



Disentangling water transport and tracer mixing mechanisms in mountainous environments influenced by volcanic features

Giovanny Mauricio Mosquera Rojas









Facultad de Ingeniería

Doctorado en Recursos Hídricos I cohorte

Disentangling water transport and tracer mixing mechanism in mountainous environments influenced by volcanic features

Trabajo de Titulación previo a la obtención del título de Doctor (PhD) en Recursos Hídricos

Autor:

Giovanny Mauricio Mosquera Rojas

CI: 0104450911

Correo electrónico:giovamosquera@gmail.com

Director:

Dr. Patricio Crespo Sánchez

CI: 0102572773

Cuenca, Ecuador

09-junio-2020



Resumen:

Las características del paisaje originadas por la actividad volcánica influyen en el transporte de agua y solutos en zonas montañosas. Sin embargo, el conocimiento sobre cómo estas características afectan el comportamiento hidrológico a diferentes escalas espaciales (desde laderas hasta cuencas) aún es escaso. La influencia de los suelos originados por la ceniza volcánica (Andosoles/Andisoles) y de la geología de origen volcánico fuertemente fracturada en el comportamiento hidrológico y la delineación de las rutas de flujo del agua es particularmente poco conocida. Para llenar estos vacíos de conocimiento, enfoqué esta disertación doctoral en la investigación de cómo los Andosoles y la geología volcánica fracturada influyen en el transporte de agua y la mezcla de trazadores. Mediciones de laboratorio, experimentales y de campo de la curva de retención de agua (CRA) de los Andosoles en combinación con datos extraídos de la literatura publicada muestran que los métodos de laboratorio estándar representan bien una pequeña porción del rango húmedo de la CRA, específicamente, desde saturación hasta potenciales matriciales 3-5 kPa (pF 1.5-1.7). Para potenciales matriciales más altos, los métodos de laboratorio estándar sobrestiman sustancialmente el contenido de agua de los suelos en comparación con las mediciones experimentales y de campo. A continuación, utilicé una evaluación combinada de datos hidrométricos, isótopos estables y de propiedades hidráulicas del suelo para investigar cómo los Andosoles influyen en el transporte de agua y la mezcla de trazadores en una ladera empinada tropical. Los resultados del análisis apuntan al predominio de las rutas de flujo vertical dentro de la matriz del suelo, a pesar de la formación de una capa de almacenamiento de agua debajo de la zona de la raíz, que se asemeja al comportamiento hidráulico de una esponja húmeda e inclinada. Finalmente, utilicé un modelo hidrológico asistido por trazadores (TraSPAN) y calibrado utilizando los isótopos estables de agua y conductividad eléctrica durante un evento de lluvia para investigar el papel de la geología volcánica fracturada en el transporte de agua y la mezcla de trazadores. La estructura del modelo que produjo las mejores simulaciones incluyó dos reservorios de agua que representan los suelos con alta capacidad de infiltración y el sistema de agua subterránea formado en el lecho de roca fracturada. Durante el evento solo el 13% de la precipitación se convirtió en caudal, con una proporción importante (75-81%) compuesta por aqua de pre-evento almacenada en la cuenca previo al evento de Iluvia. Estos hallazgos indican una alta capacidad de almacenamiento de agua del sistema en la geología volcánica fracturada.

Palabras claves: Andosol/Andisol. Roca fracturada. Isotopos estables. Transporte de agua. Trazadores hidrológicos. Modelación hidrológica. Curva de retención de agua.



Abstract:

Landscape features of volcanic origin influence the transport of water and solutes across high-elevation environments. Nevertheless, knowledge regarding how these features affect subsurface hydrological behavior at different spatial scales (from plot to catchment) is scarce. The effect of the soils originated from volcanic ash, such as Andosols (or Andisols), and the influence of highly fractured geology of volcanic origin on subsurface hydrological behavior and water flow path delineation are poorly understood. To fill this knowledge gap, I took as the main objective in the doctoral project the analysis of how Andosols and fractured volcanic geology influence flow transport and tracer mixing mechanisms. Laboratory, experimental, and field measurements of the water retention curve (WRC) of Andosols in combination with data extracted from the published literature shows that standard laboratory methods resemble well a small portion of the wet range of the WRC, specifically, from saturation to the matric potentials 3 to 5 kPa (pF 1.5-1.7). For higher matric potentials, standard laboratory methods substantially overestimate the water content of the soils in comparison to experimental and field measurements. Further, a unique set of hydrometric, stable isotope, and soil hydraulic properties data were evaluated to investigate how Andosols influence water transport and tracer mixing mechanisms at a steep tropical hillslope. The results from this analysis point to the dominance of vertical flow paths within the soil matrix, despite the formation of a perched water layer below the root zone, which mimics the hydraulic behavior of a wet, layered sloping sponge. Last, I used a tracer-aided hydrological model (TraSPAN) calibrated for the stable isotopes of water and electrical conductivity (or specific conductance) during a rainstorm event for the analysis of the role of the fractured volcanic geology on flow transport and tracer mixing at the catchment scale. The model structure that best simulated the streamflow hydrograph and the tracers concentrations during a rainfall event consisted of two water reservoirs representing the soils with high infiltration capacity and the groundwater system formed in the fractured bedrock. During the monitored event, only 13% of total precipitation was converted into runoff, with a major proportion (75-81%) corresponding to pre-event water stored in the catchment prior to the event. These findings indicate a large water storage capacity of the system in the fractured volcanic geology.

Keywords: Andosol / Andisol. Fractured bedrock. Stable isotopes. Water transport. Hydrological tracers. Hydrological modeling. Water retention curve.



Cláusula de licencia y autorización para publicación en el Repositorio Institucional

Giovanny Mauricio Mosquera Rojas en calidad de autor/a y titular de los derechos morales y patrimoniales del trabajo de titulación "Disentangling water transport and tracer mixing mechanisms in mountainous environments influenced by volcanic features", de conformidad con el Art. 114 del CÓDIGO ORGÁNICO DE LA ECONOMÍA SOCIAL DE LOS CONOCIMIENTOS, CREATIVIDAD E INNOVACIÓN reconozco a favor de la Universidad de Cuenca una licencia gratuita, intransferible y no exclusiva para el uso no comercial de la obra, con fines estrictamente académicos.

Asimismo, autorizo a la Universidad de Cuenca para que realice la publicación de este trabajo de titulación en el repositorio institucional, de conformidad a lo dispuesto en el Art. 144 de la Ley Orgánica de Educación Superior.

Cuenca, 9 de junio de 2020

Giovanny Mauricio Mosquera Rojas

C.I: 0104450911



Cláusula de Propiedad Intelectual

Giovanny Mauricio Mosquera Rojas, autor/a del trabajo de titulación "Disentangling water transport and tracer mixing mechanisms in mountainous environments influenced by volcanic features", certifico que todas las ideas, opiniones y contenidos expuestos en la presente investigación son de exclusiva responsabilidad de su autor/a.

Cuenca, 9 de junio de 2020

Giovanny Mauricio Mosquera Rojas

C.I: 0104450911



Jury committee Prof. Dr. Jan Boll, Washington State University Prof. Dr. Ricardo Sánchez-Murillo, National University of Costa Rica Dr. Edison Timbe Castro, Universidad de Cuenca Director: Prof. Dr. Patricio Crespo Sánchez. Department of Water Resources and Environmental Sciences University of Cuenca Co-directors: Prof. Dr. Rolando Célleri Alvear Department of Water Resources and Environmental Sciences University of Cuenca Dr. David Windhorst Institute for Landscape Ecology and Resources Management (ILR), Research Centre for BioSystems, Land Use and Nutrition (iFZ) Justus Liebig University Dean of the Faculty of Engineering

Prof. Eng. Julver Pino Velázquez

School of Civil Engineering



Giovanny Mauricio Mosquera Rojas
Disentangling water transport and tracer mixing mechanisms in mountainous environments influenced by volcanic features
Thesis submitted in partial fulfilment of the requirements for the degree of
Doctor of Philosophy in Water Resources



Spanish translation of the title:

Comprensión de los mecanismos de transporte de agua y la mezcla de trazadores en entornos montañosos influenciados por características volcánicas.

Refer to this work as follows:

Mosquera GM, 2020. Disentangling water transport and tracer mixing mechanisms in mountainous environments influenced by volcanic features. PhD thesis, Universidad de Cuenca, Escuela Politécnica Nacional and Universidad Técnica Particular de Loja, Ecuador.

Faculty:

Faculty of Engineering, University of Cuenca.

Department:

Department of Water Resources and Environmental Sciences, University of

Cuenca.

Universities:

Universidad de Cuenca, Escuela Politécnica Nacional y Universidad Técnica Particular de Loja.

City:

Cuenca, Ecuador.

This research was conducted under the financial support of the University of Cuenca and the Justus-Liebig-Universität Gießen (Germany) through grants awarded to the author.



"Only he who can see the invisible can do the impossible."

Frank L. Gaines





Acknowledgements

First, I thank my parents Giovanny and Ruth, my sisters Diana and Ruth A., and my awesome girlfriend Mishi for their unconditional support and motivation. I also thank all my friends around the world who became brothers and sisters throughout my journeys during the past few years in Latin America, North America, and Europe.

Special thanks to the wonderful members of my Committee, Patricio Crespo, Rolando Célleri, and David Windhorst, who provided invaluable guidance to complete this research and the best support I could have ever asked for. I also wish to acknowledge the support of my collaborators, Lutz Breuer and Catalina Segura, for their strong support of my doctoral work. Thanks are also due to two amazing individuals, Jan Feyen and Jeffrey J. McDonnell, who despite not being members of my doctoral committee, provided wise advice and support of my doctoral research, becoming my mentors on the way.

I also want to thank the support and good vibes of the members of my labs in Ecuador (Franklin, Paul, Galo, Johanna, Pachi, Juan, Elizabeth, Pablo, Irene, Enma, Darío, Mishel, Adrián, Dolores, Valeria, Mario C., Marcelo, Fausto, Jenny, Diego V., Mario M., Diego U., Ximena) and Germany (Amir, Carla, Marta, Mitchi, Philipp, Solomon, Laura, Alejandro, Jaqueline, Amani, Björn, Tobias, Sanne, Lukas, Naomi, Alicia, Ruth).

Finally, I wish to thank the support of the Central Research Unit of the University of Cuenca (Dirección de Investigación de la Universidad de Cuenca, DIUC), the German Research Foundation (DFG; Grant Numbers: BR2238/14-2, BR2238/31-1, WI4995/2-1), and the Ecuadorian National Secretary of Higher Education, Science, Technology and Innovation for providing funding for this doctoral project (Grant Number: PIC-13-ETAPA-001).



To my beloved parents, sisters, and Mishi!



Summary

Terrestrial mountain landscapes are shaped by past and present volcanic activity. The formed landscape features in turn influence the transport of water and solutes across those highelevation environments. Knowledge regarding how these features affect subsurface hydrological behavior at different spatial scales (from plot to catchment) is scarce. In this regard, the effects of the soils originated from volcanic ash, such as Andosols (or Andisols), on subsurface hydrological behavior and water flow path delineation are poorly understood. Similarly, the investigation of how the highly fractured geology of volcanic origin affects flow partitioning and hydrological behavior in catchments has been limited. To fill this knowledge gap that hinders the water management in regions where landscape features of volcanic origin dominate, I took as the main objective in the doctoral project the analysis of how Andosols and fractured volcanic geology influence flow transport and tracer mixing mechanisms. To this end, three specific objectives were proposed: 1) the determination of the water retention capacity of Andosols, 2) the conceptualization of how the properties of Andosols influence subsurface water transport and tracer mixing dynamics at the hillslope scale, and 3) the assessment of how fractured geology of volcanic origin affects the hydrological behavior and flow partitioning at the catchment scale.

Laboratory, experimental, and in-situ measurements of the water retention curve (WRC) of Andosols in combination with data extracted from the published literature shows that standard laboratory methods resemble only partially the water retention curve of these soils as compared to field conditions. These methods resemble well a small portion of the wet range of the WRC, specifically, from saturation to the matric potentials 3 to 5 kPa (pF 1.5-1.7). For higher matric potentials, standard laboratory methods substantially overestimate the water content of the soils, including the moisture content at field capacity, in comparison to experimental and field measurements. The comparison of results with data compiled from the published literature shows that this issue occurs independently of the standard laboratory method applied and the site-specific physical, chemical, and mineralogical properties of the analyzed Andosols. Findings also depict that cylindrical soil samples of small volume (<300 cm³), generally used to determine the WRC of Andosols through standard laboratory analyses, cannot capture the hydraulic behavior of these soils under field conditions. Even though an experimental method using direct soil moisture and matric potential measurement in large, undisturbed soil cores as an alternative method to characterize correctly the WRC of Andosols is presented. Future research should focus on determining the representative elementary volume of Andosol soils



and developing laboratory methods that allow the accurate characterization of their water retention capacity at reasonable logistical and financial costs.

Further, a unique set of hydrometric, stable isotope, and soil hydraulic properties data were evaluated to investigate how Andosols influence water transport and tracer mixing mechanisms at a steep tropical hillslope. The analysis of the properties of the soils along the experimental hillslope showed a little developed (52-61 cm) andic (Ah) horizon rich in organic matter (33-42%) and clay (29-31%), overlying a mineral (C) horizon. The hydrometric data revealed the formation of a perched water layer below the root zone in the Ah horizon that remains near saturation year-round. The existence of this layer is favored by the tendency of water molecules to be bounded to the high surface areas of the clay and organic matter particles, in combination with an abrupt change in saturated hydraulic conductivity between the rooted and perched layers due to the lower density of roots in the former in comparison to the latter. Despite the formation of this layer, soil water transit times (ages) were short within the whole Ah horizon (2-4 weeks). The response time to peak in soil moisture during rainfall events indicated a strongly synchronized response of soil moisture across the entire soil profile (Ah-C horizons), despite the formation of the perched layer as a result of a fast transfer of hydraulic potentials due to the exponential shape of the WRC of the soils. Overall, these findings point to the dominance of vertical flow paths within the soil matrix, despite the formation of a perched water layer below the root zone, which mimics the hydraulic behavior of a wet, layered sloping sponge.

For the analysis of the role of the fractured volcanic geology on flow transport and tracer mixing at the catchment scale, I used a tracer-aided hydrological model (Tracer-based Streamflow Partitioning ANalysis model, TraSPAN) calibrated for the stable isotopes of water (SIW) and electrical conductivity or specific conductance (EC). The model was calibrated using hydrometric and tracer data collected at high temporal frequency (<4 hours) during a rainstorm event that took place at the beginning of the fall season after a particularly dry summer. A hypothesis testing framework, in which different TraSPAN structures each one representing a different mechanism of rainfall conversion into runoff, was designed and tested. The framework was used to delineate the hydrological behavior of a temperate catchment in the U.S. Pacific Northwest. The model structure that best simulated the streamflow hydrograph and the tracers concentrations during the rainfall event consisted of two water reservoirs and a time-variant fraction of effective precipitation routed as event water. These reservoirs represent the soils with high infiltration capacity and the groundwater system formed in the fractured



bedrock. During the monitored event, precipitation totaled 155.1 mm and only 13% of it was converted into runoff, with a major proportion (75-81%) corresponding to pre-event water stored in the catchment prior to the event. These findings indicate a large water storage capacity of the system in the fractured volcanic geology. Moreover, I found that the modeling results using EC, an inexpensive and easy to measure tracer at high temporal frequency (sub-hourly), yielded remarkably similar results than the commonly used SIW, which cannot normally be collected at temporal frequencies less than a few hours. However, further testing of the suitability of EC to calibrate hydrological models at other catchments with different physiographical and climatological conditions is recommended before the proposed methodology is broadly disseminated. These results open the door to facilitate the identification of fast occurring water transport and tracer mixing processes in catchments.



Resumen

La actividad volcánica pasada y presente da forma a paisajes montañosos en la Tierra. Las características del paisaje originadas por el vulcanismo a su vez influyen en la forma en que el agua y los solutos se transportan a través de regiones de alta elevación. Sin embargo, el conocimiento sobre cómo estas características afectan el comportamiento hidrológico subsuperficial a diferentes escalas espaciales (desde laderas hasta cuencas) aún es escaso. La influencia de los suelos originados por la ceniza volcánica (Andosoles/Andisoles) en el comportamiento hidrológico y la delineación de las rutas de flujo subsuperficial del agua es particularmente poco conocida. Del mismo modo, la investigación sobre cómo la geología fuertemente fracturada de origen volcánico afecta la separación de flujo y el comportamiento hidrológico en las cuencas hidrográficas aún es escaza. Para llenar estos vacíos de conocimiento que limitan el mejoramiento de la gestión del recurso hídrico en las regiones donde estas características del paisaje se hallan comúnmente, enfoqué esta disertación doctoral en la investigación de cómo los Andosoles y la geología volcánica fracturada influyen en el transporte de agua y la mezcla de trazadores. Con este fin, se llevaron a cabo tres objetivos específicos: 1) determinar la capacidad de retención de agua de los Andosoles, 2) conceptualizar cómo las propiedades de los Andosoles influyen en la dinámica subsuperficial del transporte de agua y la mezcla del trazador a escala de ladera y 3) evaluar cómo la geología fracturada de origen volcánico afecta el comportamiento hidrológico y la separación de flujo a escala de cuenca.

Mediciones de laboratorio, experimentales e *in-situ* de la curva de retención de agua (CRA) de los Andosoles en combinación con datos extraídos de la literatura publicada muestran que los métodos de laboratorio estándar reflejan parcialmente a la capacidad de retención de agua de estos suelos en comparación con las condiciones de campo. Estos métodos representan bien una pequeña porción del rango húmedo de la CRA, específicamente, desde saturación hasta potenciales matriciales 3-5 kPa (pF 1.5-1.7). Para potenciales matriciales más altos, los métodos de laboratorio estándar sobrestiman sustancialmente el contenido de agua de los suelos, incluido el contenido de humedad a capacidad de campo, en comparación con las mediciones experimentales y de campo. La comparación de los resultados con los datos recopilados de la literatura publicada muestra que este problema ocurre independientemente del método de laboratorio estándar aplicado y las propiedades físicas, químicas y mineralógicas específicas de los diferentes sitios de estudio. Los resultados también muestran que las muestras de suelo recolectadas en cilíndros de pequeño volumen (<300 cm³), generalmente



utilizadas para determinar la CRA de los Andosoles a través de análisis de laboratorio estándar, no permiten capturar el comportamiento hidráulico de estos suelos en condiciones de campo. A pesar de que se presenta un método experimental que utiliza la medición directa de la humedad del suelo y el potencial matricial en núcleos de suelo grandes y no perturbados como un método alternativo para caracterizar correctamente la CRA de los Andosoles, la investigación futura debe centrarse en determinar el volumen elemental representativo de estos suelos y desarrollar métodos de laboratorio que permiten caracterizar la capacidad de retención de agua de estos suelos con precisión a costos logísticos y financieros accesibles.

A continuación, utilicé una evaluación combinada de datos hidrométricos, isótopos estables y de propiedades hidráulicas del suelo para investigar cómo los Andosoles influyen en el transporte de agua y la mezcla de trazadores en una ladera empinada en un ambiente tropical. La caracterización de las propiedades de los suelos a lo largo de la ladera experimental mostró un horizonte andico (Ah) poco desarrollado (52-61 cm) rico en materia orgánica (33-42%) y arcilla (29-31%), que recubre un horizonte mineral (C). Los datos hidrométricos mostraron la formación de una capa de almacenamiento de agua (perched layer) que permanece cerca de la saturación durante todo el año, debajo de la zona de la raíz en el horizonte Ah. La formación de esta capa se ve favorecida por la tendencia de las moléculas de agua a unirse a las altas áreas superficiales de las partículas de arcilla y materia orgánica, en combinación con un cambio brusco en la conductividad hidráulica saturada entre la zona de raíces y la capa de almacenamiento debido a la mayor densidad de raíces en la primera en comparación con la segunda. A pesar de la formación de esta capa, los tiempos de tránsito (edades) del agua del suelo fueron cortos dentro de todo el horizonte Ah (2-4 semanas). El tiempo de respuesta al pico de la humedad del suelo durante eventos de lluvia indicó una respuesta fuertemente sincronizada en todo el perfil del suelo (horizontes Ah-C), a pesar de la formación de la capa de almacenamiento como resultado de una rápida transmisividad de potenciales hidráulicos debido a la forma exponencial del CRA de los suelos. En general, estos hallazgos indican al predominio de las rutas de flujo vertical dentro de la matriz del suelo, a pesar de la formación de una capa de almacenamiento de agua debajo de la zona de la raíz, que se asemeja al comportamiento hidráulico de una esponja húmeda e inclinada en capas.

Con respecto al papel de la geología volcánica fracturada en el transporte de agua y la mezcla de trazadores, utilicé un modelo hidrológico asistido por trazadores (Tracer-based Streamflow Partitioning ANalysis model, TraSPAN) calibrado para los isótopos estables de agua (IEA) y conductividad eléctrica o conductancia específica (CE) para investigar la separación de flujo a



escala de cuenca. El modelo se calibró utilizando datos hidrométricos y de trazadores recolectados a alta frecuencia temporal (<4 horas) durante un evento de lluvia que tuvo lugar al comienzo de la temporada de otoño después de una temporada de verano particularmente seca en la región de estudio. Un marco de prueba de hipótesis en el que se utilizaron diferentes estructuras de TraSPAN, cada una representando un mecanismo diferente de conversión de lluvia en escorrentía, fue usado para delinear el comportamiento hidrológico en una cuenca templada en el noroeste de los EE. UU. La estructura del modelo que mejor simuló el hidrograma y las concentraciones de los trazadores durante el evento de lluvia incluyó dos reservorios de agua y una fracción de precipitación efectiva encaminada como agua de evento variable en el tiempo. Estos depósitos representan los suelos con alta capacidad de infiltración y el sistema de agua subterránea formado en el lecho de roca fracturada. Durante el evento monitoreado, la precipitación totalizó 155.1 mm y solo el 13% se convirtió en escorrentía, con una proporción importante (75-81%) compuesta por agua de pre-evento almacenada en la cuenca antes del evento de lluvia. Estos hallazgos indican una alta capacidad de almacenamiento de agua del sistema en la geología volcánica fracturada. Además, encontré que los resultados del modelado utilizando conductividad eléctrica, un trazador económico y fácil de medir a alta frecuencia temporal (sub-horaria), arrojaron resultados notablemente similares a los isótopos estables de agua utilizados de manera estándar, pero que normalmente no se pueden recolectar a una frecuencia temporal menor a unas pocas horas Si bien es necesario realizar más pruebas para evaluar la utilidad de la CE para calibrar modelos hidrológicos en otras cuencas con diferentes condiciones fisiográficas y climatológicas antes de que la metodología propuesta pueda ser ampliamente utilizada, estos resultados abren una nueva puerta para facilitar la identificación de rápidos procesos de transporte y mezcla de agua en cuencas hidrográficas.



Contents

Ackn	owled	gements
Sumr	nary	ii
Resu	men	vi
Conte	ents	ix
List o	of figu	res xiii
List o	of tabl	esxix
1. l	Introd	uction1
1.1	Im	portance of the study1
1.2	Ob	ojectives3
1.3	Stı	udy areas4
1	1.3.1	Zhurucay Ecohydrological Observatory5
1	1.3.2	Quinuas Ecohydrological Observatory6
1	1.3.3	H.J. Andrews Experimental Forest
1.4	Ου	ıtline8
2.	Water	retention capacity of volcanic ash soils11
2.1	Int	roduction
2.2	Ma	aterials and methods
2	2.2.1	Description of the experimental sites
2	2.2.2	WRC determination from in-situ (field) measurements
2	2.2.3	Collection of soil samples
2	2.2.4	WRC determination on large soil cores via a desiccation experiment19
2	2.2.5	WRC determination on small soil cores using standard laboratory methods 20
2	2.2.6	Compilation of WRC data from the published literature
2.3	Re	esults and discussion
2	2.3.1	Comparison of laboratory determined WRCs



4	2.3.2	Comparison of laboratory, experimental, and field WRCs	28
2.4	Bro	pader implications	31
2.5	Cor	nclusions	34
3. \$	Subsur	face flow dynamics at a tropical hillslope underlain by volcanic a	ash soils37
3.1	Intr	roduction	38
3.2	Exp	perimental hillslope description	40
3.3	Dat	ta collection and methods	41
3	3.3.1	Soil properties characterization	41
3	3.3.2	Hydrometric data collection	42
3	3.3.3	Isotopic data collection and analysis	43
	3.3.4 respons	Spatial-temporal variability of hydrometric data: Hydrological d	
3	3.3.5	Soil water stable isotopes: Tracer mixing and soil water ages	45
3.4	Res	sults	46
3	3.4.1	Soil properties characterization	46
3	3.4.2	Hydrological dynamics and response times	49
3	3.4.3	Tracer mixing and soil water ages	54
3.5	Dis	scussion	56
3	3.5.1	Hydrological dynamics and response times	56
3	3.5.2	Tracer mixing and soil water ages	59
3	3.5.3	Volcanic ash soils as wet, layered sloping sponges?	61
3.6	Cor	nclusions	62
4.]	Hydrol	logical behavior of a temperate catchment underlain by volcanic	geology64
4.1	Intr	roduction	65
4.2	Ma	terials and Methods	67
2	4.2.1	Study Area	67
2	1.2.2	Hydrometric Data Collection	68



4.2.3	Water Stable Isotope Data Collection and Analysis
4.2.4	Electrical Conductivity Measurements
4.2.5	Tracer-Based Hydrograph Separation Modeling
4.2.6	Model Simulations, Performance, and Uncertainty75
4.2.7	Comparison of Model Simulations for $\delta^{18}O$ and EC78
4.3 Resi	ults
4.3.1	Hydrometric and Tracer Characterization
4.3.2	Model Performance
4.3.3	Modelled Streamflow Partitioning80
4.3.4	Model Parameter Identification for the Best Model Structure84
4.3.5	Comparison of Model Results for Both Tracers86
4.4 Disc	cussion87
4.4.1 Conduct	Selection of the Best Model Structure Using Water Isotopes and Electrical tivity for Model Calibration
4.4.2 Isotopes	Comparison of Flow Partitioning Modelling Results Calibrated for Water and Electrical Conductivity
4.4.3 Modellin	On the Use of High-Temporal Resolution EC in Hydrograph Separation ng
4.4.4	Process-Based Understanding of Hydrological Behavior
4.5 Con	cluding Remarks and Future Directions91
5. Conclus	sions92
5.1 Synt	thesis92
5.2 Con	nplementary, ongoing, and future research
5.2.1	Complementary studies
5.2.2	Future research opportunities 98
References	102
Appendix A	130
Appendix B	



Supplementary material	137
About the author	148



List of figures

Figure 1.1. The Pacific Basin surrounded by volcanic arcs and major active volcanoes around
the Pacific Ring of Fire (pinkish shaded area). The study areas are located in the northern Andes
in south Ecuador (cyan star) and the Cascades range in Oregon, United States (green star).
(Adapted from Encyclopædia Britannica, Inc., https://www.britannica.com/place/Ring-of-Fire,
Last access: March 3, 2020)4
Figure 1.2. a) Dominant tussock grass vegetation on the hillslopes of the tropical alpine
(Páramo) ecosystem in south Ecuador. b) Profile of the soils of volcanic ash origin
(Andosols/Andisols) that underlie the Andean Páramo hillslopes. (Photo credits: G.M.
Mosquera)6
Figure 1.3. Photography of a stream section within the H.J. Andrews Experimental Forest.
(Photo credits: G.M. Mosquera)
Figure 1.4. Outline of the structure of the doctoral dissertation. The vertical blue arrows
indicate how each chapter relates to each of the specific objectives (SOs), as well as to the
applied approaches and scales of work used to address each SO. The horizontal orange arrow
indicates that the knowledge obtained from one chapter (initial point) was necessary to evaluate
the findings of another chapter (end point)9
Figure 2.1. Synthesis of published literature presenting data on the water retention curves
(WRCs) of Andosols. a) Evolution of the number of publications and cumulative number of
citations of the consulted studies (81 in total). The pie charts summarize the research objectives
of the consulted studies (b), the applied laboratory methods (c-e), and the volume of the soil
samples used for the determination of the WRCs (f) in the consulted studies. The laboratory
methods are classified according to different matric potential ranges (pF = logarithm of the
matric potential in cm H ₂ O). Total = number of studies reporting results for each pie chart
category13
Figure 2.2. Study site and monitoring setup for determining the water retention curves of
Andosols. a) View of the experimental plot (marked in red) located in the Zhurucay
Ecohydrological Observatory in south Ecuador; b) conceptual diagram of the spatial
distribution of Andosols in the Zhurucay Observatory hillslopes (Ah=andic horizon, C=mineral
horizon, R=bedrock); c) profile of an Andosol in the observatory; and d) experimental setup
for monitoring the soil water content and matric potential in the Ah horizon of undisturbed
Andosol soil cores (Ø=40 cm, h=32 cm) covered by tussock grass. Positions along the hillslope



in subplot b) correspond to: (A)=Toe slope, (B)=Lower slope, (C)=Middle slope, (D)=Upper slope, and (E)=Hilltop. (Photo credits: a) Galo Carrillo, c) Pablo Borja, and d) Giovanny M. Figure 2.3. Comparison of the water retention curves (WRCs) of Andosols obtained using standard laboratory methods. Soil moisture content versus matric potential relation (i.e., soil WRC, moisture release curve, or pF curve) of the Ah horizon of Andosols at different locations across the Zhurucay Ecohydrological Observatory (Figure 2.2; this study) and the WRCs of 16 published studies summarized in Table 2.2 (compiled WRC data). All data correspond to the upper horizon (depth<50 cm) of the Andosol, all covered by pristine grassland (i.e., forest cover and disturbed land use were excluded from the compiled WRC dataset). Data were generated via laboratory analysis using (i) steel rings (100 cm³ volume) in Zhurucay, and (ii) steel rings of different volume (100-230 cm³ volume) in the literature compiled WRC dataset (see Table 2.2 for details). The box plots correspond to the median and the 25 and 75 percentiles, and the whiskers to the maximum and minimum soil moisture values. The dashed vertical lines represent field capacity (FC; pF 2.52, -330 cm H₂O, or -33 kPa) and permanent wilting point (PWP; pF 4.2, -15,500 cm H₂O, or -1,550 kPa). n indicates the number of Figure 2.4. Comparison of laboratory, experimental, and *in-situ* measured water retention curves. a) Soil moisture content versus matric potential relation of the Ah horizon in the Andosols located in the middle position of the hillslope (position C in Figure 2.2a) obtained via standard laboratory methods using 100 cm³ steel rings (n=10), the experimental measurement of the soil moisture content-water potential relation (daily data shown, n=3) in large undisturbed soil cores (Ø=40 cm, h=32 cm), and field measurements of soil moisture content versus matric potential in the experimental plot of the Zhurucay Ecohydrological Observatory (data shown in **Figure 2.5**, n=2). Subplot b) shows the same results for the Ah horizon of Andosol soils in the Quinuas Ecohydrological Observatory located 35 km north of Zhurucay measured in the laboratory and experimentally on large soil cores. Data shown are the mean (x symbols connected with a thick line) and standard deviations (vertical error bars) of the measured soil moisture contents. Continuous vertical lines represent the matric potential at field capacity (FC; pF 2.52, -330 cm H₂O, or -33 kPa) and permanent wilting point (PWP; pF 4.2, -15,500 cm H₂O, or -1,550 kPa)......28 Figure 2.5. In situ measurements of daily precipitation (a), and soil moisture and matric potential monitored at half the thickness of the Ah horizon of the Andosols at the middle position (b) of the experimental plot of the Zhurucay Ecohydrological Observatory (position C



in Fig. 2b) during the period January 2012–June 2018. The matric potential and soil moisture
data correspond to the average of two monitoring stations in the experimental plot and were
used to construct the "field" water retention curve (WRC) of the Andosol soil (red line in
Figure 2.4a). The dashed horizontal lines in b) represent the soil moisture values at saturation
(green line), field capacity (blue line), and wilting point (purple line) according to the WRC
obtained using standard laboratory methods (yellow line in Figure 2.4a). The solid orange
horizontal line in b) represents the matric potential at field capacity (-33 kPa, -330 cm $\rm H_2O$,
or $pF = 2.52$), which is not reached during the study period according to the field measurements.
32
Figure 3.1. a) Experimental hillslope showing the monitoring stations of soil moisture content
and stable isotopes of soil water at the upper (UP), middle (MP), and lower (LP) positions (red
triangles) along the experimental hillslope and the position of a monitoring well used for
monitoring the groundwater level at the bottom of the hillslope (GW, blue square); b) hillslope
drainage area and monitoring stations; and c) soil profile and horizons at the UP of the hillslope
(Ah = Andic horizon, C = mineral horizon)40
Figure 3.2. Moisture release curves of the a) organic (Ah) horizon (including the curve for a
peat soil reported by Schwärzel et al. (2002) for reference) and b) the mineral (C) horizon
(including the curve of the Ah horizon for reference) of the experimental hillslope soils. The
black lines in subplots a) and b) show the exponential relation between the matric potential and
soil moisture content of the Ah horizon [Eq: $\ln{(\theta)}$ = 1.076e ⁻³ x Ψ_M – 0.3548]. Note the different
ranges of the x- and y-axes values in subplots a) and b). Data shown represent the mean (x
symbols) and standard deviation (error bars) of all samples collected at the upper (UP), middle
(MP), and lower (LP) sampling sites along the experimental hillslope for each soil horizon. 49
Figure 3.3. Hourly temporal variability of a) precipitation and soil moisture content (θ) at the
b) upper (UP), c) middle (MP), and d) lower (LP) positions along the experimental hillslope,
and e) groundwater level (GW) at the bottom of the experimental hillslope located in the
headwaters of the Quinuas River Ecohydrological Observatory for the period January 2015-
December 2017
Figure 3.4. Relation of the response times in hours (t_{peak}) to the peak value of soil moisture
during rainfall events between contiguous sampling depths at the UP (a-c), MP (d-f), and LP
(g-i) sites. Subplots j-l show the relation between the t_{peak} to the peak value of soil moisture at
different depths at the LP site and the t_{peak} to the peak value of groundwater level (GW) at the
bottom of the hillslope during rainfall events (j-l). The orange line in each subplot represents
the 1:1 ratio



Figure 3.5. Relation of the response times in hours (t_{peak}) to the peak value of soil moisture during rainfall events between contiguous sampling positions (UP, MP, and LP sites) at a depth of 5 cm (a-b), 20 cm (c-d), 45 cm (e-f), and 75 cm (g-h). The orange line in each subplot represents the 1:1 ratio. **Figure 3.6.** Temporal variability of the weekly δ^{18} O isotopic composition of precipitation (light blue line) and soil water (a, c, and e) and the δ^2 H- δ^{18} O relation in precipitation (Local Meteoric Water Line, LMWL) and soil water (b, d, and f) at the upper (UP), middle (MP), and lower (LP) positions along the experimental hillslope during the period January 2016-January 2017. The dark blue lines and the light blue shaded areas in subplots b), d), and f) represent the LMWL and the range of the isotopic variation in precipitation, respectively.54 Figure 3.7. Observed and simulated soil water δ^{18} O isotopic composition at a) 10 cm, b) 35 cm, and c) 65 cm depths at the upper position (UP) of the experimental hillslope. The open circles represent the observed isotopic composition in soil water; the blue lines represent the precipitation isotopic composition; the black lines represent the best simulated isotopic composition in soil water according to the KGE objective function; and the shaded areas....55 Figure 3.8. "A wet, layered sloping sponge". Conceptual model of the subsurface hydrological system of the experimental hillslope underlain by volcanic ash soils (Andosols) located in the headwaters of the Quinuas Ecohydrological Observatory. The size of the blue arrows represents the relative importance of vertical and lateral flow paths of water at different soil layers. The relative size of the white symbols indicates differences in the magnitude of the soil properties at each of the soil layers (values in Tables 1 and 2). ${}^{a}K_{sat}$ = saturated hydraulic conductivity in Figure 4.1. Location of Mack Creek Catchment within the H.J. Andrews Experimental Forest in Western Oregon. Black triangles indicate the locations of the meteorological stations (PRIMET, CENMET, and UPLMET) along with the location of the precipitation and stream Figure 4.2. Assumptions in TRaSPAN model structures (a) constant fraction of effective precipitation (Peff) routed as event water and a single reservoir for the event and pre-event runoff components (structure 1); (b) constant fraction of Peff routed as event water and two reservoirs in parallel for the event and pre-event runoff components (structure 2); (c) timevariable fraction of P_{eff} routed as event water and a single reservoir for the event and pre-event runoff components (structure 3); and (d) the time-variable fraction of Peff routed as event water and two reservoirs in parallel for the event and pre-event runoff components (structure 4)...75



Figure 4.3. Temporal variability of the hydrometric and tracer data during the event monitored between 28 October and 7 November 2015 at Mack Creek. (a) Rainfall (P), runoff (Q), and sample collection times. Vertical dashed lines $(t_0 - t_f)$ indicate periods described in Section 4.3.1; (b) δ^{18} O in stream and P; and (c) electrical conductivity (EC) in stream and P......78 Figure 4.4. TraSPAN modelling results of the hydrograph separation using structure 1 with δ¹⁸O (a–c) and electrical conductivity (EC) (d–f) as tracers for calibration. (a,b,d, and e) show the observed (open markers) and simulated streamflow and tracer data according to at least 100 different sets of parameters (light blue lines) yielding Nash–Sutcliffe efficiencies (NSEs) above 0.70 (behavioral parameter sets). The simulated times series with the set of parameters that yielded the highest NSEs are depicted in dark blue lines in all cases. (c and f) present the preevent water (gray shaded area) and the event water (unshaded area) contributions during the storm corresponding to the set of parameters yielding the highest NSEs......82 Figure 4.5. TraSPAN model results of the hydrograph separation using structure 4 calibrated with $\delta^{18}O$ (a–c) and electrical conductivity (EC) (d–f) as tracers. (a,b,d, and e) present observed (open markers) and simulated streamflow and tracer data according to all parameter sets (blue lines) that yield a Nash–Sutcliffe coefficient above 0.75 (behavioral parameter sets). The best simulated times series in both cases are depicted in dark blue lines. (c and f) present the preevent water (gray area) and the event water (white area) contributions during the storm, according to the best set of parameters......83 Figure 4.6. Dotty plots of the Monte Carlo simulations for the calibrated parameters using TraSPAN model structure 4 using electrical conductivity (EC). Parameter names are shown in Figure 4.7. Box plots of the calibrated parameters considering sets that yielded NSE>0.75 from the last run (i.e., 1×10^7 simulations) using model structure 4 calibrated for δ^{18} O and electrical Figure 4.8. Transit time distributions (TTDs) of the (a) event (he) and (b) pre-event (hp) flow components for model structure 4 using $\delta^{18}O$ and electrical conductivity (EC) for calibration. The solid lines represent TTDs based on the 50th percentiles of behavioral (>0.75 NSE) parameter sets. The dashed lines correspond to the TTD defined based on parameter sets representing the 25th and 75th percentiles of their distributions.......86 Figure 5.1. Schematic representation of complementary and future/ongoing research linked to this doctoral dissertation. The vertical blue arrows indicate how complementary research published in peer-reviewed journals that resulted from the thesis of 3 MSc students advised by the dissertation author (gray level) and open research questions that need to be addressed in



future (or ongoing) research (orange l	evel) ar	e linked	to the	outcomes	of each	of the	chapter
of this dissertation	(blue level))							9



List of tables

Table 2.1 Hydraulic properties of the Ah (andic) horizon of the Andosols monitored at different
positions along the hillslopes (as shown in Figure 2.2b) in the Zhurucay Ecohydrological
Observatory. The values presented in the table are the average and the standard deviation (in
parenthesis) of the properties measured in the laboratory
Table 2.2 Summary of the published literature presenting soil moisture content versus matric
potential data ^a used for the construction of the water retention curves (moisture release curves,
moisture characteristic curves, or pF curves) of volcanic ash soils with andic properties
(Andosols/Andisols) using standard laboratory methods
Table 3.1. Physical characteristics and carbon content of the soil profiles monitored at the
upper (UP), middle (MP), and lower (LP) positions along the experimental hillslope47
Table 3.2. Mean values of the hydrophysical properties of the soil at the upper (UP), middle
(MP), and lower (LP) positions along the experimental hillslope. The presented values
correspond to the average of three measurements of each of the properties and each sampling
location and depth
Table 3.3. Summary statistics of the $\delta^{18}O$ isotopic composition of precipitation (QP1) and soil
water and the soil water mean transit times (MTTs) at the upper (UP), middle (MP), and lower
(LP) positions along the experimental hillslope. MTT values in parenthesis represent the 5-
95% confidence limits of the simulated soil water MTTs
Table 4.1. Modules, equations, and parameters of the four Tracer-Based Streamflow
Partitioning Analysis (TraSPAN) model structures
Table 4.2. Parameter sets that yielded the highest NSEs values for each TraSPAN model
structure and tracer used for calibration
Table 4.3. TraSPAN model performance in terms of the mean Nash–Sutcliffe efficiency (NSE)
for discharge and tracer concentrations and the Akaike Information Criterion for discharge
(AIC ₀) and tracer (AIC _T , i.e., δ^{18} O or EC) values80





Chapter 1

1. Introduction

1.1 Importance of the study

Montane ecosystems provide key hydrological services to local and downstream populations. These services include runoff production and regulation and water storage (Beniston, 2003). As a result, catchments originated from high-elevation ecosystems are often considered the "water towers" of the planet (Viviroli et al., 2007). Runoff generated from these catchments provides the water that sustains the economic development of millions of people around the world (Messerli et al., 2004; Viviroli et al., 2011). However, hydrological knowledge in these catchments remains limited due to the difficulty to understand the complexity of mountainous landscapes and the harsh environmental conditions that limit data collection. These factors hamper the understanding of how montane headwater catchments store and release water and how these processes are affected by specific catchment features.

Despite the close link between past and present volcanic activity and the formation of mountain ranges (Gerrard, 1990; Stanley, 2004), the specific influence of landscape features of volcanic origin on the hydrological behavior of mountainous environments is not yet fully understood. Amongst these features, the influence of soils formed on volcanic ash and of highly fractured geology originated from weathered lava flows has been the least investigated. Hence, an improved understanding of how these landscape characteristics affect fundamentally hydrological relations such as flow path delineation and water transport and tracer mixing in the subsurface still needs to be further unraveled. Acquiring such understanding will not only fill knowledge gaps in hydrological sciences, but also will help to improve the water management in the regions where these features dominate.

One of the main factors behind these knowledge gaps is the lack of appropriate datasets, in combination with field-based surveys and modeling methods, to obtain a complete understanding of subsurface hydrological processes (Vereecken et al., 2015). Although commonly measured hydrometric data (e.g., precipitation, streamflow, and soil moisture) have been useful to shed light on the dynamics of hydrological systems influenced by volcanic features (e.g., Hasegawa and Sakayori, 2000; Hasegawa and Eguchi, 2002), this information alone is not sufficient to identify the dominant flow paths of water in the subsurface, neither to



understand how water mixes within these systems. The methodological limitations were resolved in other environments through the use of environmental tracers, of the stable isotopes of water in particular. These tracers have the potential to help identify the fractions of event water (or "new" water from incoming precipitation) and pre-event water (or "old" water stored in a catchment prior to a precipitation event) that contribute to discharge during rainstorm events (Klaus and Mcdonnell, 2013; von Freyberg et al., 2017), the mean transit time (or "age") of water at an outlet point of a hydrological system (Hrachowitz et al., 2016; McGuire and McDonnell, 2006), the main flow paths of water (e.g., Mueller *et al.*, 2014; Farrick and Branfireun, 2015; Klaus *et al.*, 2015; Mosquera *et al.*, 2016; Orlowski *et al.*, 2016), and the relationship between water storage and discharge (e.g., McNamara *et al.*, 2011; Birkel *et al.*, 2015; Pfister *et al.*, 2017; Lazo *et al.*, 2019). Despite their usefulness, the use of these tracers to evaluate how the aforementioned catchment features of volcanic origin affect the hydrology of mountainous environments is still limited.

The mixing and transport of water and solutes in the subsurface depends largely on the water retention capacity of porous media (Selker et al., 1999). Thus, an accurate determination of the water retention curve of a soil (WRC, the relation between the water content of the porous medium and the matric potential, a measure of the adhesion of water molecules to the soil matrix) is fundamental to investigate flow transport and mixing below ground. Past investigations about the WRC of volcanic ash soils (Andosols/Andisols) have shown contrasting results between *in-situ* measurements, considered as the true representation of the hydrological behavior of the soils under field conditions, and those obtained through the application of standard laboratory methods (Eguchi and Hasegawa, 2008; Fontes et al., 2004). Defining the reasons behind such discrepancies and how to obtain accurate representations of the WRC of Andosols is, therefore, a fundamental step in the interpretation and modeling of the subsurface hydrological, ecological, and biogeochemical processes occurring within these soils.

Another important knowledge gap is the assessment of how Andosols influence water transport and tracer mixing in the subsurface. To date, research only focused on investigating the dynamics of soil moisture and the factors controlling its hydrological behavior (e.g., Hasegawa and Eguchi, 2002; Blume *et al.*, 2009; Dec *et al.*, 2017; Tenelanda-Patiño *et al.*, 2018; Montenegro-Díaz *et al.*, 2019). Unfortunately, those investigations offer no information about water flow paths and tracer mixing mechanisms in the subsurface. Other investigations monitored the isotopic and geochemical composition of Andosols to evaluate sources of runoff



contributing to streamflow production (e.g., Muñoz-Villers and McDonnell, 2012; Mosquera *et al.*, 2016; Correa *et al.*, 2017). However, those data have not yet been used to obtain a process-based understanding of subsurface flow processes in these soils. Therefore, the analysis of a combined dataset of hydrometric, tracer, and Andosol properties is required to investigate how the properties of these soils influence the subsurface water flow paths (lateral versus vertical).

Past research focused mainly on investigating the role of vegetation (forested versus non-forested) and land use (conserved versus disturbed) on the hydrological behavior of catchments, while overlooking the effect of the highly fractured geology originated from weathered lava flows. As a result, how geology affects subsurface flow processes is still poorly understood (Gabrielli and McDonnell, 2020). In other environments, hypothesis testing frameworks (Beven et al., 2020; Pfister and Kirchner, 2017; Vaché et al., 2004) using traceraided hydrological models have been successfully used to disentangle subsurface water flow paths (Birkel and Soulsby, 2015). These models present the advantage that they do not only account for water flux dynamics (i.e., the transfer of hydraulic potentials in the subsurface), but also for the mixing of tracers (Harman, 2015; Segura et al., 2012; Weiler et al., 2003). However, the potential of these techniques to understand the role of fractured volcanic geology on the partitioning of streamflow into new and old water has not yet been taken advantage of.

In this dissertation, a combination of traditional and emerging laboratory, experimental, field, and numerical modeling techniques at different spatial scales (from plot to catchment) were applied to fill these knowledge gaps. The acquisition of such knowledge will enhance the water resources management in mountainous environments where landscape features of volcanic origin are dominant and facilitate the development of adaptation strategies as input for management and policy action.

1.2 Objectives

The general objective of this dissertation was to shed light on how landscape features of volcanic origin (soils and geology) influence the main flow paths and the transport and mixing of water in the subsurface of mountainous environments. To this end, the following specific objectives were formulated:

1) to determine the water retention capacity of volcanic ash soils (Andosols)



- 2) to conceptualize how the hydraulic properties of Andosols influence subsurface water transport and tracer mixing dynamics at the hillslope scale, and
- 3) to evaluate how fractured geology of volcanic origin affects the hydrological behavior and flow partitioning at the catchment scale.

1.3 Study areas

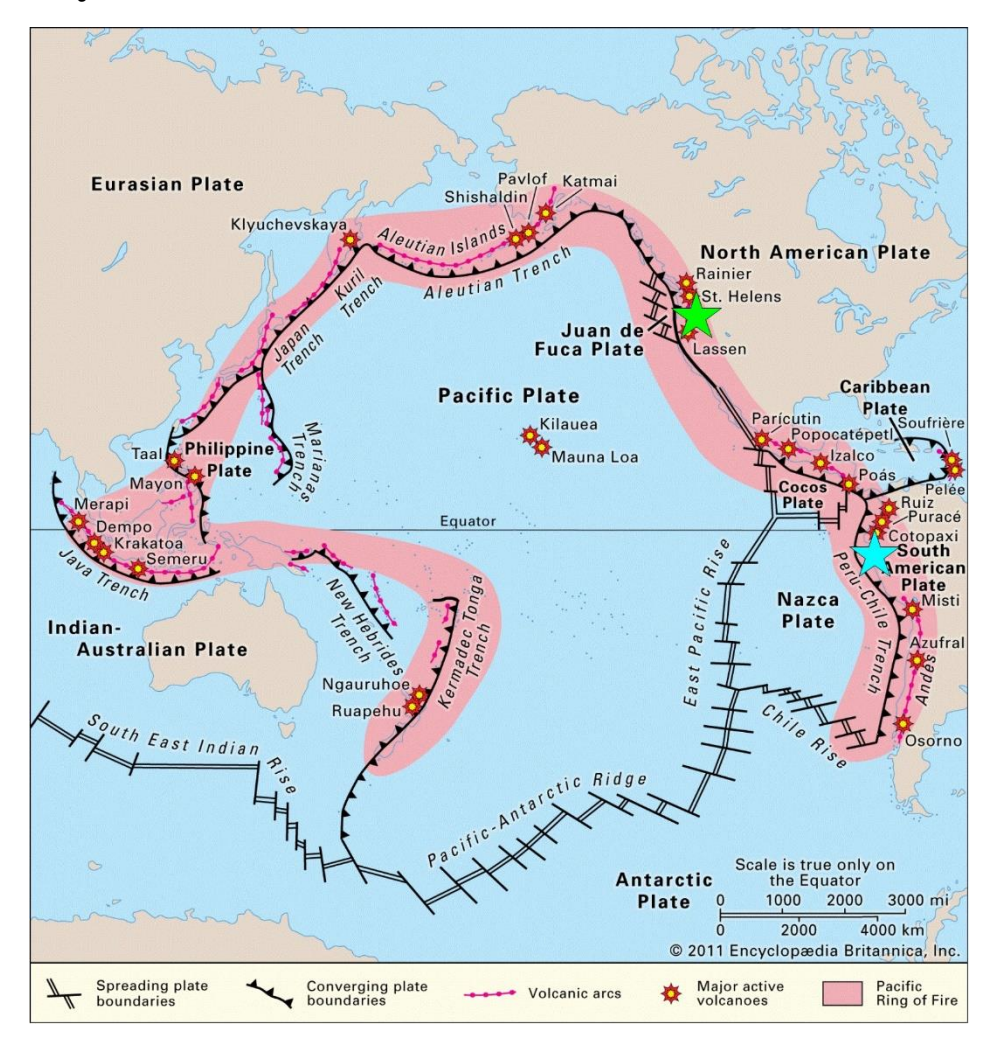


Figure 1.1. The Pacific Basin surrounded by volcanic arcs and major active volcanoes around the Pacific Ring of Fire (pinkish shaded area). The study areas are located in the northern Andes in south Ecuador (cyan star) and the Cascades range in Oregon, United States (green star). (Adapted from Encyclopædia Britannica, Inc., https://www.britannica.com/place/Ring-of-Fire, Last access: March 3, 2020).

The Pacific Ring of Fire surrounds a major area of the Pacific Basin (**Figure 1.1**). This area, geographically bounded by North, Central, and South America on the east and by an arc of islands extending from Alaska to New Zealand on the west, is largely affected by the movement of the Earth's tectonic plates (Schlanger et al., 1981). As a result, this region of the planet is



one of the most affected by volcanic activity. Volcanism along the Ring of Fire in turn has led to the formation of vast mountain ranges, such as the Cascades range and the Andean mountain range along the western edge of North and South America, respectively. As such, three experimental sites with distinctive soil and geological features of volcanic origin situated within these two mountainous ranges were selected. Two of the experimental sites were located in the northern Andes of Ecuador, where relatively young soils derived from volcanic ash are common, and the third one in the western Cascades in the Pacific Northwest of the United States, where older, fractured geology is found without the presence of volcanic ash soils. Although a detailed description of each of the experimental sites are presented in Chapter 2-4, a brief description of the most relevant characteristics is given below.

1.3.1 Zhurucay Ecohydrological Observatory

The Zhurucay Ecohydrological Observatory is located on the west slope of the Andean mountain range in southern Ecuador (3°04'S, 79°14'W) and drains towards the Pacific Ocean. The observatory is located within the tropical alpine (Páramo) ecosystem at elevations ranging from 3,400-3,900 m a.s.l. The climate in the study area is mainly influenced by air masses stemming from the Amazon forest (Esquivel-Hernández et al., 2019), despite its proximity to the Pacific Ocean (approximately 80 km). Annual precipitation in the observatory averages 1,345 mm (Mosquera et al., 2015). Precipitation is fairly uniformly distributed throughout the year showing little seasonality and falling mainly in the form of drizzle (Padrón et al., 2015). Mean annual temperature, relative humidity, and radiation at 3,780 m a.s.l. are 6.0°C, 90%, and 100 W m⁻²; Córdova et al., 2015; Ochoa-Sánchez et al., 2020). The landscape presents a U-shaped geomorphology with broad valleys at the bottom of hillslopes as a result of past glacial activity, presenting an average gradient of 17%. The geology in the region consists primarily of volcanic rock deposits compacted by glacial activity during the last ice age (Coltorti and Ollier, 2000). The Quimsacocha and Turi geologic formations dominate, both dating from the late Miocene Period (Pratt et al., 1997). The former is composed of basaltic flows and the latter of tuffaceous andesitic breccias, conglomerates, and horizontally stratified sands. The dominant soils in the observatory are Andosols/Andisols of volcanic ash origin covering approximately 72% of the area; while the remaining area is occupied by peat soils (Histosols). Andosols are commonly found on hillslopes, whereas Histosols are mainly located in the valley bottoms. These soils have resulted from the accumulation of volcanic ash deposits during the Quaternary, which in combination with cold and humid local atmospheric conditions led to the formation of organic and clay rich soils with high water holding capacity (Buytaert



et al., 2006a). The areal distribution of the soils in the observatory is highly correlated with its vegetation cover (Mosquera et al., 2016a). As such, the dominant tussock grass of the Páramo (commonly in the genera *Calamagrostis* and *Festuca*) that overlies the Andosols cover 71% of the land (**Figure 1.2**), and cushion plants (*Plantago rigida*, *Xenophyllum humile*, *Azorella*; Ramsay and Oxley, 1997; Sklenar and Jorgensen, 1999) covering the Histosols extend over 24% of the observatory. Endemic (*Polylepis*) and introduced (*Pinus*) forest patches cover the remaining area of the observatory (4%). The land cover in the observatory is mainly pristine, with little cattle grazing at the lower elevations.

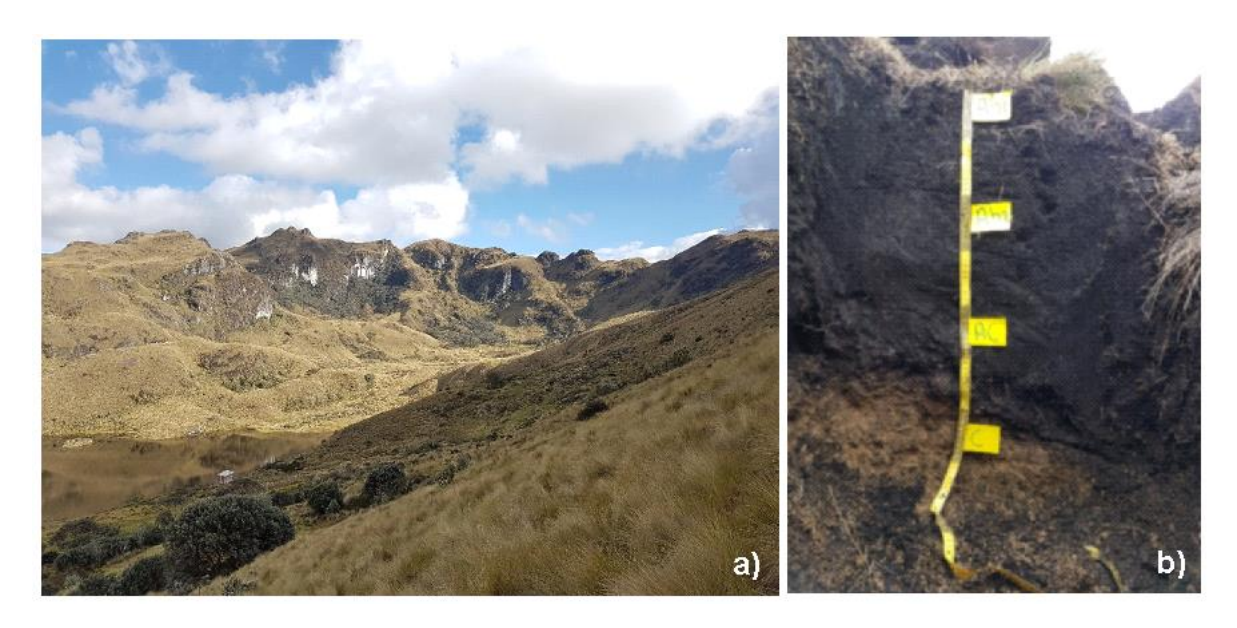


Figure 1.2. a) Dominant tussock grass vegetation on the hillslopes of the tropical alpine (Páramo) ecosystem in south Ecuador. b) Profile of the soils of volcanic ash origin (Andosols/Andisols) that underlie the Andean Páramo hillslopes. (Photo credits: G.M. Mosquera).

1.3.2 Quinuas Ecohydrological Observatory

The Quinuas Ecohydrological Observatory is approximately 35 km north of the Zhurucay Observatory, but situates on the east slope of the Andean mountain range (2°47'S, 79°13'W), draining towards the Atlantic Ocean through the Amazon basin. The observatory is also situated in the Páramo ecosystem and extends between 3,600-4,400 m a.s.l. (Pesántez et al., 2018). The upper part of the observatory, where this research was conducted (3,900-4,100 m a.s.l.), belongs to the protected El Cajas National Park. The climate and precipitation regime in the study area are similar to those described above for the Zhurucay Observatory. Annual precipitation, temperature, and relative humidity at 3,955 m a.s.l. are on average 1,021 mm, 5.4°C, and 92.1%, respectively (Carrillo-Rojas et al., 2019; Muñoz et al., 2016). The



geomorphology in the observatory is also shaped by past glaciation, although the valley bottoms are narrower and the surrounding hillslopes are steeper in comparison to Zhurucay, presenting an average gradient of 42% (Carrillo-Rojas et al., 2016). The geology is composed of the Tarqui and Celica formations, with a dominance of tuffs, lavas, agglomerates, and ignimbrites of rhyolitic composition (Hall and Calle, 1982). Similar to the Zhurucay Observatory, the dominant soils are Andosols covering mainly the hillslopes and Histosols found principally in the valley bottoms. The dominant vegetation in the observatory is tussock grass (*Calamagrostis* and *Festuca*, 67%) coexisting with forest patches (*Polylepis*, *Gynoxys*. and *Pinus*, 14%) and cushion plants and shrubs (*Plantago*, *Valerian*, and *Gentiana*, 8%). The remaining of the landscape corresponds to lakes and small water ponds (7%) and rock and bare soil (Pesántez et al., 2018). There is no influence of anthropogenic land use in the study area.

1.3.3 H.J. Andrews Experimental Forest



Figure 1.3. Photography of a stream section within the H.J. Andrews Experimental Forest. (Photo credits: G.M. Mosquera).

The H.J. Andrews Experimental Forest is located on the western Cascade Range of Oregon, United States (44°12'N, 122°15'W) and drains to the Willamette River basin that ultimately discharges into the Pacific Ocean after joining the Columbia River in the north. Differently than in the Páramo of south Ecuador, soils of volcanic ash origin (Andosols) are not commonly found in this study area. The experimental site situates in a temperate forest ecosystem at



elevations between 430 and 1,600 m a.s.l. The study region has a Mediterranean climate, with cool, wet winters and warm, dry summers. Annual precipitation averages 2,709 mm at 1,294 m a.s.l., with more than 80% falling between November and May. Snow-pack accumulation normally occurs between mid-November through the end of June at high elevations (>1,000 m a.s.l.), but snow usually does not persist for periods>2 weeks at lower elevations (Jones and Perkins, 2010). The landscape is dominated by a U-shaped geomorphology of glacial origin, with a steep average gradient of 46%. The geology in the study area is composed of multiple rock types of volcanic origin that date back from the late Miocene and Pliocene (upper Sardine Formation and Pliocene flows). Ridges in the study area are underlain by highly weathered lava flows with high porosity, and areas at lower elevation are underlain by air fall tuffs and alluvial tuffaceous sediments (Swanson and James, 1975). Highly porous Inceptisols with high infiltration rates (>1000 mm hr⁻¹) are the dominant soils in this experimental site (Brown and Parsons, 1973). Vegetation is mainly composed of coniferous forests (Dyrness and Hawk, 1972) including Douglas-fir (*Pseudotsuga menziesii*), western hemlock (*Tsuga heterophylla*), western red cedar (Thuja plicata), noble fir (Abies procera), and Pacific silver fir (Abies amabilis).

1.4 Outline

The first chapter of this dissertation provides an overview of the relevance and general background of the topics addressed in the doctoral project. In addition, the general and specific objectives of the dissertation and a brief description of the content of each of the following chapters are listed.

The outline of the main Chapters of the dissertation that summarizes the approach and scale of analysis used to address each of the specific objectives is shown in **Figure 1.4**. Chapter 2 is oriented towards the accurate determination of the water retention capacity of Andosols. To this end, a combination of laboratory and experimental techniques were used for the measurement of the WRC of the soil. The chapter also includes a compilation of data extracted from the literature published on this topic. I included and analyzed these data so that the study results are discussed in a broader context, and general conclusions about the advantages and limitations of the different measurement techniques to obtain the WRC of Andosols could be developed. The last part of Chapter 1 presents a set of recommendations in support of the interpretation and modeling of subsurface flow processes in future research.



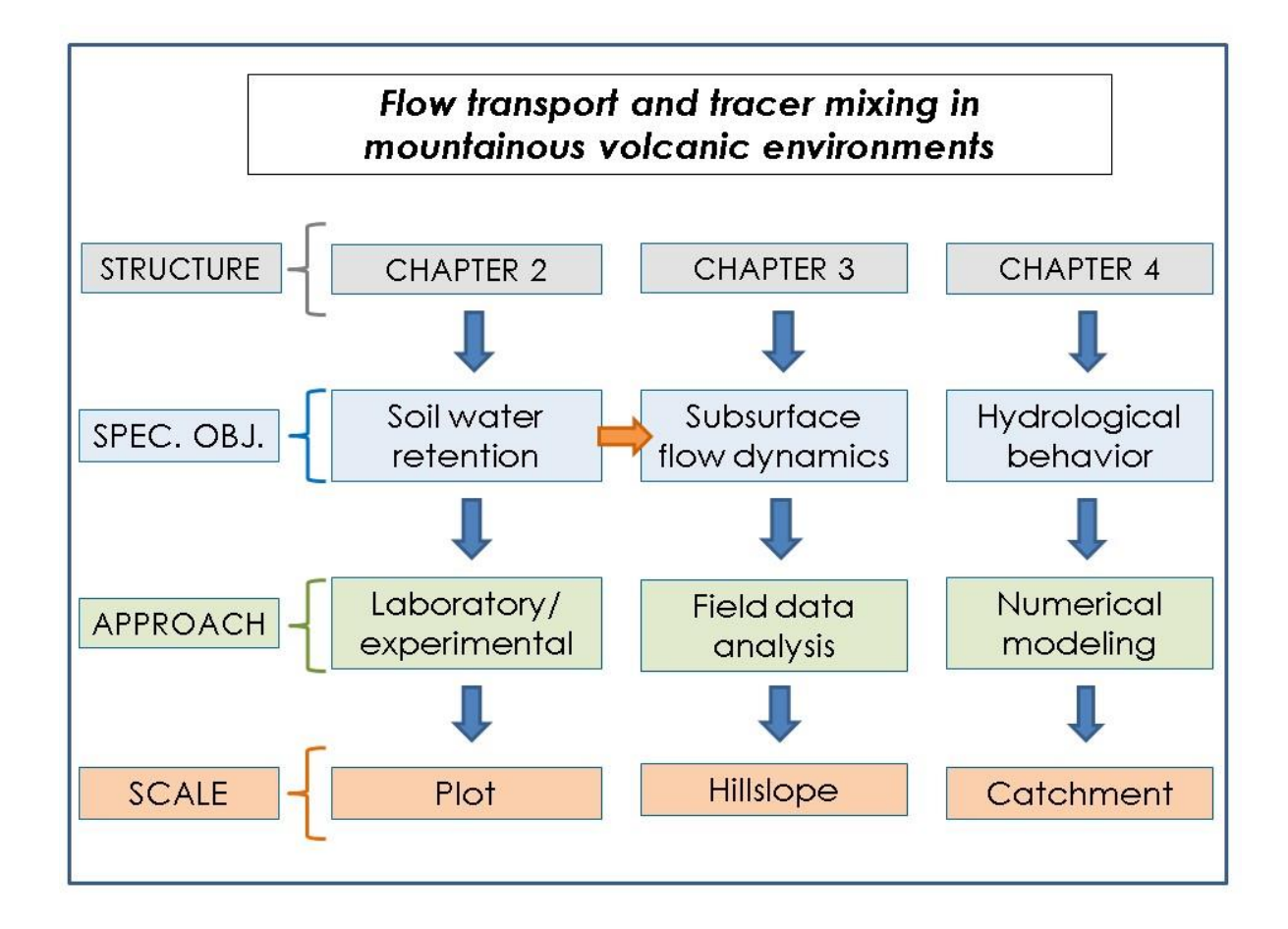


Figure 1.4. Outline of the structure of the doctoral dissertation. The vertical blue arrows indicate how each chapter relates to each of the specific objectives (SOs), as well as to the applied approaches and scales of work used to address each SO. The horizontal orange arrow indicates that the knowledge obtained from one chapter (initial point) was necessary to evaluate the findings of another chapter (end point).

Subsequently, the conceptualization of how the hydraulic properties of Andosols (including the WRC of the soils determined using the appropriate method defined in Chapter 2) control the subsurface flow dynamics at the hillslope scale is presented in Chapter 3. A spatial and temporal analysis of precipitation, soil moisture, and groundwater level dynamics was conducted in a hillslope transect covered by Andosols to unravel the flow transport along the hillslope transect. In addition, the stable isotopic composition of precipitation and soil water were analyzed to investigate the mixing of tracer and to delineate the main water flow paths in the subsurface. Finally, a process-based conceptual model on how water transport and tracer mixing mechanisms relate to the hydraulic properties of the Andosols along the experimental hillslope was developed.

Chapter 4 presents on the investigation of the role of fractured volcanic geology on the hydrological behavior and streamflow partitioning (old versus new water) at the catchment



scale. For this purpose, I used a combined set of hydrometric (precipitation and streamflow) and tracer (stable isotopes and electrical conductivity) data collected at high temporal frequency (15 minutes to 4 hr) and introduced a tracer-aided hydrological model as a hypothesis testing tool to unravel the hydrological functioning of the catchment. In addition, this chapter presents a thorough comparison of the modeling results using two tracers for calibration in terms of the modeling performance and the process-based understanding of the hydrologic system.

Finally, Chapter 5 presents a summary of the main findings of this doctoral project. In addition, a brief description of the findings of studies complementary to this work, in which I participated during the execution of the research, are included. Finally, the pathways that the findings of the doctoral project have left open for future investigations are delineated.

.



Chapter 2

2. Water retention capacity of volcanic ash soils

Volcanic ash soils with andic properties (Andosols) provide fundamental hydrological and ecological services in mountainous regions worldwide. For the study of the transport and mixing of water and solutes in the unsaturated zone of the Earth's crust the volumetric water content-matric potential relationship (the water retention curve, WRC) is an essential parameter. Through an extensive analysis of laboratory, experimental, and in-situ measured WRCs of Andosols in combination with data extracted from published literature I show that standard laboratory methods using small soil sample volumes ($\leq 300 \text{ cm}^3$) are capable of mimicking the WRC of Andosols only partially. These methods resemble well the wet range of the WRC, but overestimate substantially the water content of Andosols for high matric potentials, including the field capacity. This discrepancy occurs irrespective of site-specific land use and cover and soil properties (physical, chemical, and mineralogical), and the laboratory method applied. These findings imply that results reported in past research should be re-evaluated and future investigations should apply appropriate methods to obtain the WRC of Andosols. The latter requires the determination of the smallest volume of soil and the adaptation of standard laboratory methods to represent accurately the Andosols' hydraulic behavior under field conditions.

Related publication

Mosquera GM, Marin F, Célleri R, Feyen J, Breuer L, Windhorst D, Crespo P. Analysis of methodological issues of the water retention characteristic curve of volcanic ash soils: Do standard laboratory methods reflect field conditions? (In review, Hydrological Processes).



2.1 Introduction

Soils developed on volcanic ash, known as Andosols (IUSS Working Group WRB, 2015) or Andisols (Soil Survey Staff, 1999), possess distinctive mineralogical, chemical, and physical properties (Nanzyo, 2002; Wada, 1985). These soils have an atypical mineralogy composed of allophane with subordinate imogolite and ferrihydrite for allophanic Andosols or Al- and Fehumus complexes for non-allophanic Andosols (McDaniel, Lowe, Arnalds, & Ping, 2012; Sadao Shoji, Nanzyo, & Dahlgren, 1993). Andosols also present a high affinity for phosphate retention combined with high organic matter accumulation (Dahlgren, Saigusa, & Ugolini, 2004). The mineralogical and chemical features of these soils provide them with andic properties (Soil Survey Staff, 2010), which in turn explain their unique physical characteristics. The latter include low bulk density, high porosity, and large surface area that gives them an outstanding water holding capacity (McDaniel et al., 2012). Andosols are found worldwide, in humid montane regions with past and present volcanic activity primarily (S. Shoji et al., 1993), providing important hydrological and ecological services (Terribile et al., 2018). Because of this, even though Andosols cover only 1% of the Earth's crust, they represent an important resource supporting the water supply of approximately 10% of world's population (Neall, 2006; Ping, 2000; Sadao Shoji et al., 1993), including the densely populated tropics, where half of the world population is projected to live by 2050 (Wright et al., 2017).

Given the increasing recognition of the hydrological services produced by Andosols such as water storage and flow regulation (Buytaert et al., 2006a, 2005b; Mosquera et al., 2016a, 2015), investigations about their hydraulic properties increased during the last few decades. The correct determination of these properties, and of the water retention characteristics in particular, is fundamental to improve the understanding of subsurface hydrological, ecological, and biogeochemical processes (Selker et al., 1999) and to increase the predictive capability of numerical models to accurately represent these processes (Vereecken et al., 2016). As such, the water retention capacity of Andosols is one of the most investigated features (81 publications with ≈3,200 citations in the period 1982-2019; **Figure 2.1a**, see Appendix A for details). The published literature regarding this topic focused predominantly on the determination of the Andosols' physical and hydraulic properties (35%) and the assessment of the impacts of land use and land cover change on these properties (25%; **Figure 2.1b**). Other authors investigated the subsurface flow dynamics (6%), the hillslope stability (6%), the derivation and use of pedotransfer functions (5%), the testing of soil moisture sensors (5%), and the hydrological behavior of catchments using hydrological models (4%), among others (**Figure 2.1b**).



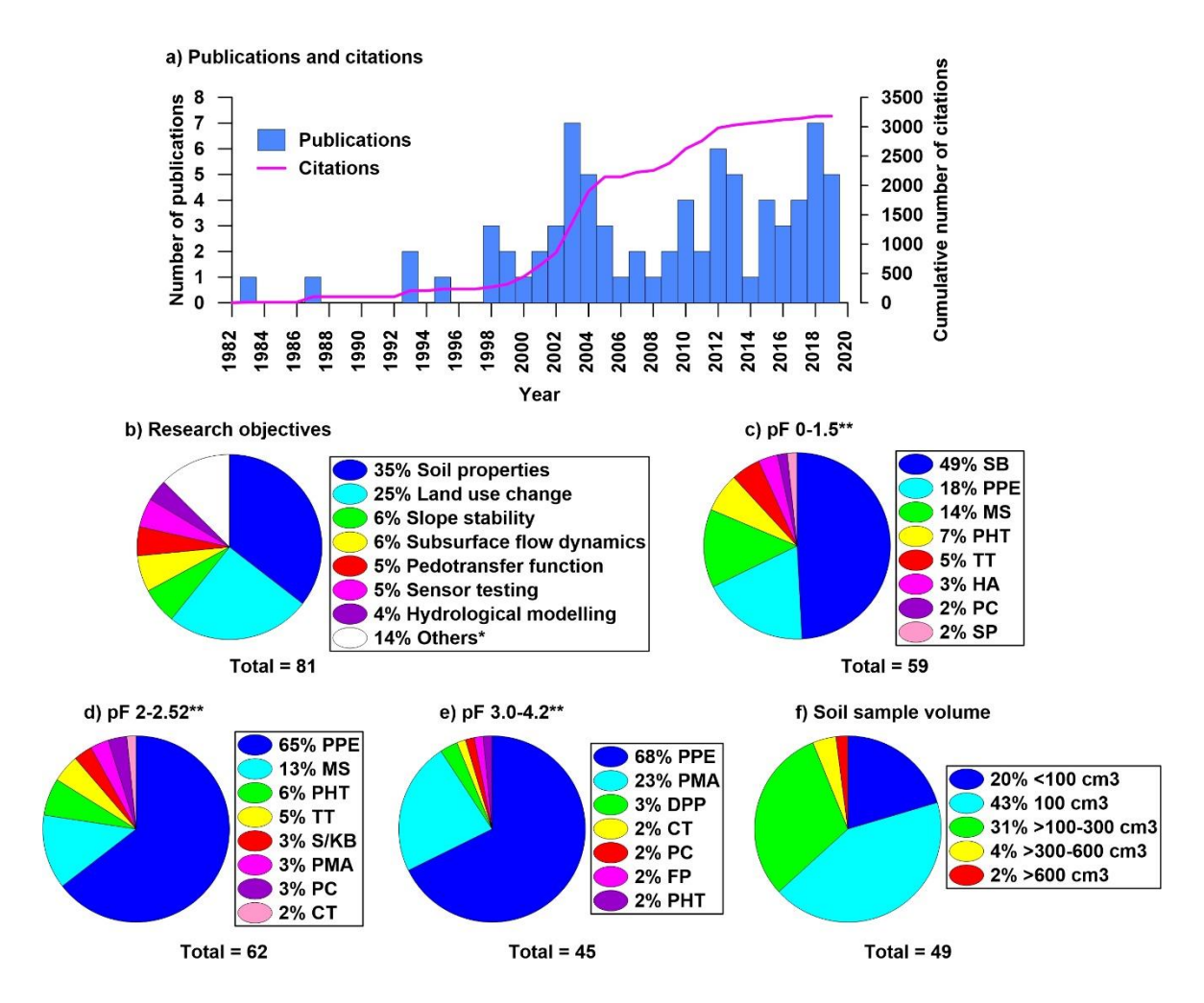


Figure 2.1. Synthesis of published literature presenting data on the water retention curves (WRCs) of Andosols. a) Evolution of the number of publications and cumulative number of citations of the consulted studies (81 in total). The pie charts summarize the research objectives of the consulted studies (b), the applied laboratory methods (c-e), and the volume of the soil samples used for the determination of the WRCs (f) in the consulted studies. The laboratory methods are classified according to different matric potential ranges (pF = logarithm of the matric potential in cm H_2O). Total = number of studies reporting results for each pie chart category.

*Others in subplot b) include: carbon stocks, soil genesis, biosolid application, ecological services, estimation of soil hydraulic parameters, soil description, spatial variability and spatial prediction of soil properties, water conservation practices, and biogeochemical modelling. **Acronyms of the laboratory methods in subplots c)-e) are as follows: SB=Sandbox, S/KB=Sand/Kaolin box, PPE=Pressure plate extractors, HA=Haines apparatus, MS=Multistep, PHT=Pressure heads by tensiometers, TT=Mini-tensiometers, PC=Pressure cells, SP=Suction plate, PMA=Pressure membrane apparatus, CT=Centrifuge, FP=Filter paper, DPP=Dew-point potentiometer.

The majority of the findings of these studies rely on the Andosols' water retention curve (WRC, also known as moisture release curve, moisture characteristic curve, or pF curve). The WRC represents the change in the soil matric potential (tension) during drying and/or wetting cycles



(Hillel, 1998) and is generally determined using standard laboratory methods. For Andosols, the sandbox (Stakman et al., 1969; 49%) and pressure plate extractor (FAO, 2002; 18%) methods are the most widely used to measure the water content of the soil at matric potentials below field capacity (i.e., the amount of water that a soil retains against gravity (Kirkham, 2014; Figure 2.1c). To determine the soil water content around field capacity, the pressure plate extractor (65%) and the multistep (van Dam et al., 1992) 13%) method are commonly used (**Figure 2.1d**). The pressure plate extractor (68%) and the pressure membrane apparatus (Richards, 1941; 23%) are applied to measure the water content at potentials above field capacity up to the permanent wilting point (i.e., the matric potential that prevents plant roots to extract water from the soil causing wilting (Kirkham, 2014; Figure 2.1e). Despite the usefulness of these methods, it is widely known that they can yield an inaccurate representation of the water retention capacity of the soils as compared to field conditions, particularly for fine textured soils (i.e., soils composed mainly of clay and silt; Bittelli and Flury, 2009; Solone et al., 2012). This issue results from a low porous material and soil sample conductance, a lack of hydrostatic equilibrium, and a lack of soil-plate contact (Bittelli and Flury, 2009; Solone et al., 2012; van Lier et al., 2019). The magnitude of the discrepancy, however, depends on the specific properties of the soils. For instance, the magnitude tends to be small in the absence of soil micro- and macrostructure (e.g., sandy soils), whereas it can be substantial for structured soils. Notwithstanding the variety of laboratory methods used to determine the Andosols' WRCs (Figure 2.1c-e), knowledge about whether these methods reflect correctly the hydraulic behavior of these soils under field conditions, as well as the magnitude of the potential discrepancy, is limited.

An important element in the accurateness of the determination of the hydraulic properties of soils using standard laboratory methods, including the WRCs, is the representativeness of the used soil sample volume. What is the smallest representative elementary volume (REV) of the soil to ensure that laboratory measurements give a correct representation of the properties in the field (Bear, 1972; Kutilek and Nielsen, 1994)? The determination of the REV for a given soil depends largely on how well the sample volume captures the soil micro- and macrostructure that controls the water movement in the porous soil material. Based on measurements of bulk density and water content in Japanese volcanic ash soils, Sato and Tokunaga (1976) reported that the REV of Andosols is 100 cm³. That is, a cylindrical sample with a cross-sectional area of 20 cm² (Ø=5 cm, h=5.1 cm). On the basis of saturated hydraulic conductivity measurements using different laboratory methods, Buytaert *et al.* (2005)



confirmed that the REV to determine the hydraulic properties of Andosols is 100 cm³. Regarding the water retention capacity of these soils, the majority of laboratory analyses have been conducted using soil samples with a volume ≤100 cm³ (63%; **Figure 2.1f**), with only 6% of the studies using volume samples>300 cm³. Despite the general application of standard laboratory methods using small sample volumes to determine the WRC of Andosols, only a few studies compared laboratory results with field measurements.

Fontes et al. (2004) compared WRCs measured in the laboratory and in the field for allophanic Andosols of the Island of Terceira (Azores) under grazed pasture. In the laboratory, they used the sand/kaolin box method (Stakman et al., 1969) to measure the water content of 100 cm³ undisturbed soil samples for potentials below field capacity. For potentials above field capacity, they used the pressure membrane apparatus and determined the water content of disturbed soil samples with a volume of 25 cm³. In parallel, they used neutron probes and mercury tensiometers to measure soil moisture and matric potential in large soil monoliths (2.5 m x 1.5 m x 1.20 m) to determine the WRC under field conditions. These authors reported that the laboratory measurements accurately described the field soil water retention for potentials lower than field capacity, but overestimated significantly the soil moisture content for potentials above field capacity. Eguchi and Hasegawa (2008) also compared the WRCs obtained via laboratory analyses and field measurements for Hydric Hapludand Andosols in a cropping field in Ibaraki, Japan. They applied the suction plate method to 314 cm³ soil samples and used time domain reflectometers and ceramic porous cups in the field to measure the WRC of the soils for matric potentials below field capacity. These authors found no difference between both methods. Despite these findings, it is yet unknown if these differences/similarities are due to local land use and/or management (i.e., both sites were impacted by different land use), the laboratory method used, the volume of the soil sample used; and/or more importantly, if they are valid for all Andosols or only for some specific subclasses/subgroups. Considering the variety of purposes for which laboratory obtained WRCs of Andosols have been and are used (Figure 2.1a), the contrasting findings reported in past investigations demand a thorough analysis of whether standard laboratory analyses using small soil samples reflect field conditions correctly.

To gain insights into this issue, I compiled and analyzed a dataset of WRCs of Andosols determined in the laboratory and in the field at experimental sites in the Ecuadorian Andes. In parallel, I searched the existing literature on this topic, and compared the results with WRC data presented in the published literature to address the overarching question of whether the



determination of the WRCs of volcanic ash soils via standard laboratory methods reflects field conditions. Addressing this question can help setup efficient monitoring strategies of soil water relations in regions where Andosols are found. This information is essential for the assessment of how changes in climate and land use will affect the water storage and flow regulation, as well as the eco-physiological functioning of vegetation in environments dominated by Andosols.

2.2 Materials and methods

2.2.1 Description of the experimental sites

Soil samples were collected at two experimental sites in the tropical alpine (Páramo) ecosystem in south Ecuador. The first site was the Zhurucay Ecohydrological Observatory located on the west slope of the western Andean mountain range (3°04′S, 79°14′W). This site covers an area of 7.53 km² and is situated between 3,400 to 3,900 m a.s.l. The second site is an experimental hillslope (3,900-4,000 m a.s.l.) located at the Quinuas Ecohydrological Observatory on the east slope of the western Andean Cordillera (2°47′S, 79°13′W), approximately 35 km north of Zhurucay. The landscape in the region is of glacial origin, resulting in the formation of a U-shaped geomorphology. Both study areas are dominated by non-allophanic Andosols (Buytaert et al., 2006b), found typically on the Páramo hillslopes, covering nearly 75 to 80% of the extent of both observatories (Mosquera et al., 2015; Pesántez et al., 2018). The Andosols at both sites are mainly covered by tussock grass, commonly the genera *Calamagrostis* and *Festuca* (Mosquera et al., 2016a). The anthropogenic disturbance in the Zhurucay Observatory is limited to light cattle grazing; whereas there is no disturbance at the Quinuas experimental hillslope as it is located in a protected national park. Detailed descriptions of the Zhurucay and Quinuas observatories are available in Mosquera *et al.* (2015) and Pesántez *et al.* (2018).



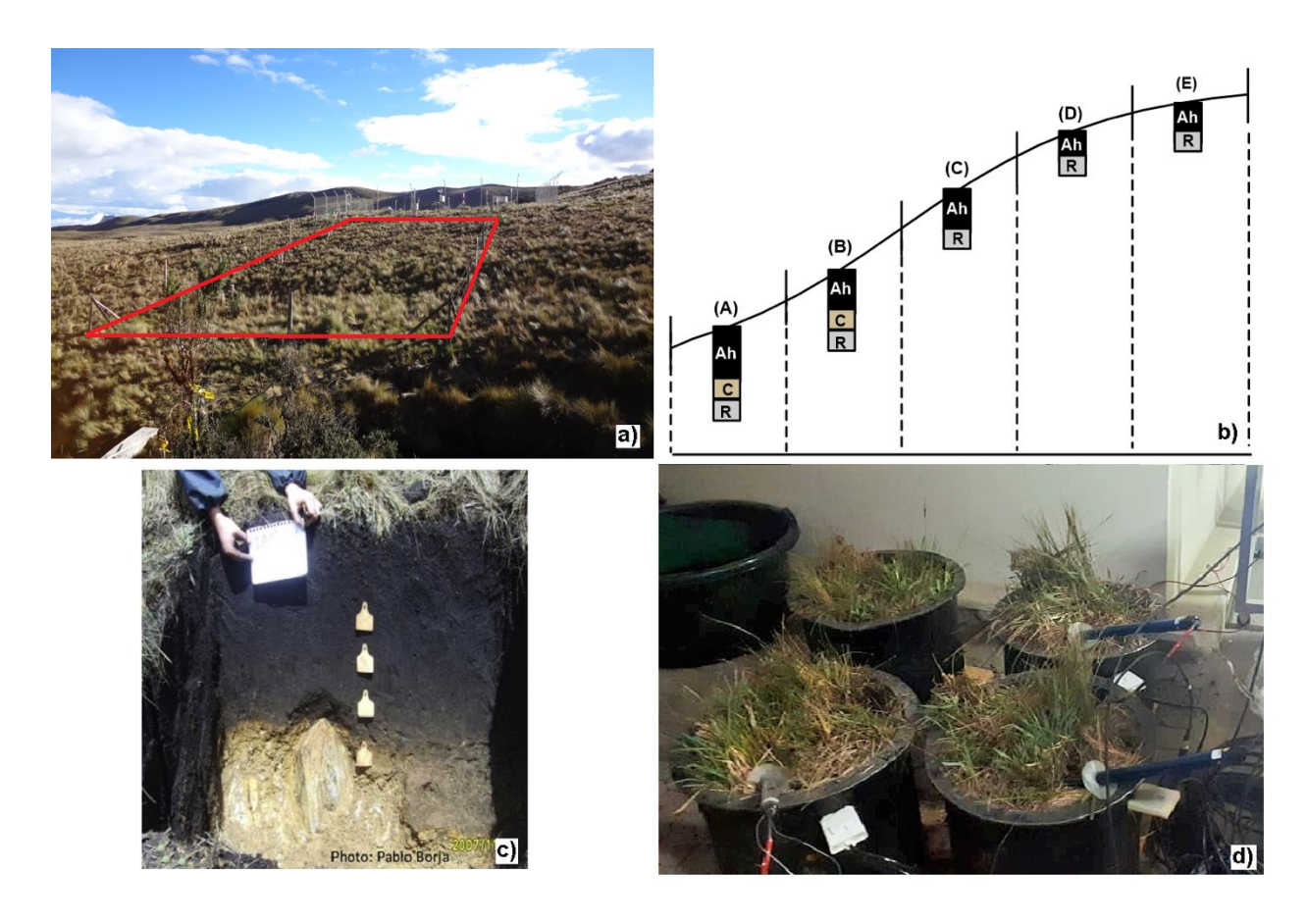


Figure 2.2. Study site and monitoring setup for determining the water retention curves of Andosols. a) View of the experimental plot (marked in red) located in the Zhurucay Ecohydrological Observatory in south Ecuador; b) conceptual diagram of the spatial distribution of Andosols in the Zhurucay Observatory hillslopes (Ah=andic horizon, C=mineral horizon, R=bedrock); c) profile of an Andosol in the observatory; and d) experimental setup for monitoring the soil water content and matric potential in the Ah horizon of undisturbed Andosol soil cores (Ø=40 cm, h=32 cm) covered by tussock grass. Positions along the hillslope in subplot b) correspond to: (A)=Toe slope, (B)=Lower slope, (C)=Middle slope, (D)=Upper slope, and (E)=Hilltop. (Photo credits: a) Galo Carrillo, c) Pablo Borja, and d) Giovanny M. Mosquera).

2.2.2 WRC determination from in-situ (field) measurements

An experimental plot (17 m x 23 m) was constructed at the upper, conserved part (3,770 m a.s.l.) of the Zhurucay Observatory to monitor the subsurface flow dynamics (Montenegro-Díaz et al., 2019). This plot was selected because the Andosol soil was covered by tussock grass and unaffected by cattle grazing (**Figure 2.2a**). To further ensure the latter, the plot was surrounded by a barbed wire fence during the monitoring period. The slope of the plot, 20% on average, was similar to the average gradient of the observatory. The plot was instrumented with water content reflectometers (WCR) (Campbell Scientific CS616, accuracy $\pm 2.5\%$, measurement range 0 to 100% moisture content) and tensiometers (UMS T8, accuracy ± 0.5



kPa, measurement range ~-85 to 0 kPa; or pF 0 to pF ~2.9). The WCR probes were calibrated to the local soil conditions to obtain an improved accuracy of the soil moisture measurements (Ochoa-Sánchez et al., 2018). The temporal variation of soil moisture and matric potential was monitored at the middle of the slope (position C in Figure 2.2b). Two sets of WCR probes and tensiometers, separated horizontally 12.8 m from each other, were installed in the organic (andic) horizon of the Andosols (the Ah horizon in Figure 2.2b, the black soil layer in Figure **2.2c**). The probes were placed below the root zone at a depth corresponding to half the thickness of this soil horizon. The WCR probes were placed horizontally and the tensiometer probes were installed vertically from the top. The soil moisture content and matric potential data were recorded continuously at 5-min intervals during the period January 2011-June 2018. The average soil moisture and matric potential values of the two sets of measurements were used to construct the in-situ WRC of the Andosols, considered in this study as the correct representation of the water retention capacity of the soils under field conditions (hereafter referred to as the field WRC). Precipitation was also recorded every 5-min during the same period using a tipping-bucket rain gauge (Texas TE525MM; resolution 0.1 mm) located approximately 10 m away from the experimental plot at 3,780 m a.s.l.

2.2.3 Collection of soil samples

Although field measurements were only conducted in the Zhurucay Observatory, soil samples to determine the WRC of the Andosols experimentally and in the laboratory were also collected at the experimental hillslope of the Quinuas Observatory.

In the Zhurucay Observatory, three large undisturbed soil cores (Ø=40 cm, h=32 cm; **Figure 2.2d**) were collected at the middle position of the slope (C in **Figure 2.2b**) for the determination of the WRC during a desiccation experiment. For direct comparison with the field WRC, the large-size cores were randomly collected from a 5 m x 5 m area centered around the site were the field measurements were conducted within the plot shown in **Figure 2.2a**. The vegetation in the cores was conserved to mimic field conditions during the desiccation of the samples. Samples from the andic horizon of the Andosols were also collected across the Zhurucay Observatory. Small, undisturbed soil samples with a volume of 100 cm³ were collected using standard steel rings (Ø=5 cm, h=5.1 cm; the REV for Andosols) and approximately 500 gr of disturbed soil for measuring the WRCs in the laboratory. Samples were collected at 14 sampling locations roughly separated 150 m from each other along three transects across the Zhurucay Observatory (41 sampling locations in total). The sampling strategy was designed such that the soil samples were collected at different positions along the hillslopes (Lazo et al.,



2019). Samples were collected accordingly at the toe, the lower, the middle, and the upper sections of the hillslopes, as well as at the hilltops (i.e., the positions A-E in Figure 2.2b). The physiographic characteristics and the properties of the soils collected at each sampling position are described in Table 2.1. The samples collected at the middle slope position (C in Figure 2.2b) were used for direct comparison with the field and experimental WRCs of the Andosols in the Zhurucay Observatory. Given that we also conducted a comparison of the WRCs of the Andosols obtained via laboratory analysis with available data from the published literature (section 2.2.6), the samples collected at different physiographic positions were used to account for the potential variability in specific terrain conditions (e.g., physiographic position and/or gradient) found in the compiled literature dataset. Undisturbed and disturbed soil samples were collected in triplicate at a depth corresponding to half the thickness of the Ah horizon at each sampling site (i.e. below the root zone at depths comparable to which the field and experimental measurements in the large soil cores were made). Considering that at a total of 123 samples were analyzed in the laboratory, it was assumed that the number of collected samples was sufficient to characterize the spatial variability of the soil properties across the observatory.

A similar soil sampling strategy was carried out in the experimental hillslope of the Quinuas Observatory. In the experimental hillslope, however, the large soil cores and small, undisturbed and disturbed soil samples were only collected at the middle slope position.

2.2.4 WRC determination on large soil cores via a desiccation experiment

The large undisturbed soil cores were wetted by capillary rise from their bottom for two months to secure saturation before the start of the desiccation cycle. Subsequently, a WCR probe (Campbell Scientific CS616) and a tensiometer (UMS T8) were placed in each soil core at half the depth of the cores (i.e., the same depth were the field measurements were conducted and the small soil samples were collected; **Figure 2.2d**). The WCR probes were placed horizontally through holes on the sides of the cores and the tensiometer probes were installed from the top at an angle of 35° from the vertical line. A correction for the inclination angle was applied according to the manufacturer's recommendations (UMS, 2011). Positive matric potential measurements from the tensiometers in each of the samples indicated saturation. After this check, I let the samples drain freely by gravity and recorded the soil moisture content and matric potential at 5-min intervals throughout the entire desiccation process. During this process, duplicate small soil samples (Ø=2.5, cm h=5 cm) were collected from each soil core to determine the "real" moisture content of the soil in the laboratory. The small samples were collected every 1 to 4 days during the first 3 weeks of the experiment, and subsequently every



10 to 15 days. These data were used to construct the calibration curve for each of the WCR probes used in the experiment to secure the accuracy of the monitored soil WRC. The experiment was carried out until the tensiometers' measurement range was reached about 50 days after its beginning. Thus, the soil water content and matric potential values recorded during the desiccation process represent the WRC of the Andosols (hereafter referred to as the experimental WRC) from saturation to pF 2.9 (-85 kPa).

2.2.5 WRC determination on small soil cores using standard laboratory methods

The 100 cm³ undisturbed samples were used to determine the soils' bulk density and soil water retention at matric potentials (or pF, defined as logarithms of the matric potentials in cm water column) below field capacity. The moisture contents were measured at pF 0 (saturation, -1 cm H_2O or -0.1 kPa), pF 0.5 (-3.2 cm H_2O or -0.31 kPa), pF 1.5 (-32 cm H_2O or -3.1 kPa), and pF 2.52 (field capacity, -330 cm H₂O or -33 kPa). Sieved, disturbed soil samples (Ø=4 cm, h=1 cm) were used to determine the water retention capacity at pF 3.4 (-2,500 cm H₂O or -245 kPa) and pF 4.2 (permanent wilting point, -15,500 cm H₂O or -1,550 kPa). The WRCs were determined using the sandbox apparatus (for pF-values 0.5-1.5) and the low (pF 2.52) and high (pF 3.4 and 4.2) pressure plate extractors (FAO, 2002) (Soil Moisture Equipment Corp., Goleta, CA, USA). I selected these methods to determine the WRC of the Andosols (hereafter referred to as the laboratory WRC) because they are the most frequently used in the compiled literature (Figure 2.1c-e). Although a direct comparison between the laboratory WRC using the REV of the Andosols (undisturbed soil samples of 100 cm³) and the field and experimental WRCs is possible until pF ~2.9 due to the measurement range of the tensiometer probes, we also present the results of the laboratory WRC for higher matric potentials (applying the standard laboratory method to the disturbed soil samples) for reference.

2.2.6 Compilation of WRC data from the published literature

I identified 81 studies that reported quantitative information (in figures or tables) about WRCs of Andosols or volcanic ash soils with andic properties (i.e., pumice soils were excluded; see Appendix A for a detailed description of the applied literature search procedure, and the list of selected documents in Appendix B). From this database, I selected the papers reporting the WRC for: (i) the organic (andic) horizon of Andosols (up to a depth of 50 cm), (ii) Andosols covered by grassland vegetation, and (iii) Andosols situated in conserved areas unaffected by changes in land use and cover. That is, for conditions comparable to the Zhurucay Observatory.



Sixteen papers that fulfilled these criteria were selected for further analysis. Information from these publications provided the data from which I reconstructed 71 WRCs. The main details about the locations, features, the physical, chemical, and mineralogical soil characteristics, and the methods and soil sample volumes used to determine these WRCs are summarized in **Table 2.2**. Information on the specific terrain conditions (e.g., physiographic position and/or gradient) are not included in the table since the majority of studies did not provide this information. However, the dataset most likely covers a wide range of terrain conditions. I will further refer to these data as the "literature compiled WRC dataset".



Table 2.1 Hydraulic properties of the Ah (andic) horizon of the Andosols monitored at different positions along the hillslopes (as shown in Figure 2.2b) in the Zhurucay Ecohydrological Observatory. The values presented in the table are the average and the standard deviation (in parenthesis) of the properties measured in the laboratory.

Position code ^a	n ^b	Slope (%)	Horizon type	Horizon depth (cm)	BD ^c (g cm ⁻³)	pF ^c 0 (cm ³ cm ⁻³)	pF ^c 0.5 (cm ³ cm ⁻³)	pF ^c 1.5 (cm ³ cm ⁻³)	pF ^c 2.52 (cm ³ cm ⁻³)	pF ^c 3.4 (cm ³ cm ⁻³)	pF ^c 4.2 (cm ³ cm ⁻³)
A	10	7 (5)	Ah	41 (2)	0.38 (0.25)	0.80 (0.10)	0.78 (0.09)	0.71 (0.06)	0.63 (0.04)	0.41 (0.14)	0.31 (0.03)
В	5	17 (14)	Ah	33 (6)	0.36 (0.10)	0.81 (0.04)	0.81 (0.04)	0.80 (0.04)	0.67 (0.00)	0.51 (0.10)	0.49 (0.10)
C	10	21 (16)	Ah	34 (7)	0.40 (0.04)	0.77 (0.03)	0.76 (0.03)	0.75 (0.04)	0.70 (0.02)	0.60 (0.08)	0.53 (0.07)
D	9	11 (9)	Ah	38 (3)	0.47 (0.16)	0.72 (0.08)	0.72 (0.08)	0.71 (0.08)	0.63 (0.05)	0.52 (0.11)	0.54 (0.06)
E	7	4 (3)	Ah	35 (11)	0.49 (0.14)	0.73 (0.06)	0.73 (0.06)	0.72 (0.06)	0.65 (0.04)	0.58 (0.06)	0.51 (0.04)

^a A=Toe slope; B=Lower slope; C=Middle slope; D=Upper slope; E=Summit.

^b n=number of locations where triplicate samples were collected and analyzed at each of the hillslope positions across the Zhurucay Ecohydrological Observatory.

^c BD=Bulk density; pF=log₁₀ matric potential in cm H₂O.



Table 2.2 Summary of the published literature presenting soil moisture content versus matric potential data^a used for the construction of the water retention curves (moisture release curves, moisture characteristic curves, or pF curves) of volcanic ash soils with andic properties (Andosols/Andisols) using standard laboratory methods.

Ref.a	Country ^b	RQc	Elevation	Slope	R	N	Soil subclass	Depth	BD	φ	pН	ОМ	Sand	Silt	Clay	Al _p /Al _o	Fe_o	\mathbf{Si}_{0}	Allophane	Lab. method ^d	Sample volume
			(m a.s.l)	(%)				(cm)	(gr cm ⁻³)	(%)		(%)	(%)	(%)	(%)	(%)	(g kg ⁻¹)	(g kg ⁻¹)	(%)		(cm ³)
[1]	ECU	LUC	3,450	-	12	-	Histic	15	0.3	-	-	33	-	-	-	-	-	-	-	MS + PPE	100
			3,970	-			0-24 24-56	0.26	83	4.8	62	29	41	31	0.92	-	-	-			
			3,850	-			0-12 12-44	0.48	73	4.6	46	32	36	32	0.82	-	-	-			
[2]	ECU	SG	3,830	-	_	8	_	0-15 15-41	0.17	82	5.3	62	40	32	29	1.08	-	-	-	PMA	100
			3,550	-				0-17 17-60	0.57	71	4.6	26	19	27	55	0.47	-	-	-		
			3,425	-				0-16 16-62		82		50	26	32	42	0.46			-		
			3,300	-				0-30	0.33	84	5.3	34	24	31	45	0.48	-	-	-		
			3,400	30	6	-	-	0-10 10-25	0.54	-	6	20	-	-	-	-	-	-	-		
[3]	ECU	LUC	3,650	22	6	-	-	0-10 10-25	0.38	-	5.2	39	-	-	-	-	-	-	-	SB + PPE	100
			>3,650	20	6	-	<u>-</u>	0-10 10-25	0.74	-	5.5	5.5 12	-	-	-	-	-	-	-		
[4]	ECU	LUC	3,650	23	-	36	-	0-50	0.64	-	4.9	29	- -	-		-	-	-	-	MS + PPE.	100
[5]	ECU	HM	3,735		 -		-	30							 -				-	MS + PPE	



Table 2.2. Cont.

Ref.a	Country ^b	RQc	Elevation	Slope	R	N	Soil subclass	Depth	BD	φ	pН	ОМ	Sand	Silt	Clay	Al _p /Al _o	$\mathbf{Fe_o}$	Si_o	Allophane	Lab. method ^d	Sample volume
			(m a.s.l)	(%)				(cm)	(gr cm ⁻³)	(%)		(%)	(%)	(%)	(%)	(%)	(g kg ⁻¹)	(g kg ⁻¹)	(%)		(cm ³)
[6]	JAP	SP	-	-	18	6	-	3-8 4-9 17-22 25-30	-	73	-	-	-	-	-	-	-	-	-	SB + PPE	100
[7]	ECU	LUC	4,000	-	4	-	-	0-20 20-40 0-30	0.85	65 80	- - -	11 28	58 9	36 65	7 26	0.72 0.96	- - -	- - -	-	PPE	-
			4,200	0- >60				0-15 15-30	0.68		4.8	11	32	54	9	0.66	0.62	1.71	-		-
[8]	ECU	LUC	4,000	0- >60	5	-	-	0-15 15-30	0.84	-	5.2	8	32	45	16	0.58	0.38	0.96	-	PPE	-
			3,700	0-40				0-15 15-30	0.78	-	5.4	12	30	54	12	0.72	0.43	0.89	-		-
[9]	СНІ	LUC	73	1	7	-	Histi-Silandic	5 15 30	0.5	-	5	31	-	-	-	-	-	-	-	SB + PPE	230
			3,500	-			Melani-Vitric (Pachic)	0-30	0.58	80	-	37	-	-	26	0.97	0.64	0.4	2		
[10]	ECU	SD	3,700	-	-	3	Melani-Vitric (Hydric)	0-30 30-45	0.38	81	-	37	-	-	35	0.99	1.23	2.4	2	PPE + PMA	100
			3,250	-			Melani-Vitric (Hydric)	0-7.5 15-50	0.33	83	-	29	-	-	51	0.96	2.07	0.45	2		



Table 2.2 Cont.

Ref. ^a	Countryb	RQc	Elevation	Slope	R	N	Soil subclass	Depth	BD	φ	pН	ОМ	Sand	Silt	Clay	Al _p /Al _o	Feo	Si_0	Allophane	Lab. method ^d	Sample volume
			(m a.s.l)	(%)				(cm)	(gr cm ⁻³)	(%)		(%)	(%)	(%)	(%)	(%)	(g kg ⁻¹)	(g kg ⁻¹)	(%)		(cm ³)
[11]	ECU	CS	3,860	14	1	-	-	0-10 10-30	0.4	-	4.5	31	-	-	12	0.93	0.85	0.14	0.9	SB + PPE	200
[12]	ECU	LUC	3,450	-			Histic	15	-	-	-									MS + PPE	100
[13]	JAP	SSF	-	6	5	-	-	7.5 15 30	0.75	-	-	-	-	-	-	-	-	-	-	SB + CT	-
[14]	TAI	SG	970 890	30 30	-	3	-	0-27 0-20	0.51 0.55	81 79	4.1 4.5	11 9	16 39	61 48	23 15	0.84 0.88	2.12 1.9	0.31 0.21	-	РМА	-
[15]	COG	SD	2,290	34		9	-	10-50	-	-	-		-	-	-	-	-		-	SB + PPE	100
[16]	NZL	SG	1,000 70	-	-	5	-	1-10 10-28 33-40 0-23	0.9 0.69	-	5.5 5.5	4	71 55	22	7 15	0.17	- - -	0.43	3.7 5	PPE	-

Abbreviations: number of replicates (R); total number of soil profiles (N); research question (RQ); porosity (ϕ); bulk density (BD); organic matter (OM); soil moisture content (θ) at pF 0 (saturation), pF 2.52 (field capacity), and pF 4.2 (permanent wilting point); not reported (-).

^a Reference: [1] (Buytaert et al., 2005b), [2] (Poulenard et al., 2003), [3] (Tonneijck et al., 2010); [4] (Podwojewski et al., 2006), [5] (Buytaert et al., 2006b), [6] (Quichimbo et al., 2012), [7] (Marín et al., 2018), [8] (Buytaert et al., 2004), [9] (Moldrup et al., 2003), [10] (Iñiguez et al., 2016), [11] (Poulenard et al., 2001), [12] (Tokumoto et al., 2010), [13] (Dörner et al., 2016), [14] (Chen et al., 1999), [15] (Dondeyne et al., 1993), [16] (Tjahyandari, 1998).

^b Country: ECU=Ecuador; JAP=Japan; CHI=Chile; COD=Democratic Republic of the Congo; NZL=New Zealand.

^c Research question: LUC=land use/cover change; SD=soil description; SG=soil genesis; SP=soil properties; SSF=subsurface flow; HM=hydrological modelling CS=carbon stocks.

^d Laboratory method: SB=sandbox, PPE=pressure plate extractors, MS=multistep, PMA=pressure membrane apparatus, CT=centrifuge.



2.3 Results and discussion

2.3.1 Comparison of laboratory determined WRCs

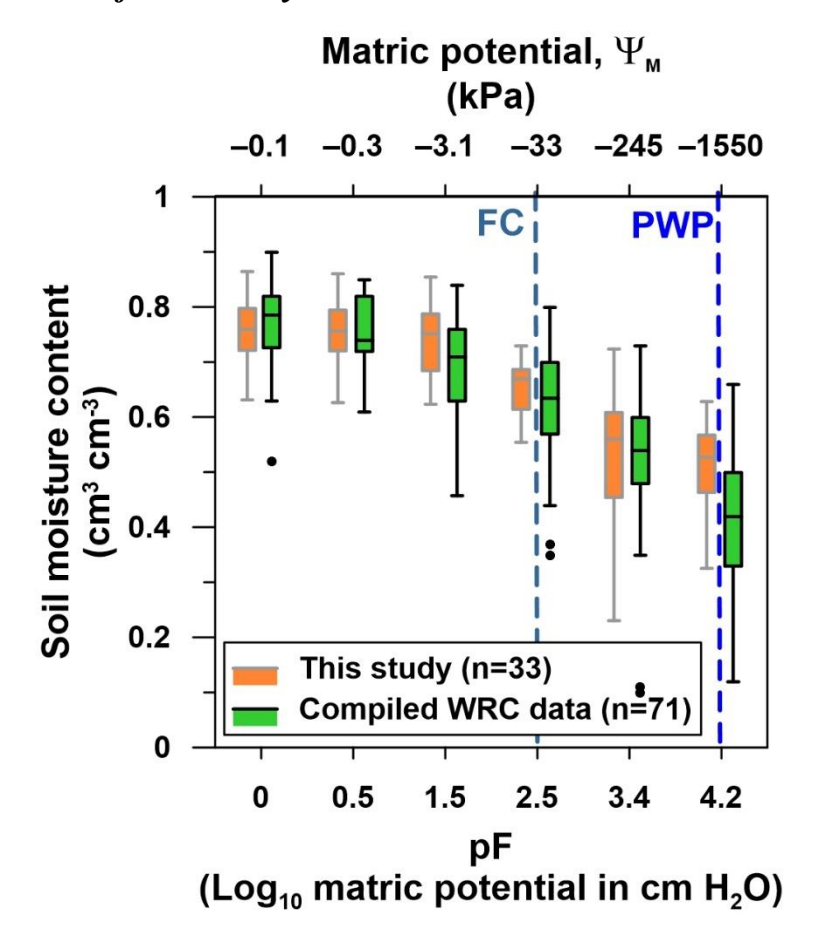


Figure 2.3. Comparison of the water retention curves (WRCs) of Andosols obtained using standard laboratory methods. Soil moisture content versus matric potential relation (i.e., soil WRC, moisture release curve, or pF curve) of the Ah horizon of Andosols at different locations across the Zhurucay Ecohydrological Observatory (**Figure 2.2**; this study) and the WRCs of 16 published studies summarized in **Table 2.2** (compiled WRC data). All data correspond to the upper horizon (depth<50 cm) of the Andosol, all covered by pristine grassland (i.e., forest cover and disturbed land use were excluded from the compiled WRC dataset). Data were generated via laboratory analysis using (i) steel rings (100 cm³ volume) in Zhurucay, and (ii) steel rings of different volume (100-230 cm³ volume) in the literature compiled WRC dataset (see **Table 2.2** for details). The box plots correspond to the median and the 25 and 75 percentiles, and the whiskers to the maximum and minimum soil moisture values. The dashed vertical lines represent field capacity (FC; pF 2.52, −330 cm H₂O, or −33 kPa) and permanent wilting point (PWP; pF 4.2, −15,500 cm H₂O, or −1,550 kPa). n indicates the number of moisture release curves used to construct the boxplots.

Figure 2.3 summarizes the laboratory results of the WRCs determined on the 100 cm³ undisturbed core samples collected across the hillslopes of the Zhurucay Observatory (**Table 2.1**). The small spatial variability of the Andosols' properties across the observatory indicates a low heterogeneity in their physical and hydraulic characteristics regardless of the hillslope



sampling position (Buytaert et al., 2006a). The figure also shows the 71 reconstructed WRCs from the 16 selected studies summarized in **Table 2.2**. The WRCs of the Andosols in Zhurucay depicted that the soil moisture content remained near saturation (0.77±0.04 cm³ cm⁻³) up to pF 1.5. A small decrease in soil moisture content was observed at pF 2.52 (0.66±0.03 cm³ cm⁻³), indicating that the soils at field capacity lost only 14% of their water content. A continuous reduction of the soils' water content was observed until pF 4.2 (permanent wilting point). At this matric potential, the moisture content of the soils was about 38% lower than at saturation (0.48±0.09 cm³ cm⁻³). These findings are in line with those reported for Andosols at nearby sites in the south Ecuadorian Andes when the WRCs were determined in the laboratory using 100 cm³ soil samples (Buytaert et al., 2005b; Iñiguez et al., 2016; Marín et al., 2018; Quichimbo et al., 2012).

Although the literature compiled WRC data were not in all cases obtained using the same laboratory methods applied in this study, they produced a similar WRC shape in comparison to the WRCs of the Andosols in the Zhurucay Observatory (**Figure 2.3**). Only a larger variability in moisture content at different matric potentials was observed in the literature compiled WRC dataset. This variability most likely reflects the differences in the site-specific conditions in this dataset (e.g., geographical location; elevation and topographic position; physical, chemical, and mineralogical properties of the Andosols; **Table 2.2**).

The remarkable similarity between both datasets suggests that different laboratory methods produce similar shapes of the Andosols' WRCs irrespective of the specific method applied. This observation is in line with the findings of Buytaert *et al.* (2005), who reported that different laboratory methods for the determination of the saturated hydraulic conductivity of non-allophanic Andosols also produced similar results. Furthermore, it is worth noting that although the Andosols in the Zhurucay Observatory are non-allophanic, the literature compiled WRC dataset included both, allophanic and non-allophanic Andosols (**Table 2.2**). This indicates that standard laboratory methods yield similar shapes of the WRCs of Andosols regardless of their specific mineralogical composition. It is also worth highlighting that although the volume of the samples analyzed in the majority of studies was 100 cm³ (**Table 2.2**), I did not find differences in the shapes of the WRCs when larger sample volumes were used (up to 230 cm³). Based on the analysis of the bulk density and water content of the Andosols using soil samples of different volume, Sato and Tokunaga (Sato and Tokunaga, 1976) concluded that the REV of volcanic ash soils with andic properties is 100 cm³. The comparative analysis of the different



standard laboratory methods for determining the WRC of Andosols supports indirectly this conclusion.

2.3.2 Comparison of laboratory, experimental, and field WRCs

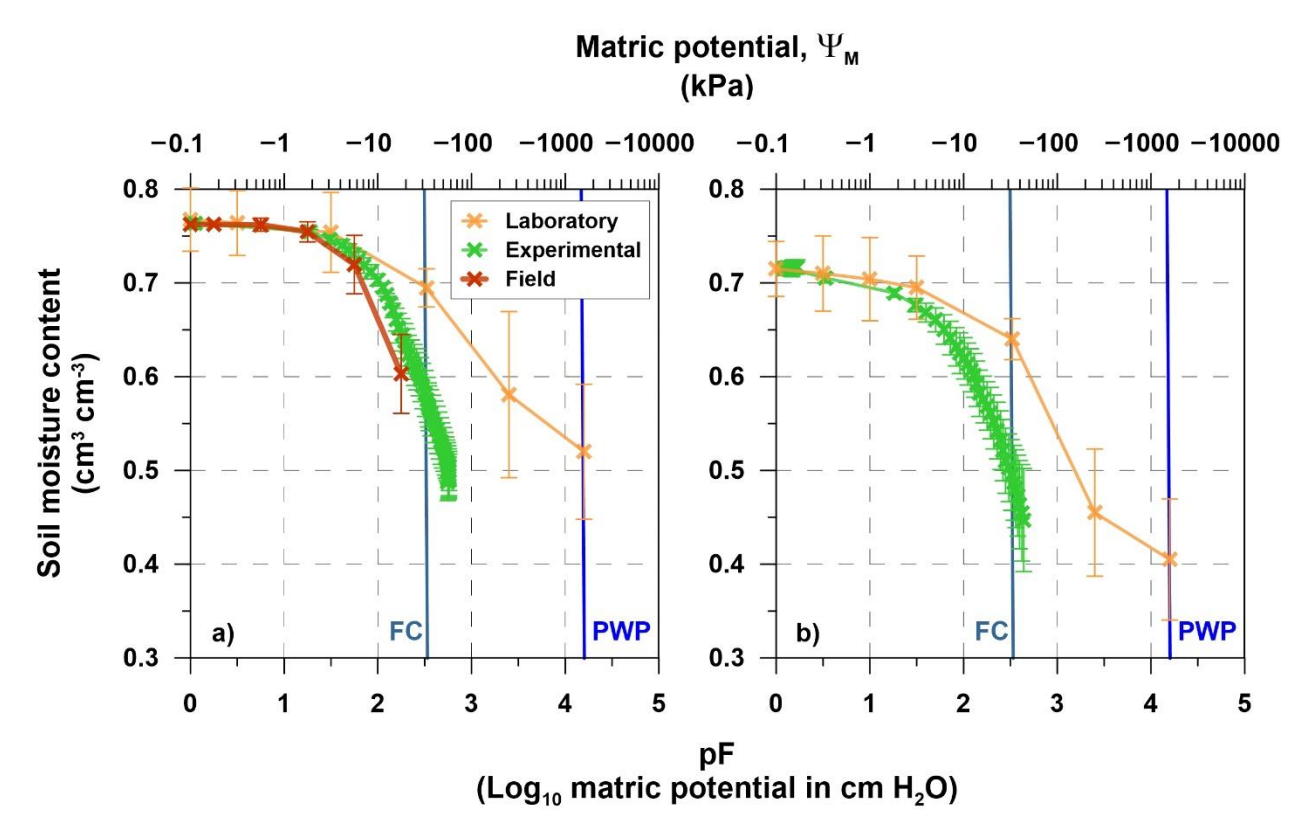


Figure 2.4. Comparison of laboratory, experimental, and *in-situ* measured water retention curves. a) Soil moisture content versus matric potential relation of the Ah horizon in the Andosols located in the middle position of the hillslope (position C in **Figure 2.2a**) obtained via standard laboratory methods using 100 cm³ steel rings (n=10), the experimental measurement of the soil moisture content-water potential relation (daily data shown, n=3) in large undisturbed soil cores (Ø=40 cm, h=32 cm), and field measurements of soil moisture content versus matric potential in the experimental plot of the Zhurucay Ecohydrological Observatory (data shown in **Figure 2.5**, n=2). Subplot b) shows the same results for the Ah horizon of Andosol soils in the Quinuas Ecohydrological Observatory located 35 km north of Zhurucay measured in the laboratory and experimentally on large soil cores. Data shown are the mean (x symbols connected with a thick line) and standard deviations (vertical error bars) of the measured soil moisture contents. Continuous vertical lines represent the matric potential at field capacity (FC; pF 2.52, −330 cm H₂O, or −33 kPa) and permanent wilting point (PWP; pF 4.2, −15,500 cm H₂O, or −1,550 kPa).

This study yielded similar shapes of the field and experimental (large core samples) WRCs for the Andosols in the Zhurucay Observatory (red and green lines in **Figure 2.4a**, respectively). That is, the soil moisture content hardly dropped between saturation (≈ 0.77 cm³ cm⁻³) up to pF 1.5. Beyond this point, both curves showed an abrupt and fast reduction in soil moisture content as the matric potential of the soil increased. Similar observations were reported by Ritter *et al.*



(2004) for volcanic ash soils in Tenerife (Canary Islands, Spain), who determined the WRC using time domain reflectometers and ceramic porous cups to monitor the soil moisture and matric potential directly in large undisturbed soil cores (Ø=45 cm, h=85 cm). The field WRC presented larger error bars than the experimental one (Figure 2.4a). This observation conforms with the hysteretic behavior of the hydraulic properties of the soils when exposed to a succession of wetting and drying cycles under field conditions (Basile et al., 2003); differently from the desiccation experiment in which the soil cores where drained only once. The field WRC did not reach field capacity (Figure 2.4a) as a result of the local environmental conditions. On the one hand, the continuous input of low-intensity precipitation (Padrón et al., 2015) sustains the recharge of soil water (Mosquera et al., 2016b, 2015). On the other hand, the high air humidity and the low temperatures year-round (Córdova et al., 2015) (mean annual relative humidity and temperature are 91% and 6.0°C at 3,780 m a.s.l.) restrict soil moisture loss by evapotranspiration. In contrast, the soil cores were dried to a matric potential beyond field capacity during the desiccation experiment (until pF≈2.9). As the experimental WRC resembled well the field WRC in the Zhurucay Observatory, I will refer to the experimental curve as representative of both conditions in the following.

The laboratory WRC in Zhurucay approximated closely the experimental observations up to pF 1.5 (i.e., soil moisture contents remained near saturation as shown in Figure 2.4a). These observations are similar to those reported by Eguchi and Hasegawa (2008) and Fontes et al. (2004) for Andosols in Japan and the Island of Terceira (Azores), respectively. These authors reported that the shape of WRCs obtained via laboratory analysis and field measurements were similar up to pF 1.7. For pF-values>1.5, the laboratory WRC in Zhurucay overestimated the water content of the Andosols in comparison to the experimental WRC. It is important to notice that the moisture content at field capacity was notoriously different between both curves. That is, the laboratory WRC overestimated the water content (0.69±0.03 cm³ cm⁻³) by 17% in comparison to the experimental curve (0.59±0.01 cm³ cm⁻³). The overestimation for the Andosols in the Quinuas experimental hillslope was even larger than in Zhurucay (33%; Figure **2.4b**). Another significant difference observed for the Andosols at both study sites was that at the soil moisture content in which the laboratory WRCs reached permanent wilting point (0.53±0.10 cm³ cm⁻³ in Zhurucay and 0.41±0.07 cm³ cm⁻³ in Quinuas), the experimental WRCs only exceeded slightly field capacity (Figure 2.4a,b). Similar discrepancies between laboratory and experimental/field derived WRCs have been reported for allophanic Andosols under disturbed land use conditions by Fontes et al. (2004). These authors reported that



laboratory methods failed to mimic field conditions for pF-values>1.7; and attributed the discrepancy to the presence of allophane in the soil. The findings for non-allophanic Andosols, however, suggest that the differences in water retention characteristics cannot be attributed solely to the allophane content of the soils. Moreover, the findings of Fontes *et al.* (2004) at disturbed sites and of this study at pristine sites also suggest that the misrepresentation of the laboratory WRCs occurs independently from the land use and/or management of the soils.

On the basis of this extensive comparative analysis I conclude that standard laboratory methods (listed in **Figure 2.1c-e**) using soil sample volumes ≤300 cm³ (corresponding to 94% of the sample volumes used for determining the WRCs of Andosols; Figure 2.1f) do not mimic accurately the water retention of Andosols under field conditions. This evaluation suggests that the observed differences occur irrespective of site-specific land use and soil properties (e.g., clay mineralogy, organic matter content, texture; Table 2.2). The observed discrepancies could partially result because small-volume soil samples do not represent correctly the soil microand macrostructure that controls the water movement of the Andosols (Guzman et al., 2019). Errors identified when applying the pressure plate laboratory method for determining the WRC of fine textured soils (for pFs>2) could also contribute to the discrepancy (e.g., Bittelli and Flury, 2009; Solone et al., 2012). These issues, which include an inadequate soil-plate hydraulic conductance, a lack of hydrostatic equilibrium, a lack of soil-plate contact, and/or soil dispersion, can cause that water does not drain properly from the soil under the applied suction and/or that hydrostatic equilibrium is not reached (Bittelli and Flury, 2009; Solone et al., 2012; van Lier et al., 2019). These methodological limitations in turn cause that the measured soil moisture content is overestimated. Taking into account that the Andosols present a moderately fine to fine texture due to their high content of small size particles (clay, silt, and organic matter) and the strong shrinkage they undergo during drying cycles (Bartoli et al., 2007; Dörner et al., 2009a), the use of standards methods could also contribute to the found laboratory misrepresentation. It is also worth noting that although the use of undisturbed versus disturbed, sieved samples for the laboratory analysis has a negative effect in the determination of the WRC of the Andosols (Kassaye et al., 2019), this factor did not have an influence in the presented results as the comparison was done in the suction range until undisturbed soil samples were used for the laboratory analysis (from saturation to pF~2.9). Furthermore, the similarities between the laboratory curves in Zhurucay and the literature compiled WRC dataset (Figure 2.3) suggest that comparing only different standard laboratory methods is



insufficient to determine the cause of the misrepresentation of the WRC of volcanic ash soils with andic properties.

2.4 Broader implications

These findings have important implications in soil hydrological research since the WRCs of Andosols obtained via standard laboratory methods are commonly used to investigate water transport and mixing in the subsurface (e.g., Blume et al., 2009; Dörner et al., 2015). The data collected in the experimental hillslope of the Zhurucay Observatory illustrates this issue when analyzing and interpreting the dynamics of soil moisture (Figure 2.5b). The WRC obtained in the laboratory (yellow line in Figure 2.4a) indicates that soil moisture at the experimental hillslope decreases rapidly from levels above field capacity to levels at or near permanent wilting point (blue and purple dashed lines in Figure 2.5b) shortly after the beginning of dry periods. A similar hydrological behavior at the hillslope scale was observed by Dörner et al. (2015) for Andosols in southern Chile. These authors attributed this phenomenon to the high unsaturated hydraulic conductivity of the soil. This explanation suggests that water molecules tightly bound to soil particles with the smallest volumes could be emptied as fast as gravitational water moving readily in the macropores of the Andosols' soil matrix. However, such a behavior cannot be physically justified, particularly for soils rich in clay minerals with high surface areas such as Andosols (Maeda et al., 1977; McDaniel et al., 2012). Our comparative analysis of the Andosols' WRCs provides a more feasible explanation for the observed dynamics. That is, the field capacity of Andosols under field conditions is reached at a much lower water content than that determined through standard laboratory methods (Figure 2.4a). This explanation is further supported by the matric potential observations in our experimental hillslope, which show that field capacity was not reached during the study period (solid orange line in Figure 2.5b). These findings do not only clearly demonstrate the misrepresentation of the WRC of the Andosols using standard laboratory methods, but also the need to determine it accurately for interpreting soil moisture dynamics and inferring subsurface hydrological behavior correctly.

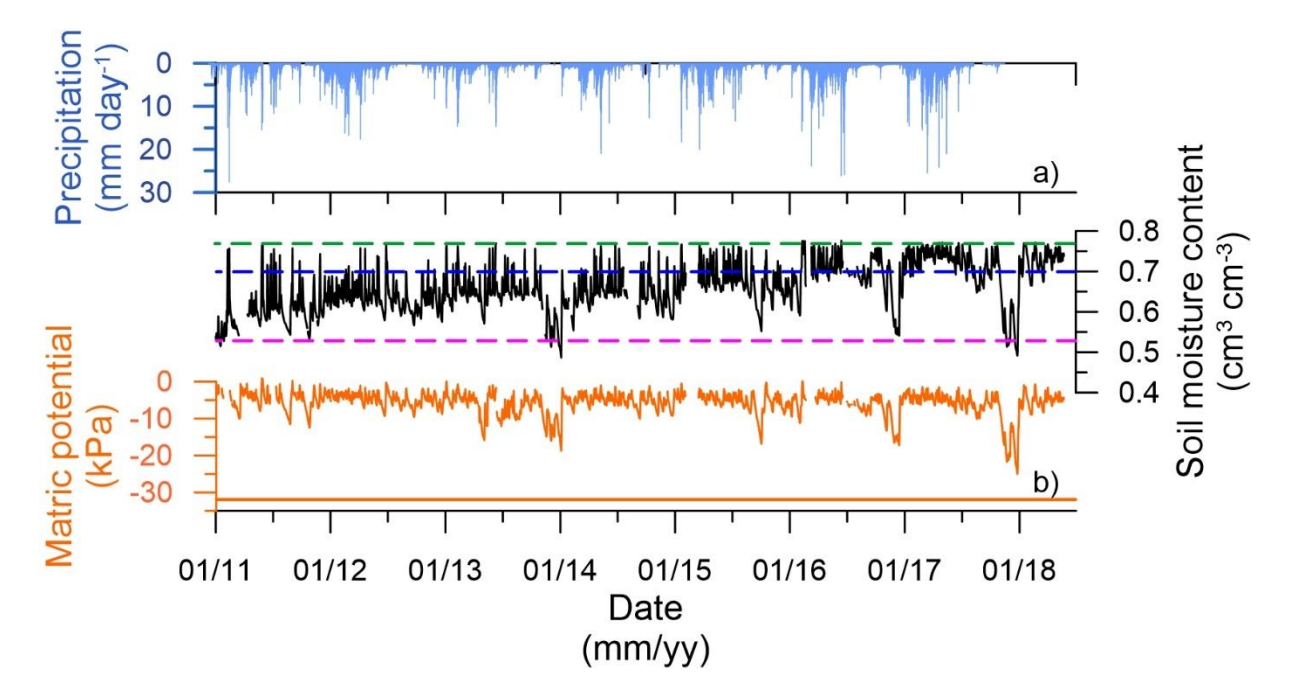


Figure 2.5. *In situ* measurements of daily precipitation (a), and soil moisture and matric potential monitored at half the thickness of the Ah horizon of the Andosols at the middle position (b) of the experimental plot of the Zhurucay Ecohydrological Observatory (position C in Fig. 2b) during the period January 2012–June 2018. The matric potential and soil moisture data correspond to the average of two monitoring stations in the experimental plot and were used to construct the "field" water retention curve (WRC) of the Andosol soil (red line in **Figure 2.4a**). The dashed horizontal lines in b) represent the soil moisture values at saturation (green line), field capacity (blue line), and wilting point (purple line) according to the WRC obtained using standard laboratory methods (yellow line in **Figure 2.4a**). The solid orange horizontal line in b) represents the matric potential at field capacity (-33 kPa, $-330 \text{ cm H}_2\text{O}$, or pF = 2.52), which is not reached during the study period according to the field measurements.

Standard laboratory methods that do not represent fully the field-based WRC of Andosols have also been used to investigate relations between the water retention characteristics of these soils and other soil properties. These properties include the Andosols' clay colloidal composition (Karube and Abe, 1998), gas diffusivity (Moldrup et al., 2003), pore size distribution and hydraulic conductivity (Poulenard et al., 2001), salinity and sodicity (Armas-Espinel et al., 2003), pH and exchangeable Ca (Van Ranst et al., 2002), topsoil structure (Negrón et al., 2019), organic matter (Pochet et al., 2007; Walczak et al., 2002), and shrinkage (Beck-Broichsitter et al., 2016; Dorel et al., 2006). Although these investigations shed light upon the relation between the mineralogical, physical, chemical, and/or biological features of these soils and their water retention capacity, my findings suggest that results from these studies should be re-evaluated to verify their validity and the real strength of the identified relations.



Past research also focused on the investigation of the impacts of land use change/management on the water retention capacity of Andosols. The land use change or management practices included crop and agroforestry (Abera and Wolde-Meskel, 2013), crop rotation (Duwig et al., 2019), overgrazing (Buytaert et al., 2005b; Podwojewski et al., 2006), forest/wetland conversion to grassland (Dec et al., 2017; Dörner et al., 2016; Roa-García et al., 2011), native forest or grassland conversion to pasture, exotic forest, or crops (Daza Torres et al., 2014; Dörner et al., 2010, 2009b; Farley et al., 2004; Marín et al., 2018; Quichimbo et al., 2012), soil compaction due to tractor traffic (Gómez-Rodríguez et al., 2013), and biosolid application (Salazar et al., 2012). Not surprisingly, Marín et al. (2018) reported that part of the aforementioned findings are not generalizable. This lack of generalization could at least be partially related to the misrepresentation of the WRCs obtained via standard laboratory methods using small soil samples (≤300 cm³). Thus, the magnitude and direction of the reported impacts should be re-evaluated using appropriate methods/REVs for characterizing the water retention of these soils, particularly for pF>1.5. Moreover, the laboratory based determination of the WRC using standard methods and soil samples of small volume should be prevented in future studies to avoid obtaining erroneous results.

The WRCs of Andosols obtained via standard laboratory methods have also been utilized as input data to implement physically-based numerical models to simulate water and nutrient fluxes (Alavi and Tomer, 2001; Asada et al., 2018), as well as hydraulic models to design landslide early warning systems (Ferrari et al., 2012; Frattini et al., 2004). Alavi and Tomer (2001) reported that simulations yielded by their hydrological model overestimated soil drainage observations by 35-138% and attributed these large errors to the soil WRCs determined in the laboratory on small volume soil samples (68 cm³). Asada *et al.* (2018) showed that a modified soil water retention function was needed to improve the simulation of nitrogen loss from soils in their biogeochemical model. These findings indicate that a correct determination of the WRCs of Andosols is required to improve the predictive capability of numerical models to simulate hydrological, hydraulic, and biogeochemical response by reducing uncertainty in model outputs (Fatichi et al., 2016; Köhne et al., 2009; Vereecken et al., 2016).

Pedotransfer functions (PTFs, i.e., relations between soil properties with different difficulty in measurement or availability (Pachepsky and van Genuchten, 2011)) and spatial predictions of the water retention characteristics of Andosols have also been developed (Borja, 2006; Guio Blanco et al., 2018; Rustanto et al., 2017; Spilling, 2018; Yáñez et al., 2015) using WRC



information obtained from standard laboratory methods. Since these functions are aimed to serve as input data for the implementation of large scale (regional to global) hydrological, ecological, land surface, and earth system models (Fan et al., 2019; Vereecken et al., 2010), the incorrect determination of the water retention characteristics of soils will increase the uncertainty and diminish the accuracy of the produced simulations (Vereecken et al., 2016). Therefore, a re-evaluation of the PTFs and spatial predictions of the water retention of Andosols is needed to better represent the hydrological and hydraulic behavior of these soils in large-scale models. This issue is of particular importance in regions where data are scarce, such as in the tropics where volcanic ash soils are an important resource (Hodnett and Tomasella, 2002; Minasny and Hartemink, 2011).

Rapid advancements in ecophysiology and ecohydrology for improving our understanding of water-soil-plant relations demand the accurate determination of the water retention characteristics of soils (Brantley et al., 2017; Sprenger et al., 2016). Although the role Andosols play in this context has not yet been investigated, a precise determination of their water retention capacity will be fundamental to fill this knowledge gap, as these soils represent an important ecological resource in mountain regions (Terribile et al., 2018).

2.5 Conclusions

The WRC is an important physical characteristic of a soil that expresses the relation between the water content of the porous medium and the matric potential, a measure of the adhesion of water molecules to the soil matrix. The matric potential defines the tendency of water to move in the subsurface, and consequently the WRC is an essential feature in most hydrological, ecological, physiological, biogeochemical, and hydraulic processes involving directly or indirectly the transport of water molecules in the vadose zone. Traditionally, the soil WRC is determined in the laboratory applying a set of standard laboratory techniques using small undisturbed and disturbed soil samples. For volcanic ash soils with andic properties (Andosols/Andisols), the determination of the WRC in the lower section of the matric potential is carried out generally using undisturbed samples of 100 cm³ (the assumed REV) as to guarantee that the sample is a true representation of the capillary structure of the soil in the field. The comparative analysis among the laboratory, experimental, and *in-situ* (field) based determination of the WRCs of Andosols revealed that standard laboratory methods using 100 cm³ soil samples corresponds well with the experimental curve (WRC measured on large soil cores or directly in the field) in the wet range from saturation to a matric potential of 3-5 kPa



(pF 1.5-1.7). For higher matric potentials, including the field capacity (pF 2.52), the laboratory defined curve overestimates considerably the water content of the soil in comparison to the experimental curve. Moreover, the outstanding similarity between the shape of the laboratory obtained WRCs and the 71 WRCs reconstructed from the data extracted from 16 articles published in high-ranked journals using small soil samples (≤300 cm³) reinforces the suspicion that the standard laboratory methods used to determine the WRC of Andosols using small soil samples are incapable of mimicking field conditions correctly. However, I cannot conclude whether this is due to the applied laboratory methods, the analyzed volume of soil sample, or both. Resolving this issue demands the identification of the factors causing the discrepancy and likely an adjustment of the standard laboratory methods used currently.

The adaptation of the laboratory methods, however, should be such that after modification the methods are not only able to accurately resemble field conditions, but also allow analyzing multiple soil samples simultaneously in relatively short time at acceptable cost. A first step towards addressing this issue will be the determination of the REV of Andosols. Results from a controlled evaporation experiment in combination with matric potential measurements using mini-tensiometers illustrated that an undisturbed core sample of 600 cm³ (Ø=8.5 cm and h=11.0 cm) produced a similar WRC than the field-based measured WRC of volcanic ash soils (Basile et al., 2003). This likely resulted because a larger soil sample is a better replica of the micro- and macrostructure of the soil and/or this alternative method is not subjected to the issues identified for determining the WRC of fine-textured soils (e.g., low plate and soil conductance, a lack of hydrostatic equilibrium, a lack of soil-plate contact, and/or soil dispersion). Although more research is needed to determine the cause behind the identified disagreement, this piece of information is crucial as it can serve as a basis for future investigations. However, this information is also linked to challenges ahead that must be overcome. For instance, if the REV of Andosols would be several times bigger than the one considered until now (100 cm³), investigating whether commonly applied laboratory methods can be accommodated to the analysis of larger soil samples requires future evaluation. Moreover, these results clearly depict that for addressing this issue, the comparison between laboratory methods and experimental measurements in large soil cores or in-situ (field) measurements is needed, as this extensive evaluation shows that the comparison between laboratory methods alone yields equivocal results. Resolving this methodological issues is essential to produce reliable information that can be used to enhance the management and conservation of soil and water resources and to develop adaptation strategies in light of changes



in climate and land use, so that a sustainable provision of ecosystem services in regions where Andosols are found can be maintained.



Chapter 3

3. Subsurface flow dynamics at a tropical hillslope underlain by volcanic ash soils

Andosol soils formed in volcanic ash provide key hydrological services in montane environments. To unravel the subsurface water transport and tracer mixing in these soils I conducted a detailed characterization of soil properties and analyzed a 3-year dataset of subhourly hydrometric and weekly stable isotope data collected at three locations along a steep hillslope. A weakly developed (52–61 cm depth), highly organic andic (Ah) horizon overlaying a mineral (C) horizon was identified, both showing relatively similar properties and subsurface flow dynamics along the hillslope. Soil moisture observations in the Ah horizon showed a fast responding (few hours) "rooted" layer to a depth of 15 cm, overlying a "perched" layer that remained near saturated year-round. The formation of the latter results from the high organic matter (33-42%) and clay (29-31%) content of the Ah horizon and an abrupt hydraulic conductivity reduction in this layer with respect to the rooted layer above. Isotopic signatures revealed that water resides within this soil horizon for short periods, both at the rooted (2) weeks) and perched (4 weeks) layer. A fast soil moisture reaction during rainfall events was also observed in the C horizon, with response times similar to those in the rooted layer. These results indicate that despite the perched layer, which helps sustain the water storage of the soil, a fast-vertical mobilization of water through the entire soil profile occurs during rainfall events. The latter being the result of the fast transfer of hydraulic potentials through the porous matrix of the Andosols, as evidenced by the exponential shape of the water retention curves of the subsequent horizons. These findings demonstrate that the hydrological behavior of volcanic ash soils resembles that of a "layered sponge", in which vertical flow paths dominate.

Related publication

Mosquera, G. M., Crespo, P., Breuer, L., Feyen, J., & Windhorst, D. (2020). Water transport and tracer mixing in volcanic ash soils at a tropical hillslope: A wet layered sloping sponge. Hydrological Processes, hyp.13733. https://doi.org/10.1002/hyp.13733



3.1 Introduction

Hillslope soils in mountainous environments are essential providers of hydrological services. They regulate the transport and mixing of water and solutes in the subsurface (Fan et al., 2019; Lin, 2010). Most of these soils are able to store large amounts of water in their matrix (e.g., organic rich soils; van Huijgevoort *et al.*, 2016; Lazo *et al.*, 2019) or to deliver it rapidly to streams via preferential and/or shallow subsurface flow (e.g., steep and forested catchments; McDonnell *et al.*, 1991; Uchida *et al.*, 1999; Anderson *et al.*, 2009). The hydrological behavior of mountain soils depends on their specific physical, and chemical properties (e.g., hydraulic conductivity, bulk density, porosity, organic matter content, texture). Despite the importance of hillslope soils in the provisioning of hydrological services, fundamental knowledge about how their properties influence water transport and mixing in the subsurface is limited (Fan et al., 2019).

Filling this knowledge gap is of particular importance in understudied hydrological systems, such as those in which subsurface flow paths are influenced by the presence of soils of volcanic ash origin. These soils are known as Andosols (IUSS Working Group WRB, 2015) or Andisols (Soil Survey Staff, 1999). Andosols are characterized by their high content of short-range order clays with high surface areas (e.g., allophane, imogolite, ferrihydrite, and/or the Al- and Fehumus complexes) and organic matter (McDaniel et al., 2012), resulting in high water holding capacity (Neall, 2006). These soils occur extensively in mountainous regions around the world with active or recently extinct volcanos (Takahashi and Shoji, 2002) and deliver important hydrological services such as water storage and flow regulation for downstream water users. Therefore, knowledge about how hillslopes underlain by Andosols store and release water is crucial to improve the management of water and soil resources in these regions. However, the understanding of how these soils and their properties influence subsurface hydrological behavior has not yet been sufficiently clarified.

One of the main factors behind this knowledge gap is the lack of datasets that allows full disentanglement of water flow and mixing processes in the subsurface (Vereecken et al., 2015). The use of hydrometric information (e.g., soil moisture and/or matric potential data) has been helpful to identify e.g.: i) spatial and/or temporal dynamics of soil moisture (Blume et al., 2009; Hasegawa and Eguchi, 2002), ii) hydrometeorological controls on soil moisture response during rainfall events (Tenelanda-Patiño et al., 2018), iii) subsurface flow processes (Eguchi and Hasegawa, 2008; Hasegawa and Sakayori, 2000), and iv) the effects of land use and/or



land cover change in soil moisture dynamics (Dec et al., 2017; Montenegro-Díaz et al., 2019) in plots and hillslopes underlain by Andosols. Nevertheless, hydrometric observations alone are insufficient to shed light on water mixing and aging within these soils.

In the last two decades, insights into subsurface mixing processes and water ages improved thanks to the monitoring of the stable isotopes of hydrogen and oxygen (²H and ¹⁸O) in soil waters (Sprenger et al., 2016). Tracer data do not only allow to investigate how incoming precipitation mixes with water previously stored in the soils, but also for the estimation of the "age" or mean transit time (MTT; i.e., the time it takes for a water molecule to travel to the outlet of a hydrological system; McGuire and McDonnell, 2006) of water mobilizing within different soil layers/horizons (e.g., Asano et al., 2002; Stumpp et al., 2009; McGuire and McDonnell, 2010; Muñoz-Villers and McDonnell, 2012; Tetzlaff et al., 2014; Lazo et al., 2019). Soil water MTT evaluations at hillslope transects have shown either a dominance of water aging with depth below the surface (e.g., Asano et al., 2002; McGuire and McDonnell, 2010; Muñoz-Villers and McDonnell, 2012) or a combination of depth and upslope contributing area (e.g., Stewart and McDonnell, 1991; Kim and Jung, 2014; Tetzlaff et al., 2014). The former indicates that vertical flow paths are dominant, and the latter that there is also a significant influence of lateral subsurface flow paths. Although soil water isotopes (SWIs) in Andosols have been used to investigate runoff generation (Mosquera et al., 2016a; Muñoz-Villers and McDonnell, 2012) and water storage (Lazo et al., 2019) in catchments, their application in combination with hydrometric observations and detailed characterization of soil properties is still inexistent. This situation hinders our ability to disentangle flow paths and mixing processes in hillslopes dominated by volcanic ash soils.

To fill this knowledge gap, a unique dataset of soil properties in combination with hydrometric and water isotope measurements in precipitation and soil water collected in an experimental hillslope transect underlain by volcanic ash soils (Andosols) is presented. The experimental hillslope is located within the tropical alpine (Páramo) ecosystem in south Ecuador. This rich set of observations was analyzed to address the following overarching question: how does water transport and mix in volcanic ash soils (Andosols) at the hillslope scale? To this end, the two objectives of this research are: i) to evaluate how Andosols' properties influence water flow and mixing in the subsurface, and ii) to conceptualize the subsurface hydrological behavior and the dominant flow paths of water occurring within the experimental hillslope.



3.2 Experimental hillslope description

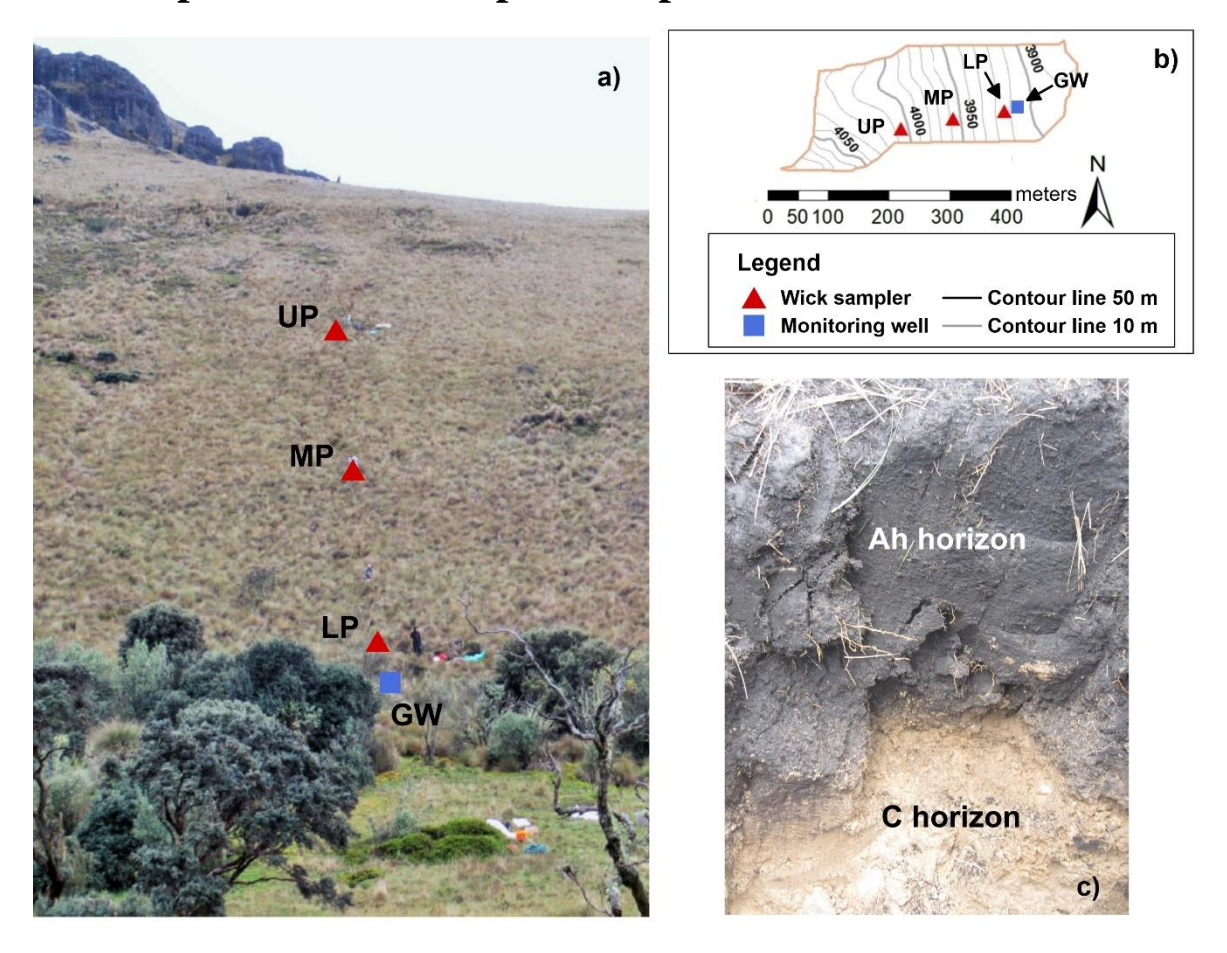


Figure 3.1. a) Experimental hillslope showing the monitoring stations of soil moisture content and stable isotopes of soil water at the upper (UP), middle (MP), and lower (LP) positions (red triangles) along the experimental hillslope and the position of a monitoring well used for monitoring the groundwater level at the bottom of the hillslope (GW, blue square); b) hillslope drainage area and monitoring stations; and c) soil profile and horizons at the UP of the hillslope (Ah = Andic horizon, C = mineral horizon).

The study was carried out at a tropical alpine (Páramo) experimental hillslope situated in the headwaters of the Quinuas Ecohydrological Observatory in south Ecuador (2°47' S, 79°13' W) between 3,900-4,100 m a.s.l. The hillslope (**Figure 3.1a**) has a steep gradient (42%; similar to the average slope of the Quinuas Observatory; Pesántez *et al.*, 2018) and is covered by the dominant Páramo vegetation, consisting primarily of tussock grass (*Calamagrotis Intermedia*), locally known as "pajonal", which covers more than 75-80% of conserved Páramo areas (Mosquera et al., 2015). The soils at the study region resulted from the accumulation of volcanic ash deposits during Quaternary activity in combination with the humid and cold local climate conditions (Buytaert et al., 2006a). These conditions have led to the formation of organic and clay rich soils with high water holding capacity (i.e., Andosols). The soils in the



study region are characterized as non-allophanic (i.e., the clay mineralogy is dominated by metal-humus complexes; Buytaert *et al.*, 2006b). The climate is mainly influenced by continental air masses originating from the Amazon basin (Esquivel-Hernández et al., 2019). Precipitation occurs throughout the year and is composed mainly of drizzle (Padrón et al., 2015). Annual precipitation during the period 2015-2018 averages 1,021 mm, with low temporal seasonality (Carrillo-Rojas et al., 2019). Average temperature and average relative humidity during the period 2011-2014 are 5.4°C and 92.1% at 3,955 m a.s.l., respectively (Muñoz et al., 2016).

3.3 Data collection and methods

3.3.1 Soil properties characterization

Soil pits were dug to characterize the soil profile at three locations along the experimental hillslope. The upper position (UP) at 4,006 m a.s.l., the middle position (MP) at 3,958 m a.s.l., and the lower position (LP) at 3,913 m a.s.l (**Figure 3.1a,b**). The length between the UP and LP sampling sites was 208 m. The UP site was located 256 m below the hilltop. The type, depth, and density of roots in each soil horizon (including the densely rooted topsoil layer) were determined according to the FAO guidelines (FAO, 2006). The distribution of coarse and fine particles and the field characterization of soil texture were carried out according to ISO 11277:2009 International Standard (ISO 11277, 2009). Soil carbon content was determined via combustion of two undisturbed soil samples collected at each sampling position and depth using a Vario EL cube device (Elementar, Germany). Carbon content (CC) was used as an indicator of soil organic matter content (OM% = CC% x 1.72; Guo and Gifford, 2002).

The hydraulic properties of the soils were also characterized at 5, 20, 45, and 75 cm depths at the same positions as the soil pits. The saturated hydraulic conductivity (k_{sat}) of the soils in the vertical direction was measured *in-situ* via the inverse auger-hole method (Oosterbaan and Nijland, 1994). The measurements were repeated three times at each position and depth, and the average k_{sat} values are reported. Three undisturbed soil samples were collected using 100 cm³ steel rings to determine bulk density (BD) and soil moisture content at saturation. The latter was determined gravimetrically as the weight difference of the samples saturated via capillary rise and subsequently oven-dried at 105°C for 24 hours. The BD and soil moisture at saturation values are reported as average values for the 3 replicates. The volume and weight of rock content (>2 mm diameter) was determined and used for correcting the BD and soil moisture content of the soil.



The moisture release curves of the organic and mineral horizons of the soils were also determined. Given the highly organic nature of the shallow horizon of the hillslope soils and the identified discrepancy between the WRCs determined experimentally and in the laboratory (section 2.3), their moisture release curves were determined from direct soil moisture content and matric potential measurements using water content reflectometers (Campbell Scientific CS616) and tensiometers (UMS T8), respectively. For this purpose, I took 3 randomly selected undisturbed soil cores (\emptyset = 40 cm, h = 32 cm) located in a 5 m x 5 m area around each of the sampling sites along the hillslope to capture the spatial variability of the moisture release characteristic. The samples were wetted from the bottom of the cores via capillary rise for two months to assure they were completely saturated. Once the samples were fully saturated, I installed one reflectometer and one tensiometer at a depth of 15 cm below the vegetation layer in each soil core. The samples were then drained freely by gravity and their soil moisture content-water potential relations were measured at 5-minute intervals until the tensiometer probes lost contact with the matrix due to desiccation.

The stoniness of the mineral horizon of the soils did not allow collecting large undisturbed soil cores to determine moisture release characteristics as described above. Thus, the soil moisture-matric potential relations were determined using 100 cm^3 undisturbed soil samples by applying traditional laboratory analyses using sandboxes (Topp and Zebchuk, 1979) and pressure chambers (FAO, 2002). Soil moisture was determined at matric potentials of 1, 3, 10, 31, 330, 2,500, and 15,000 cm H₂O, which span a range from saturation (1 cm H₂O) to theoretical permanent wilting point (~15,000 cm H₂O). Given the similarities among the water retention curves collected at each soil horizon along the hillslope, I report these results as the average \pm 1 standard deviation of all analyzed samples.

3.3.2 Hydrometric data collection

The hillslope was equipped for the monitoring of hydrometric fluxes (rainfall, soil moisture, and groundwater level) and tracer fingerprints (SWI) at the same three positions as the soil pits. A Texas TE525MM tipping bucket rain gauge with an accuracy of $\pm 1\%$ was used to record precipitation amounts 1.5 km from the experimental hillslope at an elevation of 3,955 m a.s.l. Soil moisture content was measured using Decagon Devices 5TE capacitance probes. The capacitance probes were installed at the UP, MP, and LP sampling sites (**Figure 3.1a,b**) at 5, 20, 45, and 75 cm depths. The probes were calibrated for the soils' local conditions for each of the identified horizons following the procedures described by Blume *et al.* (2009). Through calibration, an improved accuracy of $\pm 1-2\%$ ($r^2=0.95$, p-value<0.05) was obtained (Tenelanda-



Patiño et al., 2018). Rainfall amount and soil moisture content data were simultaneously monitored every 5-minutes during the period January 2015–December 2017.

I also used a monitoring well to measure groundwater level fluctuations at the bottom of the experimental hillslope (GW site in **Figure 3.1a,b**). The well consisted of 1.5 m long, 2-inch (5.1 cm) diameter galvanized tube, with a 1.05 m screen with holes of 0.8 mm diameter separated 10 mm vertically and 5 mm horizontally. Given the highly organic nature of the local soils, I designed a filter system following the recommendations of the Minnesota Board of Water & Soil Resources for hydrologic monitoring of wetlands (Minnesota Board of Water & Soil Resources, 2013). The well was wrapped with a permeable nylon textile and a 5 cm sand and gravel filter (1-20 mm diameter) to prevent sediment accumulation in the tube. Approximately 70% of the filter was composed of fine sand particles (1 mm diameter) to increase the surface area where organic matter particles could be retained. Pressure transducers (Schlumberger DI500) with a precision of ±5 mm recorded groundwater level fluctuations every 5-minutes during the period January-December 2017.

3.3.3 Isotopic data collection and analysis

Precipitation water samples were collected from a rainfall collector installed at the location of the rain gauge. The rainfall collector was covered with aluminum foil and a 5 mm mineral oil layer was added to the collector to reduce possible isotopic fractionation due to evaporation. A portion of the mobile water fraction of the soils was collected using wick samplers (Mertens and Vanderborght, 2007). The wick samplers consisted of a 30 cm x 30 cm polypropylene plate surrounded by 5 cm walls, on which a piece of 0.5 m long woven and braided 3/8" fiberglass wick (Amatex Co. Norristown, PA, US) was unraveled and covered with parent soil material. Below the polypropylene plates, the remaining part of the wicks were placed inside a flexible silicon tube and protected with a 60 cm long and 3/4" diameter plastic pipe to ensure an unhindered and constant vertical suction of approximately 60 hPa (Windhorst et al., 2014). Each silicon tube was routed to a centralized collection pipe (Ø = 50 cm) where it was connected to a 1.5 L glass bottle where collected water was stored until analysis (Pesántez et al., 2018). The wick samplers were installed at 10, 35, and 65 cm depths at each sampling site.

The precipitation and soil water samples were collected weekly for the period January-December 2016. The collected samples were filtered in the field using 0.45 μ m polytetrafluorethylene membranes and stored in 2 ml amber glass bottles in the dark to prevent evaporative fractionation until analysis (Mook, 2000). The samples were analyzed for 2 H and



¹⁸O using a Picarro L2130-i isotopic water vapor analyzer with a precision of 0.5‰ for 2 H and 0.2‰ for 18 O. The ChemCorrect software (Picarro, 2010) was used to check the samples for organic contamination. Samples that showed evidence of contamination were excluded from data analysis. The isotopic values are reported in the δ notation in reference to the Vienna Standard Mean Ocean Water V-SMOW for both measured isotopes (Craig, 1961).

3.3.4 Spatial-temporal variability of hydrometric data: Hydrological dynamics and response times

The transport of water in the subsurface was characterized through the temporal variability of hydrometric observations and the response time of soil moisture and groundwater level to rainstorm events. I first plotted and compared hourly data of precipitation, soil moisture content, and groundwater level, and carried out an examination of the response times to reach the peak value (tpeak) of soil moisture or groundwater level during rainstorm events (Zhu et al., 2014). Rainfall events were defined using the minimum inter-event time criteria (Dunkerley, 2008). That is, the minimum time span without rain between two consecutive events. Given that precipitation occurs frequently in the study region, with only few consecutive dry days throughout the year (Padrón et al., 2015), a time-lapse of 6 hr without rain was used to characterize rainfall events (Tenelanda-Patiño et al., 2018). The manufacturers' accuracy of the instruments, 0.3% volume for soil moisture and 0.5 cm H₂O for groundwater level, was applied as minimum threshold changes to differentiate instruments noise from response to rainfall during the events (Lozano-Parra et al., 2015). Only events in which data were available at all sampling locations were considered. Under these conditions, 74 rainfall events were identified. The t_{peak} information was used to compare the timing of soil moisture response along the experimental hillslope. For this purpose, scatter plots of t_{peak} between pairs of contiguous sampling positions at the same sampling depth (e.g., between the UP and MP at 5 cm depth) and contiguous sampling depths at the same sampling position (e.g., between 20 cm and 45 cm depths at the MP) were constructed and analyzed. The same approach was carried out to compare the t_{peak} between soil moisture at different depths at the LP site and the groundwater levels at the bottom of the hillslope. In these analyses, scatter points falling closely to the 1:1 ratio indicate similar response times, whereas the ones falling outside this relation indicate delays in response time between different sampling positions/depths or groundwater levels.



3.3.5 Soil water stable isotopes: Tracer mixing and soil water ages

The mixing of tracer in the system was evaluated via the attenuation of the isotopic composition of soil water (at different positions and depths) in relation to the composition of precipitation. For this purpose, I compared the weekly collected stable isotopic composition of rainfall and soil water samples. This analysis permitted a qualitative characterization of how the water within the soils mixes with rainfall water. In addition, I used δ^2H – $\delta^{18}O$ isotope plots of precipitation samples (i.e., the Local Meteoric Water Line, LMWL; Rozanski *et al.*, 1993) and soil waters to evaluate potential evaporation effects in the isotopic fractionation of soil water (i.e. non-equilibrium fractionation).

I applied a lumped convolution approach (LCA; Maloszewski and Zuber, 1996) to estimate the MTT (age) of soil water. The LCA approach aims to reproduce the attenuation of the geochemical composition of a given tracer (e.g. ²H, ¹⁸O, Cl) at the outlet of a hydrologic system based on the tracer's input signal assuming steady state conditions. Even though alternative methods for the investigation of water ages under non-stationary conditions exist (e.g., Harman, 2015; Kirchner, 2016; Benettin *et al.*, 2017), since my objective is not to investigate long-term changes in subsurface hydrological conditions, the LCA provides a valuable metric that allows for a quantitative comparison of the attenuation of the isotopic composition of soil water at different sampling positions and depths. Since it can be assumed that the experimental hillslope is subjected to the same meteorological conditions along the whole monitoring transect, such a comparison permits to identify the dominant flow paths of water in the subsurface.

Transit time distributions (TTDs) are used in the LCA to convert inputs tracer signals into output ones. TTDs are predefined mathematical functions that represent the internal transport and mixing processes within hydrologic systems (Hrachowitz et al., 2016). I applied the exponential model (EM) TTD as it has outperformed at catchment (Mosquera et al., 2016b; Muñoz-Villers et al., 2016) and hillslope (Lazo et al., 2019; Muñoz-Villers and McDonnell, 2012) scales in the Páramo and other tropical montane ecosystems in comparison to other TTDs. The model performance was evaluated using the Kling–Gupta efficiency (KGE; (Gupta et al., 2009). The model was run 10,000 times using a Monte Carlo sampling procedure to calibrate the only parameter of the EM TTD, i.e., the MTT of the system. The range of calibration parameters was 0-250 weeks (0-5 years). Simulations that yielded at least 95% of the highest KGE were considered behavioral solutions. The 5 and 95% bounds of the range of



behavioral solution parameters were used as uncertainty limits for the model simulations. Further details about the modelling procedure can be found in (Mosquera et al., 2016b).

3.4 Results

3.4.1 Soil properties characterization

Table 3.1. These were generally consistent with those reported for nearby Páramo hillslopes (Buytaert et al., 2006b; Mosquera et al., 2016a) and in a tropical forest catchment dominated by Andosol soils in central eastern Mexico (Muñoz-Villers and McDonnell, 2012). There were two well-differentiated soil horizons (**Figure 3.1c**). The shallow horizon corresponded to an andic horizon (Ah) with relatively comparable characteristics at all sampling sites. Its depth varied little (52–61 cm) along the hillslope. The Ah horizon contained a high density of fine roots ($\emptyset \le 2$ mm), with the highest density in the first 10–15 cm below the ground surface due to the presence of the root system of the overlying tussock grass vegetation. The density of large roots ($\emptyset > 2$ mm) was lower than the density of fine roots. In this horizon few coarse particles, most of them with $\emptyset \le 200$ mm, were present. Its texture was classified as clay loam. The distribution of fine particles in the Ah horizon was similar at all sampling sites (sand 29–39%, silt 32–42%, and clay 29–31%). The carbon content in the Ah horizon was high at all hillslope positions (19.5–24.5%, corresponding to organic matter contents of 33.5-42.1%).

The underlying horizon corresponded to a mineral horizon (C) with more heterogeneous characteristics. The depth of the C horizon was higher at the LP site compared to the UP and MP sites. The density of fine roots was very low and there were no large roots. The proportion of coarse particles was higher than for the Ah horizon. The majority of particles (48–57% of the total) had \varnothing >200 mm, regardless of the position along the hillslope. The texture of the C horizon was classified as sandy loam. The distribution of fine particles revealed a dominance of sand (70–73%) and low clay content (7–8%). The carbon content was much lower than in the Ah horizon and decreased with sampling site elevation from 4.4% at the UP site to 1.7% at the LP site.



Table 3.1. Physical characteristics and carbon content of the soil profiles monitored at the upper (UP), middle (MP), and lower (LP) positions along the experimental hillslope.

	Altitude				Root content		Coarse particles distribution			Fine particles distribution ^a				
Hillslope position		Horizon type	Upper boundary	Lower boundary	Fine [Ø ^b ≤ 2 mm]	Large [Ø ^b >2 mm]	2-63 mm	63-200 mm	>200 mm	Sand	Silt	Clay	Carbon Content ^b	
	(m a.s.l.)		(cm)	(cm)	(Roots per dm²)	(Roots per dm²)	(%)	(%)	(%)	(%)	(%)	(%)	(%)	
		Ah_{DRZ}	0	10	224	0	0	0	0	29	42	20	24.4	
UP	4,006	$Ah_{BDRZ} \\$	10	57	63	7	4	2	0	29	42	30 7	24.5	
		C	57	89	4	0	5	8	12	73	20	7	4.4	
		Ah_{DRZ}	0	10	280	0	0	0	0	34	35	31	33.8	
MP	3,958	$Ah_{BDRZ} \\$	10	52	57	3	4	2	0	34	33	31	19.5	
		C	52	77	11	0	10	5	20	71	71 22		2.3	
		Ah_{DRZ}	0	10	200	0	0	0	0	20	22	20	27.3	
LP	3,913	$Ah_{BDRZ} \\$	10	61	58	9	5	1	1	39	32	29	21.2	
		C	61	116	4	0	10	2	12	70	23	8	1.7	

Abbreviations: Ah = andic horizon and C = mineral horizon. Subscripts are: DRZ = densely rooted zone and BDRZ = below densely rooted zone, \emptyset = diameter of the roots

^a The distribution of fine particles in the andic (Ah) horizon was only characterized at the middle depths of the soil horizon at each sampling site.

^b The soil samples for carbon content analysis were taken at depths corresponding to half the horizon/layer thickness (i.e., the average between the upper and lower boundaries reported in the table).



The hydraulic properties of the soils along the experimental hillslope are summarized in **Table** 3.2. The BD of the Ah horizon was relatively similar at all depths (5, 20, and 45 cm) at each sampling position, with typically low values (<0.90 gr cm⁻³) expected for the Ah horizon of Andosol soils (Takahashi and Shoji, 2002). The BD varied between 0.37±0.07 gr cm⁻³ and was least variable with depth at the UP site. The BD in the C horizon (75 cm depth) was consistently higher than in the Ah horizon at all sampling sites (0.96–1.37 gr cm⁻³). The K_{sat} of the Ah horizon in the vertical direction generally decreased with depth, with values up to 1.91 cm hr ¹ at 5 cm depth, and as low as 0.25 cm hr⁻¹ at 45 cm depth. The K_{sat} of the C horizon (1.12-2.73) cm hr⁻¹) was higher than for the Ah horizon and was highest downslope. The BD and K_{sat} values for both horizons are consistent with those previously reported along hillslopes in nearby Páramo areas (Buytaert et al., 2006b; Mosquera et al., 2016a). The soil moisture content at saturation was high, as expected for soils rich in organic matter (Boelter, 1969; Letts et al., 2000), and similar at all soil depths within the Ah horizon at all sampling positions (0.78–0.84 cm³ cm⁻³). The soil moisture content at saturation in the C horizon was substantially lower than in the Ah horizon (Buytaert et al., 2006b), and varied little along the hillslope (0.48-0.59 cm³ cm^{-3}).

Table 3.2. Mean values of the hydrophysical properties of the soil at the upper (UP), middle (MP), and lower (LP) positions along the experimental hillslope. The presented values correspond to the average of three measurements of each of the properties and each sampling location and depth.

Hillslope	Altitude	Depth	Hawizan	BD ^a K _{sat} ^a		Jorizon		θ_{sat}^{a}
position	(m a.s.l.)	(cm)	Horizon	(gr cm ⁻¹)	(cm hr ⁻¹)	(cm ³ cm ⁻³)		
UP		5	Ah	0.29	1.41	0.84		
	4.006	20	Ah	0.29	0.45	0.8		
UP	4,006	45	Ah	0.3	0.25	0.85		
		75	C	1.12	1.12	0.59		
		5	Ah	0.37	1.88	0.82		
MD	2.050	20	Ah	0.46	0.65	0.78		
MP	3,958	45	Ah	0.51	0.31	0.78		
		75	C	1.37	2.28	0.48		
		5	Ah	0.33	1.91	0.84		
	2.012	20	Ah	0.39	0.42	0.84		
LP	LP 3,913 45	Ah	0.35	0.3	0.84			
		75	C	0.96	2.73	0.55		

Note: The presented values correspond to the average of three measurements of each of the properties and each sampling location and depth.

Abbreviations: BD, bulk density; Ksat, saturated hydraulic conductivity in the vertical direction; θ_{sat} , soil moisture content at saturation.



The moisture release curve of the organic horizon of the hillslope soils depicted an exponential decrease in soil moisture as matric potentials increased from saturation to ~330 cm H_2O (**Figure 3.2a**), resembling the soil moisture retention curve of peat soils (e.g., Schwärzel *et al.*, 2002) and those obtained for Andosol soils in the Terceira Island, Portugal (Fontes et al., 2004). The water retention curve of the mineral horizon resembled that of the organic horizon at potential values above field capacity, but with lower moisture contents for the same potentials (**Figure 3.2b**). This relation further showed a decrease in soil moisture with decreasing potentials to a soil moisture of 0.24 ± 0.11 cm³ cm⁻³ at permanent wilting point (~15,000 cm H_2O).

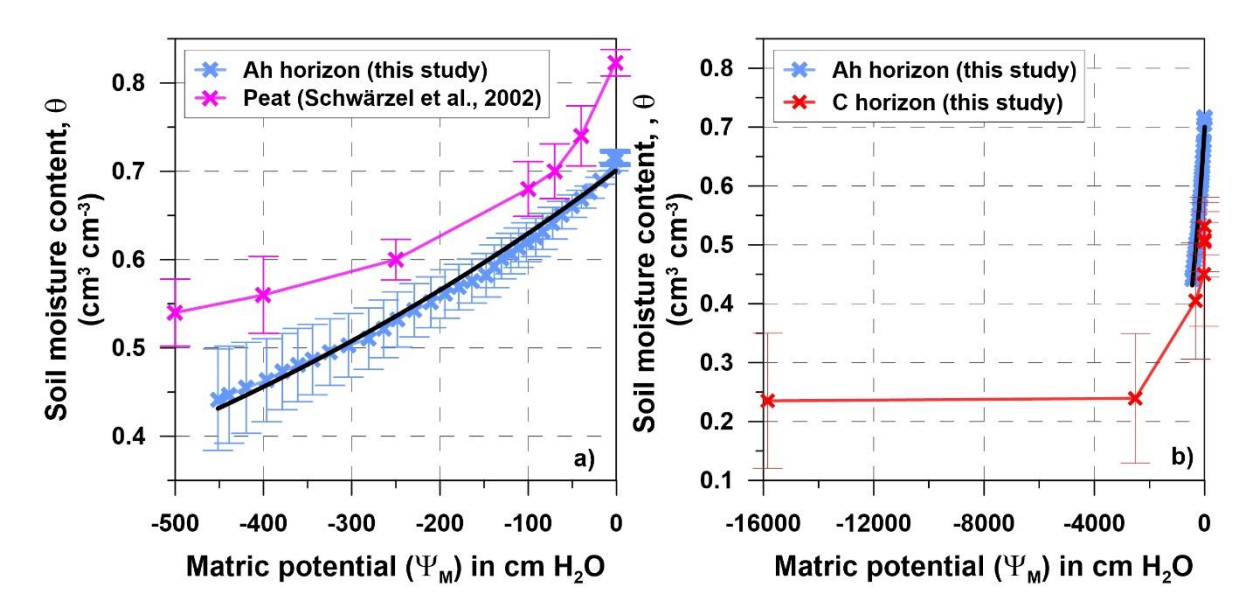


Figure 3.2. Moisture release curves of the a) organic (Ah) horizon (including the curve for a peat soil reported by Schwärzel *et al.* (2002) for reference) and b) the mineral (C) horizon (including the curve of the Ah horizon for reference) of the experimental hillslope soils. The black lines in subplots a) and b) show the exponential relation between the matric potential and soil moisture content of the Ah horizon [Eq: $\ln(\theta) = 1.076e^{-3} \times \Psi_M - 0.3548$]. Note the different ranges of the x- and y-axes values in subplots a) and b). Data shown represent the mean (x symbols) and standard deviation (error bars) of all samples collected at the upper (UP), middle (MP), and lower (LP) sampling sites along the experimental hillslope for each soil horizon.

3.4.2 Hydrological dynamics and response times

Hourly rainfall, soil moisture content, and groundwater level data are shown in **Figure 3.3**. Precipitation was uniform during the study period and fell typically as low intensity events (<2 mm hr⁻¹), although few rainstorm events had a maximum intensity that exceeded 5 mm hr⁻¹ (**Figure 3.3a**).

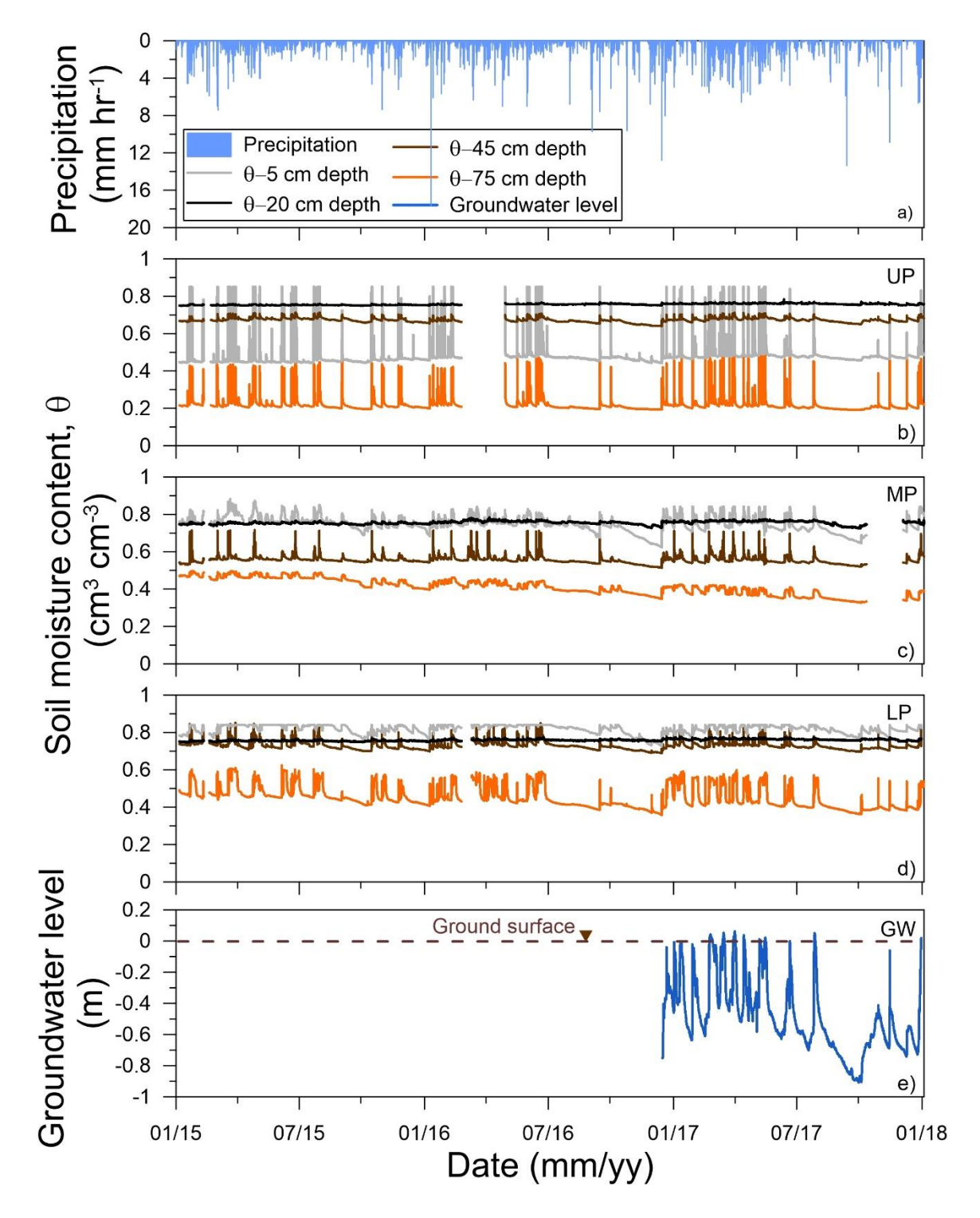


Figure 3.3. Hourly temporal variability of a) precipitation and soil moisture content (θ) at the b) upper (UP), c) middle (MP), and d) lower (LP) positions along the experimental hillslope, and e) groundwater level (GW) at the bottom of the experimental hillslope located in the headwaters of the Quinuas River Ecohydrological Observatory for the period January 2015–December 2017.



The soil moisture dynamics at 5 cm depth (the densely rooted zone of the Ah horizon; hereafter referred to as the "rooted layer") varied along the hillslope (grey lines in **Figure 3.3b–d**). At the UP site, soil moisture varied between 0.46 cm³ cm⁻³ during periods of low intensity precipitation and saturation (0.84 cm³ cm⁻³) in response to high intensity precipitation events (**Figure 3.3b**). A similar hydrological dynamic was observed at the MP site, but at higher soil moisture than at the UP site (**Figure 3.3c**). Soil moisture at the LP site varied little and remained near saturated (0.84-0.82 cm³ cm⁻³, respectively), except during relatively long dry periods (e.g., October–December 2016; **Figure 3.3d**).

At 20 cm depth, the soil moisture dynamic at all hillslope positions was very different than in the rooted layer (black lines in **Figure 3.3b-d**). That is, there was no apparent soil moisture response to the temporal variability in precipitation. Soil moisture remained high and near saturation (0.72±0.05. cm³ cm⁻³) during the entire study period, even during extended dry periods. These conditions resemble a perched water layer in the Ah horizon, and as such, this layer will hereafter be referred to as the "perched layer". Although soil moisture at 45 cm depth (the Ah horizon layer near the organic-mineral horizons interface; hereafter referred to as the "transition layer") was more responsive to the temporal variability of precipitation (brown lines in **Figure 3.3b–d**), it showed a similar behavior as the perched layer. Soil moisture varied little at the UP site during the study period (0.68 cm³ cm⁻³ to 0.71 cm³ cm⁻³). At the MP site, soil moisture varied between 0.53 cm³ cm⁻³ during low intensity precipitation periods and was 0.71 cm³ cm⁻³ during high intensity precipitation events (**Figure 3.3c**). Soil moisture at the LP site was higher (>0.72 cm³ cm⁻³) than at UP and LP sites during the whole study period, and reached saturation during precipitation events of high intensity (Figure 3.3d). Regardless of the monitoring position, soil moisture in the transition layer decreased only slightly during dry periods.

The soil moisture dynamics at a depth of 75 cm depth (i.e., within the C horizon), hereafter referred to as the "mineral layer", differed at each of the hillslope positions (orange lines in **Figure 3.3b–d**). At the UP site, soil moisture was low and remained below saturation (<0.59 cm³ cm⁻³) but was very responsive to precipitation inputs (**Figure 3.3b**). At the MP site, soil moisture remained higher in comparison to the UP site and reached saturated conditions (0.48 cm³ cm⁻³) during some rainy periods (**Figure 3.3c**). Soil moisture was the highest at the LP site and often reached saturation (0.58 cm³ cm⁻³; **Figure 3.3d**) in comparison to the other hillslope positions. Soil moisture showed only a slight decrease during dry periods at all hillslope positions.



The groundwater level at the bottom of the hillslope responded rapidly to precipitation events, but reached the surface only few times mainly during the wettest months (March-May). Groundwater levels were also more sensitive to relatively long (>1 month) periods of no to low rainfall (**Figure 3.3e**). During one of the longest dry periods (August 3-October 5, 2017), groundwater levels steadily decreased to the lowest level recorded during the monitoring period (i.e., 97 cm below the ground level) and changed at a faster rate than the soil moisture levels uphill (**Figure 3.3b-d**).

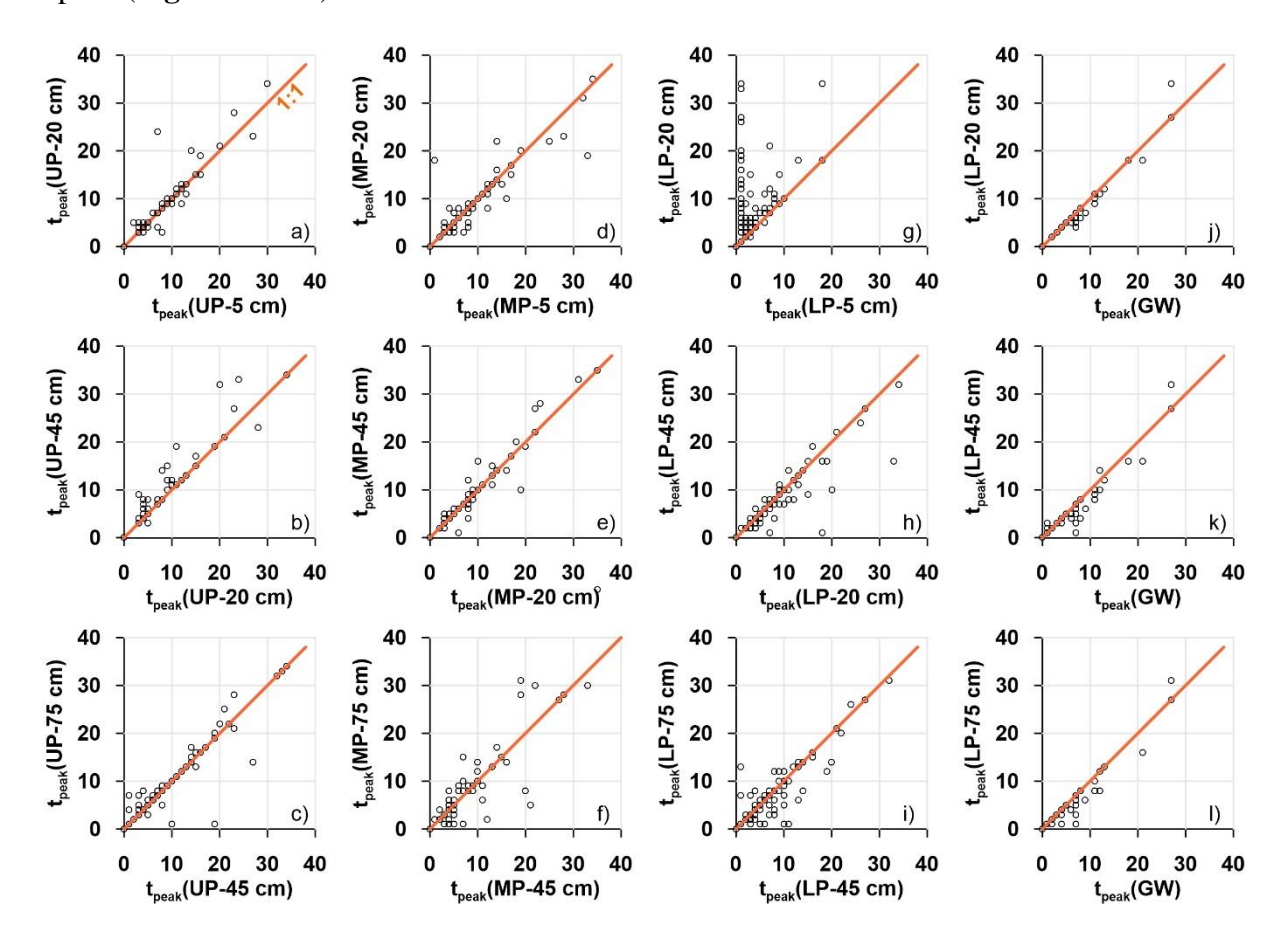


Figure 3.4. Relation of the response times in hours (t_{peak}) to the peak value of soil moisture during rainfall events between contiguous sampling depths at the UP (a-c), MP (d-f), and LP (g-i) sites. Subplots j-l show the relation between the t_{peak} to the peak value of soil moisture at different depths at the LP site and the t_{peak} to the peak value of groundwater level (GW) at the bottom of the hillslope during rainfall events (j-l). The orange line in each subplot represents the 1:1 ratio.

The response times to the peak values of soil moisture and groundwater level during precipitation events varied between 1 and 35 hours along the hillslope (**Figure 3.4** and **Figure 3.5**). These times were normally short, with an average variation of 7.2±1.6 hours among all sampling sites. The response times at contiguous sampling positions and depths were very similar and fell mostly under the 1:1 relation (**Figure 3.4** and **Figure 3.5c-h**). The only



exception was in the rooted layer, where I observed a short delay in soil moisture response at the MP site in comparison to the UP site (**Figure 3.5a**). I could not evaluate the response times at the LP site in the rooted layer as the soil usually became saturated before the other sampling positions/depths reached maximum soil moisture/groundwater level (**Figure 3.4g** and **Figure 3.5b**).

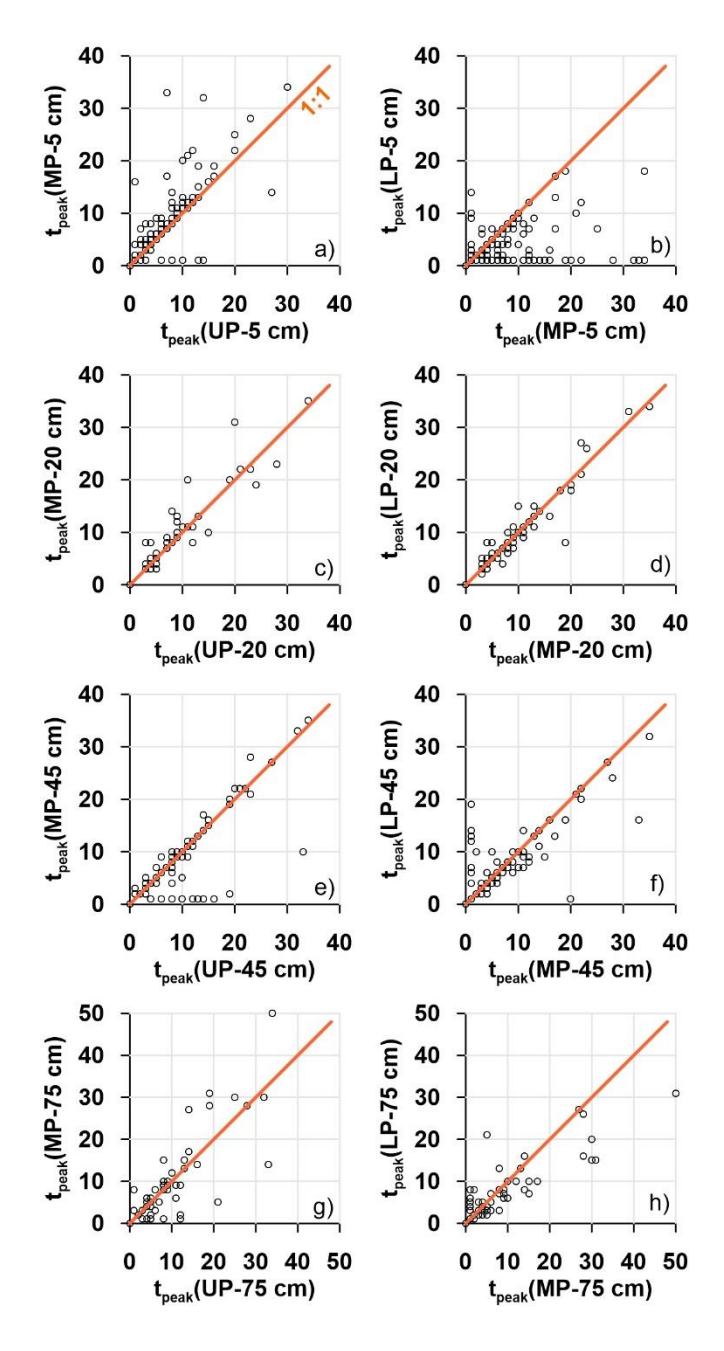


Figure 3.5. Relation of the response times in hours (t_{peak}) to the peak value of soil moisture during rainfall events between contiguous sampling positions (UP, MP, and LP sites) at a depth of 5 cm (a-b), 20 cm (c-d), 45 cm (e-f), and 75 cm (g-h). The orange line in each subplot represents the 1:1 ratio.



3.4.3 Tracer mixing and soil water ages

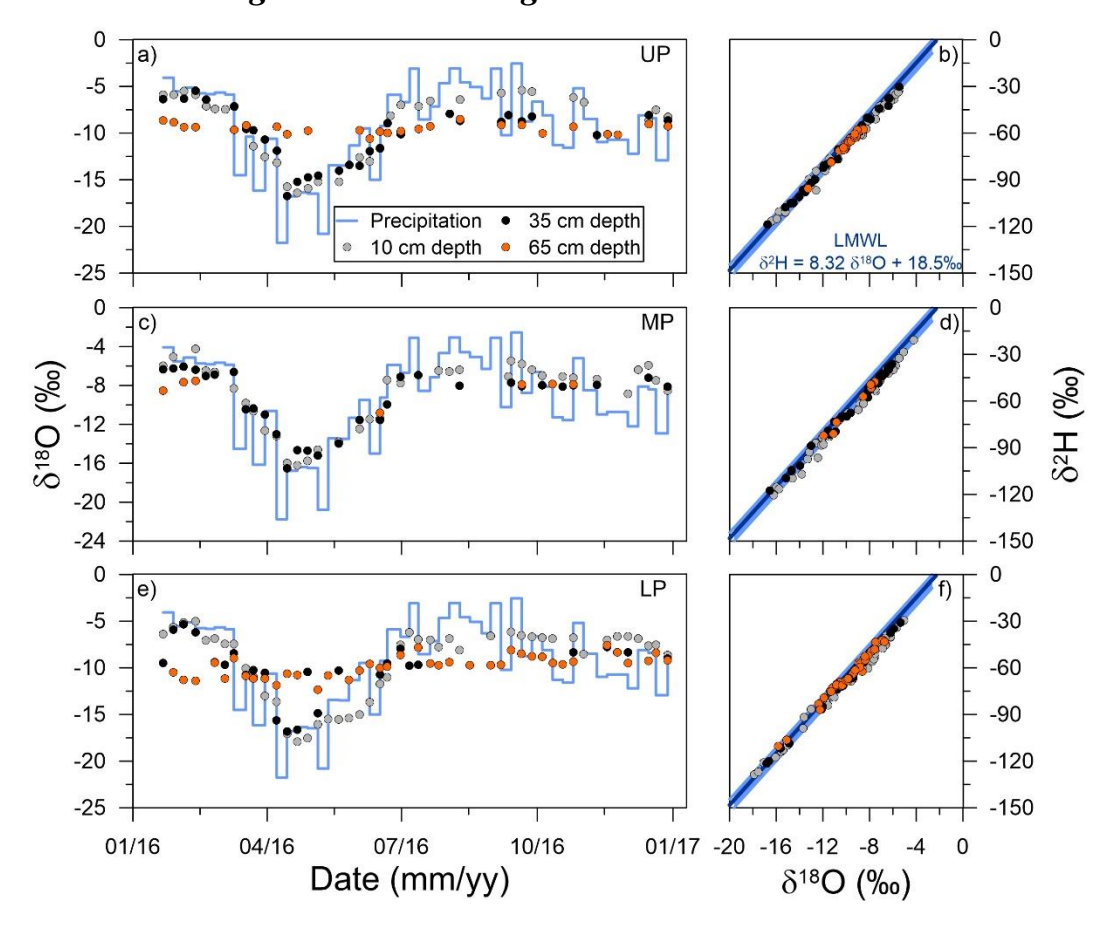


Figure 3.6. Temporal variability of the weekly δ^{18} O isotopic composition of precipitation (light blue line) and soil water (a, c, and e) and the δ^2 H- δ^{18} O relation in precipitation (Local Meteoric Water Line, LMWL) and soil water (b, d, and f) at the upper (UP), middle (MP), and lower (LP) positions along the experimental hillslope during the period January 2016-January 2017. The dark blue lines and the light blue shaded areas in subplots b), d), and f) represent the LMWL and the range of the isotopic variation in precipitation, respectively.

The temporal variability of the isotopic composition of precipitation and soil water is shown in **Figure 3.6**. The isotopic composition of soil water in the rooted and perched layers (at 10 and 35 cm depths, respectively; grey and black dots in **Figure 3.6**) followed closely the isotopic composition of precipitation. Conversely, the isotopic composition of soil water in the mineral layer (at 65 cm depth; orange dots in **Figure 3.6**) was more attenuated than the isotopic compositions of precipitation and soil water in the Ah horizon. The dual plots of δ^{18} O and δ^{2} H showed that regardless of the horizon type (i.e., organic or mineral), all soil water samples at all sampling sites plotted within the range of variation of the samples in precipitation (**Figure 3.6b,d,f**). These observations indicate that evaporative fractionation of soil water is negligible. Although transpiration does not usually modify the stable isotopic composition of water (White, 1989), it could affect soil water MTT estimations by removing important amounts of



water from the soil. Transpiration of the tussock grass vegetation that covers the experimental hillslope only affects the rooted layer of the soil profile (up to 10-15 cm depth). However, this water flux represents only a small fraction of evapotranspiration in the study region (Ochoa-Sánchez et al., 2020). Evaporation and transpiration effects on the isotopic composition of soil water are likely suppressed by the local environmental conditions. That is, high relative humidity (annual average=90%; Muñoz *et al.*, 2016), low net radiation (annual average=100 W m⁻²; Ochoa-Sánchez *et al.*, 2020), and sustained input of low intensity precipitation (Padrón *et al.*, 2015) throughout the year. Thus, the soil water MTT estimations were unaffected by evaporation and transpiration effects. Soil water MTTs increased consistently from the rooted layer to the mineral layer at all hillslope positions (**Figure 3.7** and **Table 3.3**). MTTs varied little at all monitored positions in the rooted (14.3±6.1 days) and perched (26.3±7.4 days) layers within the Ah horizon. On the contrary, there was a larger MTT variation in the mineral layer (from 256.7±34.3 days at the UP to 83.8±13.4 days at the LP; **Table 3.3**).

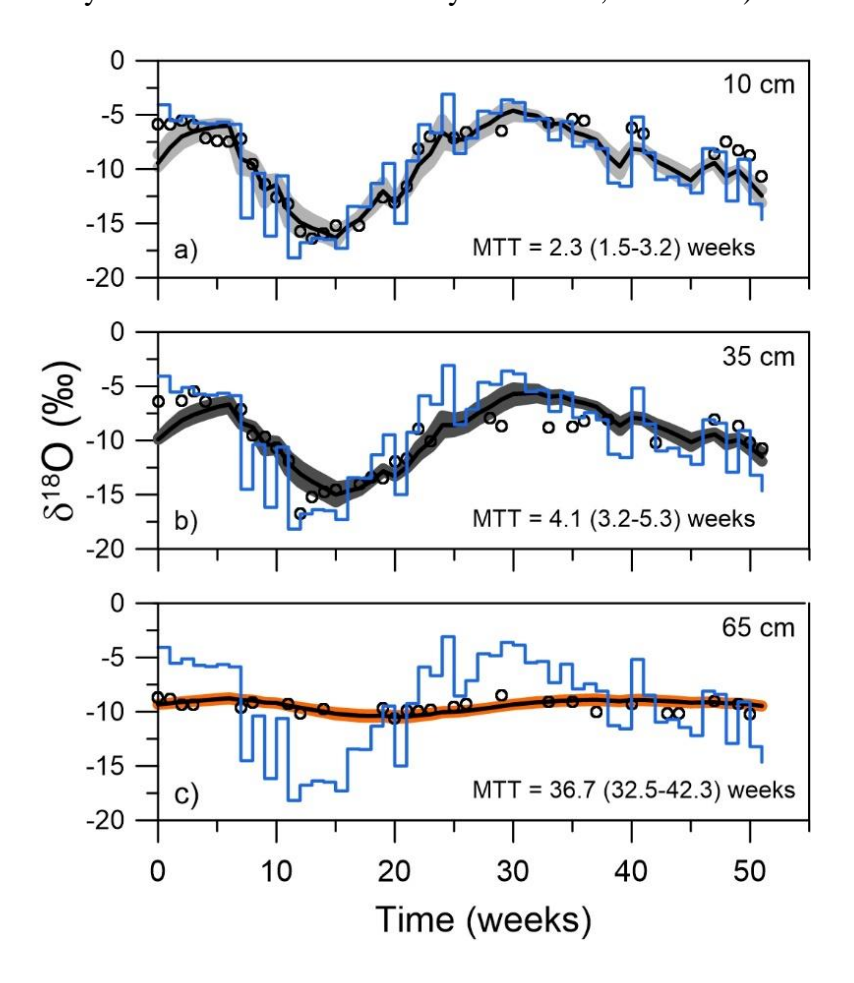


Figure 3.7. Observed and simulated soil water $\delta^{18}O$ isotopic composition at a) 10 cm, b) 35 cm, and c) 65 cm depths at the upper position (UP) of the experimental hillslope. The open circles represent the observed isotopic composition in soil water; the blue lines represent the precipitation isotopic composition; the black lines represent the best simulated isotopic composition in soil water according to the KGE objective function; and the shaded areas.



Table 3.3. Summary statistics of the δ^{18} O isotopic composition of precipitation (QP1) and soil water and the soil water mean transit times (MTTs) at the upper (UP), middle (MP), and lower (LP) positions along the experimental hillslope. MTT values in parenthesis represent the 5–95% confidence limits of the simulated soil water MTTs.

Sample	Sampling	Altitude	Depth		δ	¹⁸ O (MTT		
type station		(m a.s.l.)	m a.s.l.) (cm)		Mean	SE	Max	Min	(days)
Precipitation	oitation QP1 3,955 n/a ^b 58 -10 0.6 -2.5 -21.8 n/a		n/aª						
			10	41	-9.7	0.5	-5.4	-16.4	15.8 (10.3-22.2)
	UP	4,006	35	38	-10.7	0.5	-5.5	-16.7	29.0 (22.3-37.3)
			65	32	-9.9	0.2	-8.5	-13.3	256.8 (227.5-296.2)
	MP	3,958	10	47	-9.3	0.5	-4.2	-16.2	15.2 (9.6-22.2)
Soil water			35	47	-9.6	0.4	-6.1	-16.5	25.5 (19.0-33.2)
			65	13	-9.9	0.5	-7.6	-12.3	n/p ^b
			10	53	-9.7	0.5	-5	-17.9	11.8 (6.9-18.9)
	LP	3,913	35	27	-10.2	0.6	-5.3	-16.8	24.5 (17.4-32.8)
			65	53	-9.9	0.2	-6.7	-15.8	83.8 (72.2-99.0)

Note: MTT values in parenthesis represent the 5–95% confidence limits of the simulated soil water MTTs.

Abbreviations: Max, maximum; Min, Minimum; n, number of samples; SE, standard error.

3.5 Discussion

3.5.1 Hydrological dynamics and response times

Hydrometric observations showed higher moisture contents towards the bottom of the hillslope (**Figure 3.3b-d**). This effect likely results from an increase in the contributing drainage area towards the bottom of the hillslope, possibly combined with a decrease in slope gradient for the sampling sites closer to the valley bottom. These factors probably explain the larger changes in soil moisture contents to occur at the UP site, as soil layers at this position (particularly the rooted and mineral layers) remain drier than those at the MP and LP sites where saturated conditions occurred more frequently. Apart from this difference, soil moisture dynamics was relatively similar at each soil layer along the experimental hillslope.

The rapid response of soil moisture to precipitation inputs in the rooted layer of the Ah horizon (from the ground surface to 10-15 cm depth; **Table 3.1** and grey lines in **Figure 3.3b-d**) indicates that this soil layer was highly influenced by the temporal dynamics of incoming precipitation. The fast-hydraulic response can be explained by the combination of two factors.

^a Not applicable.

^b Not possible to estimate the soil water mean transit time since there were not enough samples to run the model due to malfunctioning of the wick sampler during the study period.



First, the activation of preferential flow paths through the layer's large density of roots, as has been previously obseverd in Japanese Andosol soils (Eguchi and Hasegawa, 2008). This rapid response can be further explained by the fast mobilization of water via matric flow through the porous soil matrix (Hasegawa and Sakayori, 2000; Neall, 2006). A similar hydrological behavior in the unsaturated zone of an organic rich soil layer was observed in a steep hillslope in Coos Bay, Oregon, USA (Torres et al., 1998). There, the observed subsurface flow dynamics were explained by the shape of the soils' water retention curves, which suggested that small changes in hydraulic potentials caused large changes in soil moisture at low matric potentials. The exponentially shaped moisture release curve of the organic horizon of the soils in the experimental hillslope (**Figure 3.2a**) behaves similarly for the same reason, reflecting a fast hydraulic dynamic in the soil system. The combination of these effects in turn result in a rapid mobilization of water during precipitation events, explaining the flashy response of soil moisture in the Ah horizon.

Deeper in the subsurface (from 10-15 cm to 30-35 cm depth), the sustained near saturated conditions year-round (black lines in **Figure 3.3b-d**) indicate a perched water layer. These findings are in line with those reported for organic rich soils in the Scottish highlands (Tetzlaff et al., 2014). The formation of this layer likely results from the abrupt vertical K_{sat} reduction in this soil layer compared to the overlying rooted layer (**Table 3.2**), caused by the lower density of fine roots (Bonell et al., 1983). Moreover, the high moisture (soil water storage) likely results from the high organic matter and clay content of the andic horizon (**Table 3.1**), to which water molecules can be easily bound (Yang et al., 2014).

The underlying transition layer (from 30-35 cm to 40-55 cm depth) also maintained a high moisture content throughout the year due to the high content of organic matter and clay of the Ah horizon (**Table 3.1**), but at a lower level than the perched layer above (brown lines in **Figure 3.3b–d**). The high water storage in the perched and transitions layers is also likely favored by the presence of a thin (few mm to few cm in thickness), cemented layer commonly found below the organic horizon of the Andosols, known as placic horizon (Soil Survey Staff, 2015). This horizon results from the illuviation of iron and organic matter from the Ah horizon and usually locates in the interface between the organic and mineral horizons (Buytaert et al., 2005a). Although irregular and discontinuous, the hard and impervious nature of the placic horizon hampers the activation of vertical flow paths throughout the entire soil profile (Ah-C horizons) during periods of little to no rainfall. This effect in turn facilitates the accumulation of water in the organic layer above the Ah-C, explaining the high water storage capacity in the



Ah horizon below the root zone. At the same time, the thin placic horizon also permits the formation a small proportion of lateral flow above the Ah-C horizons' interface during these periods (as observed in the field). During rainfall events, however, the available pore space in the transition layer was quickly recharged, leading to a fast soil moisture response as in the rooted layer. This response likely results from the exponential soil moisture-matric potential relation of the soils' organic horizon (**Figure 3.2a**) that allows incoming water to fill rapidly the available pore space in the soil matrix (Hasegawa and Eguchi, 2002; Torres et al., 1998). This effect is likely due to the precipitation intensity (<2 mm hr⁻¹), which is generally lower than the vertical K_{sat} of the organic soil horizons (**Table 3.2**), thus enhancing the transfer of hydraulic potentials during rainfall events. A noteworthy difference in this layer was observed between the UP and MP sites. This difference reflects possibly the higher content of mineral and coarse particles at the MP site, as observed in the field and indicated by the higher BD and a lower soil moisture content at saturation compared to the UP site (**Table 3.2**). This factor is also likely responsible for the observed lower moisture (water storage) at the MP site in comparison to the UP site (brown lines in **Figure 3.3b-c**, respectively).

The fast soil moisture dynamics in the underlying mineral layer (from 40-55 cm to 70-80 cm depth) indicate that this layer is quickly recharged by water from the Ah horizon during rainfall events (orange lines in **Figure 3.3b-d**). This hydrological dynamic indicates that despite the aforementioned influence of the placic horizon on the soil water storage above the Ah-C interface, the irregular and discontinuous features of this horizon allow water to transport downwards during rainfall events before reaching the C horizon. The subsequent rapid response of soil moisture in the mineral layer is likely explained by the steep gradient of the water retention curve of the C horizon at high matric potentials (**Figure 3.2b**), similar to that of the organic horizon. This soil moisture-matric potential relation facilitates a rapid transfer of hydraulic potentials through the mineral horizon, which in turn causes a fast soil moisture response to precipitation inputs of water that infiltrated through the Ah horizon during rainfall events (Torres et al., 1998). The observed soil moisture variations, however, occurred at lower water content than those within the Ah horizon. This lower moisture content reflects the lower clay fraction and organic matter content in the mineral horizon, which decreased to about a third to fourth of those in the Ah horizon (**Table 3.1**).

As lateral flow is more prone to be activated under high moisture conditions, hypothetically, if upper hillslope portions would contribute substantial moisture downslope via lateral subsurface flow, a delay in the response times in downhill positions with respect to uphill positions during



rainfall events would be observed. However, the strong synchronization of response times to the peak values of soil moisture and groundwater level along the entire experimental hillslope (i.e., most scatter points in Figs. 4 and 5 plot near the 1:1 ratio) indicates that during rainfall events a dominance of vertical flow paths of water persists. These findings are further supported by soil moisture and groundwater level observations during dry periods (e.g., September-October 2017; **Figure 3.3**). During these periods, not surprisingly, groundwater levels showed a very sharp and steady reduction at faster rates than soil moisture observations did. These findings indicate that the aforementioned hydrological dynamics, enabled by the properties of the Andosol soils, facilitate the vertical percolation of water throughout the year despite the perched layer formed below the rooted zone. Nevertheless, it is worth noting the likely occurrence of lateral subsurface flow in the thin transition zones (<few centimeters) between soil layers with marked differences in hydraulic conductivity (e.g., the transitions between the rooted and perched layers, and the C horizon and the compact bedrock), which I observed during field work, but whose hydrological dynamics could not be captured through the monitoring system used.

3.5.2 Tracer mixing and soil water ages

Precipitation affected greatly the mixing of water in the rooted layer, as evidenced by the little attenuation of the stable isotopic composition of soils water (grey dots in **Figure 3.6**). These observations further indicate that water molecules residing in this soil layer are rapidly replaced by incoming water during precipitation events (Mosquera et al., 2016a), thus explaining the short MTT of water in this soil layer (about 2 weeks at all sampling sites; **Figure 3.7a**, **Table 3.3**).

Past research suggested that a perched water layer in the subsurface implies that vertical percolation in a soil—regolith—bedrock continuum is substantially reduced, while lateral subsurface flow in the overlaying layer is favored (Dykes and Thornes, 2000; Hardie et al., 2012). Thus, solely based on soil moisture observations, I expect that the time water resided in this soil layer was much longer than the one in the fast reacting rooted layer above. Surprisingly, however, results from the SWI data and MTT analyses indicate that the isotopic composition of the water stored in the perched layer is highly influenced by the isotopic composition of precipitation (black dots in **Figure 3.6a,c,e**) and resides in the subsurface for a short time (about a month at all sampling sites; **Figure 3.7b**, **Table 3.3**). Similar MTTs have been previously reported for Andosols in a nearby Páramo catchment at 25 cm depth (35 days;



Mosquera *et al.*, 2016a; Lazo *et al.*, 2019) and in a temperate humid forest catchment in central eastern Mexico at 30 cm depth (36 ± 10 days; Muñoz-Villers and McDonnell, 2012).

The soil water MTTs at this soil horizon increased with depth at each hillslope position, but were consistently similar at each depth among all sampling sites, similar to the vertical aging of water in a tropical forest catchment dominated by Andosol soils (Muñoz-Villers and McDonnell, 2012). The sole vertical aging of soil water indicates that water from upslope areas does not significantly contribute to lower hillslope positions, and thus, that vertical flow paths of water are dominant (Asano et al., 2002; McGuire and McDonnell, 2010; Muñoz-Villers and McDonnell, 2012). These findings are concomitant with the aforementioned fast transfer of hydraulic potentials across the entire organic (andic) horizon of the hillslope soils, being the result from the fast movement of water through the porous soil matrix. Moreover, the transport and mixing of water throughout the whole Ah horizon suggests that the perched layer is hydrologically active, balancing out gains and losses of moisture during rainfall events. This behavior can be explained by the combined effect of two characteristics of the soil. On the one hand, the high content of organic matter and clay of the soil that allow water molecules to be bound to the large surface area of the soil particles. On the other hand, the rapid transport of water through the soil that enables the replacement of stored moisture by "new" water molecules during rainstorms.

Despite the fast transfer of hydraulic potentials from the organic horizon to the mineral horizon during rainfall events, soil water stored within the mineral layer was less influenced by the isotopic composition of incoming precipitation and had longer MTTs (2.8-8.5 months; **Table 3.3**) than in the organic horizon. Similar SWI signals for the mineral layer of Andosols have been reported in a nearby Páramo catchment (Lazo et al., 2019; Mosquera et al., 2016a) and in a tropical forest catchment in Veracruz, Mexico (Muñoz-Villers and McDonnell, 2012). Even though the dominance of rapid infiltration of incoming precipitation across the Ah horizon toward the mineral layer is consistent with the relatively short MTT observed at the LP site (2.8 months), this mechanism cannot explain the longer MTT at the UP site (8.5 months). A potential explanation for the long MTT at the latter could be the reduced lateral inflow at upper hillslope positions within the mineral layer due to smaller upslope contributing area in relation to the downslope sites. This effect could result in an overall lower exchange of the water stored at upslope sampling positions and hence explain (i) the generally longer MTTs of soil water in the mineral layer in relation to the organic horizon and (ii) the longer MTT and slower response times to the peak values of soil moisture during rainfall events (**Figure 3.5g,h**) at the UP site



in comparison to the LP site. The activation of lateral flow paths in this soil layer is likely favored by the compacted underlying geology observed during the excavation of the soil pits.

3.5.3 Volcanic ash soils as wet, layered sloping sponges?

The hydraulic properties of household cellulose sponges were experimentally examined and compared to soils with different characteristics by Richardson and Siccama (2000) to investigate whether the forest hydrology analogy of soils behaving like "sponges" is a fair comparison from a soil physics point of view. Their findings suggested that sponges (O-Cel-O cellulose sponges, 3M) had similar water retention and release characteristics as soils rich in organic matter, i.e., topsoil and peat. The field observations and soil properties characterization suggest that the organic layer of the Andosol soils is able to store large amounts of water and to rapidly transfer hydraulic potentials in a similar manner to the cellulose sponges. Thus, this findings provide novel field evidence to support the experimental observations reported by Richardson and Siccama (2000) and indicate that volcanic ash soils (rich in organic matter and clay) resemble a "sponge-like" hydrological behavior.

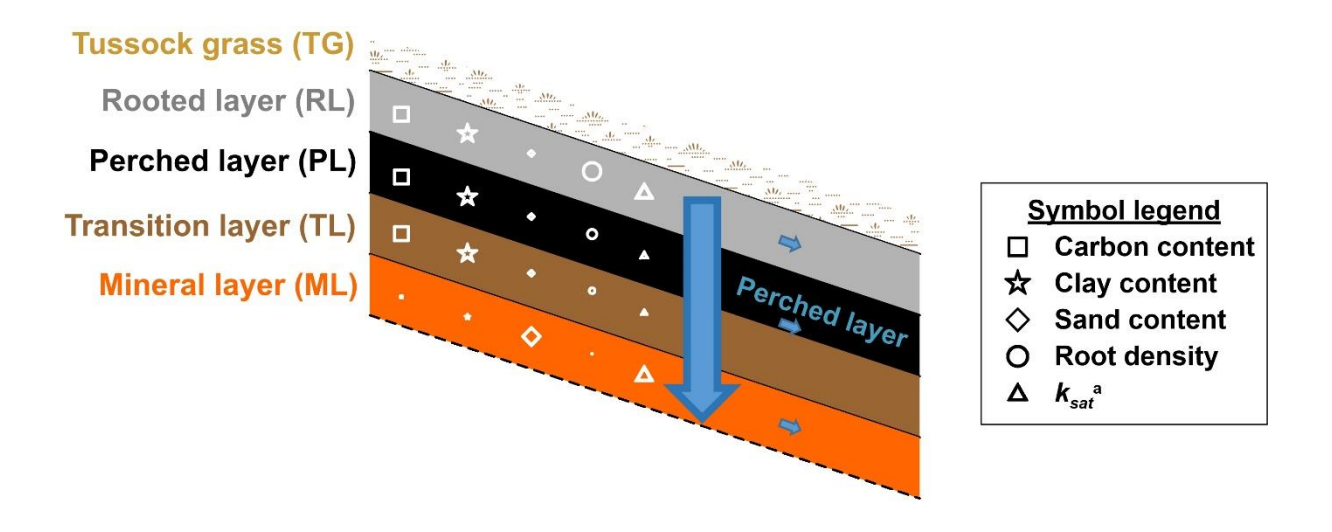


Figure 3.8. "A wet, layered sloping sponge". Conceptual model of the subsurface hydrological system of the experimental hillslope underlain by volcanic ash soils (Andosols) located in the headwaters of the Quinuas Ecohydrological Observatory. The size of the blue arrows represents the relative importance of vertical and lateral flow paths of water at different soil layers. The relative size of the white symbols indicates differences in the magnitude of the soil properties at each of the soil layers (values in Tables 1 and 2). ${}^{a}K_{sat}$ = saturated hydraulic conductivity in the vertical direction.



This natural soil system, however, presents some particularities with respect to the "ideal" sponge behavior. Even though the organic matter and clay content of the organic horizon of the soils are homogenous along the experimental hillslope, K_{sat} decreased consistently with depth at all positions. These factors allow incoming water to rapidly fill and empty the porous matrix of the unsaturated layers with high K_{sat} (the rooted layer), but tend to promote a sustained storage of high amounts of water and to transport it steadily to deeper soil layers with low K_{sat} (the perched layer). The latter phenomenon is also possible at the study site given that precipitation is distributed fairly even throughout the year, with generally low intensity compared to the K_{sat} of the soil, thus maintaining near saturation conditions in the organic layers below the highly conductive root zone. This results in the formation of a "layered sponge" system, in which a fast-conducting organic layer underlain by a lower conductivity layer helps conserve high soil moisture near saturated conditions year-round in the latter (**Figure 3.8**). This situation, in turn, provides water for vegetation throughout the year, creating a positive hydrological service. Even though topography has been found an important factor controlling subsurface flow processes (e.g., Famiglietti et al., 1998; Bachmair and Weiler, 2012), the findings illustrate clearly the dominance of vertical flow paths independent of the position along the steep hillslope. Thus, it is not unlikely that the conceptual system representation can be used to mimic the hydrological functioning of hillslopes dominated by volcanic ash soils with similar to lower slope gradients.

3.6 Conclusions

The experimental evaluation of water transport and tracer mixing helped to conceptualize the subsurface hydrological behavior of a steep experimental hillslope underlain by volcanic ash soils (Andosols). Findings reveal that the behavior resembles that of a "layered sponge" in which vertical flow paths are dominant. That is, on the one hand, the formation of a perched water layer that maintains high moisture near saturated conditions year-round due to the presence of a low conductivity layer below a layer with a higher conductivity. On the other hand, a fast-vertical transport of water due to the rapid transfer of hydraulic potentials along the entire soil profile facilitating water mobilization through the porous soil matrix. Despite the dominance of vertical flow paths, lateral flow likely develops during high intensity rainstorm events above hydraulically restrictive layers (e.g., the perched layer) due to the steep slope of the hillslope. Given that the "sponge-like" hydrological behavior of these soils largely depends on their high organic matter and clay content, the rapid breakdown of the soil organic-mineral components due to changes in land use and climate could cause severe changes in the



hydrological services provided by ecosystems in which these soils dominate. The findings of this study provide crucial information that can be used to improve the representation of the physical processes in hydrological models, which in turn will lead to a better management of the soil and water resources in these ecosystems.



Chapter 4

4. Hydrological behavior of a temperate catchment underlain by volcanic geology

Water-stable isotopic (WSI) data are widely used in hydrological modelling investigations. However, the long-term monitoring of these tracers at high-temporal resolution (sub-hourly) remains challenging due to technical and financial limitations. Thus, alternative tracers that allow continuous high-frequency monitoring for identifying fast-occurring hydrological processes via numerical simulations are needed. I used a flexible numerical flow-partitioning model (TraSPAN) that simulates tracer mass balance and water flux response to investigate the relative contributions of event (new) and pre-event (old) water fractions to total runoff. I tested four TraSPAN structures that represent different hydrological functioning to simulate storm flow partitioning for an event in a headwater forested temperate catchment in Western, Oregon, USA using four-hour WSI and 0.25-hour electrical conductivity (EC) data. Results showed strong fits of the water flux and tracer signals and a remarkable level of agreement of flow partitioning proportions and overall process-based hydrological understanding when the model was calibrated using either tracer. In both cases, the best model of the rainstorm event indicated that the proportion of effective precipitation routed as event water varies over time and that water is stored and routed through two reservoir pairs for event and pre-event. These results provide great promise for the use of sub-hourly monitored EC as an alternative tracer to WSI in hydrological modelling applications that require long-term high-resolution data to investigate non-stationarities in hydrological systems.

Related publication

Mosquera G, Segura C, Crespo P. 2018. Flow Partitioning Modelling Using High-Resolution Isotopic and Electrical Conductivity Data. Water 10 (7): 904 DOI: 10.3390/w10070904



4.1 Introduction

The identification of the water sources contributing to runoff is fundamental to understand the linkage and interactions between water and biogeochemical cycles and the transport of contaminants and solutes at the catchment and landscape scales (Burns and Kendall, 2002; Burt and Pinay, 2005; Hrachowitz et al., 2015; Kendall and McDonnell, 1998). During precipitation events total runoff can be partitioned into event — "new" water from incoming precipitation — and pre-event water — "old" water stored in the catchment prior to a given precipitation event (Buttle, 1994; Klaus and Mcdonnell, 2013). Depending on the catchment conditions (e.g., vegetation, soil type, geology, topography, antecedent moisture) and event characteristics (e.g., precipitation amount and temporal variability) the event and pre-event water fractions vary. As such, understanding the spatial and temporal variability of the contributions of different water pools to the hydrograph is not only a fundamental question in hydrological science (Heidbüchel et al., 2012), but is also needed for the implementation of effective water resources management strategies worldwide (Hrachowitz et al., 2013).

Given that the contribution of different water pools to total runoff is time dependent owing to the time variant nature of flow response processes (Bertuzzo et al., 2013; Birkel et al., 2012; Heidbüchel et al., 2012; Kirchner, 2016; van der Velde et al., 2015), we struggle to apply effective monitoring strategies in catchments with different environmental conditions (Rode et al., 2016). Conservative (e.g., water stable isotopes, ²H and ¹⁸O, and chloride) and nonconservative (e.g., electrical conductivity (EC) and silica) tracers have been used to constrain mixing models of flow partitioning at the event scale (e.g., Hooper, Christophersen, & Peters, 1990; Hooper & Shoemaker, 1986; Kronholm & Capel, 2016; Laudon & Slaymaker, 1997; Uhlenbrook & Hoeg, 2003). One of the most commonly applied methods is tracer-based twocomponent end member mixing analysis (Buttle, 1994; Klaus and Mcdonnell, 2013; Pinder and Jones, 1969; Sklash and Farvolden, 1979) to quantify the proportions of event and preevent water to total runoff using a simple mass balance (cf., Buttle (1994) and Klaus & Mcdonnell (2013) for reviews). However, since these models only account for the mixing of the tracer within a hydrological system, they provide only limited information about the combined flow and tracer mixing dynamics in response to precipitation inputs. Therefore, these models have limited ability to provide a process-based understanding of catchment behavior (Laudon et al., 2004; McDonnell and Kendall, 1992; Rice and Hornberger, 1998).



In response to this challenge, numerical models in which the tracer mass balance and the hydrological flow response are coupled have been developed (Roa-García and Weiler, 2010; Segura et al., 2012; Vaché and McDonnell, 2006; Weiler et al., 2003). These models allow for the simultaneous simulation of the streamflow hydrograph — water flux — and the tracer mixing. In general, these models account for the water flux partitioning by applying the unit hydrograph approach, and the tracer mixing using travel time distributions (TTDs) (Barnes and Bonell, 1996). The application of TTDs accounts for the estimation of the possible travel times of the tracer within the system. That is, the time that a water molecule takes to travel within a hydrological system from the moment it enters as precipitation or snowmelt to the time it exists as runoff (Kirchner et al., 2000; McGuire and McDonnell, 2006). The TTDs shapes are used to identify runoff processes (Heidbüchel et al., 2012; Hrachowitz et al., 2016; Kirchner et al., 2000; Małoszewski and Zuber, 1982) by providing information about the physical processes that influence the internal mixing of different water sources.

Despite the advantages of numerical approaches for hydrograph separation, the availability of long-term high-resolution water geochemical data remains a challenge. To date, the majority of applications of tracer-based hydrograph separation techniques have been conducted using WSIs as tracers (Klaus and Mcdonnell, 2013). Despite their recognized usefulness and reliability (being conservative), WSIs sampling at fine resolution (e.g., sub-hourly) is still sparse given high associated costs and, thus, limits the description of the rapid response of streamflow to water inputs and the inter-storm variation of the input isotopic composition (Brooks et al., 2010; Coplen et al., 2015, 2008; N.C. Munksgaard et al., 2012). This limitation has resulted in high uncertainties in the estimation of flow components (Coplen et al., 2015; McDonnell et al., 1990; N.C. Munksgaard et al., 2012). Recent studies have monitored WSIs at high-temporal resolution (every 30 min) (Berman et al., 2009; Koehler and Wassenaar, 2011; Munksgaard et al., 2011; N. C. Munksgaard et al., 2012; Pangle et al., 2013; Volkmann et al., 2016) and applied simple mixing models to partition flow components (Birkel et al., 2012; Kronholm and Capel, 2016; Tweed et al., 2015; von Freyberg et al., 2017). However, while technological developments currently allow the deployment of field analyzers to measure the WSI of inputs and outputs (e.g., rainfall and streamflow) at high temporal resolution it is unfeasible to broadly implement such analyzers. Thus, there is a need for alternative inexpensive and low maintenance water quality parameters (i.e., tracers) that allow investigating internal catchment processes at a high resolution (Kirchner et al., 2004; Rode et al., 2016).



Electrical conductivity, or specific conductance (EC) of water, is an alternative tracer often used in flow partitioning and water quality studies, either alone or in combination with WSIs (e.g., Nakamura, 1971; Pilgrim *et al.*, 1979; Sklash and Farvolden, 1979; Matsubayashi *et al.*, 1993; Laudon and Slaymaker, 1997; Johnson *et al.*, 2007; Pellerin *et al.*, 2008; Maurya *et al.*, 2011; Penna *et al.*, 2015). The main advantage of using EC is that it can be continuously monitored at high temporal resolution (seconds to minutes) using inexpensive in-stream probes (Kirchner et al., 2004; Matsubayashi et al., 1993; Rode et al., 2016). Despite the nonconservative nature of EC as it highly depends on the water contact time with the mineral substrate in particular (Carey and Quinton, 2005; Mueller et al., 2016; Pilgrim et al., 1979), EC has yielded similar streamflow partitioning results than WSIs using traditional mass balance models (Laudon and Slaymaker, 1997; Pellerin et al., 2008). However, its effectiveness has not been tested against WSI using sophisticated hydrological modeling approaches.

This study compares the results of a flow partitioning tracer-based hydrological model calibrated using WSIs and EC. The specific objectives are: (1) to evaluate different model structures (representing different assumptions of the internal catchment hydrological functioning) and determine the model structure that best simulates flow partitioning using WSI and EC data; and (2) to compare the process-based hydrological understanding obtained from the models calibrated using each tracer.

4.2 Materials and Methods

4.2.1 Study Area

This study was conducted at the Mack Creek catchment (5.8 km²) in the H.J. Andrews Experimental Forest in the Western Cascades of Oregon (**Figure 4.1**). Mack Creek is a tributary of Lookout Creek, which drains into the Blue and McKenzie rivers within the Willamette River Basin. Glaciation occurred in the catchment leaving U-shaped valley morphologies with a steep slope (average 46%). The elevation ranges between 758 and 1610 m a.s.l. (McGuire et al., 2005; Swanson and Jones, 2002). The catchment is underlain by ridge-capping andesite lava flows (upper Sardine Formation and Pliocene flows). The soils in the catchment are gravelly loams at high elevation that transition into the predominantly gravelly sandy loams that characterize over 70% of Mack Creek drainage area (Dyrness et al., 2005). The forest is dominated by 400–500 year-old coniferous trees, including Douglas fir (Psuedotsuga menziesii), western hemlock (Tsuga heterophylla), and western red cedar (Thuja plicata). The climate is Mediterranean with wet, mild winters and dry summers. Fall and winter



precipitation falls as a mix of rain and snow and may accumulate and last from early November to late June (Jennings and Jones, 2015). Mean annual precipitation (between 2002 and 2016) was 2243 and 2709 mm at the CENMET (1018 m a.s.l) and UPMET (1294 m a.s.l) meteorological stations (**Figure 4.1**), respectively. However, precipitation in 2015 — when this study was conducted — was only 51% of this 15-year average and fell almost entirely in the form of rain.

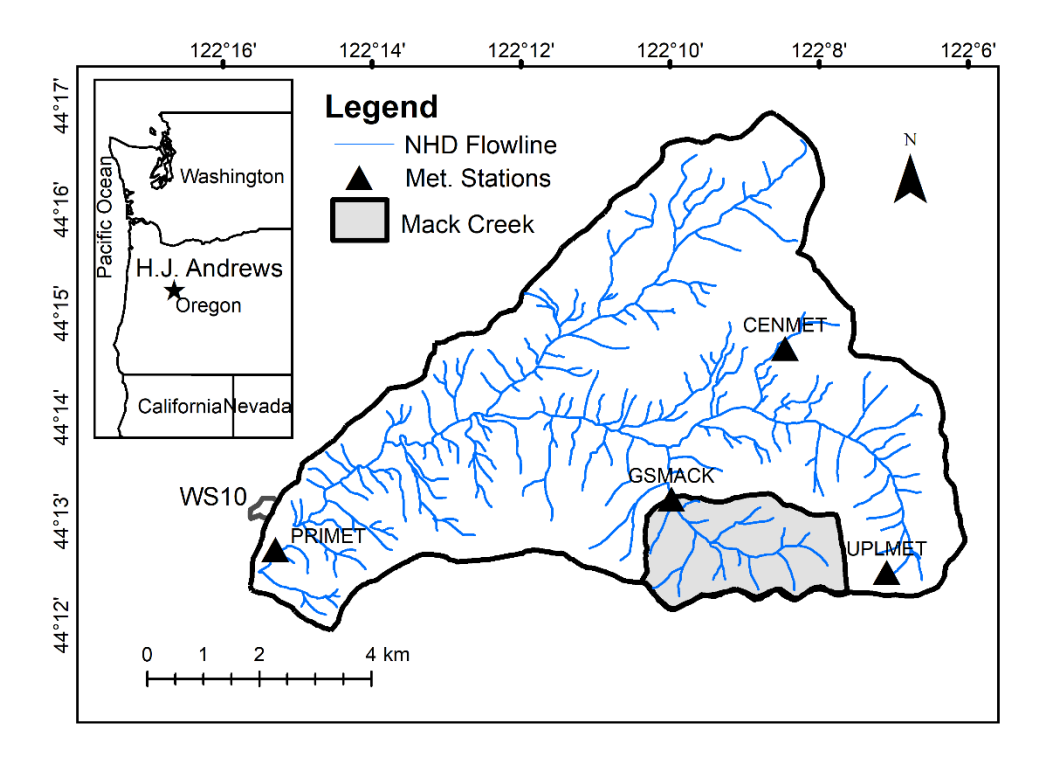


Figure 4.1. Location of Mack Creek Catchment within the H.J. Andrews Experimental Forest in Western Oregon. Black triangles indicate the locations of the meteorological stations (PRIMET, CENMET, and UPLMET) along with the location of the precipitation and stream gauging stations at Mack Creek (GSMACK).

4.2.2 Hydrometric Data Collection

Water fluxes — precipitation (P) and streamflow (Q) — were monitored during a large rainstorm event between 28 October and 7 November 2015. I used 5-min resolution P and Q data maintained as part of the NSF Long-Term Ecological Research (LTER) program (Johnson and Rothacher, 2016). Q data derived from an 18-in flume (GSMACK; **Figure 4.1**) and mean P values across the UPMET station and a precipitation tipping bucket located in the roof top of the GSMACK was used (Daly and Rothacher, 2017). The 8-in diameter GSMACK gauge is heated with a propane heater. Continuous precipitation is recorded with depth measurements using a Stevens A-35 chart recorder or a Stevens PAT water level shaft encoder. The UPMET



precipitation gauge is stand-alone composed of standing pipe with tank gauge, a propane-heated 20-inch diameter orifice, surrounded by a Valdai-style double wind fence. A temperature probe controls the orifice heating by turning a pump and heater on/off. The stand-alone rain gauge was specifically developed to withstand heavy snow with depths up to 3–4 m and windy condition.

4.2.3 Water Stable Isotope Data Collection and Analysis

Streamflow grab samples of 44,500 mL were collected every 4 h using an automatic autosampler (ISCO-3700). A grab sample was also collected before the event in order to characterize the streamflow isotopic composition during base flow conditions (i.e., pre-event). I described the event isotopic signature of precipitation at a meteorological station located at 430 m a.s.l (PRIMET; **Figure 4.1**) with a sequential rainfall sampler designed to collect up to 12 200-mL water samples to characterize the temporal variability of water stable isotopes (Brooks et al., 2010; McGuire and McDonnell, 2010). The sequential collector was located in a clearing, thus, it was assumed that the difference between the isotopic signature of direct rainfall and throughfall was minimal (Allen et al., 2014). All water samples for isotopic analysis were collected and stored in 20 mL glass bottles with conical inserts without headspace and kept in dark at relatively cool conditions (~15°C) to avoid fractionation by evaporation until their analysis was conducted at the Watershed Processes Laboratory at Oregon State University.

The water-stable isotopes (δ^{18} O) in all samples were measured using a cavity ring down spectroscopy liquid and vapor isotopic analyzer (Picarro L2130-i, Picarro Inc, Santa Clara, CA). All samples were run under high precision, including six injections per sample. The first three injections were discarded to account for memory effects. Two internal (secondary) standards (MET1, δ^{18} O= -14.49% and BB1, δ^{18} O= -7.61%) were used to develop calibration curves, while a third internal standard (ALASKA1, δ^{18} O= -11.09%) was used to estimate a drift correction equation (drift was always below 0.000152‰). All internal standards were calibrated against the IAEA primary standards for the Vienna Standard Mean Ocean Water (VSMOW2, δ^{18} O=0.0‰), Greenland Ice Sheet Precipitation (GISP, δ^{18} O=-24.76%), and Standard Light Antarctic Precipitation (SLAP2, δ^{18} O=-55.5%). The uncertainty in the secondary standards (i.e., standard deviation) is<0.01‰. Based on>50 duplicate samples (collected concurrently under comparable conditions) in rainfall and streamflow, an internal laboratory precision of 0.03‰ was estimated. The external accuracy of the laboratory was 0.06‰. This accuracy was computed as the mean difference between 60 estimated values and



a known water standard. Only the internal precision as an overall measure of accuracy was used although it is acknowledged that there are other sources of uncertainty (Dunn and Carter, 2018).

4.2.4 Electrical Conductivity Measurements

The conductance of the sequential water samples collected for the water stable isotopes analysis was measured using a Hanna® Multiparameter (HI9828) Water Quality Portable Meter and used these measurements to characterize the EC of the precipitation during the event. The portable meter was calibrated in the laboratory following manufacture guidelines. The manufacture accuracy of this instrument is 1% or 1 μS/cm (whichever is larger). Replicate measurements for 30 samples indicated a precision of<5%. The EC measurements were conducted after the 20-mL samples for water stable isotopes were collected to avoid sample contamination. Streamflow EC was continuously recorded (every 5 min) at the GSMACK gauge with a Campbell Scientific CS547A EC and temperature probe (with a 5% accuracy; Johnson, 2016). The EC data is corrected with a temperature coefficient based on YSI Pro30 conductivity instrument (Johnson, 2016).

4.2.5 Tracer-Based Hydrograph Separation Modeling

In recent years, different approaches that allow the incorporation of geochemical tracers mixing into hydrological models have been developed. The application of conceptual models using TTD functions (Birkel et al., 2015; Segura et al., 2012; Weiler et al., 2003) and ranked storage-age-selection (rSAS) functions (Harman, 2015) are amongst the most frequently applied approaches. I selected the former approach as it allows for the implementation of different model structures (representing different catchment hydrological behavior) that have been widely tested using WSI for model calibration in other studies and, thus, allow for a direct comparison with these results using both high-resolution WSIs and EC data.

The flexible modelling framework developed by (Segura et al., 2012) that considers both the tracer mass balance and the hydrological flow response during rainfall-runoff events was used. I refer to this model as TraSPAN (Tracer-based Streamflow Partitioning ANalysis model). TraSPAN shares similarities with other tracer-based hydrological models (e.g., Weiler *et al.*, 2003; Roa-García and Weiler, 2010). It allows for the implementation of different model structures to simulate different levels of hydrological complexity, assuming that rainfall-runoff can be partitioned into event and pre-event components. As such, I implemented this framework to evaluate competing hypotheses of hydrological response against observed Q and



tracer data to select the best model structure for the given hydrological system (Clark et al., 2011; Kirchner et al., 2000; Pfister and Kirchner, 2017).



Table 4.1. Modules, equations, and parameters of the four Tracer-Based Streamflow Partitioning Analysis (TraSPAN) model structures.

	Module	Danamatons and Equations	Units	Model Structure			
	Module	Parameters and Equations	Omis	1	2	3	4
		Initial antecedent rainfall index, S_o	-	X	X	X	X
	$P_{\it eff}$	Memory timescale parameter, w	time steps ^d	X	X	X	X
1ª		$P_{eff}(t) = p(t)s(t)$; Equation (1)					
Е	Equations	$s(t) = c \cdot p(t) - s(t - \Delta t) \left(1 - \frac{1}{w}\right)$; Equation (2)					
		where p is precipitation and c is the normalization constant to maintain $\sum P_{eff} = \sum Q$					
	f, constant	Fraction of effective rainfall routed as event water, f	-	X	X		
a h	f, variable	Normalization constant, c_f	15- min/m m			X	X
2 ^b	J,	Memory timescale parameter, w _f	time steps ^d			X	X
	Equations	$f(t) = c_f \cdot p(t) - f(t - \Delta t) \left(1 - \frac{1}{w_f}\right)$; Equation (3)					



Table 4.1 Cont.

Madula	Donomotous and Escations	T I 24 cc	Model Structure			
Module	Parameters and Equations	Units	1	2	3	4
	Mean transit time of event water, k_e	h	X		X	
Single Reservoir	Time delay for the event fraction response, e_{lag}	h	X		X	
Single Reservoir	Mean transit time of pre-event water k_p	h	X		X	
-	Time delay for the pre-event fraction response, pl_{ag}	h	X		X	
	$Q_e(t) = \int_0^t h_e(\tau) P_{eff}(t-\tau) f(t-\tau) d\tau$; Equation (4)					
	$Q_p(t) = \int_0^t h_p(\tau) P_{eff}(t-\tau) [1 - f(t-\tau)] d\tau$; Equation (5)					
	$he(\tau) = e_{lag} - \frac{1}{k_e} \exp\left(\frac{\tau}{k_e}\right)$; Equation (6)					
Equations	$hp(\tau) = p_{lag} - \frac{1}{k_n} \exp\left(\frac{\tau}{k_n}\right)$; Equation (7)					
	$C_t(t) = \frac{Q_e(t) C_e + Q_p(t) C_p}{Q_o + Q_h}$; Equation (8)					
	where C_e is the tracer composition of event water (rainfall) and C_p is the tracer composition in pre-event					
, с	water (e.g., baseflow prior to the rainstorm).					
	Fraction of water routed into the fast-responding reservoir of event water, q_e	-		X		Σ
	Mean transit time of the fast fraction of event water, k_{fe}	h		X		7
	Mean transit time of the slow fraction of event water, k_{se}	h		X		2
Two Parallel	Time delay for the event fraction response, e_{lag}	h				
Reservoirs	Fraction of water routed into the fast-responding reservoir of pre-event water, q_p	-		X		2
	Mean transit time of the fast fraction of pre-event water, k_{fp}	h		X		2
	Mean transit time of the slow fraction of pre-event water, \vec{k}_{se}	h		X		2
	Time delay for the pre-event fraction response, pl_{ag}	h		X		2
Equations	$he(\tau) = -\frac{q_e}{k_{fe}} \exp\left(-\frac{\tau - e_{lag}}{k_{fe}}\right) + \frac{1 - q_e}{k_{se}} \exp\left(\frac{\tau - e_{lag}}{k_{se}}\right)$; Equation (9)					
	$hp(\tau) = \frac{q_p}{k_{fp}} \exp\left(-\frac{\tau - p_{lag}}{k_{fp}}\right) + \frac{1 - q_p}{k_{sp}} \exp\left(\frac{\tau - p_{lag}}{k_{sp}}\right); \text{ Equation (10)}$					
	Equations (4), (5) and (8) are also used here.					
	Total number of parameters		7	11	8	1

^a Module 1: Effective rainfall module; ^b Module 2: Event and pre-event routing module; ^c Module 3: Event and pre-event transfer functions module; ^d 15 min time steps.



TRaSPAN is composed of three modules (**Table 4.1**). Module 1: The effective rainfall module is a non-linear routine that computes the effective rainfall (P_{eff}) as the product of precipitation (P) and the antecedent rainfall index (s) (Equations (1) and (2) in Table 4.1; Jakeman and Hornberger, 1993). Module 2: The event and pre-event routing module defines the fraction Peff routed as either event or pre-event water. Module 3: The Event and pre-event transfer functions module includes the TTDs to convolve the fractions of event and pre-event water and, thus, represents the internal hydrological behavior of the system. Modules 2 and 3 are flexible, allowing for the fraction (f) of Peff routed as event water to be constant or time-variant (i.e., to vary over the duration of the event; Equation (3) in **Table 4.1**) and for the incorporation of TTDs of varying degrees of complexity into the convolution integrals for event ant pre-event water (Equations (4) and (5)). Even though there exists a variety of theoretical TTDs that could represent tracer mixing in hydrological models, two of the most commonly applied TTDs that have been tested to represent hydrological systems in other catchments were selected (Muñoz-Villers and McDonnell, 2012; Timbe et al., 2014; Weiler et al., 2003). These are the exponential model (EM; Maloszewski and Zuber, 1996) representing a single linear reservoir (Equations (6) and (7) in **Table 4.1**) and the two-parallel linear reservoirs model (TPLR; (Weiler et al., 2003) representing two connected linear reservoirs (Equations (9) and (10) in Table 4.1). A detailed description of the model framework and its modules can be found in Segura et al. (2012). The tracer signal was also allowed to vary 10% around the concentration measured before the event to account for the uncertainty in pre-event water composition.

The fractions of event and pre-event water are routed according to the given TTD for $he(\tau)$ and $hp(\tau)$ (**Table 4.1**, **Figure 4.2**) and the resulting event (Q_e) and pre-event (Q_p) fractions are used to calculate the tracer concentration based on a mass balance approach (Equation (8), **Table 4.1**). Total discharge (Q_t) is the sum of event and pre-event water plus the baseflow (Q_b), which was subtracted from the input data prior to the modelling. The discharge prior to the beginning of the rainfall event was defined as Q_b . All the parameters in the model were estimated by the simultaneous calibration of the streamflow and tracer data (Segura et al., 2012).

Four TraSPAN model structures were explored of varying complexity depending on the treatment of the fraction of P_{eff} routed as event water and the number of reservoirs used to route the event and pre-event water fractions (**Figure 4.2**). The number of parameters fitted in each of the four model structures varied between 7 and 12 (**Table 4.1**). Structure 1 had a constant fraction f of P_{eff} routed as event water and a single reservoir for each of the event and pre-event water components (seven parameters). Structure 2 also had a constant fraction f, but two



reservoirs in parallel for routing the event and pre-event water components (11 parameters). Structure 3 had a time-variant fraction f(t) of P_{eff} routed as event and pre-event water and a single reservoir for each of the event and pre-event water components (8 parameters). Structure 4 also had a time-variant fraction f(t), but two reservoirs in parallel for each of the event and pre-event water components (12 parameters). For all the model structures, Q, $\delta^{18}O$, and EC data were computed every 15 min.

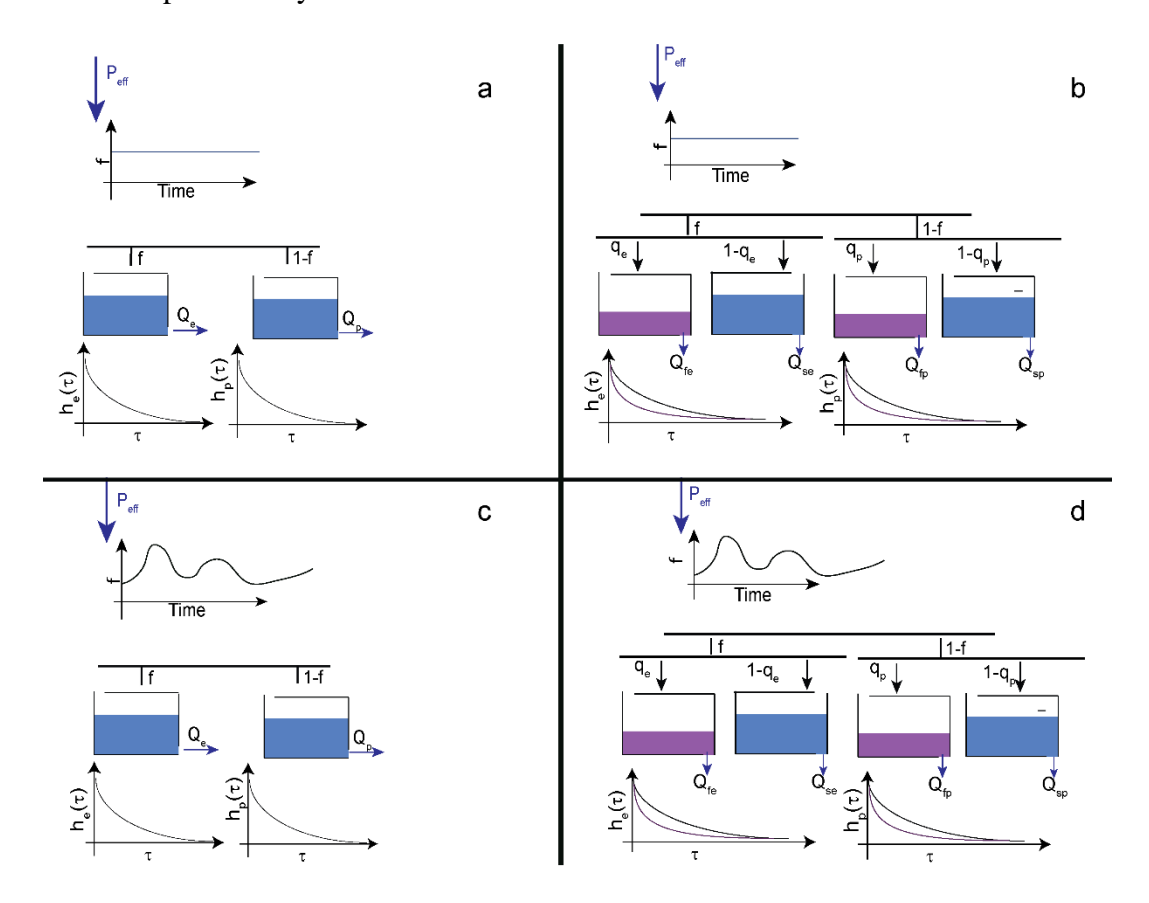


Figure 4.2. Assumptions in TRaSPAN model structures (a) constant fraction of effective precipitation (P_{eff}) routed as event water and a single reservoir for the event and pre-event runoff components (structure 1); (b) constant fraction of P_{eff} routed as event water and two reservoirs in parallel for the event and pre-event runoff components (structure 2); (c) time-variable fraction of P_{eff} routed as event water and a single reservoir for the event and pre-event runoff components (structure 3); and (d) the time-variable fraction of P_{eff} routed as event water and two reservoirs in parallel for the event and pre-event runoff components (structure 4).

4.2.6 Model Simulations, Performance, and Uncertainty

Initially, each of the model structures was ran per tracer 80 million times within a broad range of Monte Carlo-generated parameter values from uniform distributions (**Table 4.2**). The Nash-Sutcliffe efficiency (NSE) coefficient (Nash and Sutcliffe, 1970) was used during the calibration always considering the average NSE for the fits of Q and either δ^{18} O or EC. In order to improve the identification of parameters each model structure was ran 20 million additional



times using a narrower range of parameters corresponding to those that yielded a NSE of at least 80% of the maximum NSE during the first run. Given that structure 4 had a larger number of calibrated parameters, a third model run for 10 million additional times considering the values of the parameters that yielded NSE values of at least 90% of the maximum NSE of the second run as initial parameter ranges was conducted (Mosquera et al., 2016b).

Overall model performance was evaluated using the NSE as a measure of goodness of fit, and the Akaike information criterion (AIC; Akaike, 1974) — using the χ^2 statistic as the likelihood (Bevington and Robinson, 2003) — as a measure of model parsimoniousness. This was necessary considering the different number of parameters of the considered model structures (**Table 4.1**). I considered the sum of AICs for the Q and tracer data. Given that the χ^2 test requires the uncertainty in the observations, it was quantified for Q, δ^{18} O, and EC. The uncertainty in the discharge was calculated as the sum of the uncertainty associated with the stage measurements and the uncertainty associated with the rating curve. The stage uncertainty was estimated to be less than 1.2 mm considering both the instrumentation precision and observed bias. The uncertainty in the rating curve was assessed by conducting 10,000 Monte Carlo simulations, in which its parameters were randomly varied. This uncertainty varied between 0.9% and 4.31% with an average of 3.2%. The total Q resulting uncertainty for the monitored storm varied between 2% and 14%. The uncertainty in δ^{18} O was estimated to be 0.03% (Section 3.4) and the uncertainty in EC was assumed to be 5%, considering the precision of the instrument.

I evaluated the uncertainty in the model parameters based on the results of their last run using a threshold of behavioral solutions. This threshold of behavioral solutions was set up to include parameter sets that yielded NSEs above 0.70 (for model structures 1 and 3) and above 0.75 (for model structures 2 and 4). In all cases, there were>5,000 behavioral sets. The difference in threshold results from the larger number of simulations for models 1 and 3 that would have been required in order to get 5,000 parameter sets with NSE>0.75.



Table 4.2. Parameter sets that yielded the highest NSEs values for each TraSPAN model structure and tracer used for calibration.

Model	Tracer	Module 1			Module 2				Module 3								
Model Structure			So	w	f	c_f	w_f	<i>ke</i> (h)	<i>e</i> lag (h)	k_p (h)	P _{lag} (h)	q_e	k_{fe} (h)	$k_{se}\left(\mathbf{h}\right)$	q_p	k_{fp} (h)	k_{sp} (h)
1	$\delta^{18}O$	Min	0.00	1.00	0.17			15.06	0.00	13.98	0.00						
		Max	1.00	400.00	0.33			55.84	5.75	74.26	3.75						
		Best	0.99	4.03	0.28			28.18	0.25	34.07	0.00						
	EC	Min	0.00	11.03	0.16			15.96	0.00	12.67	0.00						
		Max	0.75	399.98	0.24			50.53	3.75	49.47	2.75						
		Best	0.01	390.44	0.20			21.19	0.25	19.64	0.25						
2	$\delta^{18}O$	Min	0.00	1.00	0.15				0.00		0.00	0.00	0.03	16.24	0.00	0.03	6.31
		Max	1.00	400.00	0.37				6.00		4.50	1.00	49.87	250.0	1.00	49.99	250.0
		Best	0.65	6.60	0.25				0.75		0.25	0.66	16.66	128.7	0.15	6.35	47.23
	EC	Min	0.00	1.09	0.13				0.00		0.00	0.00	0.25	17.82	0.00	0.11	5.75
		Max	1.00	400.00	0.27				5.25		4.25	1.00	47.78	250.0	1.00	46.99	250.0
		Best	0.01	190.67	0.19				0.75		1.00	0.69	6.18	122.1	0.66	4.89	208.8
3	$\delta^{18}O$	Min	0.00	1.00		0.01	1.01	17.83	0.00	18.23	0.00						
		Max	1.00	39.99		0.19	39.99	43.40	2.00	72.50	3.75						
		Best	0.08	24.90		0.02	21.33	26.10	0.00	30.61	0.00						
	EC	Min	0.00	1.00		0.01	1.00	22.80	0.00	17.50	0.00						
		Max	1.00	40.00		0.15	40.00	64.50	6.50	64.84	3.25						
		Best	0.75	2.50		0.02	12.45	37.63	0.25	35.53	0.25						
4	$\delta^{18}O$	Min	0.00	1.02		0.01	1.23		0.00		0.00	0.06	1.06	22.9	0.02	1.25	20.77
		Max	1.00	39.98		0.14	39.99		2.25		3.25	1.00	31.30	249.8	1.00	49.54	250.0
		Best	0.31	39.63		0.01	34.95		1.00		0.50	0.48	6.24	45.00	0.31	6.57	44.26
	EC	Min	0.00	1.01		0.01	1.00		0.00		0.00	0.00	0.24	27.2	0.00	0.04	13.60
		Max	1.00	40.00		0.16	39.98		3.25		3.00	1.00	49.95	250.0	1.00	38.49	249.9
		Best	0.11	21.03		0.01	32.75		0.00		0.00	0.63	20.62	140.6	0.27	3.84	59.94



4.2.7 Comparison of Model Simulations for $\delta^{18}O$ and EC

Once the model structure that best simulated the observed Q and tracer data when calibrated for both tracers (δ^{18} O and EC) was selected, I compared the results in terms of their capability to simulate the Q and tracer data observations, their distribution and ranges of behavioral parameters, and their TTDs. The TTD comparison, which provides information about the mixing and transport processes within the hydrological system, allowed for a direct comparison of the hydrological behavior determined by the model structures using each tracer.

4.3 Results

4.3.1 Hydrometric and Tracer Characterization

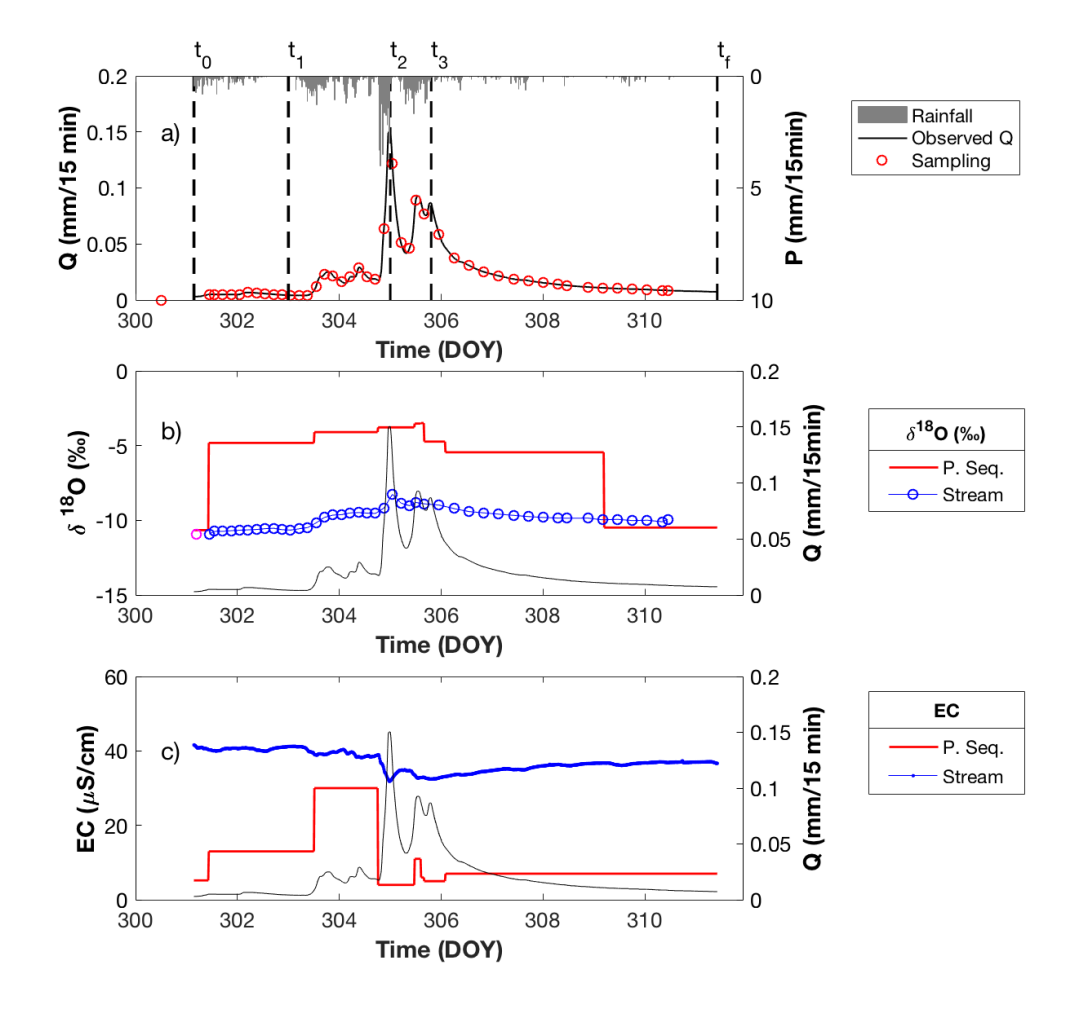


Figure 4.3. Temporal variability of the hydrometric and tracer data during the event monitored between 28 October and 7 November 2015 at Mack Creek. (a) Rainfall (P), runoff (Q), and sample collection times. Vertical dashed lines $(t_0 - t_f)$ indicate periods described in Section 4.3.1; (b) δ^{18} O in stream and P; and (c) electrical conductivity (EC) in stream and P.



The monitored rainfall-runoff event lasted for 10 days and 6.5 h ($t_0 - t_f$ in **Figure 4.3a**). During this period, total precipitation (in the form of rain; P) and total runoff (Q) reached 155.1 mm and 20.6 mm, respectively. These values corresponded to a runoff coefficient (Q/P) of 0.13. During the first 44.5 h ($t_0 - t_1$), total P was 19.9 mm with a mean intensity of 0.45 mm h⁻¹. This period was characterized by little response in the hydrograph. Subsequently ($t_1 - t_2$), Q started to increase in response to P inputs of higher intensity (0.95 mm h⁻¹). At t2 (92.5 h since t0) Q reached its maximum after a total P amount of 107.4 mm. Later ($t_2 - t_3$), the recession of the hydrograph started as P intensity decreased to 0.30 mm h⁻¹. Then, at t_3 , the last Q peak occurred 112 h after the beginning of the event. By this time, total P was 140.7 mm. Between t_3 and the end of the event (t_f), P almost completely ceased, and the hydrograph recession proceeded. During this last period ($t_3 - t_f$), total P was 14.4 mm with a mean intensity of 0.06 mm h⁻¹.

The temporal dynamics of the δ^{18} O and EC signals of P and O are shown in **Figure 4.3b** and 3c respectively. The δ^{18} O of P (δ^{18} O) at to (baseline signal) was the lowest during the event (-10.66 %) and started increasing as P inputs increased (**Figure 4.3b**). The δ^{18} O signal peaked at -3.5% in the water sample collected a few hours before the Q peak at t₃. After this time, during the recession of the hydrograph, the δ^{18} O decreased to the baseline value in the sample collected at the end of the event (t_f). Similarly, the EC signal in P (EC_P) started at a low baseline value of 5.2 μ S cm⁻¹, and increased as P inputs increased (**Figure 4.3c**). The EC_P peaked at a value of 30 µS cm⁻¹ in the sample collected a few hours before the highest peak of the hydrograph at t². After this period, EC_P decreased near the baseline value, and then peaked again (as δ^{18} O did) in the sample collected before the last Q peak (around t₃) with a value of 11 µS cm⁻¹. Then, EC_P decreased to the baseline value during the recession of the O as P inputs decreased until the end of the event (t_f). The temporal variability in the O δ^{18} O (δ^{18} O₀) was smaller (-10.92% to -8.3%; **Figure 4.3b**) than the variability observed in $\delta^{18}O_P$. The $\delta^{18}O_O$ showed a pattern related to the hydrograph, i.e., $\delta^{18}O_0$ increased as Q increased, and vice versa, in response to the dynamics of P. Similarly, the temporal change of EC in Q (EC₀) was lower $(31.8-41.6 \mu \text{S cm}^{-1}; \text{ Figure 4.3c})$ than EC_P. The EC_O variability was the mirror image of the $\delta^{18}O_0$ signal, i.e., when the $\delta^{18}O_0$ signal (and Q) increased, the EC₀ signal decreased, and vice versa (the r^2 between EC and $\delta^{18}O$ is 0.69). The Q values of the pre-event water fraction were -10.92% for δ^{18} O and $41.0 \text{ }\mu\text{S cm}^{-1}$ for EC.

4.3.2 Model Performance

A summary of the parameter values that yielded the highest NSEs and the statistics of the calibration model performance for the four structures using each tracer are presented in Tables



2 and 3 respectively. In general, all model structures using both tracers yielded strong fits (NSE>0.79) to the observed Q and tracer data (**Table 4.3**). The highest NSEs were obtained using model structures 2 and 4 (NSE = 0.87) for δ^{18} O and model structure 4 (NSE = 0.90) for EC. The evaluation of the models structures' parsimoniousness showed that the variation of the AIC values for Q (10,747–22,581) was higher than the variation of the AIC values for the tracers (213–1025) among the different model structures (**Table 4.3**). Even though model structure 4 had the largest number of fitting parameters, the sum of the AIC values for Q and the tracers (Σ AIC) showed that this model structure yielded the lowest values for both δ^{18} O (Σ AIC = 12,238) and EC (Σ AIC = 10,992).

Table 4.3. TraSPAN model performance in terms of the mean Nash–Sutcliffe efficiency (NSE) for discharge and tracer concentrations and the Akaike Information Criterion for discharge (AIC_Q) and tracer (AIC_T, i.e., δ^{18} O or EC) values.

Tracer	Model Structure	Pre-Event Fraction (%)	NSE	AICQ	AICT	ΣAIC *
$\delta^{18}O$	1	71.7	0.86	20,762	644	21,405
	2	76.2	0.87	16,987	514	17,501
	3	76.3	0.81	21,563	1025	22,589
	4	74.9	0.87	11,390	849	12,238
EC	1	79.6	0.79	20,762	448	21,209
	2	79.5	0.86	15,517	379	15,896
	3	81.7	0.86	22,581	213	22,793
	4	81.0	0.90	10,747	245	10,992

Note: Bold values indicate the best model structure considering NSE or AIC. * Σ AIC = AIC_Q + AIC_T.

4.3.3 Modelled Streamflow Partitioning

The fitted hydrographs using TRaSPAN model structure 1 (**Figure 4.2a**) for δ^{18} O and EC (**Figure 4.4a,d**) poorly resembled the temporal dynamics of Q during the monitored event. In general, the model was not able to reproduce the Q peak responses to P inputs, or the recession limbs of the hydrographs. This was particularly noticeable during the highest Q peak and rapid recession of the hydrograph on DOY 305 and by the overestimation (DOY 306–308) and underestimation (DOY 308–311) of Q during the recession limb of the hydrograph. Similarly, this model structure poorly reproduced the δ^{18} O_Q and EC_Q temporal variability during the event. The structure could not resemble the δ^{18} O_Q tracer signal dynamics at the beginning of the event (DOY 301–303) and the enriched isotopic composition during the highest Q peak response on DOY 306 (**Figure 4.4b**). During the remaining of the event, the tracer signal was better captured within the uncertainty bands of the simulations. Regarding the EC_Q temporal dynamics, the model simulations were even weaker (**Figure 4.4e**). The model poorly



reproduced this tracer's signal at the beginning of the event (DOY 301–304), during the highest Q peak response (DOY 305), and during the last part of the event's recession limb (DOY 311). The pre-event water fractions estimated using this model structure were 71.7 % for δ^{18} O and 79.6% for EC (**Table 4.3**) and the temporal dynamics of the event and pre-event water contributions to total Q are shown in **Figure 4.4c,f**, respectively. These fractions depicted similar overall model results using both tracers. These simulations also indicated an over prediction of the pre-event water fraction (i.e., $Q_e>100\%$) at the beginning of the event with δ^{18} O (DOY 301–302; **Figure 4.4c**) and at the first part of the recession limb (DOY 306–308; **Figure 4.4d**) with EC. Similar results were found for model structure 3 (time-variant fraction of P_{eff} routed as event water and single reservoirs for event and pre-event; **Figure 4.2c**). For this structure, the implementation of the time-variant routine for the fraction of P_{eff} routed as event water did not improve the simulations of the hydrograph and the temporal variation of the tracers (**Figure S2**). The pre-event water fractions estimated using this model structure were 76.3% for δ^{18} O and 81.7% for EC (**Table 4.3**) and the temporal dynamics of the event and pre-event water contributions to total Q were similar using both tracers (**Figure S2c,f**).

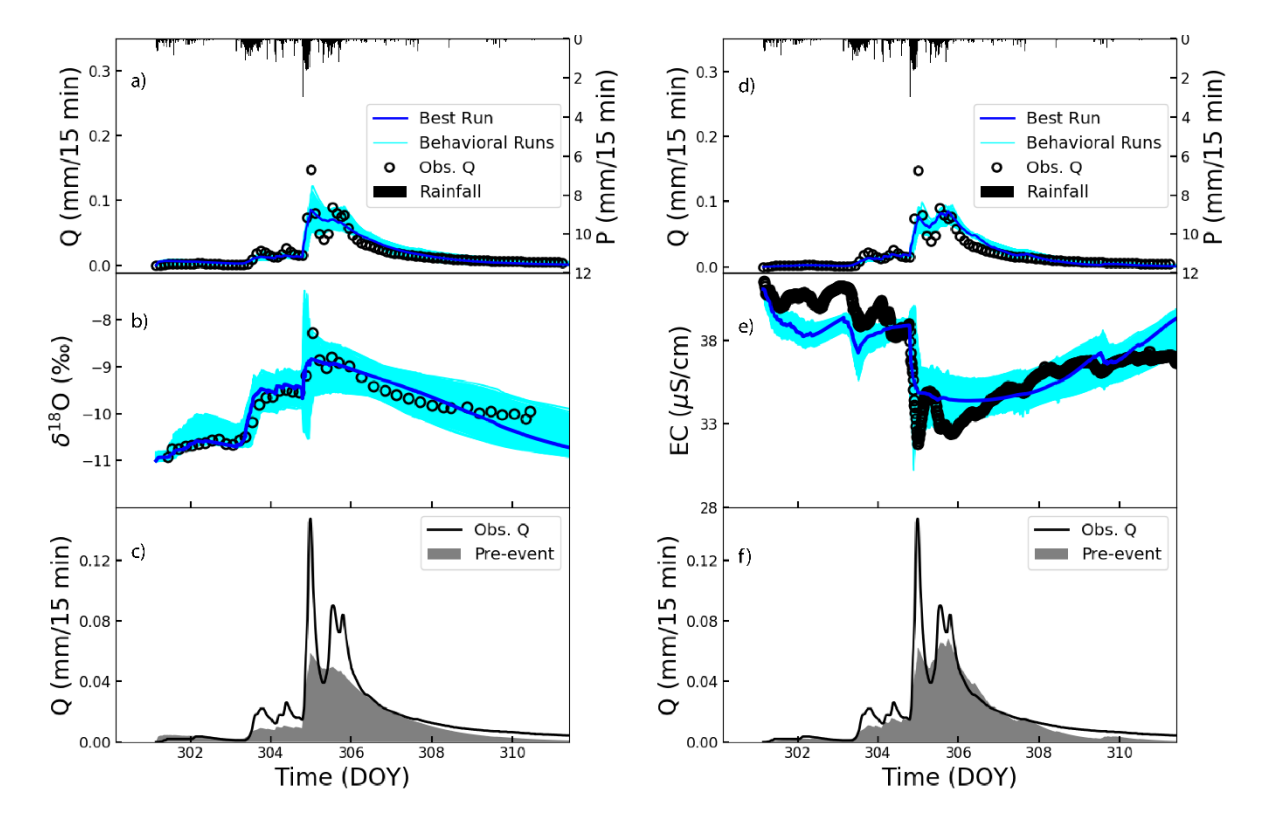


Figure 4.4. TraSPAN modelling results of the hydrograph separation using structure 1 with $\delta^{18}O$ (a–c) and electrical conductivity (EC) (d–f) as tracers for calibration. (a,b,d, and e) show the observed (open markers) and simulated streamflow and tracer data according to at least 100 different sets of parameters (light blue lines) yielding Nash–Sutcliffe efficiencies (NSEs) above 0.70 (behavioral parameter sets). The simulated times series with the set of parameters that yielded the highest NSEs are depicted in dark blue lines in all cases. (c and f) present the preevent water (gray shaded area) and the event water (unshaded area) contributions during the storm corresponding to the set of parameters yielding the highest NSEs.

The simulation results using TRaSPAN model structure 4 (i.e., the time variant fraction of P_{eff} routed as event water and two connected reservoirs for event and pre-event water; **Figure 4.2d**) showed that this structure better captured the temporal dynamics of Q using both tracers. All peaks (e.g., the highest peak produced on DOY 305) and the recession (DOY 306–311) of the hydrograph were well simulated by this model structure using $\delta^{18}O$ (**Figure 4.5a**) and EC (**Figure 4.5d**). Similarly, the temporal dynamics of the tracers' signal were well simulated by this model structure. Even though this model structure underestimated the $\delta^{18}O_Q$ enrichment (**Figure 4.5b**) and overestimated the decrease in EC_Q (**Figure 4.5e**) on DOY 304; the most enriched $\delta^{18}O_Q$ and the lowest EC_Q peak values (DOY 305), as well as the rest of the tracer dynamics, fitted the observed data well. The estimated proportions of pre-event water were 74.9% using $\delta^{18}O$ and 81% using EC (**Table 4.3**). The temporal variability of the pre-event water contributions were similar using $\delta^{18}O$ (**Figure 4.5c**) and EC (**Figure 4.5f**) and showed a dominance of pre-event water contributions, even during the peak Q generation.



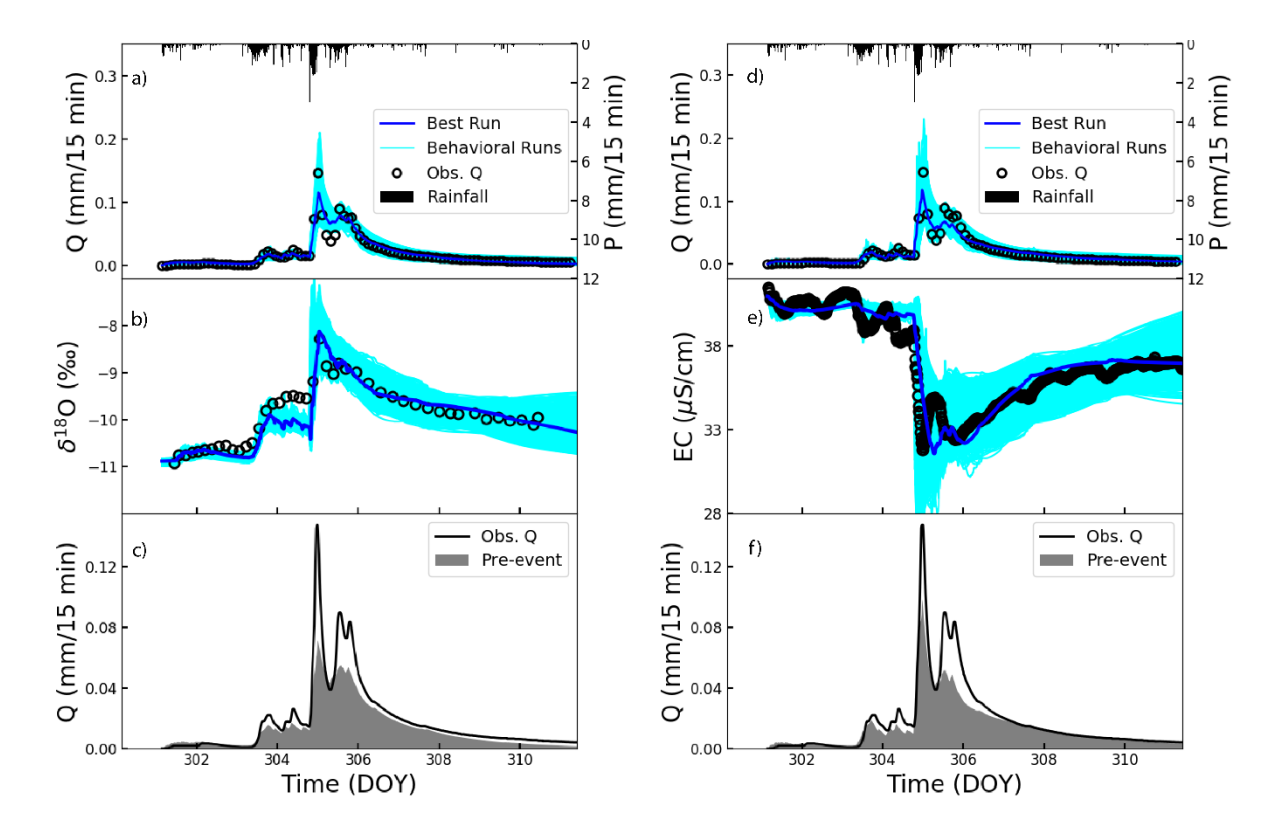


Figure 4.5. TraSPAN model results of the hydrograph separation using structure 4 calibrated with $\delta^{18}O$ (a–c) and electrical conductivity (EC) (d–f) as tracers. (a,b,d, and e) present observed (open markers) and simulated streamflow and tracer data according to all parameter sets (blue lines) that yield a Nash–Sutcliffe coefficient above 0.75 (behavioral parameter sets). The best simulated times series in both cases are depicted in dark blue lines. (c and f) present the preevent water (gray area) and the event water (white area) contributions during the storm, according to the best set of parameters.

Even though structure 2 (i.e., the constant fraction of P_{eff} routed as event water and two connected reservoirs for event and pre-event; **Figure 4.2b**), simulated the hydrograph better than structures 1 and 3 using both tracers (e.g., it captured the Q peaks better), it still had issues simulating the peak hydrograph response compared to structure 4, particularly when calibrated using $\delta^{18}O$ (**Figure S1a,b**). Structure 2 also had issues replicating the $\delta^{18}O_Q$ (**Figure S1c**) and EC_Q (**Figure S1d**), particularly when calibrated using EC during the rising limb of the hydrograph. The pre-event water fractions estimated using this model structure were 76.2% for $\delta^{18}O$ and 79.5% for EC (**Table 4.3**). However, in contrast to all of the other model structures, the temporal dynamics of the event and pre-event water contributions to total Q were different using both tracers. This structure tended to estimate lower pre-event water contributions during the rising limb of the hydrograph and higher pre-event water contributions during the recession when calibrated using $\delta^{18}O$ (**Figure S1c**). An opposite trend was observed when calibrated for EC (**Figure S1f**).



4.3.4 Model Parameter Identification for the Best Model Structure

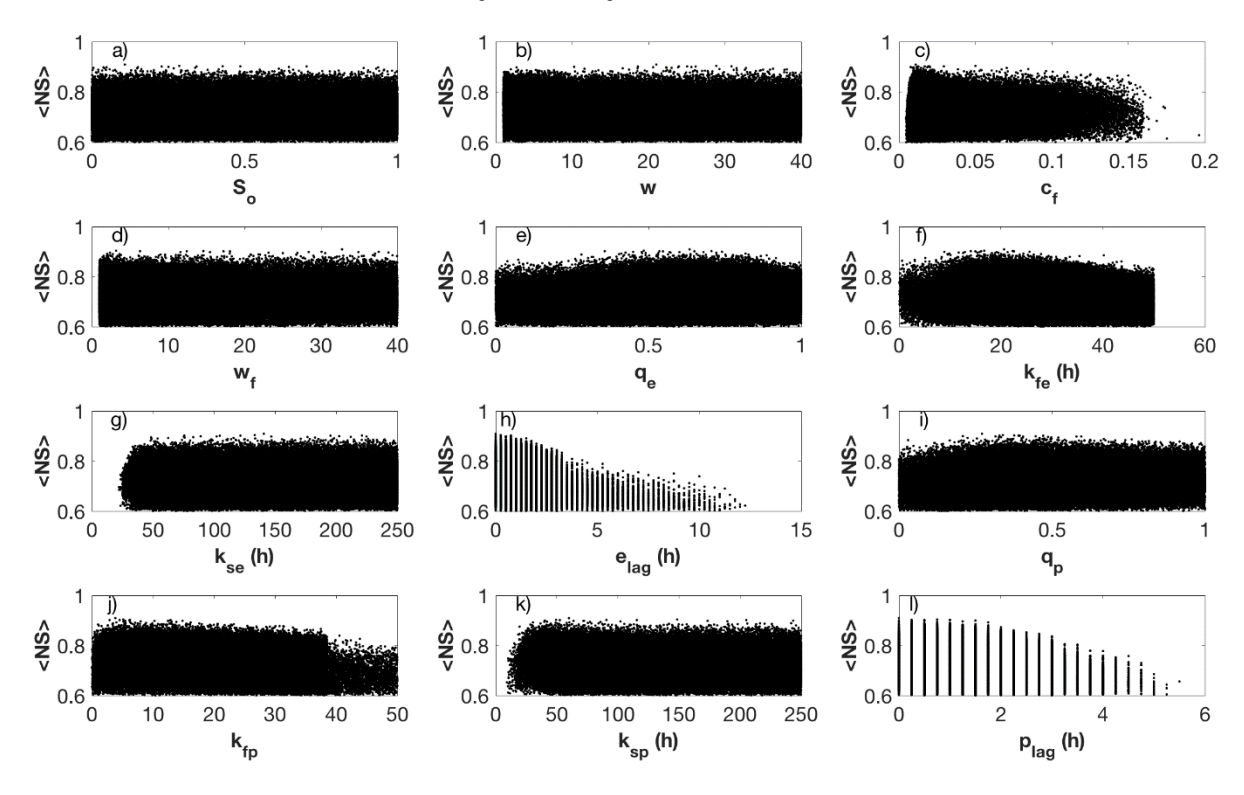


Figure 4.6. Dotty plots of the Monte Carlo simulations for the calibrated parameters using TraSPAN model structure 4 using electrical conductivity (EC). Parameter names are shown in **Table 4.1**.

According to the dotty plots (i.e., values of the NSE as a function of the calibrated parameters for a given model run), seven of the 12 parameters of model structure 4 using EC for calibration reached a single peak in the parameter space yielding the highest NSE (**Figure 4.6**). These parameters were: the normalization constant (cf = 0.01; **Figure 4.6c**; **Table 4.2**) of module 2 and the fraction of water routed into the fast-responding reservoir of event water ($q_e = 0.63$; **Figure 4.6e**), the mean transit time (MTT) of the fast fraction of event water ($k_{fe} = 20.62$ h; **Figure 4.6f**), the time delay for the event fraction response ($e_{lag} = 0$ h; **Figure 4.6h**), the fraction of water routed into the fast-responding reservoir of pre-event water ($q_p = 0.27$; **Figure 4.6i**), and the MTT of the fast fraction of pre-event water ($k_{fp} = 3.84$ h; **Figure 4.6j**), and the time delay for the pre-event fraction response ($p_{lag} = 0$ h; **Figure 4.6l**) of module 3. Both parameters of module 1 (So; **Figure 4.6a** and w; **Figure 4.6b**), the memory timescale parameter (wf) of module 2 (**Figure 4.6d**), and the slow fractions of event (k_{se} ; **Figure 4.6g**) and pre-event (k_{sp} ; **Figure 4.6k**) water of module 3 showed equifinality (Beven and Freer, 2001). That is, these parameters did not reach a single peak associated to the highest NSE in their parameter space distributions. The distributions of the model parameters for model structure 4 calibrated using



 δ^{18} O was similar (**Figure S9**) and the ranges of calibrated parameters using both tracers were in strong agreement (**Figure 4.7**).

Similar results were found for model structure 2 using EC for calibration. For this structure, the module 3 parameters q_e , k_{fe} , e_{lag} , q_p , k_{fp} , and p_{lag} , as well as the constant fraction of effective rainfall routed as event water parameter f (module 2) reached a single peak in the parameter space yielding the highest NSE (i.e., seven out of 11 parameters; **Figure S6**). However, even tough for the same model structure calibrated using δ^{18} O, the parameters q_p and k_{fp} did not reach a single peak in the parameter space (i.e., only five out of 11 parameters did; **Figure S5**), the ranges of calibrated parameters using both tracers were in agreement (**Figure S11**).

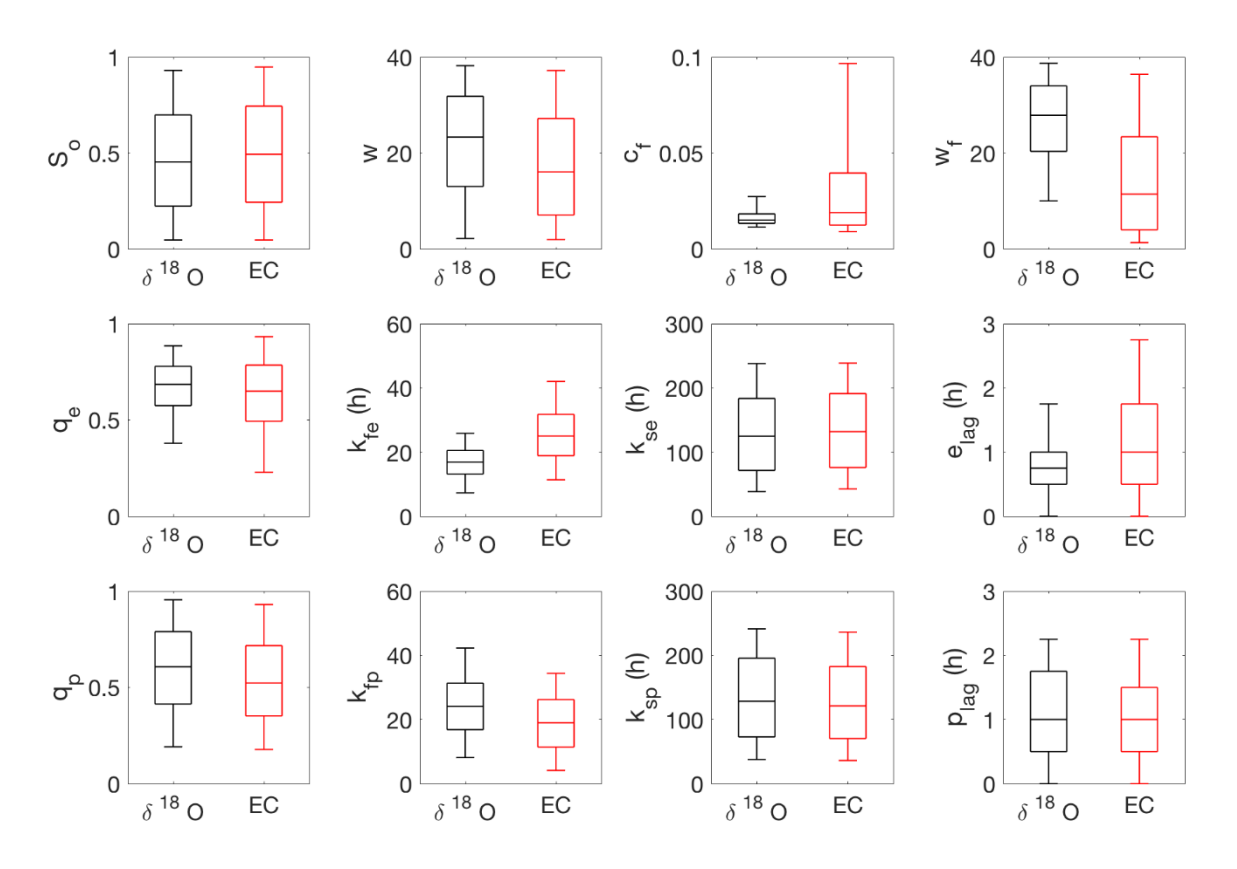


Figure 4.7. Box plots of the calibrated parameters considering sets that yielded NSE>0.75 from the last run (i.e., 1×10^7 simulations) using model structure 4 calibrated for δ^{18} O and electrical conductivity (EC) data. Parameter names are shown in **Table 4.1**.

For model structure 1 calibrated using EC, none of the parameters of module 1 reached a single peak in the parameter space, whereas the parameters f (module 2), and k_e , e_{lag} , k_p , and p_{lag} (module 3) did (i.e., five out of seven parameters; **Figure S4**). The calibration of structure 1 using δ^{18} O, showed that the parameter w (module 1) reached a single peak in the parameter space in addition to those that did for the model calibrated for EC (i.e., six out of seven



parameters; **Figure S3**). Similarly, the ranges of the calibrated parameters for both tracers were not in agreement (**Figure S10**). For model structure 3 calibrated using EC, only the cf parameter (module 2), and the k_e , k_p , and e_{lag} parameters (module 3) reached a single peak in the parameter space (i.e., four out of eight parameters; **Figure S8**). The same parameters reach a single peak in the parameter space when structure 3 was calibrated using $\delta^{18}O$ (**Figure S7**) and the ranges of calibrated parameters using both tracers were in agreement (**Figure S12**).

4.3.5 Comparison of Model Results for Both Tracers

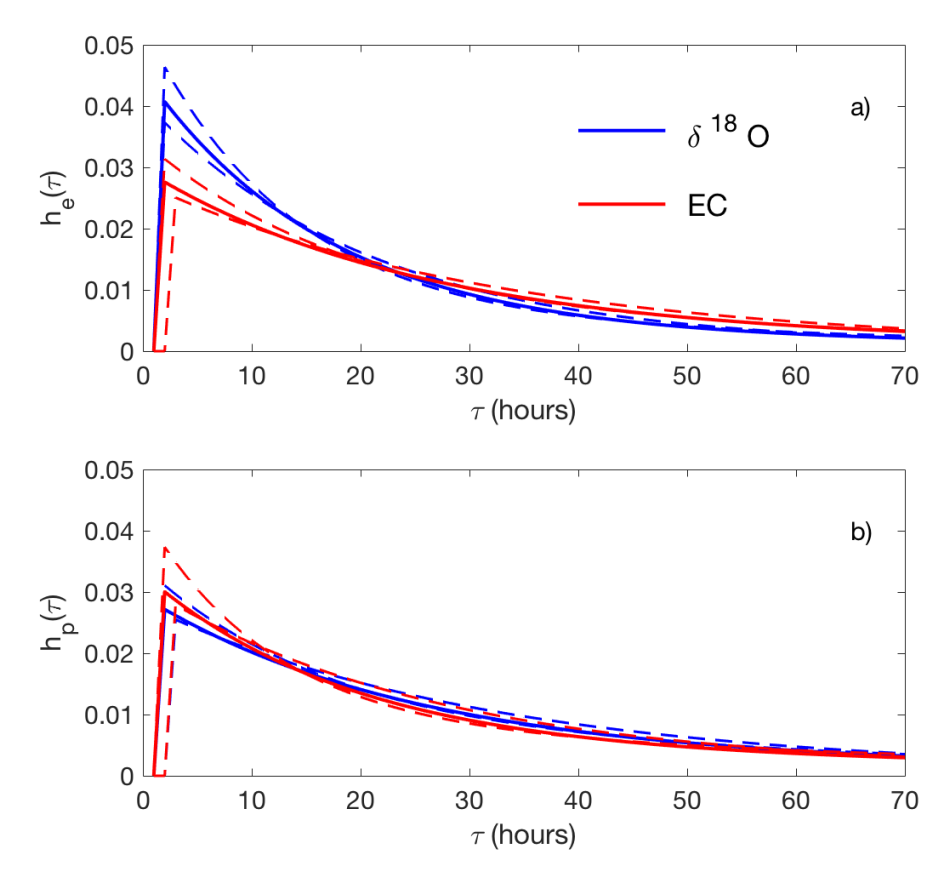


Figure 4.8. Transit time distributions (TTDs) of the (a) event (he) and (b) pre-event (hp) flow components for model structure 4 using $\delta^{18}O$ and electrical conductivity (EC) for calibration. The solid lines represent TTDs based on the 50th percentiles of behavioral (>0.75 NSE) parameter sets. The dashed lines correspond to the TTD defined based on parameter sets representing the 25th and 75th percentiles of their distributions.

Even though the TTDs of the event fractions using both tracers were similar for transit times (τ) longer than 20 h (**Figure 4.8**), there was some discrepancy in the τ distributions shorter than 20 h. For shorter τ , the calibration with $\delta^{18}O$ yielded a TTD with a predominance of shorter τ in comparison to the calibration of the model calibrated with EC (**Figure 4.8a**). The shape of the TTDs of the pre-event water fractions (**Figure 4.8b**) were opposite to those of the event



water fraction. That is, for shorter MTTs (<10 h), there was a predominance of shorter MTTs for the calibration with EC compared to the calibration with δ^{18} O.

4.4 Discussion

4.4.1 Selection of the Best Model Structure Using Water Isotopes and Electrical Conductivity for Model Calibration

The various TraSPAN model structures can be used to test different hypothesis about the processes that control streamflow generation (Clark et al., 2011; Pfister and Kirchner, 2017) or as a rejectionist framework to improve knowledge about the hydrological behavior of a given catchment (Vaché and McDonnell, 2006). Thus, the modeler can hypothesize and test different hydrological behaviors and assumptions in a catchment by building and testing conceptual models that represent different catchment functions (Birkel et al., 2010; Fenicia et al., 2011).

In this study, the four tested model structures (i.e., competing hypotheses; Chamberlin, 1965; Elliott and Brook, 2007) provided strong fits in terms of the NSE objective function using both tracers for calibration (NSEs>0.79; **Table 4.3**). However, further evaluation of the models' parsimoniousness, depicted important differences among the evaluated structures (**Table 4.3**). The simplest TraSPAN structures, including a single reservoir for the event and pre-event water transit times assuming either constant (structure 1 with 7 parameters; **Figure 4.2a**) or a time variant (structure 3 with 8 parameters; **Figure 4.2c**) fraction of P_{eff} routed as event water, provided less parsimonious results than the more complex structures 2 and 4. Between structures 2 and 4, which represented the catchment response with two connected linear reservoirs for each the event and pre-event water fractions and a constant (structure 2 with 11 parameters; **Figure 4.2b**) or time variant (structure 4 with 12 parameters; **Figure 4.2d**) fraction of P_{eff} routed as event water; structure 4 was the most parsimonious to represent the internal catchment response using both tracers (**Table 4.3**).

Regarding the results of the simulations of the observed Q and tracer data, the simplest structures 1 and 3 poorly resembled the hydrograph. These structures did not reproduce the peak responses and the recessions that followed them (DOY 306–311; **Figure 4.4a,d**, **Figure S2a,d**). Regarding the simulation of the tracer dynamics, these structures captured relatively well the δ^{18} O_Q decrease and EC_Q increase during the hydrograph falling limb but poorly resembled the tracer dynamics at the beginning of the event (**Figure 4.4b,e**, **Figure S2b,e**). These results indicate that the hydrological behavior of Mack Creek is not well represented when a single reservoir is used to route the event and pre-event water fractions regardless of



the treatment of the P_{eff} as constant or time variant. On the other hand, structures 2 and 4 provided better representations of the hydrograph and the tracers' dynamics. Both of these structures calibrated with both tracers were able to better resemble the highest Q peak (DOY 305) and the following rapid recession (Figure 4.5a,d, Figure S1a,d). These results suggest that the Mack Creek hydrological system is better represented by two connected linear reservoirs for each the event and pre-event water fractions. Regarding the tracer dynamics, structure 4 provided the best fits of the tracer data in comparison with structure 2 for both tracers (Figure 4.5b,e, Figure S1b,e). These results indicate that the system is not only better represented by two connected reservoirs, but that the internal mixing of the tracer is better represented when the P_{eff} routed as event water is treated as time-variant (structure 4) than when it is treated as constant (structure 2). Even though not directly investigated at Mack Creek evidence of non-stationary flow conditions and tracer dynamics have been shown for WS10, a 0.1 km² catchment located near the outlet of the H.J. Andrews Forest (Figure 4.1; McGuire and McDonnell, 2010; Klaus *et al.*, 2015; Rodriguez *et al.*, 2018).

4.4.2 Comparison of Flow Partitioning Modelling Results Calibrated for Water Isotopes and Electrical Conductivity

The ranges of the calibrated parameters for TraSPAN structure 4 were remarkably similar using both WSI and EC for calibration (**Figure 4.6**, **Figure 4.7**, and **Figure S8**, **Table 4.2**). In addition, the temporal variation (**Figure 4.5c,f**) and the estimated proportions of pre-event water yielded by the model calibrated for each tracer were in agreement (74.9% for δ^{18} O and 81.0% for EC, **Table 4.3**). Even though previous hydrograph separation investigations using simple tracer mixing models have found contradictory results regarding the reliability of the event and pre-event water contributions when EC is used as a tracer due to its non-conservative nature (Caissie et al., 1996; Cey et al., 1998; Kronholm and Capel, 2016; Laudon and Slaymaker, 1997; Matsubayashi et al., 1993; Nakamura, 1971; Nolan and Hill, 1990; Pellerin et al., 2008; Pilgrim et al., 1979), these findings suggest that this issue could be related to the lack of simultaneous representation of the water flow transport in addition to the tracer mixing within a given hydrological system. I was able to account for both using the TraSPAN numerical modeling approach.

Similar findings were reported by Mosquera *et al.* (2016b) in a study conducted to evaluate the baseflow transit times in a nested system of tropical alpine (páramo) catchments in South America. These authors found that the spatial variability of transit time estimates for their



nested system of catchments—based on the calibration of a lumped conceptual model using $\delta^{18}O$ —was highly correlated with the catchments' mean yearly baseflow EC ($r^2 = 0.89$) and suggested that average EC values could be used as an inexpensive proxy to estimate baseflow transit times. Even though these results cannot be generalized until additional investigations are carried out in different environments, the results from Mosquera *et al.* (2016b) and this study highlight the potential advantages of high-resolution monitoring of EC for hydrological modelling applications, particularly when flow dynamics are accounted for.

4.4.3 On the Use of High-Temporal Resolution EC in Hydrograph Separation Modelling

It is worth noting that the structure 4 simulation results yielded better model performance, both in terms of goodness of fit and parsimoniousness, when calibrated with the finer temporal resolution of EC data than when calibrated for $\delta^{18}O$ (**Table 4.3**). The simulation results also showed that a higher accuracy to represent the hydrograph and tracer dynamics was obtained when structure 4 was calibrated using the higher-resolution EC data (sub-hourly), than when calibrated for WSI data collected every 4 h. For instance, the hydrograph highest peak and following recession on DOY 305 (**Figure 4.5a,c**) and the rapid $\delta^{18}O$ increase/EC decrease on DOY 304–305 (**Figure 4.5b,d**) were better represented by the model calibrated using EC data. These results indicate that even though the model calibrated for both tracers depicted similar hydrological behavior (see Section 4.4 for details), the calibration for the higher-resolution EC data allowed better capturing of the fast occurrence of flow transport and solute mixing processes. These simulations resulted in the release of higher amounts of pre-event water for the model calibrated for EC (81%), particularly during the highest hydrograph peak on DOY 305 (**Figure 4.5f**), with respect to the calibration for $\delta^{18}O$ (75%; **Figure 4.5c**).

Other investigations have also reported higher accuracy to represent the temporal variability of the tracer's signal, and further interpretation of water routing in hydrological systems when using high-temporal resolution tracer data (Stockinger et al., 2016; Timbe et al., 2015). This results do not only support the findings from these authors, but also demonstrate the potential of the inexpensive collection of EC data at high-temporal resolution to improve understanding of fast occurring (seconds to minutes) hydrological processes.

4.4.4 Process-Based Understanding of Hydrological Behavior

The similarity in hydrological behavior of the transport and mixing of water within the Mack Creek catchment was evaluated based on the shapes of TTDs provided by the best model



structure calibrated for each tracer. Despite the overall similarities of the TTDs' shapes for both tracers (**Figure 4.8**) with dominance of long transit times (τ >10 h), results showed small differences for shorter transit times (τ <20 h for the event water fractions, **Figure 4.8a**; τ <10 h for the pre-event water fractions, **Figure 4.8b**). This discrepancy could be related to different temporal resolution of the data used for calibration, as reported in other studies (Stockinger et al., 2016). In other words, the use of finer temporal resolution EC data (every 0.25 h) in comparison to the WSI data (every 4 h).

From a process-based perspective, the TTDs obtained from the model calibration using both tracers indicate that the catchment acts as a connected system of two water reservoirs each with a fast and a slow transit function contributing large amounts of pre-event water (75–81%) to discharge (**Table 4.3**). These two reservoirs likely represent: (1) fast event and pre-event water moving through the shallow permeable soils and (2) slow event and pre-event water moving through the fractured parent material (hereafter referred to as the groundwater reservoir, GW). That is, this catchment has poorly developed gravelly loam soils with high infiltration rates (>500 cm h-1) that are overlaying highly weathered and fractured bedrock (McGuire et al., 2005). Baseflow MTT at Mack Creek was estimated around 2 ± 0.49 years, i.e., one of the longest within the H.J. Andrews catchments (McGuire et al., 2005). This MTT estimation indicates that water is likely stored in the GW reservoir, as has been observed in other headwater catchments with relatively permeable geology (e.g., Timbe et al., 2014; Hale and McDonnell, 2016; Muñoz-Villers et al., 2016). Stored water that can be released rapidly to streams during rainfall events given the connectivity between hillslopes and riparian areas. Such connectivity has been observed near the study area at WS10 (Figure 4.1; McGuire and McDonnell, 2010). Additionally, even though high amounts of pre-event water were released as streamflow during the monitored event, the total runoff (20.6 mm) accounted for only 13% of the total precipitation input (155.1 mm). Again, given the permeable soils and fractured bedrock of the catchment, and the dry antecedent moisture conditions during the monitoring period (28 October-7 November)—which corresponded to the beginning of the fall season after the summer period in the particularly dry water year 2015—only a small fraction of total precipitation was converted into Peff. These results from the hydrometric analysis indicate that the rest of water inputs must have filled the initially low water storage of the GW reservoir after the dry summer. In this context, the strong goodness of fit of the model to simulate the high temporal variability of the streamflow and tracer data dynamics (**Figure 4.5a–d**) indicates that through the simultaneous calibration of water and solute fluxes, the model was not only



capable to successfully account for the water flux and tracer mixing dynamics, but also for the recharge of water in the groundwater system.

4.5 Concluding Remarks and Future Directions

Our evaluation of a tracer-based hydrological model (TraSPAN) demonstrated that the assessment of different modeling structures—each representing a different rainfall-runoff response—allowed for a better identification of the hydrological system functioning. For the analyzed rainfall event at the H.J. Andrews experimental forest, I found that the same model structure was best at representing hydrographic and tracer dynamics using either electrical conductivity/specific conductance (EC) or water-stable isotopes (WSIs) collected at high temporal resolution for calibration. The model results using both tracers not only showed a remarkable agreement to fit the observed data and the calibrated parameter distributions, but also in terms of the process-based understanding of the hydrological system. Moreover, the use of sub-hourly (0.25 h) collected EC data also allowed to better simulate the catchment hydrological response in comparison to the 4 h δ^{18} O data. These findings highlight the potential of using low-cost EC data collected at high temporal resolution in combination with a flexible hydrological modelling framework to better understand catchment hydrological behavior.

Despite the advantages of the applied methodology, it is acknowledged that before the widespread application of this approach, future research should focus on understanding site-dependent geochemical conditions under which the applicability of EC as a conservative tracer is suitable. Future research should also focus on implementing monitoring strategies that allow for the combined collection of water isotopes and geochemical data at the highest possible temporal resolution during a variety of climatic conditions (i.e., wet, transition, and dry periods). Such efforts are encouraged, as these data would provide information about the spatial and temporal variability in weathering rates to better establish the conditions under which the use of high-resolution EC observations would yield robust datasets to investigate important, but yet unresolved, questions in catchment hydrology that require the identification of fast-occurring hydrological processes, while reducing monitoring costs and the degree of uncertainty in simulated flow components.



Chapter 5

5. Conclusions

5.1 Synthesis

The influence of volcanic activity in the evolution of mountainous landscapes is well-known. In contrast, knowledge about how catchment features originated from volcanic material affect the behavior of hydrological systems has not been sufficiently investigated. The definition of flow paths in the unsaturated zone of volcanic ash soils and the influence of fractured volcanic geology on how catchments store and release water are still not completely understood. To improve knowledge about this, I focused the doctoral research on the investigation of the role of volcanic catchment features on the water transport and tracer mixing mechanisms in mountainous environments. In a first step, the water retention characteristics of volcanic ash soils with andic properties (Andosols/Andisols; Chapter 2) were evaluated. Subsequently, the influence of Andosols in the delineation of subsurface flow paths at the hillslope scale was analyzed (Chapter 3). Lastly, the impact of a highly weathered volcanic geology on streamflow partitioning at catchment scale was studied (Chapter 4).

The water retention capacity of the soils is a fundamental parameter in the analysis of the transport and mixing of water and solutes in porous media. Previous comparative research using in-situ (field) and standard laboratory methods to determine the relationship between soil moisture content and soil matric potential (the water retention curve, WRC) of Andosols showed contrasting results. Since it is yet unknown whether such discrepancy depends on site-specific features, the applied laboratory method, and/or the volume of the soil sample, a thorough comparison among standard laboratory methods and direct measurements in large soil cores and in the field (in-situ) was conducted (Chapter 2). High-elevation experimental observatories in south Ecuador were selected as study sites given that the formation of the local soils is highly influenced by the accumulation of volcanic ash from past volcanic activity. This evaluation showed that soil moisture content and matric potential measurements in large, undisturbed soil cores (\emptyset =40 cm, h=32 cm) resemble accurately the WRC of the Andosols in comparison to direct measurements in the field. However, this evaluation in combination with data compiled from the published literature on this topic demonstrated that standard laboratory methods reflect only partially the hydraulic behavior of the Andosols under field conditions.



These methods resembled well the wet range of the WRC of the soils (up to 3-5 kPa or pF 1.5-1.7), but overestimated greatly the water retention capacity of the soils for the dry range of the WRC, including the field capacity (i.e., the amount of water that a soil retains against gravity). It is worth mentioning that this discrepancy occurred independently of the site-specific land use, land cover, and physical, chemical, and mineralogical properties of the Andosols. Importantly, this analysis also indicated that soil samples of small volume ($\leq 300 \text{ cm}^3$), which are traditionally used in laboratory analyses (corresponding to 94% of the sample volumes used in the published literature), do not represent the field hydraulic behavior of these soils. This, most likely because small-volume soil samples do not represent correctly the macro-porosity of the Andosols and/or produce the dead end of preferential flow paths that in turn causes an underestimation of the large-scale conductivity of the soil. I also demonstrated that for the determination of the representative elementary volume (i.e., the smallest soil sample volume that resembles the field hydraulic behavior of the soils in the laboratory, REV) of Andosols, currently considered as a soil sample of 100 cm³ volume (a cylindrical sample with a crosssectional area of 20 cm²; i.e., Ø=5 cm, h=5.1 cm), the comparison among different standard laboratory methods yielded equivocal results. As a result, future comparisons against field and/or experimental observations are required to determine the REV of these soils.

Further research was focused on the analysis of how the properties of Andosols influence subsurface flow dynamics in a steep hillslope underlain by Andosols in a tropical alpine (Páramo) ecosystem in the south of Ecuador (Chapter 3). An extensive dataset of soil moisture measurements, soil water stable isotopes, and a detailed characterization of the soil properties was used and led to a profound understanding of the dominant water flow paths (vertical versus lateral) that control the water transport and tracer mixing within the studied hillslope soils. The findings from Chapter 2 were crucial to apply an appropriate method (direct soil moisture and matric potential measurements in large soil cores) for the accurate representation of the water retention characteristics of the Andosol soil along the experimental hillslope. The characterization of soil properties along the experimental hillslope depicted two welldifferentiated soil horizons. A poorly developed andic horizon (52-61 cm, Ah horizon) rich in organic matter (33.5-42.1 %) and clay (29-31 %) in comparison to the underlying mineral (C) horizon that presented much lower organic matter (2.9-7.6 %) and clay (7-8 %) contents, with a dominance of the sand fraction (70-73 %). In the Ah horizon, soil moisture data in the rooted layer (from the ground surface to 10-15 cm depth) showed a fast response to rainfall. Differently, below the root zone, a perched water layer (from 10-15 cm to 35-40 cm depth) that



remained near saturation during the 3-year monitoring period was observed. The presence of a perched layer is the result from the combination of two factors. On the one hand, the abrupt decrease in saturated hydraulic conductivity of the soil between the highly conductive rooted layer and the unrooted layer below. On the other hand, the high organic matter and clay content of the Ah horizon that increases the water storage capacity of the soil. Interestingly, the isotopic data showed that the mixing of tracer within the entire Ah horizon was highly influenced by the isotopic composition of precipitation, and that despite the perched layer, the mean transit time (MTT, or the age of the water) was short (2-4 weeks). This information indicates that water molecules in the soil matrix of the Ah horizon are rapidly replenished by incoming water during rainfall events. This effect is likely explained by the rapid transfer of hydraulic potentials through the porous soil matrix as evidenced by the exponential shape of the WRC of the soils in the Ah horizon. In the C layer, the soil moisture data responded fast during rainfall events with response times similar to those observed in the rooted layer of the Ah horizon. The fast soil moisture dynamics of this layer indicates that the C horizon is rapidly recharged by water that percolates vertically through the entire Ah horizon during rainfall events. Soil water in this horizon was less influenced by the isotopic composition of precipitation and presented longer MTTs (2.8-8.5 months) in comparison to the Ah horizon. These findings suggest that the storage of water in the C horizon is not only maintained by vertical contributions stemming from the Ah horizon above, but also by an overall lower exchange of the water stored at upslope sampling positions. Despite the dominance of vertical flow paths in the subsurface of the experimental hillslope, lateral flow likely occurs during high intensity rainstorm events above the hydraulically restrictive layers (e.g., the perched layer) due to the steep gradient of the hillslope. Together, the combination of different sources of information (i.e., hydrometric, isotopic, and soil properties data) led to the following conclusion: the hydrologic behavior of volcanic ash soils resembles the hydrologic functioning of a wet layered sloping sponge in which vertical flow paths dominate despite the formation of a perched water layer that helps sustain water storage in the andic horizon of the soils.

Moving beyond the role of volcanic ash soils on the hydrological behavior of mountainous environments, Chapter 4 examined how highly weathered volcanic geology influences the hydrological behavior at the catchment scale. A catchment presenting fractured bedrock geology but without the influence of soils developed on volcanic ash in the Pacific Northwest of the United States was selected as the study site in order to discard the influence of the latter on flow transport and tracer mixing mechanisms. For this purpose, a hypothesis testing



framework consisting of a flow partitioning tracer-aided hydrological model was applied to quantify the contribution of event (new) and pre-event (old) water to total runoff. The hypotheses were represented as four different model structures, each representing a different mechanism (or competing hypothesis) of conversion of precipitation into runoff during a rainstorm event in which hydrometric (streamflow and precipitation) and tracer (water-stable isotopes (WSIs) and electrical conductivity or specific conductance (EC)) data were collected at high temporal frequency (few hours to sub-hourly). The model structure that best simulated the transport (streamflow hydrograph) and mixing (the tracers' signals in streamflow) of water was represented by two-parallel linear reservoirs. From a process-based perspective, the two reservoirs represent the poorly developed gravelly loam soil with high infiltration rates (>500 cm h⁻¹) and the highly weathered, fractured bedrock that conforms the groundwater (GW) reservoir of the system. During the event, which lasted for 10 days and took place at the beginning of the fall season in the dry 2015 water year, only 13% of the total precipitation input during the monitored storm (155.1 mm) was released as streamflow. The modeling results showed that the streamflow hydrograph was mainly composed of pre-event water (or water stored in the catchment prior to the rainstorm event, 75-81%). These results indicate that incoming precipitation infiltrated rapidly through the permeable soils and contributed mainly to recharge the storage of the GW reservoir, whereas only a small fraction of water was released to the stream. The latter was composed principally of pre-event water. These findings do not only contribute to improve the process-based understanding of how catchments dominated by fractured geology generate streamflow, but also to the knowledge of how they store water. The latter is a fundamental hydrological feature that cannot be directly quantified by traditional hydrometric measurements or observed in the field, but that can be inferred from the use and the modeling of isotopic and geochemical signals as shown in this work.

An additional contribution from Chapter 4 was the evaluation of whether a low cost and easy to measure at high temporal frequency (sub-hourly) "non-conservative" tracer (EC) yield similar model calibration results than conservative tracers (WSIs) commonly collected at a lower temporal frequency (few hours to monthly). The comparative analysis depicted a remarkable agreement between the flow partitioning modeling results produced by both tracers. This, not only in terms of the modeling performance (hydrometric and tracer data fitting and calibrated parameter distributions), but also with regard to the process-based understanding of the system. These findings provide a great promise for the utility of EC in combination with tracer-aided hydrologic models to investigate fast occurring catchment hydrological behavior,



particularly in remote areas where harsh field conditions limit the capacity to acquire WSI information at high temporal frequency.

The research presented in this doctoral dissertation fills important knowledge gaps and highlights other important ones that require urgent attention regarding the influence of catchment features of volcanic origin (soils and geology) in the subsurface hydrology of montane ecosystems. The findings in Chapter 2 highlight that we, as a community, have not been able to develop appropriate methods to characterize correctly the water retention capacity of volcanic ash soils. Although an accurate, yet expensive and unsuitable method to be implemented at large spatial scale is available, it is urgent that future research is devoted to identify the REV of Andosols and laboratory methods that allow the characterization of this fundamental soil property at accessible logistical and financial costs.

At the hillslopes scale, volcanic ash soils (Andosols) facilitate the vertical percolation of water within the soil profile during rainfall events, despite the formation of a perched water layer that sustains the near saturation water holding capacity of the soil below the root zone (Chapter 3). It is important to highlight that to develop this knowledge, the combination of traditional hydrometric measurements and not so commonly used techniques in vadose zone investigations, such as the use of stable isotope fingerprints and mean transit time modeling, was crucial. It is also worth noting that an accurate determination of the water retention capacity of the soils is fundamental to interpret hydrometric and isotopic observations, but more importantly, to develop a process-based understanding of subsurface flow processes.

Finally, at the catchment scale, the highly weathered, fractured volcanic geology (groundwater reservoir) contributed substantially to water storage, with only a small amount of water previously stored in the catchment (pre-event water) being released as streamflow during the first fall season rainstorm event after a long, dry summer season (Chapter 4). Similar to Chapter 3, the combination of hydrometric and tracer data with numerical modeling methods was vital to obtain an improved understanding of catchment hydrological behavior. In this sense, in addition to the developed process-based understanding presented in this doctoral dissertation, this work also contributes as a methodological guidelines for the investigation of similar issues in other mountainous environments. Importantly, if we would not have had access to different, but complementary, sources of information, it is pretty likely that our conclusions would have been different, and presumably erroneous.



5.2 Complementary, ongoing, and future research

5.2.1 Complementary studies

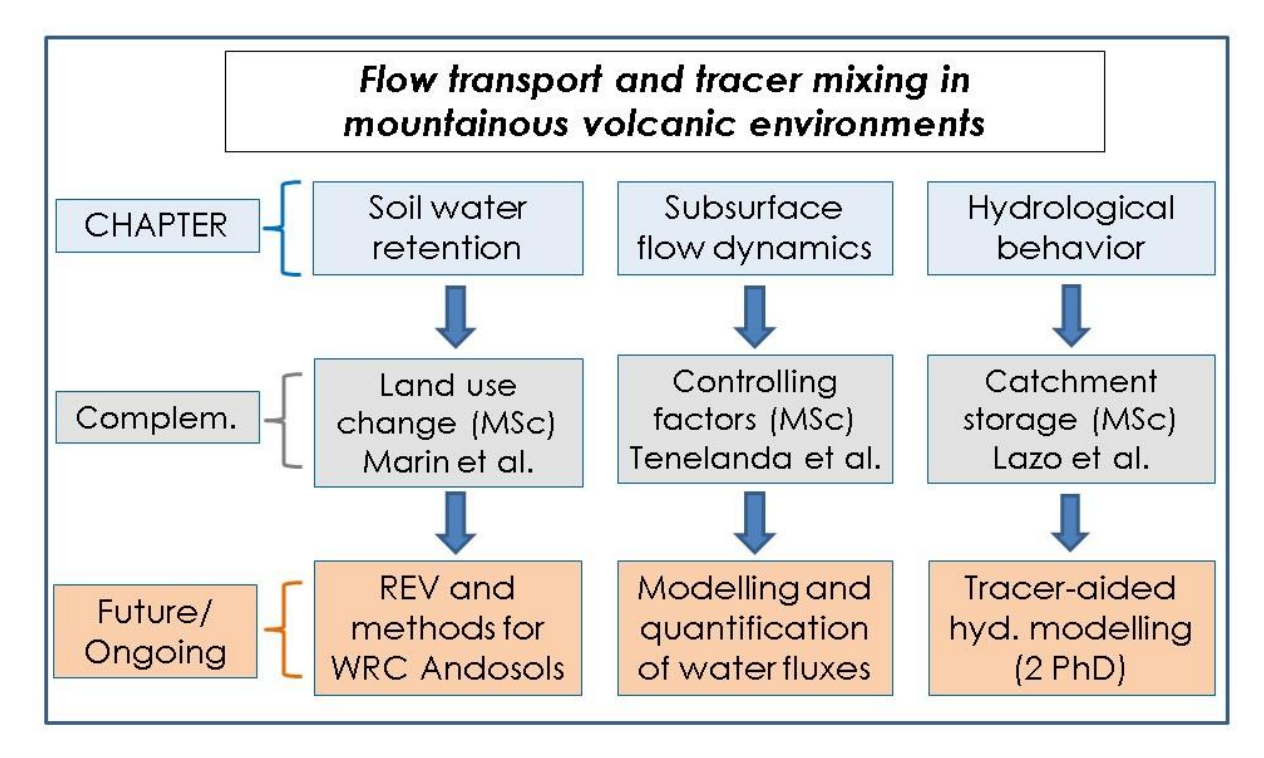


Figure 5.1. Schematic representation of complementary and future/ongoing research linked to this doctoral dissertation. The vertical blue arrows indicate how complementary research published in peer-reviewed journals that resulted from the thesis of 3 MSc students advised by the dissertation author (gray level) and open research questions that need to be addressed in future (or ongoing) research (orange level) are linked to the outcomes of each of the chapters of this dissertation (blue level).

The research presented in this dissertation was closely related to several studies conducted in parallel (grey boxes in **Figure 5.1**). These studies correspond to the work of MSc students in the Ecohydrology Program at the University of Cuenca, in which I participated as a tutor, codirector, or director of the students' theses. One of these studies was focused on the investigation of how land use change (LUC), from native forests and grasslands to pastures or pine forests specifically, affect the hydraulic properties of Andosols in the Andean highlands (Marín et al., 2018). Results revealed that the impacts of changes in the properties of the soils, including their water retention capacity, cannot be generalized across the study region mainly because their effects depend on previous land management. Similar to the outcomes presented in Chapter 2, these findings add up to the general knowledge about the hydraulic properties of these soils. However, given the demonstrated lack of representativeness of the dry range of the WRC of Andosols using standard laboratory methods (Chapter 2), and that such methods were



used in our study, the effects of LUC on soil parameters dependent on the dry portion of the curve (e.g., field capacity, wilting point, plant available water) ought to be reevaluated using appropriate techniques.

Regarding the dynamics of subsurface flow in Andosol soils at the hillslope scale, we studied the factors that control maximum soil moisture changes in response to precipitation events (Tenelanda-Patiño et al., 2018). Parameters based on precipitation, evapotranspiration, and soil wetness during and prior to rainstorm events were used as potential variables that control soil moisture dynamics during dry, transition, and wet periods (wetness states) at the same experimental hillslope studied in Chapter 3. We demonstrated that regardless of the wetness state of the system, the total volume and the intensity of precipitation during the monitored events were the main factors that triggered soil moisture response along the experimental hillslope. These complementary findings to those reported in Chapter 3 contribute to an enhanced understanding of the role of Andosols in the dynamics of subsurface flow at the hillslope scale.

In relation to the hydrological behavior at the catchment scale, we analyzed how catchment features (e.g., vegetation, soil type and distribution, precipitation, evapotranspiration) influence the water storage of a nested system of tropical alpine catchments (Lazo et al., 2019) by applying an approach analogous to the one presented in Chapter 4. That is, we used a combination of hydrometric, tracer, and modelling techniques that allowed to obtain improved process-based understanding of the hydrologic functioning of the catchment. The study revealed that the areal extent of riparian soils (wetlands), which cover only 15-25% of the study catchments, control the passive storage (or total volume of storage available for tracer mixing), whereas precipitation intensity controls the dynamic storage (the storage active in the water balance) of the catchments. Similar to the findings presented in Chapter 4, this study filled knowledge gaps about the influence of landscape features on streamflow production and water storage. In addition, both studies present emerging methods that can be applied to unravel efficiently the hydrological behavior of other catchments.

5.2.2 Future research opportunities

The findings in this dissertation lead to important research questions, challenges, and opportunities for future investigations (orange boxes in **Figure 5.1**). What is the REV of Andosols that allows to resemble the hydraulic behavior of these soils accurately in the laboratory (Chapter 2)? Resolving this issue is fundamental to continue advancing the



understanding of the hydrological, ecological, and biogeochemical processes in regions where these soils dominate. Another important issue to resolve is to define whether or not standard laboratory methods can be used or adapted, if necessary, to determine the WRC of Andosols using soil samples of larger dimensions. Although I demonstrated that direct soil moisture and matric potential measurements in large, undisturbed soil cores provide an accurate representation of the water retention capacity of these soils, using this method is not logistically and economically sustainable. One of the main issues related to this method is that the collection of large samples across large areas is difficult as it requires the construction and transportation of the cores to the field, and large man-power to collect the samples in the field, particularly at steep, mountainous areas where these soils are commonly found. Given that this procedure also requires conducting soil moisture and matric potential measurements during the desiccation of the saturated samples at environmental conditions, obtaining the curve requires long observation periods in the order of several months. Additionally, the use of often expensive probes increases the cost of this method. These financial and logistical constraints limit the applicability of the method almost exclusively to research applications and to small spatial scale studies (e.g., from plot to hillslope transect). Therefore, the identification of the REV of the Andosols and the identification/adaptation of methods that allow the analysis of several soil samples in short time periods at accessible cost is more than relevant and opens opportunities for future research. It is also worth highlighting that once these issues are resolved, reevaluation of past research that yielded conclusions based on the incorrectly determined WRC of Andosols using the up to now standard laboratory methods is required.

Once the Andosols' influence on the delineation of the main water flow paths and the subsurface hydrological behavior at the hillslope scale has been conceptualized based on field observations (Chapter 3), the next step is to quantify these fluxes. Taking advantage of the detailed characterization of the hydraulic properties of the soils and the available high-frequency hydrometric data along the experimental hillslope, the application of a process-based hydrological model to quantify how much water is distributed laterally and vertically in the subsurface, as well as how much of it is lost via soil evaporation and plant transpiration is the next obvious step. Another issue that requires further attention, is the dynamics of soil water storage along the hillslope. The available datasets could help to unravel how soil moisture storage changes over time and what hydrometeorological factors and/or properties of the soils along the hillslope control its spatial-temporal variation. Resolving these issues will not only be helpful in filling knowledge gaps in hydrological sciences, but also improve water



management in the study region, the tropical Andes, where these soils are an important resource that sustains the regional economic development.

The investigation of the hydrologic behavior and flow partitioning at catchment scale using hydrometric, geochemical, and numerical modelling techniques also opened new opportunities for future investigations. During the development of the dissertation, I proposed two ideas for potential doctoral projects that surfaced from the findings presented in Chapter 4. The evolution of these ideas was partially triggered by the fact that I participated as co-director of a research project co-funded by the International Atomic Energy Agency and the Central Research Unit of the University of Cuenca (DIUC), which recently lead to the initiation of two doctoral projects that since mid-2018 are being implemented by two doctoral students of the Water Resources Program at the University of Cuenca. One of the projects relates to the use of a tracer-aided hydrological model, which can be used as a hypothesis testing framework similar to the one applied in Chapter 4, to obtain improved understanding of the hydrologic behavior of catchments. This project seeks to improve the transport and mix of water and stable isotopes within a tropical alpine experimental catchment, and how the catchment's hydrological behavior varies over time in response to time-varying environmental conditions. This research project will contribute to improve the understanding of the hydrology of tropical alpine environments and the general knowledge about the usefulness of tracer-aided numerical models to unravel runoff generation mechanisms.

Given the difficulty to obtain reliable conservative tracer data (i.e., stable isotopes) in precipitation and streamflow at high-temporal frequency to identify the fractions of old and new water contributing to streamflow during a variety of flow conditions (from droughts to extremely wet conditions), it is most relevant to identify easy to collect/measure, inexpensive alternative tracers that provide the same information at a fraction of the cost associated with the acquisition of stable isotope data. In Chapter 4, the potential use of electrical conductivity in combination with a tracer-aided hydrological model was tested for this purpose. However, determining the usefulness of the combination of these techniques in other catchments with different landscape and/or environmental conditions requires further testing. To this end, the objective of the second doctoral project I proposed is to evaluate whether electrical conductivity and/or other geochemical tracers collected *in-stream* at a high temporal frequency (sub-hourly) produce similar flow partitioning modeling results than those yielded when the model is calibrated for stable isotopes in a tropical alpine setting. The findings obtained from this research project will not only allow to fill knowledge gaps about rainfall conversion into



runoff in tropical alpine catchments, but also to the rapidly growing interest of the hydrological and biogeochemical community to obtain *in-stream* high-frequency water quality data that allows investigating fast occurring, non-stationary hydrological behavior in catchments.



References

- Abera, G., Wolde-Meskel, E., 2013. Soil Properties, and Soil Organic Carbon Stocks of Tropical Andosol under Different Land Uses. Open J. Soil Sci. 03, 153–162. https://doi.org/10.4236/ojss.2013.33018
- Akaike, H., 1974. A new look at the statistical model identification. IEEE Trans. Automat. Contr. 19, 716–723. https://doi.org/10.1109/TAC.1974.1100705
- Alavi, G., Tomer, M.D., 2001. Estimation of soil hydraulic parameters to simulate water flux in volcanic soils. New Zeal. J. For. Sci. 31, 51–65.
- Allen, S.T., Brooks, J.R., Keim, R.F., Bond, B.J., McDonnell, J.J., 2014. The role of pre-event canopy storage in throughfall and stemflow by using isotopic tracers. Ecohydrology 7, 858–868. https://doi.org/10.1002/eco.1408
- Anderson, A.E., Weiler, M., Alila, Y., Hudson, R.O., 2009. Subsurface flow velocities in a hillslope with lateral preferential flow. Water Resour. Res. 45, W11407. https://doi.org/10.1029/2008WR007121
- Armas-Espinel, S., Hernández-Moreno, J.M., Muñoz-Carpena, R., Regalado, C.M., 2003. Physical properties of "sorriba"-cultivated volcanic soils from Tenerife in relation to andic diagnostic parameters. Geoderma 117, 297–311. https://doi.org/10.1016/S0016-7061(03)00130-7
- Asada, K., Eguchi, S., Ikeba, M., Kato, T., Yada, S., Nakajima, Y., Itahashi, S., 2018. Modeling nitrogen leaching from Andosols amended with different composted manures using LEACHM. Nutr. Cycl. Agroecosystems 110, 307–326. https://doi.org/10.1007/s10705-017-9899-x
- Asano, Y., Uchida, T., Ohte, N., 2002. Residence times and flow paths of water in steep unchannelled catchments, Tanakami, Japan. J. Hydrol. 261, 173–192. https://doi.org/10.1016/S0022-1694(02)00005-7
- Bachmair, S., Weiler, M., 2012. Hillslope characteristics as controls of subsurface flow variability. Hydrol. Earth Syst. Sci. 16, 3699–3715. https://doi.org/10.5194/hess-16-3699-2012



- Barnes, C.J., Bonell, M., 1996. Application of unit hydrograph techniques to solute transport in catchments. Hydrol. Process. 10, 793–802. https://doi.org/10.1002/(SICI)1099-1085(199606)10:6<793::AID-HYP372>3.0.CO;2-K
- Bartoli, F., Begin, J.C., Burtin, G., Schouller, E., 2007. Shrinkage of initially very wet soil blocks, cores and clods from a range of European Andosol horizons. Eur. J. Soil Sci. 58, 378–392. https://doi.org/10.1111/j.1365-2389.2006.00889.x
- Basile, A., Ciollaro, G., Coppola, A., 2003. Hysteresis in soil water characteristics as a key to interpreting comparisons of laboratory and field measured hydraulic properties. Water Resour. Res. 39. https://doi.org/10.1029/2003WR002432
- Bear, J., 1972. Dynamics of Fluids in Porous Media. Elsevier, Mineaola, NY.
- Beck-Broichsitter, S., Fleige, H., Goebel, M.-O., Dörner, J., Bachmann, J., Horn, R., 2016. Shrinkage potential and pore shrinkage capacity of differently developed volcanic ash soils under pastures in southern Chile. J. Plant Nutr. Soil Sci. 179, 799–808. https://doi.org/10.1002/jpln.201600110
- Benettin, P., Soulsby, C., Birkel, C., Tetzlaff, D., Botter, G., Rinaldo, A., 2017. Using SAS functions and high resolution isotope data to unravel travel time distributions in headwater catchments. Water Resour. Res. https://doi.org/10.1002/2016WR020117
- Beniston, M., 2003. Climatic Change in Mountain Regions: A Review of Possible Impacts. Clim. Change 59, 5–31. https://doi.org/10.1023/A:1024458411589
- Berman, E.S.F., Gupta, M., Gabrielli, C., Garland, T., McDonnell, J.J., 2009. High-frequency field-deployable isotope analyzer for hydrological applications. Water Resour. Res. 45. https://doi.org/10.1029/2009WR008265
- Bertuzzo, E., Thomet, M., Botter, G., Rinaldo, A., 2013. Catchment-scale herbicides transport: Theory and application. Adv. Water Resour. 52, 232–242. https://doi.org/10.1016/j.advwatres.2012.11.007
- Beven, K., Asadullah, A., Bates, P., Blyth, E., Chappell, N., Child, S., Cloke, H., Dadson, S., Everard, N., Fowler, H.J., Freer, J., Hannah, D.M., Heppell, K., Holden, J., Lamb, R., Lewis, H., Morgan, G., Parry, L., Wagener, T., 2020. Developing observational methods to drive future hydrological science: Can we make a start as a community? Hydrol. Process. 34, 868–873. https://doi.org/10.1002/hyp.13622



- Beven, K., Freer, J., 2001. Equifinality, data assimilation, and uncertainty estimation in mechanistic modelling of complex environmental systems using the GLUE methodology. J. Hydrol. 249, 11–29. https://doi.org/10.1016/S0022-1694(01)00421-8
- Bevington, P.R., Robinson, D.K., 2003. Data Reduction and Error Analysis for the Physical Sciences. McGraw-Hill, New York.
- Birkel, C., Dunn, S.M., Tetzlaff, D., Soulsby, C., 2010. Assessing the value of high-resolution isotope tracer data in the stepwise development of a lumped conceptual rainfall-runoff model. Hydrol. Process. 24, 2335–2348. https://doi.org/10.1002/hyp.7763
- Birkel, C., Soulsby, C., 2015. Advancing tracer-aided rainfall-runoff modelling: a review of progress, problems and unrealised potential. Hydrol. Process. 29, 5227–5240. https://doi.org/10.1002/hyp.10594
- Birkel, C., Soulsby, C., Tetzlaff, D., 2015. Conceptual modelling to assess how the interplay of hydrological connectivity, catchment storage and tracer dynamics controls nonstationary water age estimates. Hydrol. Process. 29, 2956–2969. https://doi.org/10.1002/hyp.10414
- Birkel, C., Soulsby, C., Tetzlaff, D., Dunn, S., Spezia, L., 2012. High-frequency storm event isotope sampling reveals time-variant transit time distributions and influence of diurnal cycles. Hydrol. Process. 26, 308–316. https://doi.org/10.1002/hyp.8210
- Bittelli, M., Flury, M., 2009. Errors in Water Retention Curves Determined with Pressure Plates. Soil Sci. Soc. Am. J. 73, 1453–1460. https://doi.org/10.2136/sssaj2008.0082
- Blume, T., Zehe, E., Bronstert, A., 2009. Use of soil moisture dynamics and patterns at different spatio-temporal scales for the investigation of subsurface flow processes. Hydrol. Process. 13, 1215–1233.
- Boelter, D.H., 1969. Physical properties of peats as related to degree of decomposition. Soil Sci. Soc. Am. Proc. 33, 606-609.
- Bonell, M., Cassells, D.S., Gilmour, D.A., 1983. Vertical soil water movement in a tropical rainforest catchment in northeast queensland. Earth Surf. Process. Landforms 8, 253–272. https://doi.org/10.1002/esp.3290080307
- Borja, P., 2006. Desarrollo de las funciones de edafo transferencia para la caracterizacion hidraulica de andosoles. Universidad de Cuenca.



- Brantley, S.L., Eissenstat, D.M., Marshall, J.A., Godsey, S.E., Balogh-Brunstad, Z., Karwan, D.L., Papuga, S.A., Roering, J., Dawson, T.E., Evaristo, J., Chadwick, O., McDonnell, J.J., Weathers, K.C., 2017. Reviews and syntheses: on the roles trees play in building and plumbing the critical zone. Biogeosciences 14, 5115–5142. https://doi.org/10.5194/bg-14-5115-2017
- Brooks, J.R., Barnard, H.R., Coulombe, R., McDonnell, J.J., 2010. Ecohydrologic separation of water between trees and streams in a Mediterranean climate. Nat. Geosci. 3, 100–104. https://doi.org/10.1038/ngeo722
- Brown, R.B., Parsons, R.B., 1973. Soils of the reference stands—Oregon, IBP, Coniferous For. Biome Internal Rep. 128., 76 pp. [WWW Document]. URL http://ir.library.oregonstate.edu/dspace/bitstream/1957/7809/1/Internal Report_128.pdf
- Burns, D.A., Kendall, C., 2002. Analysis of δ^{15} N and δ^{18} O to differentiate NO $_3$ $^-$ sources in runoff at two watersheds in the Catskill Mountains of New York. Water Resour. Res. 38, 9-1-9–11. https://doi.org/10.1029/2001WR000292
- Burt, T.P., Pinay, G., 2005. Linking hydrology and biogeochemistry in complex landscapes. Prog. Phys. Geogr. 29, 297–316. https://doi.org/10.1191/0309133305pp450ra
- Buttle, J.M., 1994. Isotope hydrograph separations and rapid delivery of pre-event water from drainage basins. Prog. Phys. Geogr. 18, 16–41. https://doi.org/10.1177/030913339401800102
- Buytaert, W., Célleri, R., De Bièvre, B., Cisneros, F., Wyseure, G., Deckers, J., Hofstede, R., 2006a. Human impact on the hydrology of the Andean páramos. Earth-Science Rev. 79, 53–72. https://doi.org/10.1016/j.earscirev.2006.06.002
- Buytaert, W., De Bièvre, B., Wyseure, G., Deckers, J., 2004. The use of the linear reservoir concept to quantify the impact of changes in land use on the hydrology of catchments in the Andes. Hydrol. Earth Syst. Sci. 8, 108–114. https://doi.org/10.5194/hess-8-108-2004
- Buytaert, W., Deckers, J., Wyseure, G., 2006b. Description and classification of nonallophanic Andosols in south Ecuadorian alpine grasslands (páramo). Geomorphology 73, 207–221. https://doi.org/10.1016/j.geomorph.2005.06.012
- Buytaert, W., Sevink, J., De Leeuw, B., Deckers, J., 2005a. Clay mineralogy of the soils in the south Ecuadorian páramo region. Geoderma 127, 114–129.



- https://doi.org/10.1016/j.geoderma.2004.11.021
- Buytaert, W., Wyseure, G., De Bièvre, B., Deckers, J., 2005b. The effect of land-use changes on the hydrological behaviour of Histic Andosols in south Ecuador 3997, 3985–3997. https://doi.org/10.1002/hyp.5867
- Caissie, D., Pollock, T.L., Cunjak, R.A., 1996. Variation in stream water chemistry and hydrograph separation in a small drainage basin. J. Hydrol. 178, 137–157. https://doi.org/10.1016/0022-1694(95)02806-4
- Carey, S.K., Quinton, W.L., 2005. Evaluating runoff generation during summer using hydrometric, stable isotope and hydrochemical methods in a discontinuous permafrost alpine catchment. Hydrol. Process. 19, 95–114. https://doi.org/10.1002/hyp.5764
- Carrillo-Rojas, G., Silva, B., Córdova, M., Célleri, R., Bendix, J., 2016. Dynamic Mapping of Evapotranspiration Using an Energy Balance-Based Model over an Andean Páramo Catchment of Southern Ecuador. Remote Sens. 8, 160. https://doi.org/10.3390/rs8020160
- Carrillo-Rojas, G., Silva, B., Rollenbeck, R., Célleri, R., Bendix, J., 2019. The breathing of the Andean highlands: Net ecosystem exchange and evapotranspiration over the páramo of southern Ecuador. Agric. For. Meteorol. 265, 30–47. https://doi.org/10.1016/J.AGRFORMET.2018.11.006
- Cey, E.E., Rudolph, D.L., Parkin, G.W., Aravena, R., 1998. Quantifying groundwater discharge to a small perennial stream in southern Ontario, Canada. J. Hydrol. 210, 21–37. https://doi.org/10.1016/S0022-1694(98)00172-3
- Chamberlin, T.C., 1965. The Method of Multiple Working Hypotheses: With this method the dangers of parental affection for a favorite theory can be circumvented. Science 148, 754–9. https://doi.org/10.1126/science.148.3671.754
- Chen, Z.S., Asio, V.B., Yi, D.F., 1999. Characteristics and genesis of volcanic soils along a toposequence under a subtropical climate in Taiwan. Soil Sci. 164, 510–524.
- Clark, M.P., Kavetski, D., Fenicia, F., 2011. Pursuing the method of multiple working hypotheses for hydrological modeling. Water Resour. Res. 47, n/a-n/a. https://doi.org/10.1029/2010WR009827
- Coltorti, M., Ollier, C.., 2000. Geomorphic and tectonic evolution of the Ecuadorian Andes. Geomorphology 32, 1–19. https://doi.org/10.1016/S0169-555X(99)00036-7



- Coplen, T.B., Neiman, P.J., White, A.B., Landwehr, J.M., Ralph, F.M., Dettinger, M.D., 2008. Extreme changes in stable hydrogen isotopes and precipitation characteristics in a landfalling Pacific storm. Geophys. Res. Lett. 35, L21808. https://doi.org/10.1029/2008GL035481
- Coplen, T.B., Neiman, P.J., White, A.B., Ralph, F.M., 2015. Categorisation of northern California rainfall for periods with and without a radar brightband using stable isotopes and a novel automated precipitation collector. Tellus B 67. https://doi.org/10.3402/tellusb.v67.28574
- Córdova, M., Carrillo-Rojas, G., Crespo, P., Wilcox, B., Célleri, R., 2015. Evaluation of the Penman-Monteith (FAO 56 PM) Method for Calculating Reference Evapotranspiration Using Limited Data. http://dx.doi.org/10.1659/MRD-JOURNAL-D-14-0024.1.
- Correa, A., Windhorst, D., Tetzlaff, D., Crespo, P., Célleri, R., Feyen, J., Breuer, L., 2017. Temporal dynamics in dominant runoff sources and flow paths in the Andean Páramo. Water Resour. Res. https://doi.org/10.1002/2016WR020187
- Craig, H., 1961. Standard for Reporting Concentrations of Deuterium and Oxygen-18 in Natural Waters. Science 133, 1833–4. https://doi.org/10.1126/science.133.3467.1833
- Dahlgren, R.A., Saigusa, M., Ugolini, F.C., 2004. The Nature, Properties and Management of Volcanic Soils. Adv. Agron. 82, 113–182. https://doi.org/10.1016/S0065-2113(03)82003-5
- Daly, C., Rothacher, J., 2017. Precipitation measurements from historic and current standard, storage and recording rain gauges at the Andrews Experimental Forest, 1951 to present. In Forest Science Data Bank; Andrews Experimental Forest and Long-Term Ecological Research [WWW Document]. For. Sci. Data Bank; Andrews Exp. For. Long-Term Ecol. Res. URL http://andlter.forestry.oregonstate.edu/data/abstract.aspx?dbcode=MS004 (accessed 12.29.17).
- Daza Torres, M.C., Hernández Flórez, F., Triana, F.A., 2014. Efecto del Uso del Suelo en la Capacidad de Almacenamiento Hídrico en el Páramo de Sumapaz Colombia. Rev. Fac. Nac. Agron. 67, 7189–7200. https://doi.org/10.15446/rfnam.v67n1.42642
- Dec, D., Zúniga, F., Thiers, O., Paulino, L., Valle, S., Villagra, V., Tadich, I., Horn, R., Dörner, J., 2017. Water and temperature dynamics of Aquands under different uses in southern



- Chile. J. Soil Sci. Plant Nutr. 17, 141–154. https://doi.org/10.4067/S0718-95162017005000011
- Dondeyne, S., Deckers, J.A., Chapelle, J., 1993. The soils and vegetation of the Bisoke Volcano (Rwanda): habitat of mountain gorillas. Pedologie 43, 301–322.
- Dorel, M., Roger-Estrade, J., Manichon, H., Delvaux, B., 2006. Porosity and soil water properties of Caribbean volcanic ash soils. Soil Use Manag. 16, 133–140. https://doi.org/10.1111/j.1475-2743.2000.tb00188.x
- Dörner, J., Dec, D., Peng, X., Horn, R., 2010. Effect of land use change on the dynamic behaviour of structural properties of an Andisol in southern Chile under saturated and unsaturated hydraulic conditions. Geoderma 159, 189–197. https://doi.org/10.1016/J.GEODERMA.2010.07.011
- Dörner, J., Dec, D., Peng, X., Horn, R., 2009a. Change of shrinkage behavior of an Andisol in southern Chile: Effects of land use and wetting/drying cycles. Soil Tillage Res. 106, 45–53. https://doi.org/10.1016/J.STILL.2009.09.013
- Dörner, J., Dec, D., Peng, X., Horn, R., 2009b. Efecto del cambio de uso en la estabilidad de la estructura y la función de los poros de un Andisol (typic hapludand) del sur de Chile. Rev. la Cienc. del suelo y Nutr. Veg. 9, 190–209. https://doi.org/10.4067/S0718-27912009000300003
- Dörner, J., Dec, D., Thiers, O., Paulino, L., Zúñiga, F., Valle, S., Martínez, O., Horn, R., 2016. Spatial and temporal variability of physical properties of Aquands under different land uses in southern Chile. Soil Use Manag. 32, 411–421. https://doi.org/10.1111/sum.12286
- Dörner, J., Huertas, J., Cuevas, J.G., Leiva, C., Paulino, L., Arumí, J.L., 2015. Water content dynamics in a volcanic ash soil slope in southern Chile. J. Plant Nutr. Soil Sci. 178, 693–702. https://doi.org/10.1002/jpln.201500112
- Dunkerley, D., 2008. Identifying individual rain events from pluviograph records: a review with analysis of data from an Australian dryland site. Hydrol. Process. 22, 5024–5036.
- Dunn, P.J.H., Carter, J.F., 2018. Publication of the second edition of the FIRMS good practice guide for isotope ratio mass spectrometry. Isotopes Environ. Health Stud. 54, 656–657. https://doi.org/10.1080/10256016.2018.1531495
- Duwig, C., Prado, B., Tinet, A.-J., Delmas, P., Dal Ferro, N., Vandervaere, J.P., Denis, H.,



- Charrier, P., Gastelum Strozzi, A., Morari, F., 2019. Impacts of land use on hydrodynamic properties and pore architecture of volcanic soils from the Mexican Highlands. Soil Res. 57, 629. https://doi.org/10.1071/SR18271
- Dykes, A.P., Thornes, J.B., 2000. Hillslope hydrology in tropical rainforest steeplands in Brunei. Hydrol. Process. 14, 215–235. https://doi.org/10.1002/(SICI)1099-1085(20000215)14:2<215::AID-HYP921>3.0.CO;2-P
- Dyrness, C.T., Hawk, G., 1972. Vegetation and soils of the Hi-15 watersheds, H.J. Andrews Experimental Forest. Coniferous For. Biome, Internal Rep. 43, 28 pp., University of Washington, Seattle, Washington.
- Dyrness, C.T., Norgren, J., Lienkaemper, G., 2005. Soil Survey (1964, Revised in 1994). In Forest Science Data Bank; Andrews Experimental Forest and Long-Term Ecological Research [WWW Document]. For. Sci. Data Bank. URL http://dx.doi.org/10.6073/pasta/7929a43cec090cc21e2e164ef624ddf3 (accessed 11.11.17).
- Eguchi, S., Hasegawa, S., 2008. Determination and Characterization of Preferential Water Flow in Unsaturated Subsoil of Andisol. Soil Sci. Soc. Am. J. 72, 320. https://doi.org/10.2136/sssaj2007.0042
- Elliott, L.P., Brook, B.W., 2007. Revisiting Chamberlin: Multiple Working Hypotheses for the 21st Century. Bioscience 57, 608–614. https://doi.org/10.1641/B570708
- Esquivel-Hernández, G., Mosquera, G.M., Sánchez-Murillo, R., Quesada-Román, A., Birkel, C., Crespo, P., Célleri, R., Windhorst, D., Breuer, L., Boll, J., 2019. Moisture transport and seasonal variations in the stable isotopic composition of rainfall in Central American and Andean Páramo during El Niño conditions (2015-2016). Hydrol. Process. 33, 1802–1817. https://doi.org/10.1002/hyp.13438
- Famiglietti, J.S., Rudnicki, J.W., Rodell, M., 1998. Variability in surface moisture content along a hillslope transect: Rattlesnake Hill, Texas. J. Hydrol. 210, 259–281. https://doi.org/10.1016/S0022-1694(98)00187-5
- Fan, Y., Clark, M., Lawrence, D.M., Swenson, S., Band, L.E., Brantley, S.L., Brooks, P.D., Dietrich, W.E., Flores, A., Grant, G., Kirchner, J.W., Mackay, D.S., McDonnell, J.J., Milly, P.C.D., Sullivan, P.L., Tague, C., Ajami, H., Chaney, N., Hartmann, A.,



- Hazenberg, P., McNamara, J., Pelletier, J., Perket, J., Rouholahnejad-Freund, E., Wagener, T., Zeng, X., Beighley, E., Buzan, J., Huang, M., Livneh, B., Mohanty, B.P., Nijssen, B., Safeeq, M., Shen, C., Verseveld, W., Volk, J., Yamazaki, D., 2019. Hillslope Hydrology in Global Change Research and Earth System Modeling. Water Resour. Res. 55, 1737–1772. https://doi.org/10.1029/2018WR023903
- FAO, 2006. Guidelines for soil description, Fourth. ed. FAO-ISRIC Press, Rome, Italy.
- FAO, 2002. Procedures for Soil Analysis, 6th ed. FAO, Roma, Italy.
- Farley, K., Kelly, E., Hofstede, R., 2004. Soil Organic Carbon and Water Retention after Conversion of Grasslands to Pine Plantations in the Ecuadorian Andes. Ecosystems 7, 729–739.
- Farrick, K.K., Branfireun, B.A., 2015. Flowpaths, source water contributions and water residence times in a Mexican tropical dry forest catchment. J. Hydrol. 529, 854–865. https://doi.org/10.1016/j.jhydrol.2015.08.059
- Fatichi, S., Vivoni, E.R., Ogden, F.L., Ivanov, V.Y., Mirus, B., Gochis, D., Downer, C.W., Camporese, M., Davison, J.H., Ebel, B., Jones, N., Kim, J., Mascaro, G., Niswonger, R., Restrepo, P., Rigon, R., Shen, C., Sulis, M., Tarboton, D., 2016. An overview of current applications, challenges, and future trends in distributed process-based models in hydrology. J. Hydrol. 537, 45–60. https://doi.org/10.1016/J.JHYDROL.2016.03.026
- Fenicia, F., Kavetski, D., Savenije, H.H.G., 2011. Elements of a flexible approach for conceptual hydrological modeling: 1. Motivation and theoretical development. Water Resour. Res. 47, n/a-n/a. https://doi.org/10.1029/2010WR010174
- Ferrari, A., Eichenberger, J., Fern, J., Ebeling, P., Laloui, L., 2012. Experimental and Numerical Analysis of an Unsaturated Volcanic Ash Deposit for the Establishment of an Early Warning System in a Quarry in Costa Rica, in: GeoCongress 2012. American Society of Civil Engineers, Reston, VA, pp. 2512–2521. https://doi.org/10.1061/9780784412121.257
- Fontes, J.C., Gonçalves, M.C., Pereira, L.S., 2004. Andosols of Terceira, Azores: measurement and significance of soil hydraulic properties. CATENA 56, 145–154. https://doi.org/10.1016/J.CATENA.2003.10.008
- Frattini, P., Crosta, G.B., Fusi, N., Dal Negro, P., 2004. Shallow landslides in pyroclastic soils:



- a distributed modelling approach for hazard assessment. Eng. Geol. 73, 277–295. https://doi.org/10.1016/J.ENGGEO.2004.01.009
- Gabrielli, C.P., McDonnell, J.J., 2020. Modifying the Jackson index to quantify the relationship between geology, landscape structure, and water transit time in steep wet headwaters. Hydrol. Process. hyp.13700. https://doi.org/10.1002/hyp.13700
- Gerrard, J., 1990. Mountain environments: an examination of the physical geography of mountains. MIT Press.
- Gómez-Rodríguez, K., Camacho-Tamayo, J.H., Vélez-Sánchez, J.E., 2013. Changes in water availability in the soil due to tractor traffic. Eng. Agrícola 33, 1156–1164. https://doi.org/10.1590/S0100-69162013000600008
- Guio Blanco, C.M., Brito Gomez, V.M., Crespo, P., Ließ, M., 2018. Spatial prediction of soil water retention in a Páramo landscape: Methodological insight into machine learning using random forest. Geoderma 316, 100–114. https://doi.org/10.1016/J.GEODERMA.2017.12.002
- Guo, L., Gifford, R.M., 2002. Soil carbon stocks and land use change: A meta analysis. Glob. Chang. Biol. 8, 345–360. https://doi.org/10.1046/j.1354-1013.2002.00486.x
- Gupta, H. V., Kling, H., Yilmaz, K.K., Martinez, G.F., 2009. Decomposition of the mean squared error and NSE performance criteria: Implications for improving hydrological modelling. J. Hydrol. 377, 80–91. https://doi.org/10.1016/j.jhydrol.2009.08.003
- Guzman, C.D., Hoyos-Villada, F., Da Silva, M., Zimale, F.A., Chirinda, N., Botero, C., Morales Vargas, A., Rivera, B., Moreno, P., Steenhuis, T.S., 2019. Variability of soil surface characteristics in a mountainous watershed in Valle del Cauca, Colombia: Implications for runoff, erosion, and conservation. J. Hydrol. 576, 273–286. https://doi.org/10.1016/J.JHYDROL.2019.06.002
- Hale, V.C., McDonnell, J.J., 2016. Effect of bedrock permeability on stream base flow mean transit time scaling relations: 1. A multiscale catchment intercomparison. Water Resour. Res. 52, 1358–1374. https://doi.org/10.1002/2014WR016124
- Hall, M.L., Calle, J., 1982. Geochronological control for the main tectonic-magmatic events of Ecuador. Earth-Science Rev. 18, 215–239. https://doi.org/10.1016/0012-8252(82)90038-1



- Hardie, M.A., Doyle, R.B., Cotching, W.E., Lisson, S., 2012. Subsurface Lateral Flow in Texture-Contrast (Duplex) Soils and Catchments with Shallow Bedrock. Appl. Environ. Soil Sci. 2012, 1–10. https://doi.org/10.1155/2012/861358
- Harman, C.J., 2015. Time-variable transit time distributions and transport: Theory and application to storage-dependent transport of chloride in a watershed. Water Resour. Res. 51, 1–30. https://doi.org/10.1002/2014WR015707
- Hasegawa, S., Eguchi, S., 2002. Soil water conditions and flow characteristics in the subsoil of a volcanic ash soil: Findings from field monitoring from 1997 to 1999. Soil Sci. Plant Nutr. 48, 227–236. https://doi.org/10.1080/00380768.2002.10409195
- Hasegawa, S., Sakayori, T., 2000. Monitoring of matrix flow and bypass flow through the subsoil in a volcanic ash soil. Soil Sci. Plant Nutr. 46, 661–671. https://doi.org/10.1080/00380768.2000.10409131
- Heidbüchel, I., Troch, P.A., Lyon, S.W., Weiler, M., 2012. The master transit time distribution of variable flow systems. Water Resour. Res. 48, W06520. https://doi.org/10.1029/2011WR011293
- Hillel, D., 1998. Environmental soil physics. Academic Press, San Diego, CA.
- Hodnett, M.G., Tomasella, J., 2002. Marked differences between van Genuchten soil waterretention parameters for temperate and tropical soils: a new water-retention pedo-transfer functions developed for tropical soils. Geoderma 108, 155–180. https://doi.org/10.1016/S0016-7061(02)00105-2
- Hooper, R.P., Christophersen, N., Peters, N.E., 1990. Modelling streamwater chemistry as a mixture of soilwater end-members An application to the Panola Mountain catchment, Georgia, U.S.A. J. Hydrol. 116, 321–343. https://doi.org/10.1016/0022-1694(90)90131-G
- Hooper, R.P., Shoemaker, C.A., 1986. A Comparison of Chemical and Isotopic Hydrograph Separation. Water Resour. Res. 22, 1444–1454. https://doi.org/10.1029/WR022i010p01444
- Hrachowitz, M., Benettin, P., van Breukelen, B.M., Fovet, O., Howden, N.J.K., Ruiz, L., van der Velde, Y., Wade, A.J., 2016. Transit times-the link between hydrology and water quality at the catchment scale. Wiley Interdiscip. Rev. Water 3, 629–657.



- https://doi.org/10.1002/wat2.1155
- Hrachowitz, M., Fovet, O., Ruiz, L., Savenije, H.H.G., 2015. Transit time distributions, legacy contamination and variability in biogeochemical 1/f ^α scaling: how are hydrological response dynamics linked to water quality at the catchment scale? Hydrol. Process. 29, 5241–5256. https://doi.org/10.1002/hyp.10546
- Hrachowitz, M., Savenije, H.H.G., Blöschl, G., McDonnell, J.J., Sivapalan, M., Pomeroy, J.W., Arheimer, B., Blume, T., Clark, M.P., Ehret, U., Fenicia, F., Freer, J.E., Gelfan, A., Gupta, H.V., Hughes, D.A., Hut, R.W., Montanari, A., Pande, S., Tetzlaff, D., Troch, P.A., Uhlenbrook, S., Wagener, T., Winsemius, H.C., Woods, R.A., Zehe, E., Cudennec, C., 2013. A decade of Predictions in Ungauged Basins (PUB)—a review. Hydrol. Sci. J. 58, 1198–1255. https://doi.org/10.1080/02626667.2013.803183
- Iñiguez, V., Morales, O., Cisneros, F., Bauwens, W., Wyseure, G., 2016. Analysis of the drought recovery of Andosols on southern Ecuadorian Andean páramos. Hydrol. Earth Syst. Sci. 20, 2421–2435. https://doi.org/10.5194/hess-20-2421-2016
- ISO 11277, 2009. Soil Quality Determination of Particle Size Distribution in Mineral Soil
 Material Method by Sieving and Sedimentation, Reference Number ISO 11277:2009(E). Geneva, Switzerland.
- IUSS Working Group WRB, 2015. World reference base for soil resources 2014. International soil classification system for naming soils and creating legends for soil maps, World Soil Resources Reports No. 106. Rome. https://doi.org/10.1017/S0014479706394902
- Jakeman, A.J., Hornberger, G.M., 1993. How much complexity is warranted in a rainfall-runoff model? Water Resour. Res. 29, 2637–2649. https://doi.org/10.1029/93WR00877
- Jennings, K., Jones, J.A., 2015. Precipitation-snowmelt timing and snowmelt augmentation of large peak flow events, western Cascades, Oregon. Water Resour. Res. 51, 7649–7661. https://doi.org/10.1002/2014WR016877
- Johnson, M.S., Weiler, M., Couto, E.G., Riha, S.J., Lehmann, J., 2007. Storm pulses of dissolved CO ₂ in a forested headwater Amazonian stream explored using hydrograph separation. Water Resour. Res. 43. https://doi.org/10.1029/2007WR006359
- Johnson, S., 2016. Stream specific conductance and temperature from small watersheds in the Andrews Forest. In Forest Science Data Bank; Andrews Experimental Forest and Long-



- Term Ecological Research [WWW Document]. URL http://dx.doi.org/10.6073/pasta/e3a1ecbada19c89fe6798681456b7cd0 (accessed 6.25.18).
- Johnson, S., Rothacher, J., 2016. Stream discharge in gaged watersheds at the Andrews Experimental Forest, 1949 to present. In Forest Science Data Bank; Andrews Experimental Forest and Long-Term Ecological Research [WWW Document]. For. Sci. Data Bank. URL http://dx.doi.org/10.6073/pasta/ce70a42e1f637cd430d7b0fb64faefb4 (accessed 6.25.18).
- Jones, J.A., Perkins, R.M., 2010. Extreme flood sensitivity to snow and forest harvest, western Cascades, Oregon, United States. Water Resour. Res. 46. https://doi.org/10.1029/2009WR008632
- Karube, J., Abe, Y., 1998. Water Retention by Colloidal Allophane and Imogolite with Different Charges. Clays Clay Miner. 46, 322–329. https://doi.org/10.1346/CCMN.1998.0460311
- Kassaye, K.T., Boulange, J., Saito, H., Watanabe, H., 2019. Calibration of capacitance sensor for Andosol under field and laboratory conditions in the temperate monsoon climate. Soil Tillage Res. 189, 52–63. https://doi.org/10.1016/J.STILL.2018.12.020
- Kendall, C., McDonnell, J.J. (Eds.), 1998. Isotope Tracers in Catchment Hydrology. Elsevier, Amsterdam.
- Kim, S., Jung, S., 2014. Estimation of mean water transit time on a steep hillslope in South Korea using soil moisture measurements and deuterium excess. Hydrol. Process. 28, 1844–1857. https://doi.org/10.1002/hyp.9722
- Kirchner, J.W., 2016. Aggregation in environmental systems Part 1: Seasonal tracer cycles quantify young water fractions, but not mean transit times, in spatially heterogeneous catchments. Hydrol. Earth Syst. Sci. 20, 279–297. https://doi.org/10.5194/hess-20-279-2016
- Kirchner, J.W., Feng, X., Neal, C., 2000. Fractal stream chemistry and its implications for contaminant transport in catchments. Nature 403, 524–527. https://doi.org/10.1038/35000537
- Kirchner, J.W., Feng, X., Neal, C., Robson, A.J., 2004. The fine structure of water-quality



- dynamics: the(high-frequency) wave of the future. Hydrol. Process. 18, 1353–1359. https://doi.org/10.1002/hyp.5537
- Kirkham, M.B., 2014. Field Capacity, Wilting Point, Available Water, and the Nonlimiting Water Range, in: Kirkham, M.B. (Ed.), Principles of Soil and Plant Water Relations. Academic Press, Boston, MA, pp. 153–170. https://doi.org/10.1016/B978-0-12-420022-7.00010-0
- Klaus, Chun, K.P., McGuire, K.J., McDonnell, J.J., 2015. Temporal dynamics of catchment transit times from stable isotope data. Water Resour. Res. 51, 4208–4223. https://doi.org/10.1002/2014WR016247
- Klaus, J., Mcdonnell, J.J., 2013. Hydrograph separation using stable isotopes: Review and evaluation. J. Hydrol. 505, 47–64. https://doi.org/10.1016/j.jhydrol.2013.09.006
- Klaus, J., McDonnell, J.J., Jackson, C.R., Du, E., Griffiths, N.A., 2015. Where does streamwater come from in low-relief forested watersheds? A dual-isotope approach. Hydrol. Earth Syst. Sci. 19, 125–135. https://doi.org/10.5194/hess-19-125-2015
- Koehler, G., Wassenaar, L.I., 2011. Realtime Stable Isotope Monitoring of Natural Waters by Parallel-Flow Laser Spectroscopy. Anal. Chem. 83, 913–919. https://doi.org/10.1021/ac102584q
- Köhne, J.M., Köhne, S., Šimůnek, J., 2009. A review of model applications for structured soils:

 a) Water flow and tracer transport. J. Contam. Hydrol. 104, 4–35. https://doi.org/10.1016/J.JCONHYD.2008.10.002
- Kronholm, S.C., Capel, P.D., 2016. Estimation of time-variable fast flow path chemical concentrations for application in tracer-based hydrograph separation analyses. Water Resour. Res. 52, 6881–6896. https://doi.org/10.1002/2016WR018797
- Kutilek, M., Nielsen, D.R., 1994. Soil Hydrology. Catena Verlag, Cremlingen, Germany.
- Laudon, H., Seibert, J., Köhler, S., Bishop, K., 2004. Hydrological flow paths during snowmelt: Congruence between hydrometric measurements and oxygen 18 in meltwater, soil water, and runoff. Water Resour. Res. 40. https://doi.org/10.1029/2003WR002455
- Laudon, H., Slaymaker, O., 1997. Hydrograph separation using stable isotopes, silica and electrical conductivity: An alpine example. J. Hydrol. 201, 82–101. https://doi.org/10.1016/S0022-1694(97)00030-9



- Lazo, P.X., Mosquera, G.M., McDonnell, J.J., Crespo, P., 2019. The role of vegetation, soils, and precipitation on water storage and hydrological services in Andean Páramo catchments. J. Hydrol. 572, 805–819. https://doi.org/10.1016/J.JHYDROL.2019.03.050
- Letts, M.G., Roulet, N.T., Comer, N.T., Skarupa, M.R., Verseghy, D.L., 2000. Parametrization of peatland hydraulic properties for the Canadian land surface scheme. Atmosphere-Ocean 38, 141–160. https://doi.org/10.1080/07055900.2000.9649643
- Lin, H., 2010. Earth's Critical Zone and hydropedology: concepts, characteristics, and advances. Hydrol. Earth Syst. Sci 14, 25–45.
- Lozano-Parra, J., Schaik, N.L.M.B. Van, Schnabel, S., Gómez-gutiérrez, Á., 2015. Soil moisture dynamics at high temporal resolution in a semiarid Mediterranean watershed with scattered tree cover. https://doi.org/10.1002/hyp.10694
- Maeda, T., Takenaka, H., Warkentin, B.P., 1977. Physical Properties of Allophane Soils. Adv. Agron. 29, 229–264. https://doi.org/10.1016/S0065-2113(08)60220-5
- Maloszewski, P., Zuber, A., 1996. Lumped parameter models for the interpretation of environmental tracer data, in: Manual on Mathematical Models in Isotope Hydrogeology. TECDOC-910.
- Małoszewski, P., Zuber, A., 1982. Determining the turnover time of groundwater systems with the aid of environmental tracers. J. Hydrol. 57, 207–231. https://doi.org/10.1016/0022-1694(82)90147-0
- Marín, F., Dahik, C., Mosquera, G., Feyen, J., Cisneros, P., Crespo, P., 2018. Changes in Soil Hydro-Physical Properties and SOM Due to Pine Afforestation and Grazing in Andean Environments Cannot Be Generalized. Forests 10, 17. https://doi.org/10.3390/f10010017
- Matsubayashi, U., Velasquez, G.T., Takagi, F., 1993. Hydrograph separation and flow analysis by specific electrical conductance of water. J. Hydrol. 152, 179–199. https://doi.org/10.1016/0022-1694(93)90145-Y
- Maurya, A.S., Shah, M., Deshpande, R.D., Bhardwaj, R.M., Prasad, A., Gupta, S.K., 2011. Hydrograph separation and precipitation source identification using stable water isotopes and conductivity: River Ganga at Himalayan foothills. Hydrol. Process. 25, 1521–1530. https://doi.org/10.1002/hyp.7912
- McDaniel, P.A., Lowe, D.J., Arnalds, O., Ping, C.-L., 2012. Andisols, in: Huang, P.M., Li, Y.,



- Summer, M.E. (Eds.), Handbook of Soil Sciences: Properties and Processes. CRC Press (Taylor & Francis), Boca Raton, FL, pp. 29–48.
- McDonnell, J., Owens, I., Stewart, M., 1991. A case study of shallow flow paths in a steep zero-order basin. J. Am. Water Resour. Assoc. 27, 679–685. https://doi.org/10.1111/j.1752-1688.1991.tb01469.x
- McDonnell, J.J., Bonell, M., Stewart, M.K., Pearce, A.J., 1990. Deuterium variations in storm rainfall: Implications for stream hydrograph separation. Water Resour. Res. 26, 455–458. https://doi.org/10.1029/WR026i003p00455
- McDonnell, J.J., Kendall, C., 1992. Isotope tracers in hydrology. Eos, Trans. Am. Geophys. Union 73, 260–260. https://doi.org/10.1029/91EO00214
- McGuire, K.J., McDonnell, J.J., 2010. Hydrological connectivity of hillslopes and streams: Characteristic time scales and nonlinearities. Water Resour. Res. 46, W10543. https://doi.org/10.1029/2010WR009341
- McGuire, K.J., McDonnell, J.J., 2006. A review and evaluation of catchment transit time modeling. J. Hydrol. 330, 543–563. https://doi.org/10.1016/j.jhydrol.2006.04.020
- McGuire, K.J., McDonnell, J.J., Weiler, M., Kendall, C., McGlynn, B.L., Welker, J.M., Seibert, J., 2005. The role of topography on catchment-scale water residence time. Water Resour. Res. 41, n/a-n/a. https://doi.org/10.1029/2004WR003657
- McNamara, J.P., Tetzlaff, D., Bishop, K., Soulsby, C., Seyfried, M., Peters, N.E., Aulenbach, B.T., Hooper, R., 2011. Storage as a Metric of Catchment Comparison. Hydrol. Process. 25, 3364–3371. https://doi.org/10.1002/hyp.8113
- Mertens, J., Vanderborght, J., 2007. Numerical Analysis of Passive Capillary Wick Samplers prior to Field Installation 35–42. https://doi.org/10.2136/sssaj2006.0106
- Messerli, B., Viviroli, D., Weingartner, R., 2004. Mountains of the world: vulnerable water towers for the 21st century. Ambio Spec No 13, 29–34.
- Minasny, B., Hartemink, A.E., 2011. Predicting soil properties in the tropics. Earth-Science Rev. 106, 52–62. https://doi.org/10.1016/J.EARSCIREV.2011.01.005
- Minnesota Board of Water & Soil Resources, 2013. Hydrologic Monitoring of Wetlands.

 Minnesota Board of Water & Soil Resources, St. Paul, MN, Unites States.



- Moldrup, P., Yoshikawa, S., Olesen, T., Komatsu, T., Rolston, D.E., 2003. Gas Diffusivity in Undisturbed Volcanic Ash Soils. Soil Sci. Soc. Am. J. 67, 41. https://doi.org/10.2136/sssaj2003.4100
- Montenegro-Díaz, P., Ochoa-Sánchez, A., Célleri, R., 2019. Impact of tussock grasses removal on soil water content dynamics of a tropical mountain hillslope. Ecohydrology 12, e2146. https://doi.org/10.1002/eco.2146
- Mook, W.G., 2000. Introduction: Theory, methods, review, in: Mook, W.G. (Ed.), Environmental Isotopes in the Hydrological Cycle: Principles and Applications. IAEA and UNESCO, Paris / Vienna.
- Mosquera, G.M., Célleri, R., Lazo, P.X., Vaché, K.B., Perakis, S.S., Crespo, P., 2016a. Combined Use of Isotopic and Hydrometric Data to Conceptualize Ecohydrological Processes in a High-Elevation Tropical Ecosystem. Hydrol. Process. https://doi.org/10.1002/hyp.10927
- Mosquera, G.M., Lazo, P.X., Célleri, R., Wilcox, B.P., Crespo, P., 2015. Runoff from tropical alpine grasslands increases with areal extent of wetlands. CATENA 125, 120–128. https://doi.org/10.1016/j.catena.2014.10.010
- Mosquera, G.M., Segura, C., Vaché, K.B., Windhorst, D., Breuer, L., Crespo, P., 2016b. Insights into the water mean transit time in a high-elevation tropical ecosystem. Hydrol. Earth Syst. Sci. 20, 2987–3004. https://doi.org/10.5194/hess-20-2987-2016
- Mueller, M.H., Alaoui, A., Alewell, C., 2016. Water and solute dynamics during rainfall events in headwater catchments in the Central Swiss Alps under the influence of green alder shrubs and wetland soils. Ecohydrology 9, 950–963. https://doi.org/10.1002/eco.1692
- Mueller, M.H., Alaoui, A., Kuells, C., Leistert, H., Meusburger, K., Stumpp, C., Weiler, M., Alewell, C., 2014. Tracking water pathways in steep hillslopes by δ18O depth profiles of soil water. J. Hydrol. 519, 340–352. https://doi.org/10.1016/j.jhydrol.2014.07.031
- Munksgaard, N.C., Wurster, C.M., Bass, A., Bird, M.I., 2012. Extreme short-term stable isotope variability revealed by continuous rainwater analysis. Hydrol. Process. 26, 3630–3634. https://doi.org/10.1002/hyp.9505
- Munksgaard, N. C., Wurster, C.M., Bass, A., Zagorskis, I., Bird, M.I., 2012. First continuous shipboard δ18O and δD measurements in sea water by diffusion sampling—cavity ring-



- down spectrometry. Environ. Chem. Lett. 10, 301–307. https://doi.org/10.1007/s10311-012-0371-5
- Munksgaard, N.C., Wurster, C.M., Bird, M.I., 2011. Continuous analysis of δ 18 O and δD values of water by diffusion sampling cavity ring-down spectrometry: a novel sampling device for unattended field monitoring of precipitation, ground and surface waters. Rapid Commun. Mass Spectrom. 25, 3706–3712. https://doi.org/10.1002/rcm.5282
- Muñoz-Villers, L.E., Geissert, D.R., Holwerda, F., Mcdonnell, J.J., 2016. Factors influencing stream baseflow transit times in tropical montane watersheds. Hydrol. Earth Syst. Sci 20, 1621–1635. https://doi.org/10.5194/hess-20-1621-2016
- Muñoz-Villers, L.E., McDonnell, J.J., 2012. Runoff generation in a steep, tropical montane cloud forest catchment on permeable volcanic substrate. Water Resour. Res. 48, W09528. https://doi.org/10.1029/2011WR011316
- Muñoz, P., Célleri, R., Feyen, J., 2016. Effect of the Resolution of Tipping-Bucket Rain Gauge and Calculation Method on Rainfall Intensities in an Andean Mountain Gradient. Water 8, 534. https://doi.org/10.3390/w8110534
- Nakamura, R., 1971. Runoff analysis by electrical conductance of water. J. Hydrol. 14, 197–212. https://doi.org/10.1016/0022-1694(71)90035-7
- Nanzyo, M., 2002. Unique Properties of Ash Volcanic Soils. Glob. Environ. Res. 6, 99–112.
- Nash, J.E., Sutcliffe, J.V., 1970. River flow forecasting through conceptual models part I A discussion of principles. J. Hydrol. 10, 282–290. https://doi.org/10.1016/0022-1694(70)90255-6
- Neall, V.E., 2006. Volcanic soils, in: Verheye, W. (Ed.), Land Use and Land Cover, Encyclopaedia of Life Support Systems (EOLSS). EOLSS Publishers with UNESCO, Oxford, U.K., pp. 1–24.
- Negrón, M., López, I., Dörner, J., 2019. Consequences of intensive grazing by dairy cows of contrasting live weights on volcanic ash topsoil structure and pasture dynamics. Soil Tillage Res. 189, 88–97. https://doi.org/10.1016/j.still.2018.12.025
- Nolan, K.M., Hill, B.R., 1990. Storm-runoff generation in the Permanente Creek drainage basin, west central California — An example of flood-wave effects on runoff composition. J. Hydrol. 113, 343–367. https://doi.org/10.1016/0022-1694(90)90183-X



- Ochoa-Sánchez, A., Crespo, P., Carrillo-Rojas, G., Marín, F., Célleri, R., 2020. Unravelling evapotranspiration controls and components in tropical Andean tussock grasslands. Hydrol. Process. hyp.13716. https://doi.org/10.1002/hyp.13716
- Ochoa-Sánchez, A., Crespo, P., Célleri, R., 2018. Quantification of rainfall interception in the high Andean tussock grasslands. Ecohydrology e1946. https://doi.org/10.1002/eco.1946
- Oosterbaan, R.J., Nijland, H.J., 1994. Determining the saturated hydraulic conductivity, in: Ritzema, H. (Ed.), Drainage Principles and Applications. International Institute for Land Reclamation and Improvement (ILRI), Wageningen, The Netherlands, pp. 435–476.
- Orlowski, N., Kraft, P., Pferdmenges, J., Breuer, L., 2016. Exploring water cycle dynamics by sampling multiple stable water isotope pools in a developed landscape in Germany. Hydrol. Earth Syst. Sci 20, 3873–3894. https://doi.org/10.5194/hess-20-3873-2016
- Pachepsky, Y.A., van Genuchten, M.T., 2011. Pedotransfer Functions. Springer, Dordrecht, pp. 556–561. https://doi.org/10.1007/978-90-481-3585-1 109
- Padrón, R.S., Wilcox, B.P., Crespo, P., Célleri, R., 2015. Rainfall in the Andean Páramo: New Insights from High-Resolution Monitoring in Southern Ecuador. J. Hydrometeorol. 16, 985–996. https://doi.org/10.1175/JHM-D-14-0135.1
- Pangle, L.A., Klaus, J., Berman, E.S.F., Gupta, M., McDonnell, J.J., 2013. A new multisource and high-frequency approach to measuring δ 2 H and δ 18 O in hydrological field studies. Water Resour. Res. 49, 7797–7803. https://doi.org/10.1002/2013WR013743
- Pellerin, B.A., Wollheim, W.M., Feng, X., Vörösmarty, C.J., 2008. The application of electrical conductivity as a tracer for hydrograph separation in urban catchments. Hydrol. Process. 22, 1810–1818. https://doi.org/10.1002/hyp.6786
- Penna, D., van Meerveld, H.J., Oliviero, O., Zuecco, G., Assendelft, R.S., Dalla Fontana, G., Borga, M., 2015. Seasonal changes in runoff generation in a small forested mountain catchment. Hydrol. Process. 29, 2027–2042. https://doi.org/10.1002/hyp.10347
- Pesántez, J., Mosquera, G.M., Crespo, P., Breuer, L., Windhorst, D., 2018. Effect of land cover and hydro-meteorological controls on soil water DOC concentrations in a high-elevation tropical environment. Hydrol. Process. 32, 2624–2635. https://doi.org/10.1002/hyp.13224
- Pfister, L., Kirchner, J.W., 2017. Debates-Hypothesis testing in hydrology: Theory and practice. Water Resour. Res. 53, 1792–1798. https://doi.org/10.1002/2016WR020116



- Pfister, L., Martínez-Carreras, N., Hissler, C., Klaus, J., Carrer, G.E., Stewart, M.K., McDonnell, J.J., 2017. Bedrock geology controls on catchment storage, mixing, and release: A comparative analysis of 16 nested catchments. Hydrol. Process. 31, 1828–1845. https://doi.org/10.1002/hyp.11134
- Picarro, 2010. ChemCorrect TM -Solving the Problem of Chemical Contaminants in H20 Stable Isotope Research, PICARRO INC, California, USA.
- Pilgrim, D.H., Huff, D.D., Steele, T.D., 1979. Use of specific conductance and contact time relations for separating flow components in storm runoff. Water Resour. Res. 15, 329–339. https://doi.org/10.1029/WR015i002p00329
- Pinder, G.F., Jones, J.F., 1969. Determination of the ground-water component of peak discharge from the chemistry of total runoff. Water Resour. Res. 5, 438–445. https://doi.org/10.1029/WR005i002p00438
- Ping, C.-L., 2000. Volcanic soils, in: Sigurdsson, H. (Ed.), Encyclopedia of Volcanoes. Academic Press, San Diego, pp. 1259–1270.
- Pochet, G., Van der Velde, M., Vanclooster, M., Delvaux, B., 2007. Hydric properties of high charge, halloysitic clay soils from the tropical South Pacific region. Geoderma 138, 96–109. https://doi.org/10.1016/J.GEODERMA.2006.10.019
- Podwojewski, P., Poulenard, J., Zambrana, T., Hofstede, R., 2006. Overgrazing effects on vegetation cover and properties of volcanic ash soil in the páramo of Llangahua and La Esperanza (Tungurahua, Ecuador). Soil Use Manag. 18, 45–55. https://doi.org/10.1111/j.1475-2743.2002.tb00049.x
- Poulenard, J., Podwojewski, P., Herbillon, A.J., 2003. Characteristics of non-allophanic Andisols with hydric properties from the Ecuadorian páramos. Geoderma 117, 267–281. https://doi.org/10.1016/S0016-7061(03)00128-9
- Poulenard, J., Podwojewski, P., Janeau, J.-L., Collinet, J., 2001. Runoff and soil erosion under rainfall simulation of Andisols from the Ecuadorian Páramo: Effect of tillage and burning. Catena 45, 185–207. https://doi.org/10.1016/S0341-8162(01)00148-5
- Pratt, W.T., Figueroa, J.F., Flores, B.G., 1997. Geology and Mineralization of the Area between 3 and 48S. Western Cordillera, Ecuador. Open File Report, WCr97r28. British Geological Survey.



- Quichimbo, P., Tenorio, G., Borja, P., Cárdenas, I., Crespo, P., Célleri, R., 2012. Efectos sobre las propiedades físicas y químicas de los suelos por el cambio de la cobertura vegetal y uso del suelo: páramo de Quimsacocha al sur del Ecuador. Suelos Ecuatoriales 42, 138–153.
- Ramsay, P.M., Oxley, E.R.B., 1997. The growth form composition of plant communities in the ecuadorian páramos. Plant Ecol. 131, 173–192. https://doi.org/10.1023/A:1009796224479
- Rice, K.C., Hornberger, G.M., 1998. Comparison of hydrochemical tracers to estimate source contributions to peak flow in a small, forested, headwater catchment. Water Resour. Res. 34, 1755–1766. https://doi.org/10.1029/98WR00917
- Richards, L.A., 1941. A pressure-membrane extraction apparatus for soil solution. Soil Sci. 51, 377–386.
- Richardson, A.D., Siccama, T.G., 2000. Are soils like sponges? J. Am. Water Resour. Assoc. 36, 913–918. https://doi.org/10.1111/j.1752-1688.2000.tb04316.x
- Ritter, A., Muñoz-Carpena, R., Regalado, C.M., Vanclooster, M., Lambot, S., 2004. Analysis of alternative measurement strategies for the inverse optimization of the hydraulic properties of a volcanic soil. J. Hydrol. 295, 124–139. https://doi.org/10.1016/J.JHYDROL.2004.03.005
- Roa-García, M.C., Brown, S., Schreier, H., Lavkulich, L.M., 2011. The role of land use and soils in regulating water flow in small headwater catchments of the Andes. Water Resour. Res. 47, W05510. https://doi.org/10.1029/2010WR009582
- Roa-García, M.C., Weiler, M., 2010. Integrated response and transit time distributions of watersheds by combining hydrograph separation and long-term transit time modeling. Hydrol. Earth Syst. Sci. 14, 1537–1549. https://doi.org/10.5194/hess-14-1537-2010
- Rode, M., Wade, A.J., Cohen, M.J., Hensley, R.T., Bowes, M.J., Kirchner, J.W., Arhonditsis, G.B., Jordan, P., Kronvang, B., Halliday, S.J., Skeffington, R.A., Rozemeijer, J.C., Aubert, A.H., Rinke, K., Jomaa, S., 2016. Sensors in the Stream: The High-Frequency Wave of the Present. Environ. Sci. Technol. 50, 10297–10307. https://doi.org/10.1021/acs.est.6b02155
- Rodriguez, N.B., McGuire, K.J., Klaus, J., 2018. Time-Varying Storage-Water Age



- Relationships in a Catchment With a Mediterranean Climate. Water Resour. Res. 54, 3988–4008. https://doi.org/10.1029/2017WR021964
- Rustanto, A., Booij, M.J., Wösten, H., Hoekstra, A.Y., 2017. Application and recalibration of soil water retention pedotransfer functions in a tropical upstream catchment: case study in Bengawan Solo, Indonesia. J. Hydrol. Hydromechanics 65, 307–320. https://doi.org/10.1515/johh-2017-0020 Open access PDF
- Salazar, I., Millar, D., Lara, V., Nuñez, M., Parada, M., Alvear, M., Baraona, J., 2012. Effects of the application of biosolids on some chemical, biological and physical properties in an Andisol from southern Chile. J. soil Sci. plant Nutr. 12, 441–450. https://doi.org/10.4067/S0718-95162012005000006
- Sato, T., Tokunaga, K., 1976. The fundamental studies on the soil sampling method: II. Analysis of sampled area variation of the distribution of the physical properties of soils found in large area farm land. Trans Jpn Soc Irrig Drain Reclam Eng 63, 1–7,.
- Schlanger, S.O., Jenkyns, H.C., Premoli-Silva, I., 1981. Volcanism and vertical tectonics in the Pacific Basin related to global Cretaceous transgressions. Earth Planet. Sci. Lett. 52, 435–449. https://doi.org/10.1016/0012-821X(81)90196-5
- Schwärzel, K., Renger, M., Sauerbrey, R., Wessolek, G., 2002. Soil physical characteristics of peat soils. J. Plant Nutr. Soil Sci. 165, 479. https://doi.org/10.1002/1522-2624(200208)165:4<479::AID-JPLN479>3.0.CO;2-8
- Segura, C., James, A.L., Lazzati, D., Roulet, N.T., 2012. Scaling relationships for event water contributions and transit times in small-forested catchments in Eastern Quebec. Water Resour. Res. 48, n/a-n/a. https://doi.org/10.1029/2012WR011890
- Selker, J.S., Keller, C.K., McCord, J.T., 1999. Vadose zone processes. Lewis Publishers, Boca Raton, FL.
- Shoji, S., Dahlgren, R., Nanzyo, M., 1993. Chapter 1 Terminology, Concepts and Geographic Distribution of Volcanic Ash Soils. Dev. Soil Sci. 21, 1–5. https://doi.org/10.1016/S0166-2481(08)70262-9
- Shoji, Sadao, Nanzyo, M., Dahlgren, R., 1993. Volcanic ash soils: Genesis, properties and utilization, Statewide Agricultural Land Use Baseline 2015. Development in Soil Science 21, London. https://doi.org/10.1017/CBO9781107415324.004



- Sklash, M.G., Farvolden, R.N., 1979. The role of groundwater in storm runoff. J. Hydrol. 43, 45–65. https://doi.org/10.1016/0022-1694(79)90164-1
- Sklenar, P., Jorgensen, P.M., 1999. Distribution patterns of paramo plants in Ecuador. J. Biogeogr. 26, 681–691. https://doi.org/10.1046/j.1365-2699.1999.00324.x
- Soil Survey Staff, 2015. Illustrated guide to soil taxonomy, version 2., 2nd ed. U.S. Department of Agriculture, Natural Resources Conservation Service, National Soil Survey Center, Lincoln, Nebraska.
- Soil Survey Staff, 2010. Keys to Soil Taxonomy, 11th ed. Washington, DC.
- Soil Survey Staff, 1999. Soil Taxonomy, 2nd ed. USDA-NRCS, Agriculture Handbook No.436.
- Solone, R., Bittelli, M., Tomei, F., Morari, F., 2012. Errors in water retention curves determined with pressure plates: Effects on the soil water balance. J. Hydrol. 470–471, 65–74. https://doi.org/10.1016/J.JHYDROL.2012.08.017
- Spilling, K.H., 2018. Pedotransfer functions for predicting hydraulic properties of nonallophanic Andosols and Histosols in the Páramo of southern Ecuador. Norwegian University of Life Sciences.
- Sprenger, M., Leistert, H., Gimbel, K., Weiler, M., 2016. Illuminating hydrological processes at the soil-vegetation-atmosphere interface with water stable isotopes. Rev. Geophys. https://doi.org/10.1002/2015RG000515
- Stakman, W.D., Valk, G.A., Van Der Harst, G.G., 1969. Determination of soil moisture retention curves. I. Sandbox apparatus. Range pF 0 to 2.7. Wageningen.
- Stanley, S.M., 2004. Earth system history. W.H. Freeman.
- Stewart, M.K., McDonnell, J.J., 1991. Modeling Base Flow Soil Water Residence Times From Deuterium Concentrations. Water Resour. Res. 27, 2681–2693. https://doi.org/10.1029/91WR01569
- Stockinger, M.P., Bogena, H.R., Lücke, A., Diekkrüger, B., Cornelissen, T., Vereecken, H., 2016. Tracer sampling frequency influences estimates of young water fraction and streamwater transit time distribution. J. Hydrol. 541, 952–964. https://doi.org/10.1016/j.jhydrol.2016.08.007



- Stumpp, C., Maloszewski, P., Stichler, W., Fank, J., 2009. Environmental isotope (δ18O) and hydrological data to assess water flow in unsaturated soils planted with different crops: Case study lysimeter station "Wagna" (Austria). J. Hydrol. 369, 198–208. https://doi.org/10.1016/j.jhydrol.2009.02.047
- Swanson, F.J., James, M.E., 1975. Geology and geomorphology of the H.J. Andrews Experimental Forest, western Cascades, Oregon. Res. Pap. PNW-188, 14 p. U.S. Dep. of Agric., For. Serv., Pac. Northwest For. and Range Exp. Stn., Portland, Oregon.
- Swanson, F.J., Jones, J.A., 2002. Geomorphology and hydrology of the HJ Andrews experimental forest, Blue River, Oregon, in: Moore, G.W. (Ed.), Field Guide to Geologic Processes in Cascadia. Oregon Department of Geology and Mineral Industries, pp. 289–313.
- Takahashi, T., Shoji, S., 2002. Distribution and Classification of Volcanic Ash Soils. Glob. Environ. Res. 6, 83–97.
- Tenelanda-Patiño, D., Crespo-Sánchez, P., Mosquera-Rojas, G., 2018. Umbrales en la respuesta de humedad del suelo a condiciones meteorológicas en una ladera Altoandina. MASKANA 9, 53–65. https://doi.org/10.18537/mskn.09.02.07
- Terribile, F., Iamarino, M., Langella, G., Manna, P., Mileti, F.A., Vingiani, S., Basile, A., 2018. The hidden ecological resource of andic soils in mountain ecosystems: evidence from Italy. Solid Earth 9, 63–74. https://doi.org/10.5194/se-9-63-2018
- Tetzlaff, D., Birkel, C., Dick, J., Geris, J., Soulsby, C., 2014. Storage dynamics in hydropedological units control hillslope connectivity, runoff generation, and the evolution of catchment transit time distributions. Water Resour. Res. 50, 969–985. https://doi.org/10.1002/2013WR014147
- Timbe, E., Windhorst, D., Celleri, R., Timbe, L., Crespo, P., Frede, H.-G., Feyen, J., Breuer, L., 2015. Sampling frequency trade-offs in the assessment of mean transit times of tropical montane catchment waters under semi-steady-state conditions. Hydrol. Earth Syst. Sci 19, 1153–1168. https://doi.org/10.5194/hess-19-1153-2015
- Timbe, E., Windhorst, D., Crespo, P., Frede, H.-G., Feyen, J., Breuer, L., 2014. Understanding uncertainties when inferring mean transit times of water trough tracer-based lumped-parameter models in Andean tropical montane cloud forest catchments. Hydrol. Earth



- Syst. Sci. 18, 1503–1523. https://doi.org/10.5194/hess-18-1503-2014
- Tjahyandari, D., 1998. Characteristics of volcanic ash soils of southern area of Mount Ruapehu, North Island, New Zealand. Massey University.
- Tokumoto, I., Noborio, K., Koga, K., 2010. Coupled water and heat flow in a grass field with aggregated Andisol during soil-freezing periods. Cold Reg. Sci. Technol. 62, 98–106. https://doi.org/10.1016/j.coldregions.2010.03.005
- Tonneijck, F.H., Jansen, B., Nierop, K.G.J., Verstraten, J.M., Sevink, J., De Lange, L., 2010. Towards understanding of carbon stocks and stabilization in volcanic ash soils in natural Andean ecosystems of northern Ecuador. Eur. J. Soil Sci. 61, 392–405. https://doi.org/10.1111/j.1365-2389.2010.01241.x
- Topp, G.C., Zebchuk, W., 1979. The determination of soil-water desorption curves for soil cores. Can. J. Soil Sci. 59, 19–26. https://doi.org/10.4141/cjss79-003
- Torres, R., Dietrich, W.E., Montgomery, D.R., Anderson, S.P., Loague, K., 1998. Unsaturated zone processes and the hydrologic response of a steep, unchanneled catchment. Water Resour. Res. 34, 1865–1879. https://doi.org/10.1029/98WR01140
- Tweed, S., Munksgaard, N., Marc, V., Rockett, N., Bass, A., Forsythe, A.J., Bird, M.I., Leblanc, M., 2015. Continuous monitoring of stream δ 18 O and δ 2 H and stormflow hydrograph separation using laser spectrometry in an agricultural catchment. Hydrol. Process. 30, n/a-n/a. https://doi.org/10.1002/hyp.10689
- Uchida, T., Kosugi, K., Mizuyama, T., 1999. Runoff characteristics of pipeflow and effects of pipeflow on rainfall-runoff phenomena in a mountainous watershed. J. Hydrol. 222, 18–36. https://doi.org/10.1016/S0022-1694(99)00090-6
- Uhlenbrook, S., Hoeg, S., 2003. Quantifying uncertainties in tracer-based hydrograph separations: a case study for two-, three- and five-component hydrograph separations in a mountainous catchment. Hydrol. Process. 17, 431–453. https://doi.org/10.1002/hyp.1134
- UMS, 2011. T8 Long-term Monitoring Tensiometer User Manual. München, Germany.
- Vaché, K.B., McDonnell, J.J., 2006. A process-based rejectionist framework for evaluating catchment runoff model structure. Water Resour. Res. 42, n/a-n/a. https://doi.org/10.1029/2005WR004247



- Vaché, K.B., McDonnell, J.J., Bolte, J., 2004. On the use of multiple criteria for a posteriori model rejection: Soft data to characterize model performance. Geophys. Res. Lett. 31, n/a-n/a. https://doi.org/10.1029/2004GL021577
- van Dam, J.C., Stricker, J.N.M., Droogers, P., 1992. Inverse Method for Determining Soil Hydraulic Functions from One-Step Outflow Experiments. Soil Sci. Soc. Am. J. 56, 1042. https://doi.org/10.2136/sssaj1992.03615995005600040007x
- van der Velde, Y., Heidbüchel, I., Lyon, S.W., Nyberg, L., Rodhe, A., Bishop, K., Troch, P.A., 2015. Consequences of mixing assumptions for time-variable travel time distributions. Hydrol. Process. 29, 3460–3474. https://doi.org/10.1002/hyp.10372
- van Huijgevoort, M.H.J., Tetzlaff, D., Sutanudjaja, E.H., Soulsby, C., 2016. Using high resolution tracer data to constrain water storage, flux and age estimates in a spatially distributed rainfall-runoff model. Hydrol. Process. 30, 4761–4778. https://doi.org/10.1002/hyp.10902
- van Lier, Q. de J., Pinheiro, E.A.R., Inforsato, L., van Lier, Q. de J., Pinheiro, E.A.R., Inforsato, L., 2019. Hydrostatic Equilibrium between Soil Samples and Pressure Plates Used in Soil Water Retention Determination: Consequences of a Questionable Assumption. Rev. Bras. Ciência do Solo 43. https://doi.org/10.1590/18069657rbcs20190014
- Van Ranst, E., Utami, S., Shamshuddin, J., 2002. Andisols on Volcanic Ash from Java Island, Indonesia: Physico-chemical Properties and Classification. Soil Sci. 167, 68–79.
- Vereecken, H., Huisman, J.A., Hendricks Franssen, H.J., Brüggemann, N., Bogena, H.R., Kollet, S., Javaux, M., van der Kruk, J., Vanderborght, J., 2015. Soil hydrology: Recent methodological advances, challenges, and perspectives. Water Resour. Res. 51, 2616–2633. https://doi.org/10.1002/2014WR016852
- Vereecken, H., Schnepf, A., Hopmans, J.W., Javaux, M., Or, D., Roose, T., Vanderborght, J., Young, M.H., Amelung, W., Aitkenhead, M., Allison, S.D., Assouline, S., Baveye, P., Berli, M., Brüggemann, N., Finke, P., Flury, M., Gaiser, T., Govers, G., Ghezzehei, T., Hallett, P., Hendricks Franssen, H.J., Heppell, J., Horn, R., Huisman, J.A., Jacques, D., Jonard, F., Kollet, S., Lafolie, F., Lamorski, K., Leitner, D., McBratney, A., Minasny, B., Montzka, C., Nowak, W., Pachepsky, Y., Padarian, J., Romano, N., Roth, K., Rothfuss, Y., Rowe, E.C., Schwen, A., Šimůnek, J., Tiktak, A., Van Dam, J., van der Zee, S.E.A.T.M., Vogel, H.J., Vrugt, J.A., Wöhling, T., Young, I.M., 2016. Modeling Soil



- Processes: Review, Key Challenges, and New Perspectives. Vadose Zo. J. 15, 0. https://doi.org/10.2136/vzj2015.09.0131
- Vereecken, H., Weynants, M., Javaux, M., Pachepsky, Y., Schaap, M.G., Genuchten, M.T. van, 2010. Using Pedotransfer Functions to Estimate the van Genuchten–Mualem Soil Hydraulic Properties: A Review. Vadose Zo. J. 9, 795. https://doi.org/10.2136/vzj2010.0045
- Viviroli, D., Archer, D.R., Buytaert, W., Fowler, H.J., Greenwood, G.B., Hamlet, A.F., Huang, Y., Koboltschnig, G., Litaor, M.I., López-Moreno, J.I., Lorentz, S., Schädler, B., Schreier, H., Schwaiger, K., Vuille, M., Woods, R., 2011. Climate change and mountain water resources: overview and recommendations for research, management and policy. Hydrol. Earth Syst. Sci. 15, 471–504. https://doi.org/10.5194/hess-15-471-2011
- Viviroli, D., Dürr, H.H., Messerli, B., Meybeck, M., Weingartner, R., 2007. Mountains of the world, water towers for humanity: Typology, mapping, and global significance. Water Resour. Res. 43, n/a-n/a. https://doi.org/10.1029/2006WR005653
- Volkmann, T.H.M., Haberer, K., Gessler, A., Weiler, M., 2016. High-resolution isotope measurements resolve rapid ecohydrological dynamics at the soil-plant interface. New Phytol. 210, 839–849. https://doi.org/10.1111/nph.13868
- von Freyberg, J., Studer, B., Kirchner, J.W., 2017. A lab in the field: high-frequency analysis of water quality and stable isotopes in stream water and precipitation. Hydrol. Earth Syst. Sci. 21, 1721–1739. https://doi.org/10.5194/hess-21-1721-2017
- Wada, K., 1985. The Distinctive Properties of Andosols. Springer, New York, NY, pp. 173–229. https://doi.org/10.1007/978-1-4612-5088-3_4
- Walczak, R., Rovdan, E., Witkowska-Walczak, B., 2002. Water retention characteristics of peat and sand mixtures. Int. Agrophysics 16, 161–165.
- Weiler, M., McGlynn, B.L., McGuire, K.J., McDonnell, J.J., 2003. How does rainfall become runoff? A combined tracer and runoff transfer function approach. Water Resour. Res. 39, n/a-n/a. https://doi.org/10.1029/2003WR002331
- White, J.W.C., 1989. Stable Hydrogen Isotope Ratios in Plants: A Review of Current Theory and Some Potential Applications. Springer, New York, NY, pp. 142–162. https://doi.org/10.1007/978-1-4612-3498-2_10



- Windhorst, D., Kraft, P., Timbe, E., Frede, H.-G., Breuer, L., 2014. Stable water isotope tracing through hydrological models for disentangling runoff generation processes at the hillslope scale. Hydrol. Earth Syst. Sci. 18, 4113–4127. https://doi.org/10.5194/hess-18-4113-2014
- Wright, C., Kagawa-Viviani, A., Gerlein-Safdi, C., Mosquera, G.M., Poca, M., Tseng, H., Chun, K.P., 2017. Advancing ecohydrology in the changing tropics: Perspectives from early career scientists. Ecohydrology e1918. https://doi.org/10.1002/eco.1918
- Yáñez, N., Dec, D., Clunes, J., Dörner, J., 2015. Estimación de la curva de retención de agua de un Andisol bajo un cultivo de arándano, a través de funciones de pedotransferencia. Agro Sur 43, 63–72. https://doi.org/10.4206/agrosur.2015.v43n3-07
- Yang, Fei, Zhang, G.-L., Yang, J.-L., Li, D.-C., Zhao, Y.-G., Liu, F., Yang, R.-M., Yang, Fan, 2014. Organic matter controls of soil water retention in an alpine grassland and its significance for hydrological processes. J. Hydrol. 519, 3086–3093. https://doi.org/10.1016/J.JHYDROL.2014.10.054
- Zhu, Q., Nie, X., Zhou, X., Liao, K., Li, H., 2014. Soil moisture response to rainfall at different topographic positions along a mixed land-use hillslope. CATENA 119, 61–70. https://doi.org/10.1016/J.CATENA.2014.03.010



Appendix A

Methodology used for the compilation of the published literature reporting on the water retention characteristics of volcanic ash soils with andic properties (Andosols/Andisols).

The literature review of studies presenting water retention curve (WRC) data for Andosols included articles published in international peer-reviewed journals indexed in the Scopus, Web of Science, and SciELo databases. We used the following search terms with logical operators: ("Andosol" OR "Andisol" OR "Volcanic ash") AND ("Water retention curve" OR "Moisture release curve" OR "Moisture characteristic curve" OR "pF curve"). Further on, the literature search was extended by conducting a "citation chasing" of papers referenced within the documents selected in the initial search and what we identified as relevant information, including PhD and MSc dissertations. From this search, we selected papers that reported quantitative information (figures or tables) about WRCs of Andosols or volcanic ash soils with andic properties (i.e., pumice soils were excluded). We found 81 studies that met these criteria (the list of selected documents can be found as Supplementary Appendix S1 online). The literature search was first used to identify (i) the research objectives for which WRCs of Andosols have been used, (ii) the measuring methods applied, and (iii) the volume of the soil samples used for the determination of the WRCs (data summarized in Figure 2.1).



Appendix B

List of the 81 consulted studies presenting the water retention curves of Andosols.

- Abera G, Wolde-Meskel E. 2013. Soil Properties, and Soil Organic Carbon Stocks of Tropical Andosol under Different Land Uses. Open Journal of Soil Science 03 (03): 153– 162 DOI: 10.4236/ojss.2013.33018
- 2. Alavi G, Tomer MD. 2001. Estimation of soil hydraulic parameters to simulate water flux in volcanic soils. New Zealand Journal of Forestry Science 31 (1): 51–65 Available at: https://www.scionresearch.com/services/science-publications/new-zealand-journal-of-forestry-science/nzjfs-volume-31 [Accessed 25 September 2019]
- 3. Armas-Espinel S, Hernández-Moreno JM, Muñoz-Carpena R, Regalado CM. 2003. Physical properties of "sorriba"-cultivated volcanic soils from Tenerife in relation to andic diagnostic parameters. Geoderma 117 (3–4): 297–311 DOI: 10.1016/S0016-7061(03)00130-7
- 4. Asada K, Eguchi S, Ikeba M, Kato T, Yada S, Nakajima Y, Itahashi S. 2018. Modeling nitrogen leaching from Andosols amended with different composted manures using LEACHM. Nutrient Cycling in Agroecosystems 110 (2): 307–326 DOI: 10.1007/s10705-017-9899-x
- 5. Basile A, Ciollaro G, Coppola A. 2003a. Hysteresis in soil water characteristics as a key to interpreting comparisons of laboratory and field measured hydraulic properties. Water Resources Research 39 (12) DOI: 10.1029/2003WR002432
- 6. Basile A, Mele G, Terribile F. 2003b. Soil hydraulic behaviour of a selected benchmark soil involved in the landslide of Sarno 1998. Geoderma 117 (3–4): 331–346 DOI: 10.1016/S0016-7061(03)00132-0
- 7. Beck-Broichsitter S, Fleige H, Goebel M-O, Dörner J, Bachmann J, Horn R. 2016. Shrinkage potential and pore shrinkage capacity of differently developed volcanic ash soils under pastures in southern Chile. Journal of Plant Nutrition and Soil Science 179 (6): 799–808 DOI: 10.1002/jpln.201600110
- 8. Blume T, Zehe E, Bronstert A. 2009. Use of soil moisture dynamics and patterns at different spatio-temporal scales for the investigation of subsurface flow processes. Hydrological Processes 13 (7): 1215–1233
- 9. Borja P. 2006. Desarrollo de las funciones de edafo transferencia para la caracterizacion hidraulica de andosoles.Universidad de Cuenca. Available at: http://dspace.ucuenca.edu.ec/handle/123456789/20330
- 10. Buytaert W, De Bièvre B, Wyseure G, Deckers J. 2004. The use of the linear reservoir concept to quantify the impact of changes in land use on the hydrology of catchments in the Andes. Hydrology and Earth System Sciences 8 (1): 108–114 DOI: 10.5194/hess-8-108-2004
- 11. Buytaert W, Deckers J, Wyseure G. 2006. Regional variability of volcanic ash soils in south Ecuador: The relation with parent material, climate and land use. Catena 70 (2): 143–154 DOI: 10.1016/j.catena.2006.08.003



- 12. Buytaert W, Wyseure G, De Bièvre B, Deckers J. 2005. The effect of land-use changes on the hydrological behaviour of Histic Andosols in south Ecuador. 3997 (August): 3985–3997 DOI: 10.1002/hyp.5867
- 13. Chen ZS, Asio VB, Yi DF. 1999. Characteristics and genesis of volcanic soils along a toposequence under a subtropical climate in Taiwan. Soil Science 164 (7): 510–524
- 14. Daza Torres MC, Hernández Flórez F, Triana FA. 2014. Efecto del Uso del Suelo en la Capacidad de Almacenamiento Hídrico en el Páramo de Sumapaz Colombia. Revista Facultad Nacional de Agronomía 67 (1): 7189–7200 DOI: 10.15446/rfnam.v67n1.42642
- 15. Dec D, Zúniga F, Thiers O, Paulino L, Valle S, Villagra V, Tadich I, Horn R, Dörner J. 2017. Water and temperature dynamics of Aquands under different uses in southern Chile. Journal of Soil Science and Plant Nutrition 17 (1): 141–154 DOI: 10.4067/S0718-95162017005000011
- 16. Dondeyne S, Deckers JA, Chapelle J. 1993. The soils and vegetation of the Bisoke Volcano (Rwanda): habitat of mountain gorillas. Pedologie 43 (2): 301–322
- 17. Dorel M, Roger-Estrade J, Manichon H, Delvaux B. 2006. Porosity and soil water properties of Caribbean volcanic ash soils. Soil Use and Management 16 (2): 133–140 DOI: 10.1111/j.1475-2743.2000.tb00188.x
- 18. Dörner J, Dec D, Feest E, Vásquez N, Díaz M. 2012. Dynamics of soil structure and pore functions of a volcanic ash soil under tillage. Soil and Tillage Research 125: 52–60 DOI: 10.1016/J.STILL.2012.05.019
- 19. Dörner J, Dec D, Peng X, Horn R. 2009a. Change of shrinkage behavior of an Andisol in southern Chile: Effects of land use and wetting/drying cycles. Soil and Tillage Research 106 (1): 45–53 DOI: 10.1016/J.STILL.2009.09.013
- 20. Dörner J, Dec D, Peng X, Horn R. 2009b. Efecto del cambio de uso en la estabilidad de la estructura y la función de los poros de un Andisol (typic hapludand) del sur de Chile. Revista de la ciencia del suelo y nutrición vegetal 9 (3): 190–209 DOI: 10.4067/S0718-27912009000300003
- 21. Dörner J, Dec D, Peng X, Horn R. 2010. Effect of land use change on the dynamic behaviour of structural properties of an Andisol in southern Chile under saturated and unsaturated hydraulic conditions. Geoderma 159 (1–2): 189–197 DOI: 10.1016/J.GEODERMA.2010.07.011
- 22. Dörner J, Dec D, Thiers O, Paulino L, Zúñiga F, Valle S, Martínez O, Horn R. 2016. Spatial and temporal variability of physical properties of Aquands under different land uses in southern Chile. Soil Use and Management 32 (3): 411–421 DOI: 10.1111/sum.12286
- 23. Dörner J, Dec D, Zúñiga F, Sandoval P, Horn R. 2011. Effect of land use change on Andosol's pore functions and their functional resilience after mechanical and hydraulic stresses. Soil and Tillage Research 115–116: 71–79 DOI: 10.1016/J.STILL.2011.07.002
- 24. Dörner J, Huertas J, Cuevas JG, Leiva C, Paulino L, Arumí JL. 2015. Water content dynamics in a volcanic ash soil slope in southern Chile. Journal of Plant Nutrition and Soil Science 178 (4): 693–702 DOI: 10.1002/jpln.201500112
- 25. Duwig C, Prado B, Tinet A-J, Delmas P, Dal Ferro N, Vandervaere JP, Denis H, Charrier P, Gastelum Strozzi A, Morari F. 2019. Impacts of land use on hydrodynamic properties and pore architecture of volcanic soils from the Mexican Highlands. Soil Research 57 (6): 629 DOI: 10.1071/SR18271



- 26. Eguchi S, Hasegawa S. 2008. Determination and Characterization of Preferential Water Flow in Unsaturated Subsoil of Andisol. Soil Science Society of America Journal 72 (2): 320 DOI: 10.2136/sssaj2007.0042
- 27. Farley K, Kelly E, Hofstede R. 2004. Soil Organic Carbon and Water Retention after Conversion of Grasslands to Pine Plantations in the Ecuadorian Andes. Ecosystems 7: 729–739
- 28. Ferrari A, Eichenberger J, Fern J, Ebeling P, Laloui L. 2012. Experimental and Numerical Analysis of an Unsaturated Volcanic Ash Deposit for the Establishment of an Early Warning System in a Quarry in Costa Rica. In GeoCongress 2012American Society of Civil Engineers: Reston, VA; 2512–2521. DOI: 10.1061/9780784412121.257
- 29. Fontes JC, Gonçalves MC, Pereira LS. 2004. Andosols of Terceira, Azores: measurement and significance of soil hydraulic properties. CATENA 56 (1–3): 145–154 DOI: 10.1016/J.CATENA.2003.10.008
- 30. Frattini P, Crosta GB, Fusi N, Dal Negro P. 2004. Shallow landslides in pyroclastic soils: a distributed modelling approach for hazard assessment. Engineering Geology 73 (3–4): 277–295 DOI: 10.1016/J.ENGGEO.2004.01.009
- 31. Garcia-Rodeja E, Silva BM, Macías F. 1987. Andosols developed from non-volcanic materials in Galicia, NW Spain. Journal of Soil Science 38 (4): 573–591 DOI: 10.1111/j.1365-2389.1987.tb02156.x
- 32. Gerding V, Thiers O. 2002. Caracterización de suelos bajo bosques de Nothofagus betuloides (Mirb) Blume, en Tierra del Fuego, Chile. Revista chilena de historia natural 75 (4): 819–833 DOI: 10.4067/S0716-078X2002000400015
- 33. Gómez-Rodríguez K, Camacho-Tamayo JH, Vélez-Sánchez JE. 2013. Changes in water availability in the soil due to tractor traffic. Engenharia Agrícola 33 (6): 1156–1164 DOI: 10.1590/S0100-69162013000600008
- 34. Greco R, Guida A, Damiano E, Olivares L. 2010. Soil water content and suction monitoring in model slopes for shallow flowslides early warning applications. Physics and Chemistry of the Earth, Parts A/B/C 35 (3–5): 127–136 DOI: 10.1016/J.PCE.2009.12.003
- 35. Guio Blanco CM, Brito Gomez VM, Crespo P, Ließ M. 2018. Spatial prediction of soil water retention in a Páramo landscape: Methodological insight into machine learning using random forest. Geoderma 316: 100–114 DOI: 10.1016/J.GEODERMA.2017.12.002
- 36. Hernandez O, Cordão Neto MP, Caicedo B. 2018. Structural features and hydromechanical behaviour of a compacted andesitic volcanic soil. Géotechnique Letters 8 (3): 195–200 DOI: 10.1680/jgele.18.00056
- 37. Hernández Z, Almendros G. 2012. Biogeochemical factors related with organic matter degradation and C storage in agricultural volcanic ash soils. Soil Biology and Biochemistry 44 (1): 130–142 DOI: 10.1016/J.SOILBIO.2011.08.009
- 38. Hincapié Gómez E, Tobón Marín C. 2012. Dinámica del Agua en Andisoles Bajo Condiciones de Ladera. Revista Facultad Nacional de Agronomía 65 (2): 6765–6777 Available at: http://www.scielo.org.co/scielo.php?script=sci_arttext&pid=S0304-28472012000200020 [Accessed 19 October 2018]
- 39. Iñiguez V, Morales O, Cisneros F, Bauwens W, Wyseure G. 2016. Analysis of the drought recovery of Andosols on southern Ecuadorian Andean páramos. Hydrology and Earth System Sciences 20 (6): 2421–2435 DOI: 10.5194/hess-20-2421-2016



- 40. Iwata Y, Miyamoto T, Kameyama K, Nishiya M. 2017. Effect of sensor installation on the accurate measurement of soil water content. European Journal of Soil Science 68 (6): 817–828 DOI: 10.1111/ejss.12493
- 41. Karube J, Abe Y. 1998. Water Retention by Colloidal Allophane and Imogolite with Different Charges. Clays and Clay Minerals 46 (3): 322–329 DOI: 10.1346/CCMN.1998.0460311
- 42. Kassaye KT, Boulange J, Saito H, Watanabe H. 2019. Calibration of capacitance sensor for Andosol under field and laboratory conditions in the temperate monsoon climate. Soil and Tillage Research 189: 52–63 DOI: 10.1016/J.STILL.2018.12.020
- 43. Kawamoto K, Moldrup P, Komatsu T, de Jonge LW, Oda M. 2007. Water Repellency of Aggregate Size Fractions of a Volcanic Ash Soil. Soil Science Society of America Journal 71 (6): 1658 DOI: 10.2136/sssaj2006.0284
- 44. Lorenzoni P, Mirabella A, Bidini D, Lulli L. 1995. Soil genesis on trachytic and leucititic lavas of Cimini volcanic complex (Latium, Italy). Geoderma 68 (1–2): 79–99 DOI: 10.1016/0016-7061(95)00027-L
- 45. Maeda T, Soma K, Warkentin BP. 1983. Physical and Engineering Characteristics of Volcanic Ash Soils in Japan Compared with Those in Other Countries. Journal of Irrigation Engineering and Rural Planning 1983 (3): 16–31 DOI: 10.11408/jierp1982.1983.16
- 46. La Manna L. 2005. Caracterización de los suelos bajo bosque de Austrocedrus chilensis a través de un gradiente climático y topográfico en Chubut, Argentina. Bosque (Valdivia) 26 (2): 137–153 DOI: 10.4067/S0717-92002005000200017
- 47. Marín F, Dahik C, Mosquera G, Feyen J, Cisneros P, Crespo P. 2018. Changes in Soil Hydro-Physical Properties and SOM Due to Pine Afforestation and Grazing in Andean Environments Cannot Be Generalized. Forests 10 (1): 17 DOI: 10.3390/f10010017
- 48. Miyamoto T, Annaka T, Chikushi J. 2003. Soil Aggregate Structure Effects on Dielectric Permittivity of an Andisol Measured by Time Domain Reflectometry. Vadose Zone Journal 2 (1): 90 DOI: 10.2136/vzj2003.9000
- 49. Moldrup P, Yoshikawa S, Olesen T, Komatsu T, Rolston DE. 2003. Gas Diffusivity in Undisturbed Volcanic Ash Soils. Soil Science Society of America Journal 67 (1): 41 DOI: 10.2136/sssaj2003.4100
- 50. Negrón M, López I, Dörner J. 2019. Consequences of intensive grazing by dairy cows of contrasting live weights on volcanic ash topsoil structure and pasture dynamics. Soil and Tillage Research 189: 88–97 DOI: 10.1016/j.still.2018.12.025
- 51. Neris J, Jiménez C, Fuentes J, Morillas G, Tejedor M. 2012. Vegetation and land-use effects on soil properties and water infiltration of Andisols in Tenerife (Canary Islands, Spain). CATENA 98: 55–62 DOI: 10.1016/J.CATENA.2012.06.006
- 52. Ordóñez I, López IF, Kemp PD, Descalzi CA, Horn R, Zúñiga F, Dec D, Dörner J. 2018. Effect of pasture improvement managements on physical properties and water content dynamics of a volcanic ash soil in southern Chile. Soil and Tillage Research 178: 55–64 DOI: 10.1016/J.STILL.2017.11.013
- 53. Pochet G, Van der Velde M, Vanclooster M, Delvaux B. 2007. Hydric properties of high charge, halloysitic clay soils from the tropical South Pacific region. Geoderma 138 (1–2): 96–109 DOI: 10.1016/J.GEODERMA.2006.10.019
- 54. Podwojewski P, Poulenard J, Zambrana T, Hofstede R. 2006. Overgrazing effects on vegetation cover and properties of volcanic ash soil in the páramo of Llangahua and La



- Esperanza (Tungurahua, Ecuador). Soil Use and Management 18 (1): 45–55 DOI: 10.1111/j.1475-2743.2002.tb00049.x
- 55. Poulenard J, Podwojewski P, Herbillon AJ. 2003. Characteristics of non-allophanic Andisols with hydric properties from the Ecuadorian páramos. Geoderma 117 (3): 267–281 DOI: 10.1016/S0016-7061(03)00128-9
- 56. Poulenard J, Podwojewski P, Janeau J-L, Collinet J. 2001. Runoff and soil erosion under rainfall simulation of Andisols from the Ecuadorian Páramo: Effect of tillage and burning. Catena 45 (3): 185–207 DOI: 10.1016/S0341-8162(01)00148-5
- 57. Quichimbo P, Tenorio G, Borja P, Cárdenas I, Crespo P, Célleri R. 2012. Efectos sobre las propiedades físicas y químicas de los suelos por el cambio de la cobertura vegetal y uso del suelo: páramo de Quimsacocha al sur del Ecuador. Suelos Ecuatoriales 42 (2): 138–153
- 58. Van Ranst E, Utami S, Shamshuddin J. 2002. Andisols on Volcanic Ash from Java Island, Indonesia: Physico-chemical Properties and Classification. Soil Science 167 (1): 68–79
- 59. Raviv M, Wallach R, Silber A, Medina S, Krasnovsky A. 1999. The effect of hydraulic characteristics of volcanic materials on yield of roses grown in soilless culture. Journal of the American Society for Horticultural Science 124 (2): 205–209
- 60. Ritter A, Muñoz-Carpena R, Regalado CM, Vanclooster M, Lambot S. 2004. Analysis of alternative measurement strategies for the inverse optimization of the hydraulic properties of a volcanic soil. Journal of Hydrology 295 (1–4): 124–139 DOI: 10.1016/J.JHYDROL.2004.03.005
- 61. Roa-García MC, Brown S, Schreier H, Lavkulich LM. 2011. The role of land use and soils in regulating water flow in small headwater catchments of the Andes. Water Resources Research 47 (5): W05510 DOI: 10.1029/2010WR009582
- 62. Rudiyanto, Toride N, Sakai M, Šimůnek J. 2013. A Hysteretic Model of Hydraulic Properties for Dual-Porosity Soils. Soil Science Society of America Journal 77 (4): 1182–1188 DOI: 10.2136/sssaj2012.0339n
- 63. Rustanto A, Booij MJ, Wösten H, Hoekstra AY. 2017. Application and recalibration of soil water retention pedotransfer functions in a tropical upstream catchment: case study in Bengawan Solo, Indonesia. Journal of Hydrology and Hydromechanics 65 (3): 307–320 DOI: 10.1515/johh-2017-0020 Open access PDF
- 64. Salazar I, Millar D, Lara V, Nuñez M, Parada M, Alvear M, Baraona J. 2012. Effects of the application of biosolids on some chemical, biological and physical properties in an Andisol from southern Chile. Journal of soil science and plant nutrition 12 (3): 441–450 DOI: 10.4067/S0718-95162012005000006
- 65. da Silva FF, Wallach R, Chen Y. 1993. Hydraulic properties of sphagnum peat moss and tuff (scoria) and their potential effects on water availability. Plant and Soil 154 (1): 119–126 DOI: 10.1007/BF00011080
- 66. Spilling KH. 2018. Pedotransfer functions for predicting hydraulic properties of non-allophanic Andosols and Histosols in the Páramo of southern Ecuador.Norwegian University of Life Sciences.
- 67. Strachan IB, Arnalds Ó, Palmason F, Porgeirsson H, Sigurdsson BD, Sigurdardottir H, Novoselac G. 1998. Soils of the Gunnarsholt experimental plantation. Iceland Agricultural Sciences 12: 27–38
- 68. Subedi S, Kawamoto K, Karunarathna AK, Moldrup P, Wollesen de Jonge L, Komatsu T. 2013a. Mini Tensiometer-Time Domain Reflectometry Coil Probe for Measuring Soil



- Water Retention Properties. Soil Science Society of America Journal 77 (5): 1517 DOI: 10.2136/sssaj2012.0106
- 69. Subedi S, Komatsu K, Komatsu T, Moldrup P, Wollesen de Jonge L, Müller K, Clothier B. 2013b. Contact Angles of Water-repellent Porous Media Inferred by Tensiometer- TDR Probe Measurement Under Controlled Wetting and Drying Cycles. Soil Science Society of America Journal 77 (6): 1944 DOI: 10.2136/sssaj2013.05.0203
- 70. Tejedor M, Jiménez C, Díaz F. 2003. Volcanic materials as mulches for water conservation. Geoderma 117 (3–4): 283–295 DOI: 10.1016/S0016-7061(03)00129-0
- 71. Terribile F, Iamarino M, Langella G, Manna P, Mileti FA, Vingiani S, Basile A. 2018. The hidden ecological resource of andic soils in mountain ecosystems: evidence from Italy. Solid Earth 9 (1): 63–74 DOI: 10.5194/se-9-63-2018
- 72. Tjahyandari D. 1998. Characteristics of volcanic ash soils of southern area of Mount Ruapehu, North Island, New Zealand.Massey University.
- 73. Tokumoto I, Noborio K, Koga K. 2010. Coupled water and heat flow in a grass field with aggregated Andisol during soil-freezing periods. Cold Regions Science and Technology 62 (2–3): 98–106 DOI: 10.1016/j.coldregions.2010.03.005
- 74. Tonneijck FH, Jansen B, Nierop KGJ, Verstraten JM, Sevink J, De Lange L. 2010. Towards understanding of carbon stocks and stabilization in volcanic ash soils in natural Andean ecosystems of northern Ecuador. European Journal of Soil Science 61 (3): 392–405 DOI: 10.1111/j.1365-2389.2010.01241.x
- 75. van der Velde M, Green SR, Gee GW, Vanclooster M, Clothier BE. 2005. Evaluation of Drainage from Passive Suction and Nonsuction Flux Meters in a Volcanic Clay Soil under Tropical Conditions. Vadose Zone Journal 4 (4): 1201 DOI: 10.2136/vzj2005.0011
- 76. Vingiani S, Mele G, De Mascellis R, Terribile F, Basile A. 2015. Volcanic soils and landslides: a case study of the island of Ischia (southern Italy) and its relationship with other Campania events. Solid Earth 6 (2): 783–797 DOI: 10.5194/se-6-783-2015
- 77. Walczak R, Rovdan E, Witkowska-Walczak B. 2002. Water retention characteristics of peat and sand mixtures. International Agrophysics 16: 161–165
- 78. Watanabe K, Osada Y. 2017. Simultaneous measurement of unfrozen water content and hydraulic conductivity of partially frozen soil near 0 °C. Cold Regions Science and Technology 142: 79–84 DOI: 10.1016/J.COLDREGIONS.2017.08.002
- 79. Wijewardana NS, Müller K, Moldrup P, Clothier B, Komatsu T, Hiradate S, de Jonge LW, Kawamoto K. 2016. Soil-water repellency characteristic curves for soil profiles with organic carbon gradients. Geoderma 264: 150–159 DOI: 10.1016/J.GEODERMA.2015.10.020
- 80. Yáñez N, Dec D, Clunes J, Dörner J. 2015. Estimación de la curva de retención de agua de un Andisol bajo un cultivo de arándano, a través de funciones de pedotransferencia. Agro Sur 43 (3): 63–72 DOI: 10.4206/agrosur.2015.v43n3-07
- 81. Zúñiga F, Horn R, Rostek J, Peth S, Uteau D, Dörner J. 2019. Anisotropy of intensity—capacity parameters on Aquands with contrasting swelling—shrinkage cycles. Soil and Tillage Research 193: 101–113 DOI: 10.1016/J.STILL.2019.05.019



Supplementary material

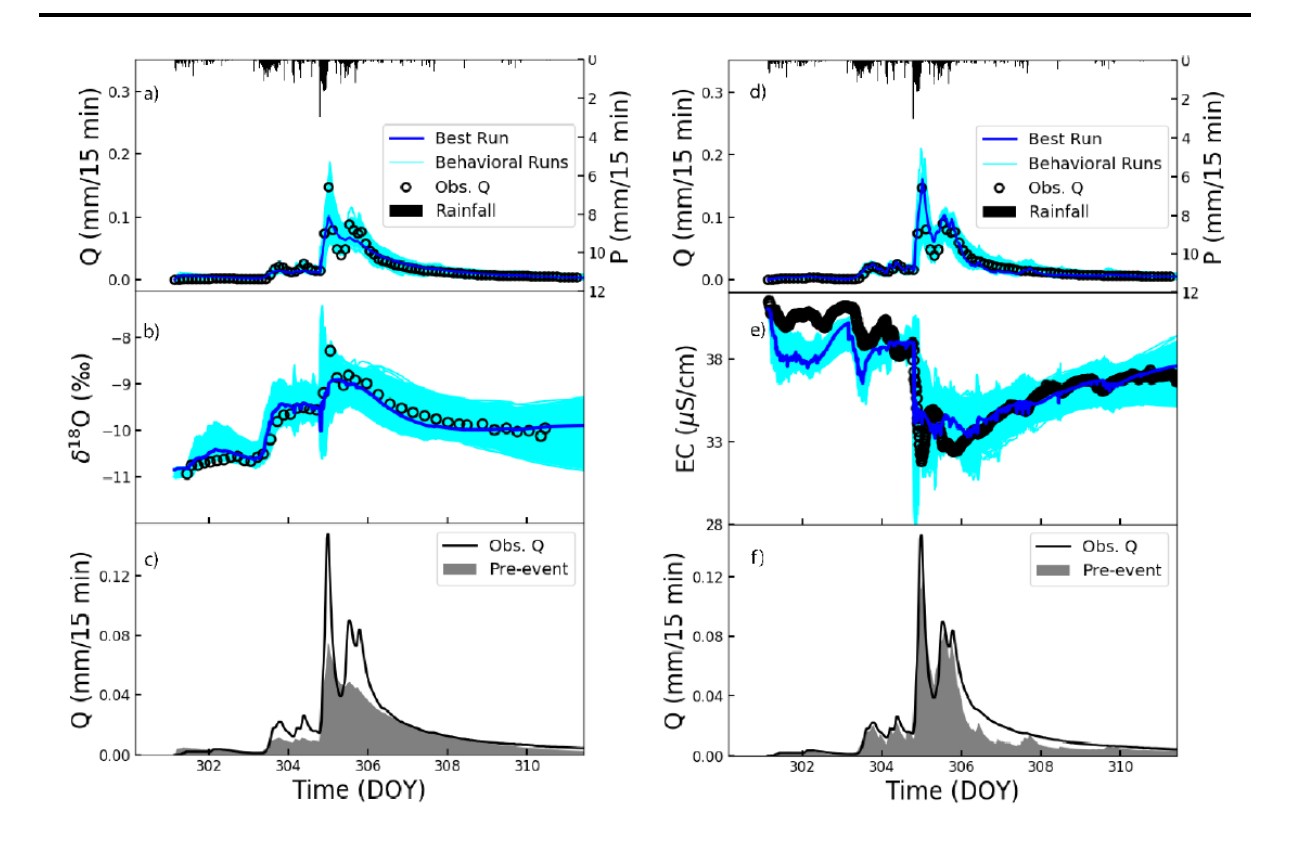


Figure S1. TraSPAN modelling results of the hydrograph separation using structure 2 with $\delta^{18}O$ (a–c) and electrical conductivity (EC) (d–f) as tracers. (a, b, d, and e) show the observed (open markers) and simulated streamflow and tracer data according to at least 100 different sets of parameters (light blue lines) yielding Nash-Sutcliffe efficiencies (NSEs) above 0.75. The simulated times series with the set of parameters that yielded the highest NSEs are depicted in dark blue in all cases. (c and f) present the pre-event water (gray shaded area) and the event water (unshaded area) contributions during the storm corresponding to the set of parameters yielding the higher NSEs.

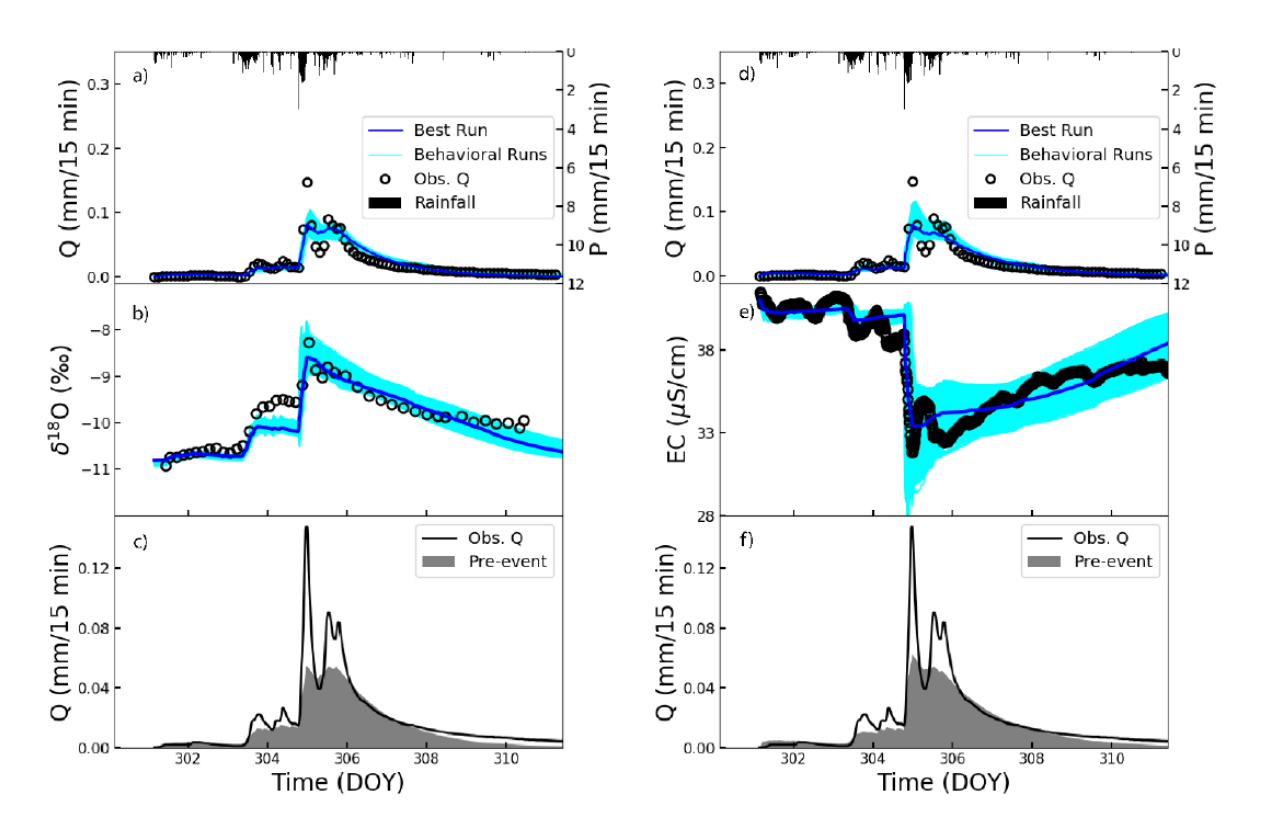


Figure S2. TraSPAN modelling results of the hydrograph separation using structure 3 with $\delta^{18}O$ (a–c) and electrical conductivity (EC) (d–f) as tracers. (a, b, d, and e) show the observed (open markers) and simulated streamflow and tracer data according to at least 100 different sets of parameters (light blue lines) yielding Nash-Sutcliffe efficiencies (NSEs) above 0.75. The simulated times series with the set of parameters that yielded the highest NSEs are depicted in dark blue in all cases. (c and f) present the pre-event water (gray shaded area) and the event water (unshaded area) contributions during the storm corresponding to the set of parameters yielding the higher NSEs.

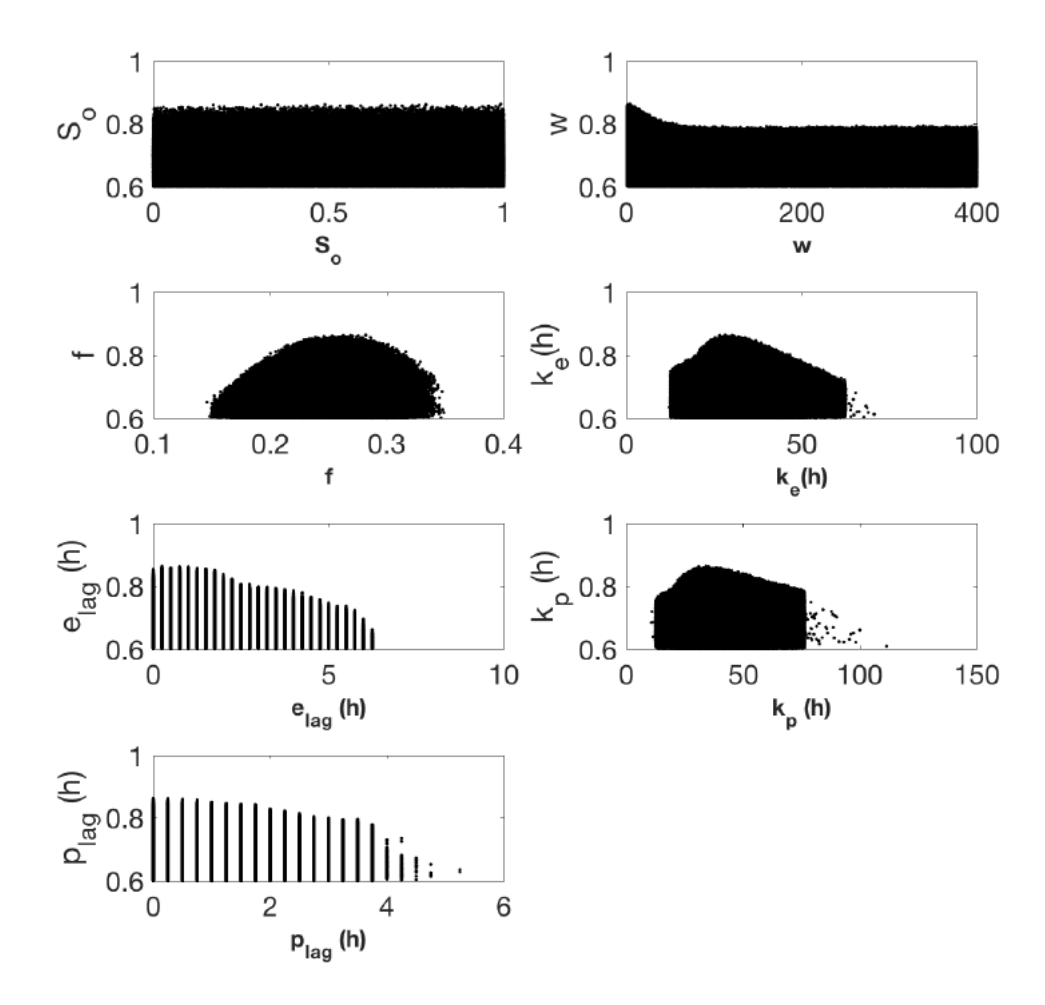


Figure S3. Dotty plots of the Monte Carlo simulation for the calibrated parameters using the TraSPAN model structure 1 for δ^{18} O. Parameter names are shown in **Table 4.1**.

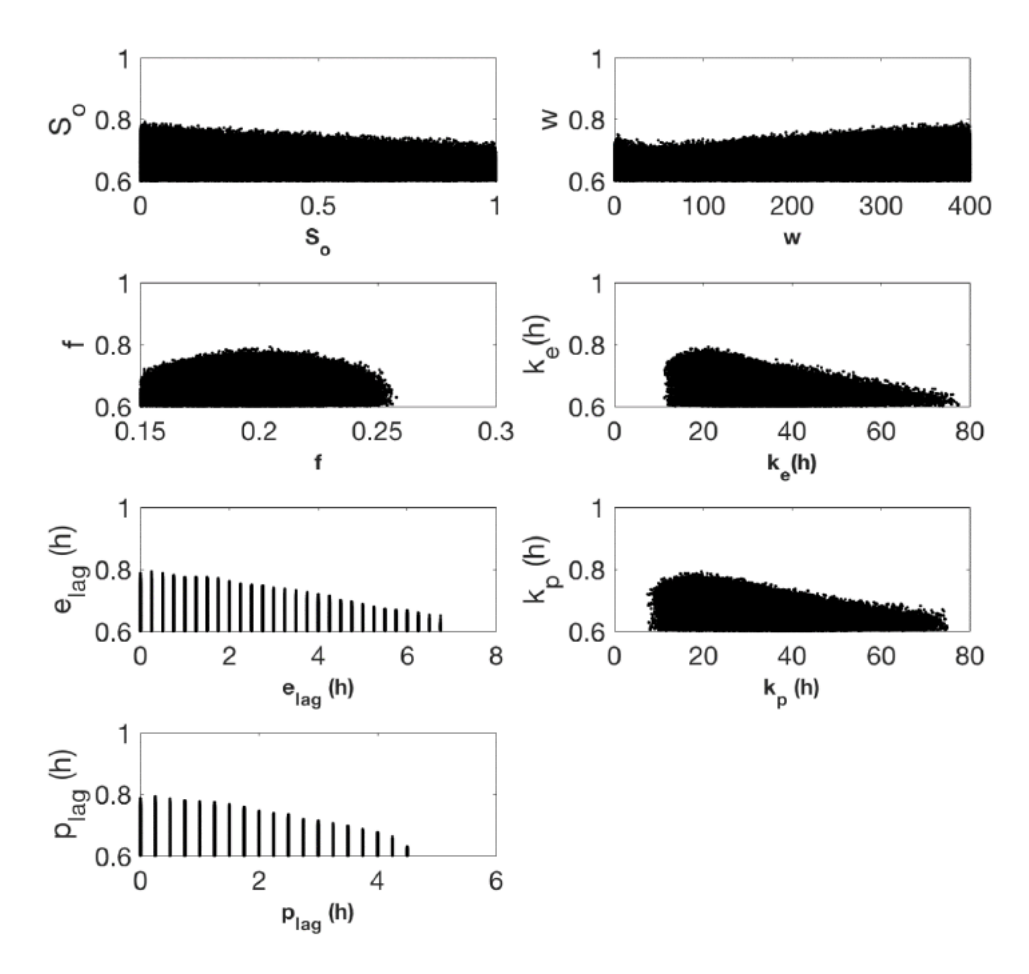


Figure S4. Dotty plots of the Monte Carlo simulation for the calibrated parameters using the TraSPAN model structure 1 for electrical conductivity (EC). Parameter names are shown in **Table 4.1**.

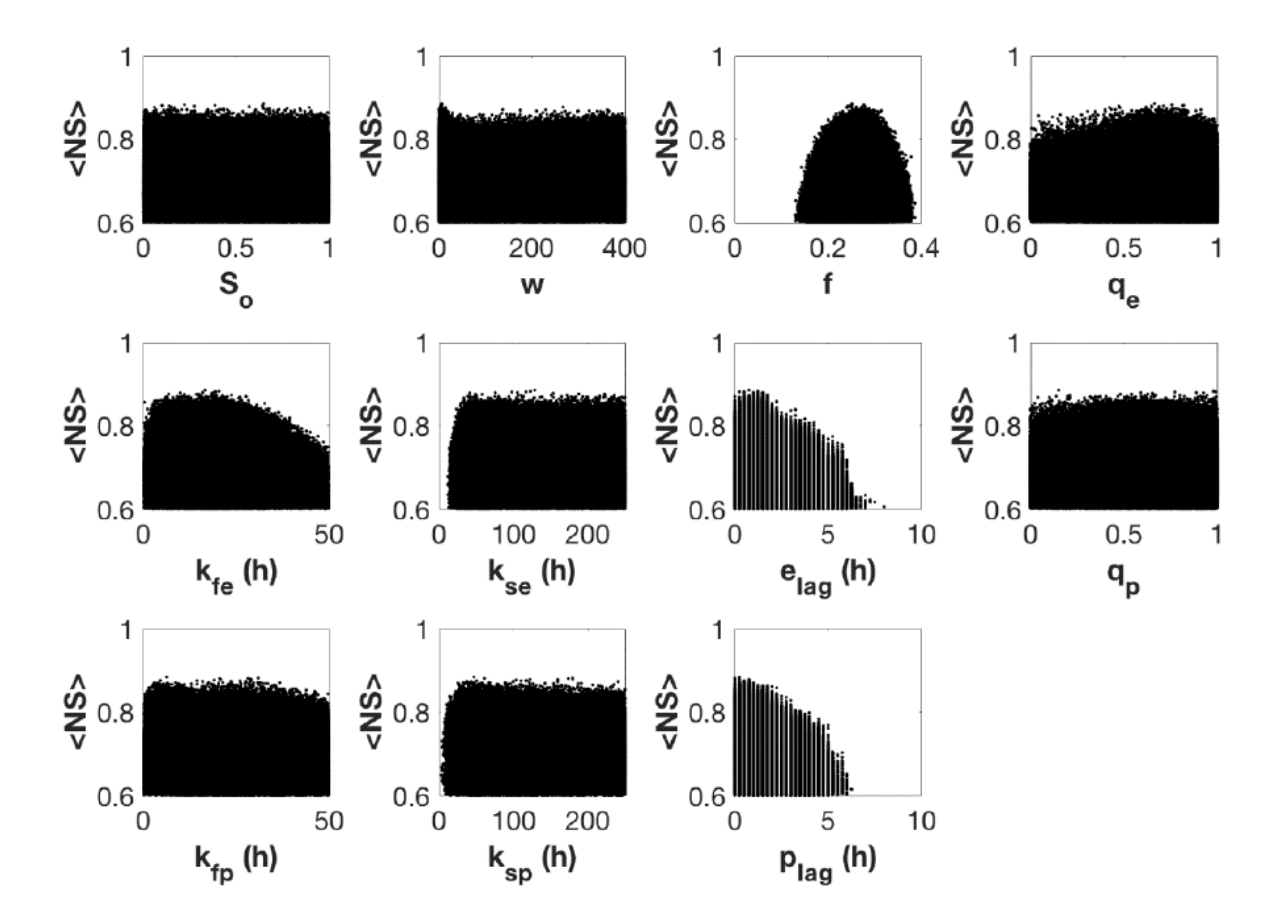


Figure S5. Dotty plots of the Monte Carlo simulation for the calibrated parameters using the TraSPAN model structure 2 for δ^{18} O. Parameter names are shown in **Table 4.1**.

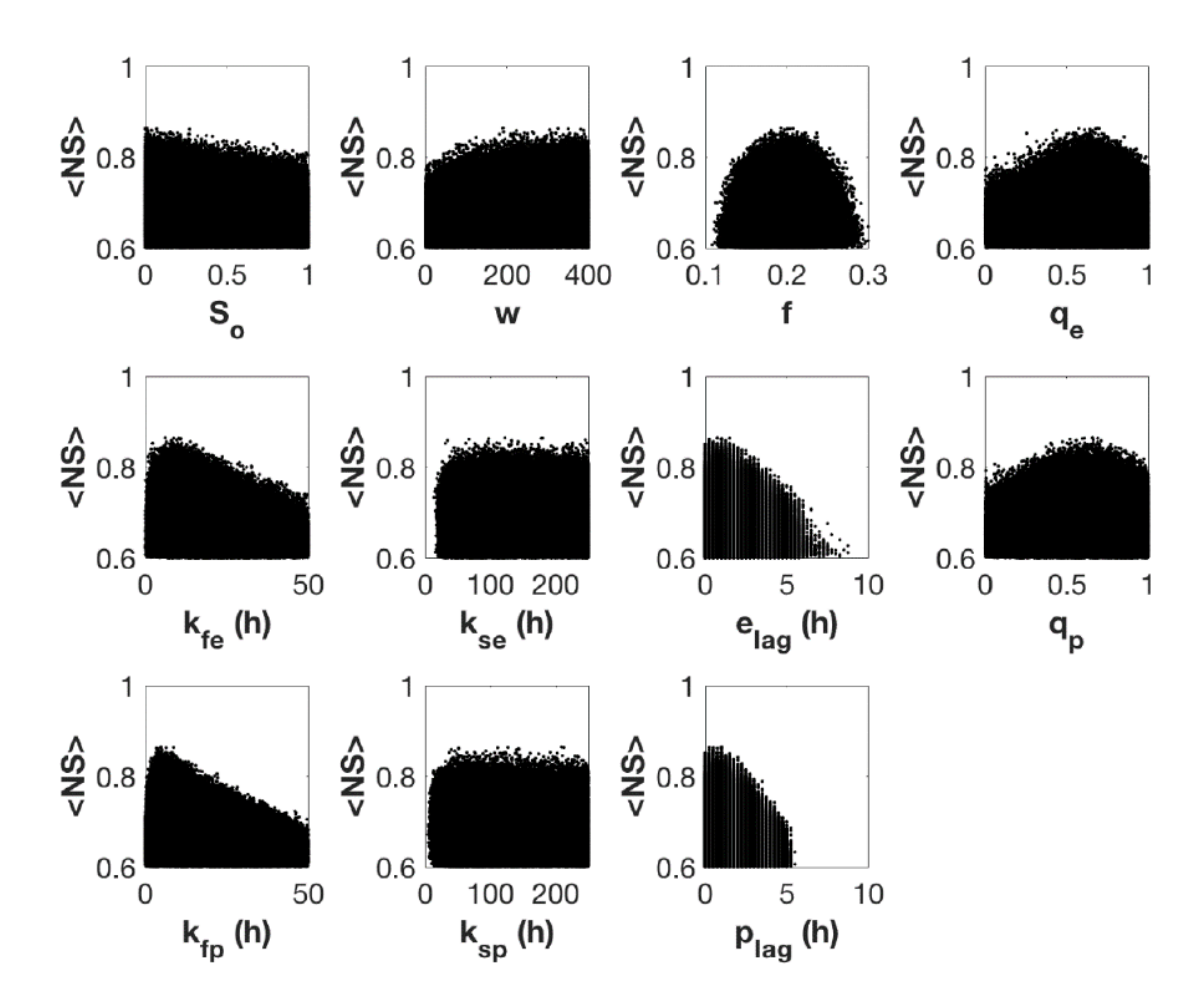


Figure S6. Dotty plots of the Monte Carlo simulation for the calibrated parameters using the TraSPAN model structure 2 for electrical conductivity (EC). Parameter names are shown in **Table 4.1**.

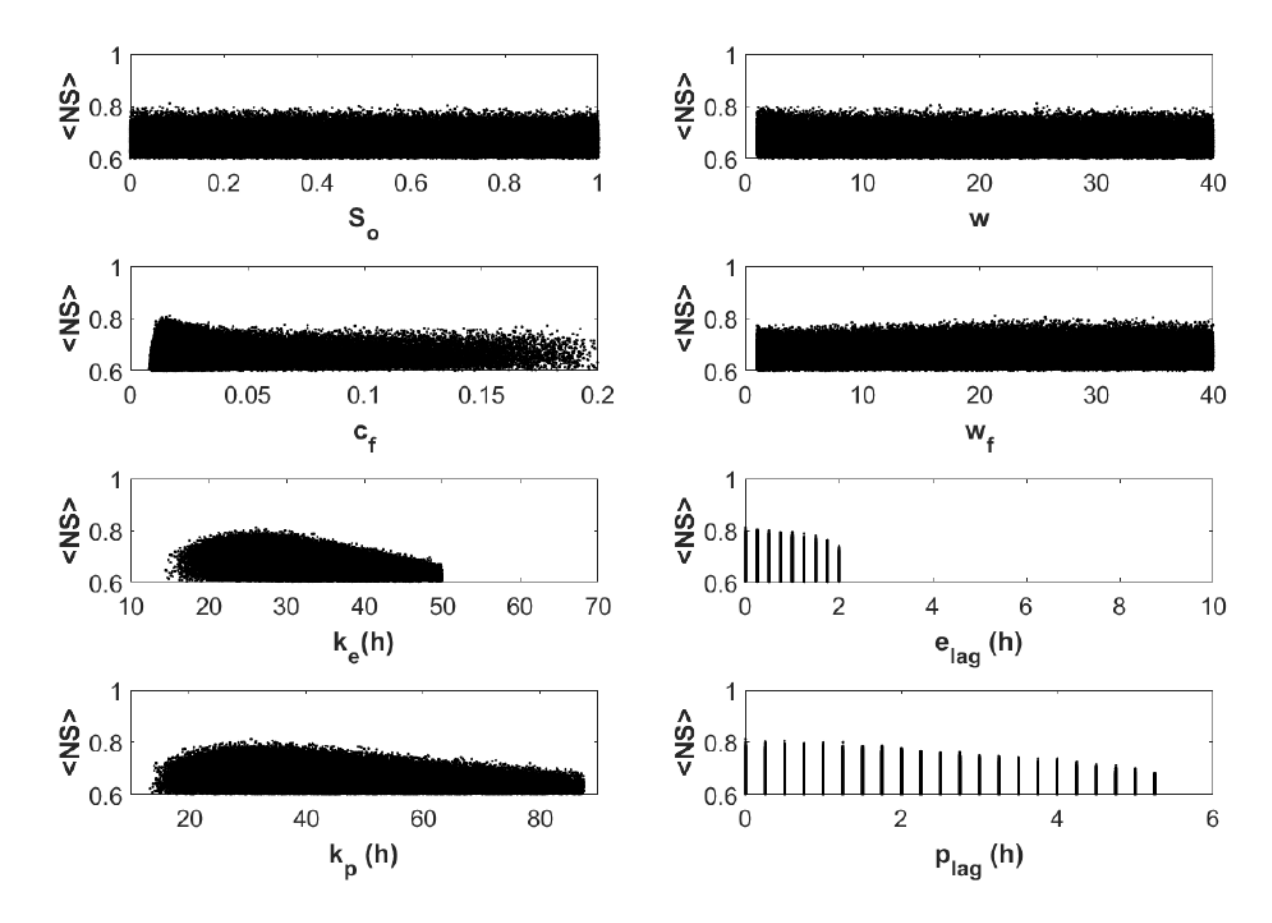


Figure S7. Dotty plots of the Monte Carlo simulation for the calibrated parameters using the TraSPAN model structure 3 for δ^{18} O. Parameter names are shown in **Table 4.1**.

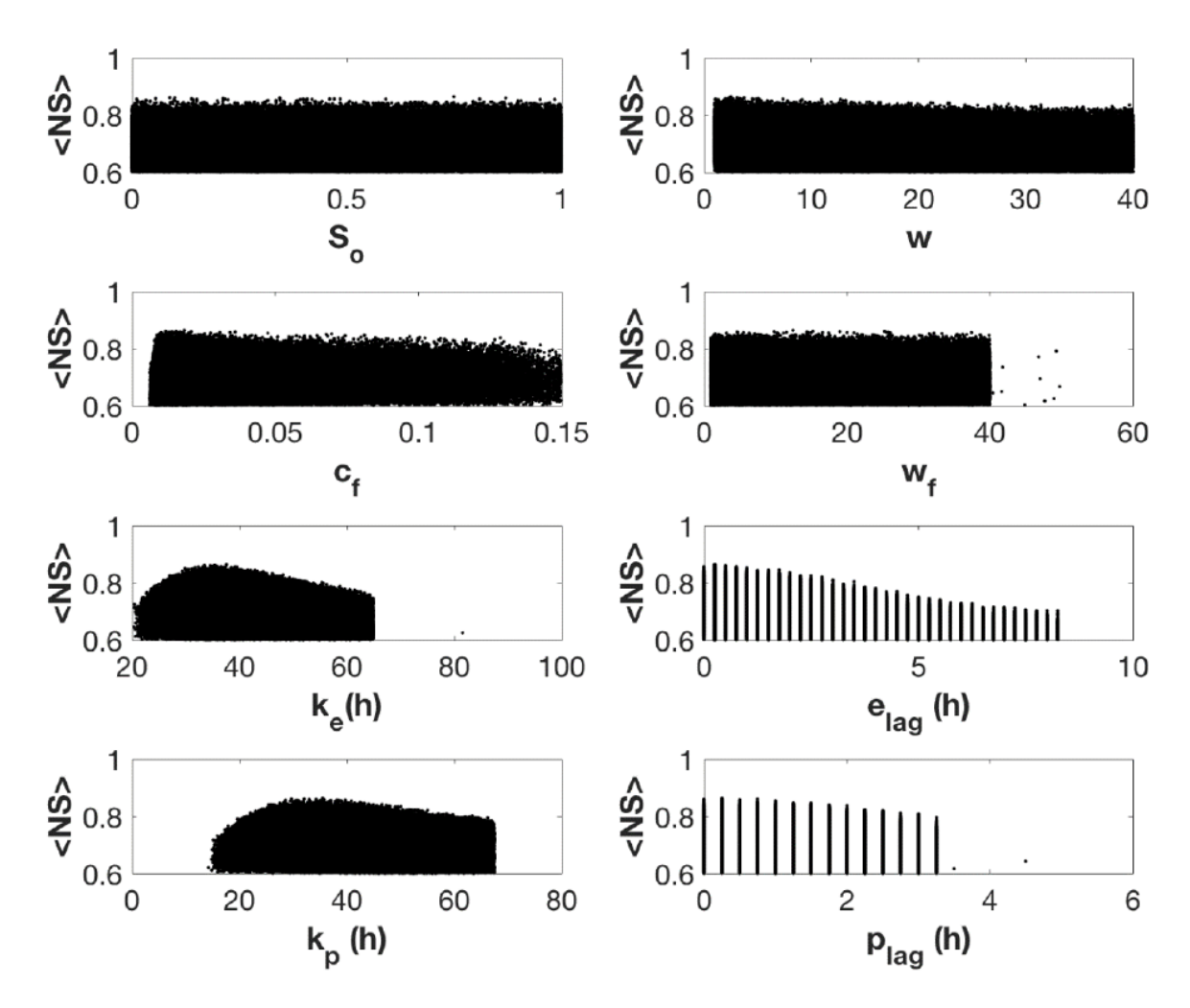


Figure S8. Dotty plots of the Monte Carlo simulation for the calibrated parameters using the TraSPAN model structure 3 for electrical conductivity (EC). Parameter names are shown in **Table 4.1**.

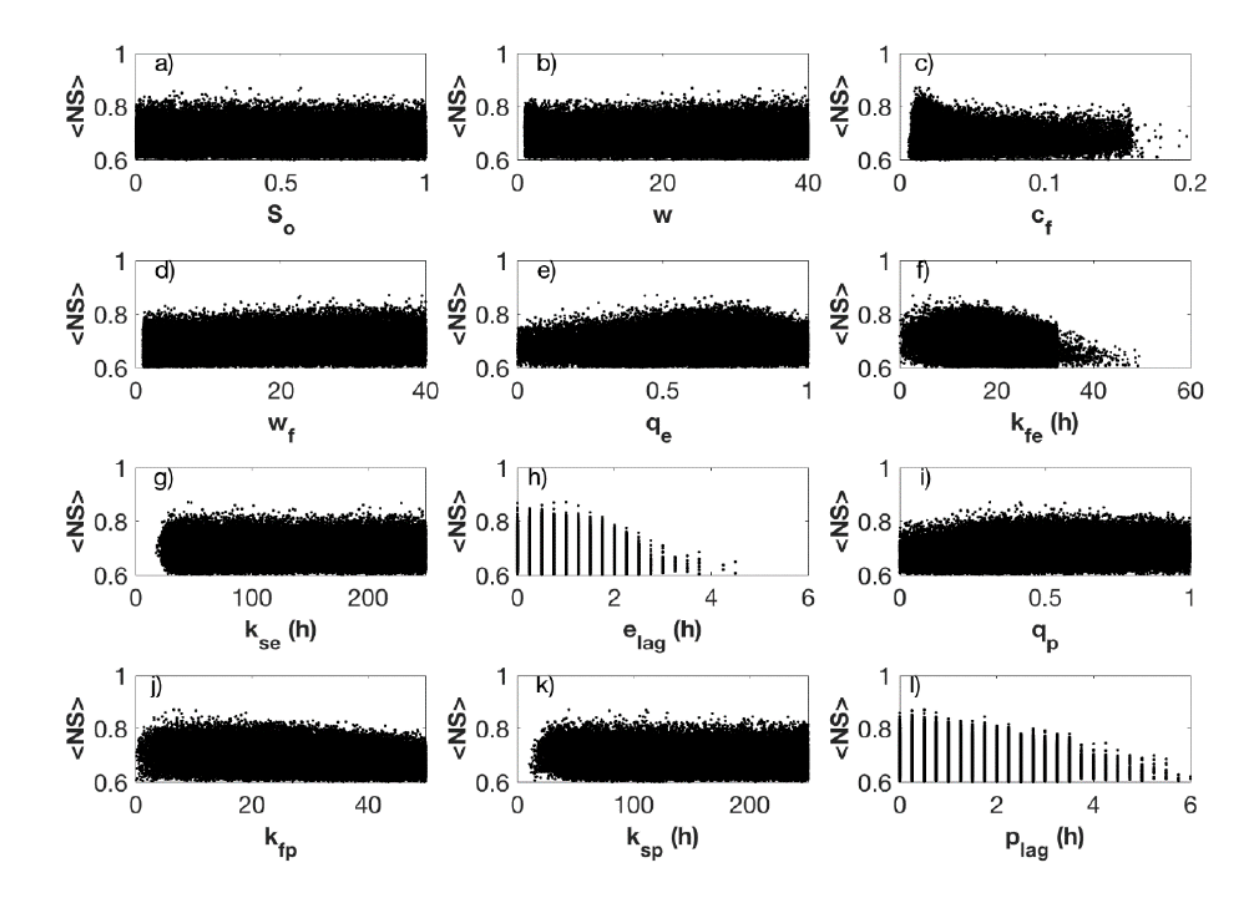


Figure S9. Dotty plots of the Monte Carlo simulation for the calibrated parameters using the TraSPAN model structure 4 for δ^{18} O. Parameter names are shown in **Table 4.1**.

erial

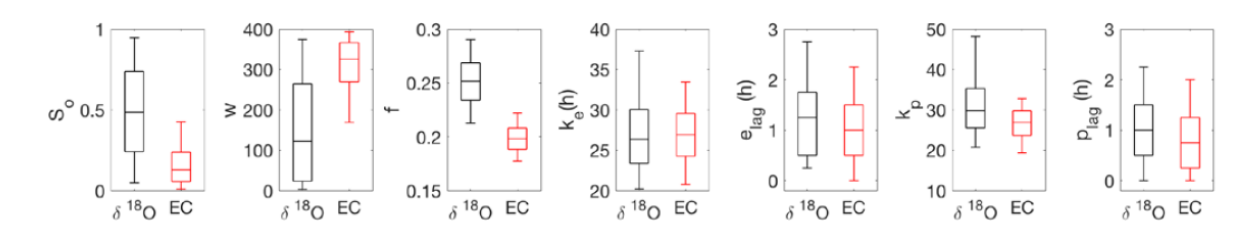


Figure S10. Box plots of the calibrated parameters considering sets that yield NS>0.75 from the last run (i.e., 1×10^7 simulations) using model structure 1 for δ^{18} O and electrical conductivity (EC). Parameter names are included in **Table 4.1**.

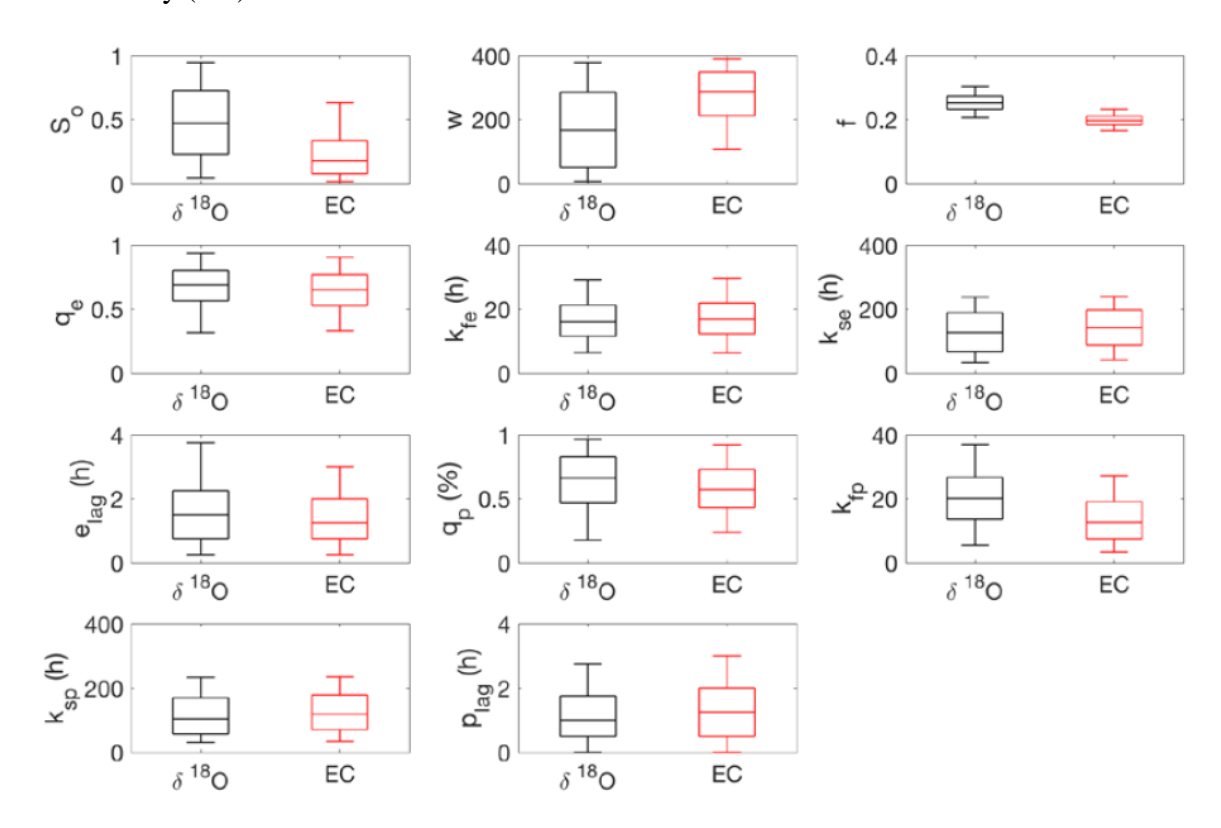


Figure S11. Box plots of the calibrated parameters considering sets that yield NS>0.75 from the last run (i.e., 1×10^7 simulations) using model structure 2 for δ^{18} O and electrical conductivity (EC). Parameter names are included in **Table 4.1**.

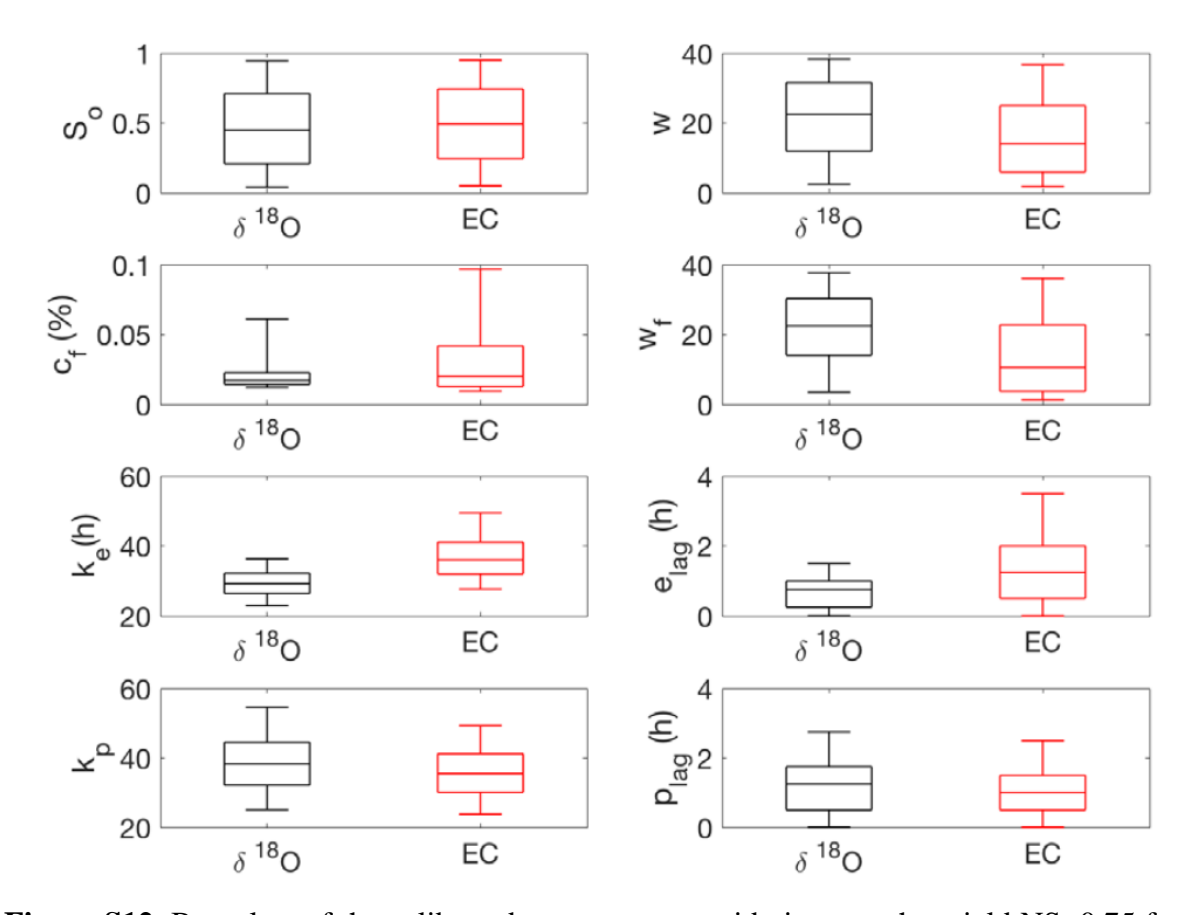


Figure S12. Box plots of the calibrated parameters considering sets that yield NS>0.75 from the last run (i.e., 1×10^7 simulations) using model structure 3 for $\delta^{18}O$ and electrical conductivity (EC). Parameter names are included in **Table 4.1**.



About the author

I was born in Cuenca, Ecuador, on March 19th, 1987. I obtained a BSc degree in Civil Engineering from the Faculty of Engineering at the University of Cuenca (Ecuador) in 2012. I continued my graduate education at Oregon State University (United States), where I obtained an MSc degree in Water Resources Science. My main research interests are related to the use of environmental tracers, field techniques, and numerical models for various applications in hydrology, ecohydrology, biogeochemistry, hydrometeorology, water quality, land use change, and urban hydrology. My research experience includes the publication of 13 articles in scientific journals indexed in ISI Web of Science and SCOPUS, the direction and tutoring of 9 theses in the MSc Program in Hydrology of the University of Cuenca, the direction and codirection of 2 research projects and participation in several research projects with international cooperation, participation as a representative of the Early Career Committee of the International Association of Hydrological Sciences, contribution as peer reviewer for 8 scientific journals indexed in ISI Web of Science and SCOPUS, and instructor of several courses in the MSc Program in Hydrology and short specialization courses at the University of Cuenca.

Peer-reviewed publications

- 1. <u>Mosquera GM</u>, Lazo PX, Célleri R, Wilcox BP, Crespo P. 2015. Runoff from tropical alpine grasslands increases with areal extent of wetlands. CATENA 125: 120–128 DOI: 10.1016/j.catena.2014.10.010
- Mosquera GM, Célleri R, Lazo PX, Vaché KB, Perakis SS, Crespo P. 2016a. Combined Use of Isotopic and Hydrometric Data to Conceptualize Ecohydrological Processes in a High-Elevation Tropical Ecosystem. Hydrological Processes DOI: 10.1002/hyp.10927
- 3. <u>Mosquera GM</u>, Segura C, Vaché KB, Windhorst D, Breuer L, Crespo P. 2016b. Insights into the water mean transit time in a high-elevation tropical ecosystem. Hydrology and Earth System Sciences 20 (7): 2987–3004 DOI: 10.5194/hess-20-2987-2016
- 4. Aparecido LMT, Teodoro GS, <u>Mosquera G</u>, Brum M, de V. Barros F, Pompeu PV, Rodas M, Lazo P, Müller CS, Mulligan M, et al. 2017. Ecohydrological drivers of Neotropical vegetation in montane ecosystems. Ecohydrology: e1932 DOI: 10.1002/eco.1932



- 5. Wright C, Kagawa-Viviani A, Gerlein-Safdi C, <u>Mosquera GM</u>, Poca M, Tseng H, Chun KP. 2017. Advancing ecohydrology in the changing tropics: Perspectives from early career scientists. Ecohydrology: e1918 DOI: 10.1002/eco.1918
- Esquivel-Hernández G, Sánchez-Murillo R, Quesada-Román A, <u>Mosquera GM</u>, Birkel C, Boll J. 2018. Insight into the stable isotopic composition of glacial lakes in a tropical alpine ecosystem: Chirripó, Costa Rica. Hydrological Processes DOI: 10.1002/hyp.13286
- 7. Marín F, Dahik C, <u>Mosquera G</u>, Feyen J, Cisneros P, Crespo P. 2018. Changes in Soil Hydro-Physical Properties and SOM Due to Pine Afforestation and Grazing in Andean Environments Cannot Be Generalized. Forests 10 (1): 17 DOI: 10.3390/f10010017
- 8. <u>Mosquera G</u>, Segura C, Crespo P. 2018. Flow Partitioning Modelling Using High-Resolution Isotopic and Electrical Conductivity Data. Water 10 (7): 904 DOI: 10.3390/w10070904
- Pesántez J, Mosquera GM, Crespo P, Breuer L, Windhorst D. 2018. Effect of land cover and hydro-meteorological controls on soil water DOC concentrations in a high-elevation tropical environment. Hydrological Processes 32 (17): 2624–2635 DOI: 10.1002/hyp.13224
- Tenelanda-Patiño D, Crespo-Sánchez P, <u>Mosquera G</u>. 2018. Umbrales en la respuesta de humedad del suelo a condiciones meteorológicas en una ladera Altoandina. MASKANA 9
 53–65 DOI: 10.18537/mskn.09.02.07
- 11. Esquivel-Hernández G, <u>Mosquera GM</u>, Sánchez-Murillo R, Quesada-Román A, Birkel C, Crespo P, Célleri R, Windhorst D, Breuer L, Boll J. 2019. Moisture transport and seasonal variations in the stable isotopic composition of rainfall in Central American and Andean Páramo during El Niño conditions (2015-2016). Hydrological Processes 33 (13): 1802–1817 DOI: 10.1002/hyp.13438
- Lazo PX, <u>Mosquera GM</u>, McDonnell JJ, Crespo P. 2019. The role of vegetation, soils, and precipitation on water storage and hydrological services in Andean Páramo catchments. Journal of Hydrology 572: 805–819 DOI: 10.1016/J.JHYDROL.2019.03.050
- 13. Campozano L, Mendoza D, <u>Mosquera G</u>, Palacio-Baus K, Célleri R, Crespo P. 2020. Wavelet analyses of neural networks based river discharge decomposition. Hydrological Processes: hyp.13726 DOI: 10.1002/hyp.13726
- 14. <u>Mosquera GM</u>, Crespo P, Breuer L, Feyen J, Windhorst D. 2020. Water transport and tracer mixing in volcanic ash soils at a tropical hillslope: A wet layered sloping sponge. Hydrological Processes: hyp.13733 DOI: 10.1002/hyp.13733



Research projects

- June 2018-June 2022 (ongoing). Principal Investigator (PI).
 Project title: "Identification of tap water sources and water supply structure in a mesoscale tropical Andean city". Co-funded by the International Atomic Energy Agency and the Central Research Unit of the University of Cuenca (USD\$ 35,000.00).
- June 2018-June 2022 (ongoing). Co-PI.
 Project title: "Evaluation of Non-Stationary Hydrological Conditions in the Andean Páramo". Co-funded by the International Atomic Energy Agency and the Central Research Unit of the University of Cuenca (USD\$ 40,000.00).

Selected presentations at scientific meetings since 2016 (*Presenting author)

- 1. <u>Mosquera*, G.M.</u>; Lazo, P.X.; Crespo, P.; Célleri, R. (2019) "The Role of Andean Peatlands in the Hydrology of Tropical Alpine Catchments" 27th IUGG General Assembly/IAHS Symposium. July, 8-18, Montreal, Canada. (Oral presentation).
- Mosquera*, G.M.; Windhorst, D.; Breuer, L.; McDonnell, J.J., Crespo, P. (2019) "How Do Organo-Mineral Soils Influence Subsurface Hydrological Connectivity at the Hillslope Scale?" Catchment Science Gordon Research Conference: Interactions of Hydrology, Biology & Geochemistry. June 23-27, Andover, NH, United States. (Poster presentation).
- 3. Mosquera*, G.M.; Lazo, P.X.; Crespo, P.; Célleri, R. (2019) "Water storage of tropical alpine catchments at the top of the Andes". 2019 Isotope Hydrology Symposium: Advancing the Understanding of Water Cycle Processes. May 20-24, 2019, Vienna, Austria. (Oral presentation).
- 4. Mosquera*, G.M.; Segura, C., Crespo, P. (2019) "High-resolution modeling of flow partitioning using water isotopes and electrical conductivity for model calibration". 2019 Isotope Hydrology Symposium: Advancing the Understanding of Water Cycle Processes. May 20-24, 2019, Vienna, Austria. (Poster presentation).
- 5. <u>Mosquera*, G.M.</u>; Lazo, P.X.; Crespo, P.; Célleri, R. (2018). "How do wetlands and grasslands influence the ecohydrological functioning of the Andean Páramo". IsoEcol 2018. July 29-August 3, 2018, Vina del Mar, Chile. (Oral presentation).
- Mosquera*, G.M.; Lazo, P.X.; Célleri, R.; Crespo, P. (2017). "ZREO: Seven years of hydrogeochemical research at the top of the Andes". Catchment Science Gordon Research Conference: Interactions of Hydrology, Biology & Geochemistry. June 25-30, Lewiston, ME, United States. (Poster Presentation).



- 7. Mosquera*, G.M.; Célleri, R.; Crespo, P. (2017). "Critical Zone Observations in the Tropical Andes". Critical Zone Science Workshop: Current Advances and Future Opportunities Conference. June 4-6, Arlington, VA, United States. (Poster Presentation)
- 8. <u>Mosquera*, G.M.</u>; Lazo, P.X.; Crespo, P.; Célleri, R. (2016). "Illuminating the hydrology of a high-elevation tropical ecosystem: Runoff generation in the páramo". 2016 AGU Fall Meeting. December 12-16, 2016, San Francisco, CA. (Oral presentation).
- 9. Mosquera*, G.M.; Timbe, E.; Célleri, R.; Windhorst, D.; Breuer, L.; Crespo, P. (2016). "Insights on the Rainfall-Runoff Response Controls in two High-Elevation Tropical Ecosystems". AGU Chapman Conference, Emerging Issues in Tropical Ecohydrology. June 5-9, Cuenca, Ecuador. (Poster Presentation).

Session/event organization at scientific meetings:

- Co-convener of session "Tracers for Understanding the Sources, Pathways and Fate of Pollutants in the Hydrological Cycle" at IUGG 2019, Montreal, Canada (with Christine Stumpp and Maki Tsujimura).
- Co-organizer of the short course "How to write and publish a paper in hydrology" at IUGG 2019, Montreal, Canada (with Svenja Fischer and Joris Eekhout).
- 3. Co-organizer of the short course "Science Communication" at IUGG 2019, Montreal, Canada (with Joris Eekhout).

Student supervision

- 1. Patricio Lazo, University of Cuenca, Department of Water Resources and Environmental Sciences, Ecohydrology MSc program. Thesis title: "How vegetation, soils, and precipitation control passive and dynamic storage change in high–elevation tropical catchments?" (Co-advisor, defended winter 2018; published in Journal of Hydrology).
- Juan Pesántez, University of Cuenca, Department of Water Resources and Environmental Sciences, Ecohydrology MSc program. Thesis title: "Effect of land cover and hydrometeorological controls on soil water leachate DOC concentrations in a high-elevation tropical environment". (Co-advisor, defended winter 2018; published in Hydrological Processes).
- 3. Franklin Marin, University of Cuenca, Department of Water Resources and Environmental Sciences, Ecohydrology MSc program. Thesis title: Impacts of natural land cover conversion into pine plantations and pasture on the hydrophysical properties of soils in



- high-elevation Andean ecosystem of south Ecuador (Co-advisor, defended spring 2018; published in Forests).
- 4. Daniel Tenelanda, University of Cuenca, Department of Water Resources and Environmental Sciences, Ecohydrology MSc program. Thesis title: Soil moisture dynamics during rain events in different topographic positions and depths in an Andean páramo hillslope. (Co-advisor, defended spring 2018; published in Maskana).
- 5. Karina Larco, Universidad de Cuenca, Department of Civil Engineering, Hydrology MSc program. Thesis title: Factors controlling the spatio-temporal variability of transit times in tropical alpine catchments (Major advisor).
- 6. Braulio Lahuatte, University of Cuenca, Department of Civil Engineering, Hydrology MSc program. Thesis title: Soil water hydrological dynamics under native and introduced forests in a montane tropical ecosystem (Major advisor).
- 7. Darío Zhiña, University of Cuenca, Department of Civil Engineering, Hydrology MSc program. Thesis title: Factors controlling precipitation formation in the Andes of South Ecuador (Major advisor).
- 8. Viviana Arizaga, University of Cuenca, Department of Civil Engineering, Hydrology MSc program. Thesis title: Quantifying export of water quality parameters in a pristine tropical alpine catchment (Co-tutor).
- 9. Pablo Peña, University of Cuenca, Department of Civil Engineering, Hydrology MSc program. Thesis title: Evaluation of concentration—discharge hysteresis effects of water quality parameters on biogeochemical and hydrological processes in a pristine tropical alpine catchment (Co-tutor).

Teaching

- 1. Summer 2019: Instructor of the short course "The hydrology of Andean Ecosystems: Introduction to ecohydrology and environmental tracers", University of Cuenca
- 2. Winter 2019: Tracers in Hydrology, MS in Hydrology, University of Cuenca.
- 3. Spring 2017: Lecturer Database Management module, Advanced Hydrometry course, MS in Hydrology, University of Cuenca.
- 4. Spring 2016: Lecturer Tracer Hydrology module, Hydrogeochemistry course, MS in Hydrology, University of Cuenca.

Awards

1. 2019 Hydrology Journal Travel Award (May 2019, 800 US\$)



- 2. Canadian Young Hydrological Society Travel Award (March 2019, CA\$250)
- 3. IAHS Sivapalan Young Scientists Travel Award (SYSTA) (February 2019, €1810)
- 4. 2018 Ignacio Rodriguez-Iturbe Publication Award for best publication in the Scientific Journal Ecohydrology
- 5. Gordon Research Conference (GRC) Carl Storm International Diversity Award (January 2019, US\$1,250)
- 6. IsoEcol 2018 Student Fellowship (US\$250 plus registration waiver)
- 7. EGU General Assembly 2018 Early Career Scientist's Travel Support (ECSTS) (March 2018, €300 plus registration and abstract waiver)
- 8. NSF Travel Award (April 2015, \$3,080).
- 9. OSU Graduate Student Travel Award (March 2015, \$800).
- 10. AGU Fall Meeting 2014 Student Travel Award (December 2014, \$500).
- 11. SENESCYT Environmental Scientific Research Award in Natural Resources Management (August 2014, \$5,000).
- 12. Oregon State University (OSU) Graduate Student Travel Award (June 2014, \$500).
- 13. Third prize Fresh Ideas Poster Competition at the PNWS AWWA Annual Conference (May 2014).
- 14. PNWS AWWA Student Travel Scholarship (April 2014, \$350).
- 15. SENESCYT Travel Award (April 2013, \$5,000).
- 16. Ecuadorian National Secretary of Higher Education, Science, Technology, and Innovation (SENESCYT). Full grant (2 years) for MS studies (August 2012, \$104,000).

Doctoral Courses

- 1. Spatial Analysis with Geographical Information Systems, 2016.
- 2. Advanced Statistics, 2016.
- 3. Numerical methods, 2016.
- 4. Scientific writing, 2016.
- 5. Water Resources Planning and Management, 2016.

Complementary courses

 May 2018: Training Course on Advances in Data Processing and Interpretation Applied to Isotope Hydrology Studies. International Atomic Energy Agency Headquarters, Vienna, Austria.



- 2. August 2016: Aberdeen Catchment Science Summer School, University of Aberdeen, Aberdeen, Scotland.
- 3. May 2016: DIES ProGRANT, Proposal Writing for Research Grants. Organized and funded by the University of Cologne (Germany) and the German Academic Exchange Service (DAAD). Universidad Nacional, Bogota, Colombia.

Professional and academic service

- November 2018-June 2021 (ongoing): Early Career Committee member of the International Association of Hydrological Sciences (IAHS) in representation of the International Commission on Tracers.
- 2. Peer reviewer for: Water Resources Research; Hydrology and Earth System Sciences; Scientific Reports; Journal of Hydrology; Hydrological Processes; Ecohydrology; Water, Air, & Soil Pollution; Vadose Zone Journal.

Non peer-reviewed publications

- 1. Mosquera, G.M.; Córdova, M.; Célleri, R. (2016). Ecohydrological observatories in highelevation tropical ecosystems: Field guide and research results. AGU Chapman Conference, Emerging Issues in tropical ecohydrology. Cuenca, Ecuador. p. 1-44.
- Mosquera, G.M.; Lazo, P.X.; Crespo, P.; Célleri, R. (2015). Water isotopes as tools for identifying water sources in high-elevation tropical ecosystems: a case of study in the Ecuadorian Andes. Book of extended synopses, Oral presentations, 2015 Isotope Hydrology Symposium: Revisiting Foundations and Exploring Frontiers. Vienna, Austria. p. 151-155.